



**WYDZIAŁ BIOLOGII
I OCHRONY ŚRODOWISKA**
Uniwersytet Łódzki

Stacjonarne Studia Doktoranckie
Biochemiczno-Biofizyczne

Krzysztof Sztefura

Nanonośniki różu bengalskiego w terapii fotodynamicznej raka podstawnokomórkowego skóry

Nanosystems as carriers for rose bengal in
photodynamic therapy of basal cell carcinoma

Praca doktorska

wykonana w Katedrze Biofizyki Ogólnej
Instytutu Biofizyki Uniwersytetu Łódzkiego

Promotor:

- Prof. dr hab. Barbara Klajnert-
Maculewicz

Promotor pomocniczy:

- Dr Michał Gorzkiewicz



Łódź, 2022

Składam serdeczne podziękowania

Pani prof. dr hab. Barbarze Klajnert-Maculewicz
za okazaną pomoc, cierpliwość i zaufanie.

Panu dr. Michałowi Gorzkiewiczowi
za życzliwość i przekazaną pasję do nauki.

Dziękuję pracownikom oraz doktorantom
Katedry Biofizyki Ogólnej Uniwersytetu Łódzkiego
za miłą atmosferę i okazaną pomoc
podczas wykonywania badań.

Dziękuję również mojej żonie Aleksandrze oraz Rodzicom
za nieustające wsparcie i wiarę,
które dodawały siłę w trudnych momentach.

Spis treści

| | | |
|--------|--|----|
| 1. | Źródła finansowania badań prowadzonych w ramach pracy doktorskiej..... | 5 |
| 2. | Współpraca..... | 5 |
| 3. | Spis publikacji wchodzących w skład rozprawy doktorskiej..... | 6 |
| 4. | Omówienie celu naukowego i uzyskanych wyników | 7 |
| 4.1. | Wprowadzenie | 7 |
| 4.2. | Cel pracy i hipoteza badawcza | 12 |
| 4.3. | Metodyka badań | 12 |
| 4.4. | Omówienie wyników | 14 |
| 4.5. | Podsumowanie i wnioski..... | 18 |
| 5. | Streszczenie w języku polskim..... | 19 |
| 6. | Streszczenie w języku angielskim | 20 |
| 7. | Dorobek naukowy | 21 |
| 7.1. | Spis publikacji niewchodzących w skład rozprawy doktorskiej..... | 21 |
| 7.2. | Doniesienia konferencyjne | 22 |
| 7.2.1. | Wystąpienia ustne | 22 |
| 7.2.2. | Plakaty | 22 |
| 7.3. | Działalność naukowa..... | 23 |
| 7.3.1. | Projekty..... | 23 |
| 7.3.2. | Stáže zagraniczne..... | 23 |
| 7.3.3. | Zgłoszenie patentowe..... | 23 |

Załączniki

1. Kopie publikacji wchodzących w skład rozprawy doktorskiej
2. Oświadczenia współautorów publikacji wchodzących w skład rozprawy doktorskiej

1. Źródła finansowania badań prowadzonych w ramach pracy doktorskiej



Projekt OPUS „Dendrymery fosforowe jako nośniki fotouczulaczy - badania in vivo”, 2017/25/B/NZ7/01304



COST Action CA17140 „Nano2Clinic Cancer Nanomedicine – from the bench to the bedside”

2. Współpraca



Laboratory of Coordination Chemistry of CNRS, Tuluza, Francja



Leibniz Institute of Polymer Research Dresden, Niemcy



PolitoMedLab, Department of Mechanical and Aerospace Engineering, Politecnico di Torino, Włochy



Department of Organic Chemistry and Inorganic Chemistry, University of Alcalá, Hiszpania

3. Spis publikacji wchodzących w skład rozprawy doktorskiej

1. **Sztandera K.**, Gorzkiewicz M., Klajnert-Maculewicz B. (2020). Nanocarriers in photodynamic therapy- in vitro and in vivo studies. *Wiley Interdisciplinary Reviews: Nanomedicine and Nanobiotechnology*, 12(3), e1509. **(IF: 9,182; MEiN: 140 pkt.)**
2. **Sztandera K.**, Marcinkowska M., Gorzkiewicz M., Janaszewska A., Laurent R., Zabłocka M., Mignani S., Majoral J.P., Klajnert-Maculewicz B. (2020). In search of a phosphorus dendrimer-based carrier of rose bengal: tyramine linker limits fluorescent and phototoxic properties of a photosensitizer. *International Journal of Molecular Sciences*, 21(12), 4456. **(IF: 5,923; MEiN: 140 pkt.)**
3. **Sztandera K.**, Gorzkiewicz M., Dias Martins A.S., Pallante L., Zizzi E.A., Miceli M., Bątał M., Pinto Reis C., Deriu M.A., Klajnert-Maculewicz B. (2021). Noncovalent interactions with PAMAM and PPI dendrimers promote the cellular uptake and photodynamic activity of rose bengal: the role of the dendrimer structure. *Journal of Medicinal Chemistry*, 64(21), 15758-15771. **(IF: 7,446; MEiN: 200 pkt.)**
4. **Sztandera K.**, Gorzkiewicz M., Bątał M., Arkhipova V., Knauer N., Sánchez-Nieves J., de la Mata FJ., Gómez R., Apartsin E., Klajnert-Maculewicz, B. (2022). Triazine-carbosilane dendrimersomes enhance cellular uptake and phototoxic activity of rose bengal in basal cell skin carcinoma cells. *International Journal of Nanomedicine*, 17, 1139-1154. **(IF: 6,4; MEiN: 140 pkt)**
5. **Sztandera K.**, Gorzkiewicz M., Wang X., Appelhans D., Klajnert-Maculewicz B. (2022). Colloids and Surfaces B: Biointerfaces (w trakcie recenzji) pH-stable polymersome as nanocarrier for post-loaded rose bengal in photodynamic therapy **(IF: 5,268; MEiN: 100 pkt)**

Sumaryczny współczynnik wpływu (*ang. Impact Factor, IF*) publikacji wchodzących w skład rozprawy doktorskiej: 34,219

Łączna liczba punktów według listy czasopism punktowanych MEiN: 720

4. Omówienie celu naukowego i uzyskanych wyników

4.1. Wprowadzenie

Nowotwory skóry (w tym podstawnocomórkowy nowotwór skóry) są obecnie jednymi z najczęściej występujących nowotworów u ludzi. Z roku na rok liczba wykrywanych przypadków rośnie¹. Najczęściej występują one u mężczyzn o jasnym kolorze skóry na terenach o największej ekspozycji na promieniowanie UV. Ryzyko zachorowania rośnie z wiekiem, a mediana wieku zachorowania wynosi 68 lat². Należy jednak zauważyć, że równocześnie wzrasta świadomość społeczeństwa dotycząca profilaktyki raka podstawnocomórkowego skóry, co w konsekwencji prowadzi do wzrostu liczby wykrywanych przypadków.

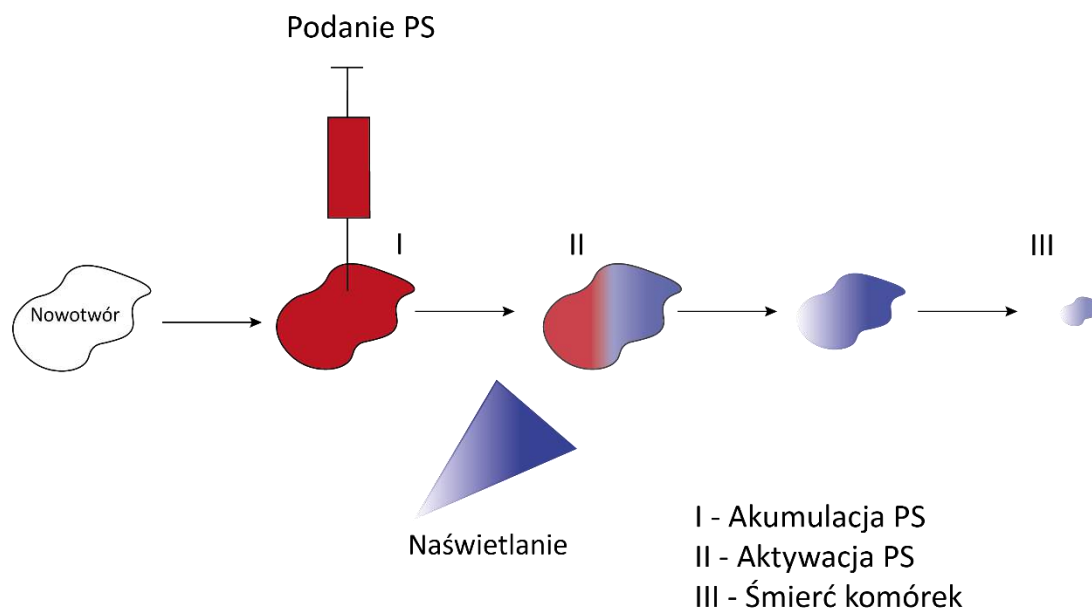
Bez względu jednak na przyczynę tego wzrostu, koniecznym pozostaje opracowanie skutecznych metod leczenia. Do obecnie stosowanych metod można zaliczyć chemioterapię, radioterapię czy terapię chirurgiczną, która jest najczęściej wykorzystywana w przypadku leczenia podstawnocomórkowego nowotworu skóry. Niestety techniki te powodują wiele efektów ubocznych³, których obecny stan wiedzy pozwala uniknąć opracowując skuteczniejsze terapie.

Terapia fotodynamiczna to nowoczesna metoda leczenia nowotworów, która wykorzystuje trzy elementy: światłoczuły lek, tzw. fotouczulacz, źródło światła oraz tlen cząsteczkowy. Ich połączenie prowadzi do rozpoczęcia kaskady reakcji prowadzących do śmierci komórek. Terapia ta nosi znamiona terapii celowanej, wywołując śmierć komórkową jedynie w miejscu naświetlenia (**Rysunek 1**).

¹ Jones O.T. et al. (2020) *Adv Ther.*, 37(1):603-616.

² Peris K. et al. (2019) *European Journal of cancer* 118: 10-34.

³ Kirby JS, Miller CJ. (2010) *J Am Acad Dermatol.* 63(4):689-702.

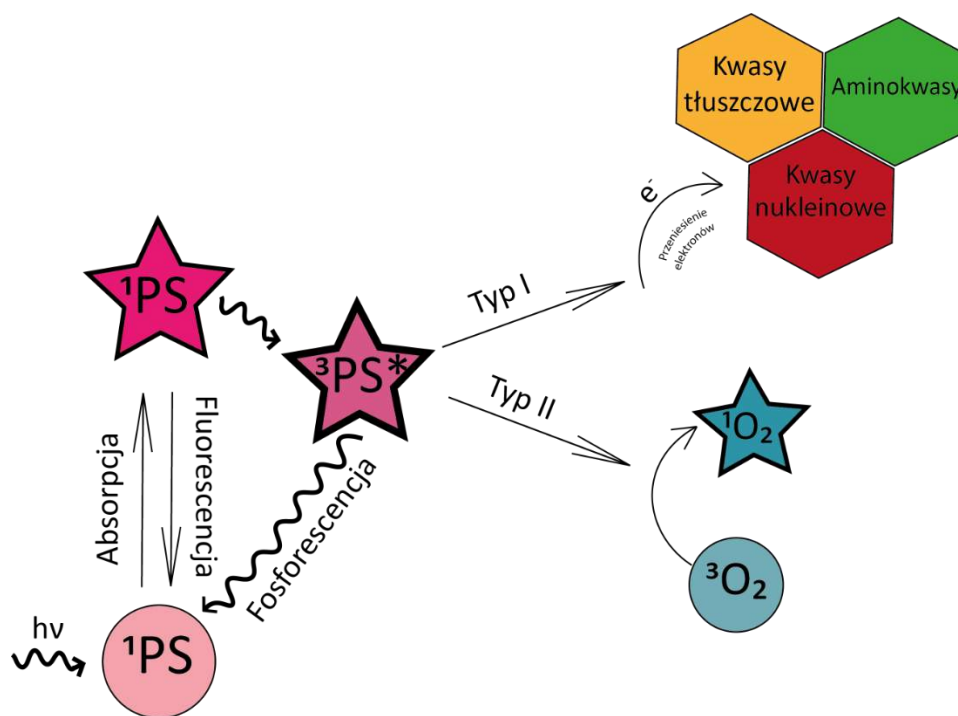


Rys. 1. Mechanizm działania terapii fotodynamicznej. Źródło: Sztandera K. et al. (2020), WIREs: Nanomedicine and Nanobiotechnology, zmodyfikowano.

Naświetlenie substancji fotouczulającej światłem o odpowiedniej długości fali prowadzi do absorpcji fotonów przez fotouczulacz, a następnie do przejścia z podstawowego poziomu energetycznego w niestabilny, singletowy stan wzbudzony. Wzbudzona cząsteczka fotouczulacza może ulec przejściu bezpromienistemu w znacznie stabilniejszy stan trypletowy lub energia może zostać uwolniona w postaci fluorescencji. W stanie trypletowym energia może zostać uwolniona w postaci ciepła, fosforescencji lub reakcji fotodynamicznych odpowiedzialnych za wywołanie efektu terapeutycznego.

Wyróżnia się dwa rodzaje reakcji fotodynamicznych. W pierwszym typie reakcji dochodzi do przeniesienia elektronu ze wzbudzonej cząsteczki fotouczulacza bezpośrednio na składniki wewnątrzkomórkowe takie jak aminokwasy, kwasy tłuszczowe lub nukleinowe. Reakcja ta prowadzi do powstania wolnych rodników, takich jak anionorodnik ponadtlenkowy czy rodnik wodoronadtlenkowy, które uszkadzają struktury komórkowe lub mogą reagować z tlenem tworząc wewnątrzkomórkowe reaktywne formy tlenu (RFT). W drugim typie reakcji energia przenoszona jest na tlen cząsteczkowy, prowadząc do powstania tlenu singletowego, również będącego silnym utleniaczem. Reakcje te odpowiadają za efekt cytotoksyczny oraz wywołują silne reakcje zapalne prowadząc do śmierci komórek (**Rysunek 2**). To, która reakcja przeważa, zależy od dostępności tlenu oraz

zastosowanego fotouczulacza, dlatego też dla otrzymania pożądanego efektu terapeutycznego niezbędne jest dobranie odpowiedniej substancji fotouczulającej.



Rys. 2. Schemat aktywacji fotouczulacza. Źródło: Sztandera K. et al. (2020), WIREs: *Nanomedicine and Nanobiotechnology*, zmodyfikowano.

Jednym z wyróżniających się fotouczulaczy jest róż bengalski (**Rysunek 3**). Jest to należąca do rodziny ksantanów pochodna fluoresceiny wykazująca właściwości fluorescencyjne. Pierwotnie róż bengalski był stosowany jako barwnik wełny, ale później znalazł zastosowanie w medycynie i obecnie jest powszechnie stosowany w okulistyce w celu wykrywania uszkodzeń spojówki oraz rogówki⁴, a także bywa stosowany w leczeniu nowotworów skóry⁵, przetyku czy głowy i szyi⁶. Róż bengalski może być również stosowany w terapii fotodynamicznej raka podstawnokomórkowego skóry⁷, lecz jego użycie w tej terapii jest ograniczone ze względu na krótki okres półtrwania w organizmie, tendencję do agregacji oraz ujemny ładunek, co powoduje ograniczony transport dkomórkowy⁸.

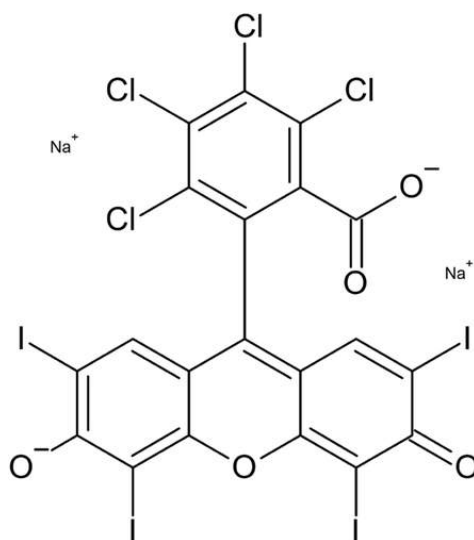
⁴ Doughty. (2013) *Contact Lens and Anterior Eye*, 36.6: 272-280.

⁵ Thompson et al. (2008) *Melanoma research*, 18.6: 405-411.

⁶ Wang et al. (2014) *Biomaterials*, 35.6: 1954-1966.

⁷ Collier et al. (2020) *Molecules*, 25.22: 5398.

⁸ Demartis et al. (2021) *Dyes and Pigments*, 188, 109236.



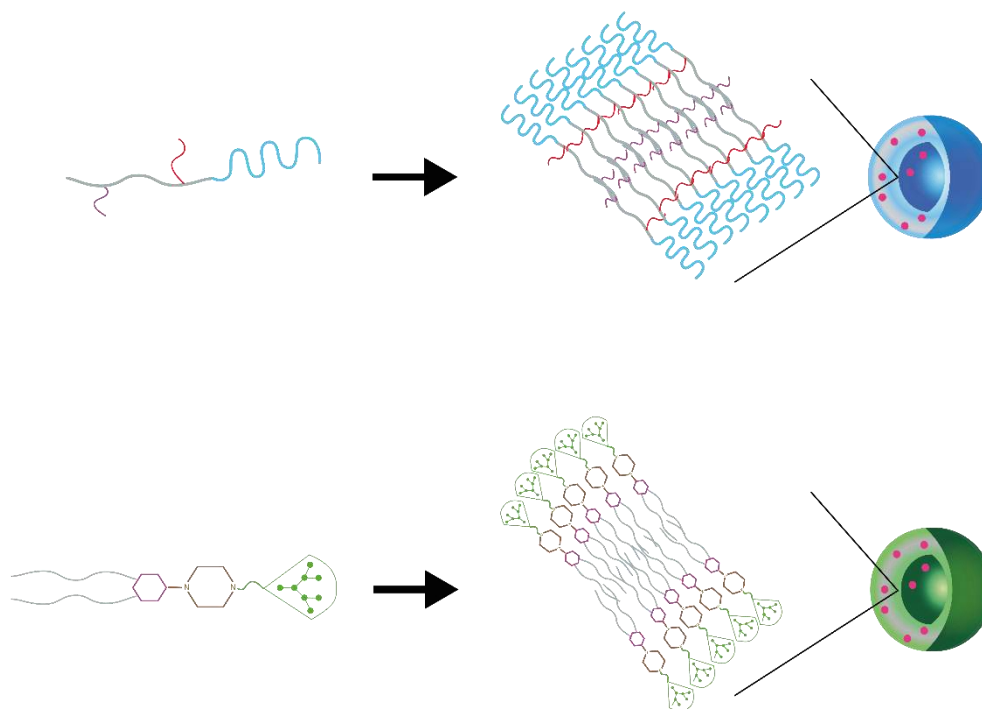
Rys. 3. Struktura chemiczna rózu bengalskiego

Dzisiejszy stan wiedzy z zakresu nanotechnologii umożliwia zastosowanie nanoukładów jako nośników rózu bengalskiego. Zadaniem takiego nośnika jest ochrona leku przed degradacją, zwiększenie jego rozpuszczalności, wydłużenie okresu półtrwania w organizmie, a także transport celowany i uwolnienie leku bezpośrednio w obrębie komórek nowotworowych. Wśród dużej liczby dostępnych obecnie i dobrze scharakteryzowanych nanoukładów należy wyróżnić dendrymery oraz dendrymersomy i polimersomy.

Dendrymery to rozbudowane związki organiczne, które cechują się symetryczną, dobrze scharakteryzowaną strukturą. Są to trójwymiarowe polimery, których kształt zbliża się do kulistego wraz ze wzrostem generacji (liczby przyłączonych warstw monomerów). Zbudowane są z rdzenia, od którego promieniście rozchodzą się ramiona zwane dendronami. Na ich końcu znajdują się grupy funkcyjne, które w dużej mierze odpowiadają za właściwości całego dendrymeru. Ta budowa umożliwia przyłączenie leku za pomocą niekwalencyjnych oddziaływań na zewnątrz i wewnątrz struktury, a także przez znacznie stabilniejsze, kowalencyjne wiązania. W pierwszym rozwiązaniu nie dochodzi do jakiegokolwiek modyfikacji struktury fotouczulacza, czego skutkiem jest brak zmian jego właściwości fotodynamicznych, jednakże kompleks taki może być mniej stabilny w warunkach *in vivo* w porównaniu do kowalencyjnego koniugatu⁹.

⁹ Jiang, Yan-Yan, et al. (2010) *Journal of drug targeting*, 18.5: 389-403.

Alternatywnym rozwiązaniem jest enkapsulacja różu bengalskiego wewnątrz polimersomu lub dendrymersomu. Są to związki zbudowane z amfifilowych monomerów, które w środowisku wodnym ulegają samoorganizacji. Prowadzi to do powstania struktur posiadających dwuwarstwową błonę, podobnych do liposomów (**Rysunek 4**).



Rys. 4. Schemat budowy: (A) polimersomu oraz (B) dendrymersomu.

Oba rodzaje nanopęcherzyków posiadają w swojej budowie również elementy wrażliwe na zmianę pH, które w środowisku kwaśnym ulegają protonacji, powodując rozluźnienie struktury błony. Właściwość ta umożliwia enkapsulację leku wewnątrz struktury, przetransportowanie go do docelowego miejsca działania i uwalnianie zależne od pH środowiska. Do głównych różnic między tymi dwoma nanoukładami można zaliczyć skład ich błony: dendrymersomy zbudowane są z amfifilowych dendronów, natomiast polimersomy z kopolimeru blokowego. Zastosowany w niniejszej pracy polimersom dodatkowo w swojej strukturze posiada ugrupowanie chemiczne umożliwiające sieciowanie światłem UV. Proces ten stabilizuje strukturę polimersomu uniemożliwiając jej reorganizację.

4.2. Cel pracy i hipoteza badawcza

Głównym celem niniejszej pracy było opracowanie najbardziej wydajnego nośnika różu bengalskiego oraz jego charakterystyka biofizyczna i ocena potencjału fotodynamicznego nanoukładów składających się z badanego nanoukładu oraz różu bengalskiego w badaniach *in vitro*.

Hipoteza badawcza zakładała, że badane nanoukłady zwiększą efektywność transportu dokomórkowego, co w konsekwencji zwiększy aktywność fotodynamiczną różu bengalskiego.

4.3. Metodyka badań

Badania przeprowadzono z zastosowaniem czterech nanoukładów składających się z:

1. Kompleksów komercyjnie dostępnych dendrymerów poliamidoaminowych (ang. poly(amidoamine), PAMAM)¹⁰ oraz polipropylenoiminowych (ang. poly(propyleneimine), PPI)¹¹ generacji trzeciej oraz czwartej połączonych z różem bengalskim za pomocą oddziaływań niekowalencyjnych (PAMAM G3:RB, PAMAM G4:RB, PPI G3:RB, PPI G4:RB)
2. Koniugatów dendrymerów fosforowych¹² pierwszej, drugiej oraz trzeciej generacji połączonych z różem bengalskim za pomocą wiązania kowalencyjnego z użyciem tyraminy (G1-TYR-RB, G2-TYR-RB, G3-TYR-RB). Badane związki zostały zsyntezowane przez zespół prof. Jeana Pierra Majorala z Laboratory of Coordination Chemistry of CNRS w Tuluzie oraz dr Monikę Marcinkowską z Katedry Biofizyki Ogólnej.
3. Polimersomów składających się z syntetycznego, amifilowego blokopolimeru z enkapsulowanym różem bengalskim (Psome RB). Blokopolimer ten został zsyntezowany przez zespół prof. Dietmara Appelhansa z Leibniz Institute of Polymer Research w Dreźnie.
4. Dendrymersomów składających się z dendronów triazynowo-karbokrzemowych generacji drugiej oraz trzeciej z enkapsulowanym różem bengalskim (Dsome G2/G3 RB), zsyntezowanych przez zespół dr. Evgeny'a Apartsina z Laboratory of Coordination Chemistry of CNRS w Tuluzie.

¹⁰ Tomalia, Rookmaker, (2009) *Oxford University Press*, pp. 979–982

¹¹ Meijer, (1993) *Angew. Chem. Int. Ed. Engl.*, 32: 1308-1311.

¹² Caminade, Majoral, (2004) *Accounts of chemical research*, 37.6 (2004): 341-348.

Jako model *in vitro* posłużyły trzy mysie linie komórkowe raka podstawnkomórkowego skóry (AsZ, BsZ, CsZ) otrzymane od Dr. Ervina Epsteina z Children's Hospital Oakland Research Institute w USA. Badane linie komórkowe wykazywały mutację w genie PTCH1 występującą u pacjentów ze skłonnością do rozwijania raka podstawnkomórkowego skóry. Dodatkowo linie BsZ oraz CsZ miały wyciszony gen P53, który koduje białko supresorowe nowotworów. Guzy u myszy indukowane były przy użyciu promieniowania UV- linia komórkowa AsZ oraz promieniowania jonizującego- linia komórkowa BsZ, natomiast myszy od których wyizolowano linię CsZ nie były poddane naświetlaniu. Należy podkreślić, że mimo różnic występujących między badanymi liniami komórkowymi uzyskane wyniki dla wszystkich linii były zbliżone, co świadczy o uniwersalnym charakterze obserwacji.

Badania przeprowadzono przy użyciu poniższych materiałów oraz metod:

1. Pomiar intensywności fluorescencji w celu:
 - a. określenia wpływu koniugacji RB z dendrymerem fosforowym (G-TYR-RB), kompleksowania RB z dendrymerami PAMAM/PPI (PAMAM G3:RB, PAMAM G4:RB, PPI G3:RB, PPI G4:RB), enkapsulacji RB w dendrymersomie (Dsome G2/G3 RB) i polimersomie (Psome RB)
 - b. Oznaczenia stechiometrii reakcji tworzenia kompleksów różu bengalskiego z dendrymerami PAMAM/PPI
 - c. Oceny wydajności enkapsulacji RB w dendrymersomie i polimersomie
2. Ocena średnicy hydrodynamicznej badanych nanoukładów za pomocą pomiaru dynamicznego rozpraszania światła (*ang. Dynamic Light Scattering, DLS*).
3. Ocena powierzchniowego potencjału elektrostatycznego badanych nanoukładów przy pomocy pomiaru potencjału zeta.
4. Pomiar szybkości uwalniania leku z koniugatów oraz dendrymersomów i polimersomów z enkapsulowanym różem bengalskim w pH 5 oraz pH 7,4 za pomocą dializy równowagowej.
5. Pomiar produkcji tlenu singletowego przez wolny róż bengalski, nanoukłady z różem bengalskim i bez przy użyciu sondy fluorescencyjnej (SOSG lub ABDA).
6. Pomiar produkcji reaktywnych form tlenu przez wolny róż bengalski oraz badane nanoukłady w mysich liniach komórkowych AsZ, BsZ, CsZ przy użyciu sondy H₂DCFDA.

7. Transport dokomórkowy badanych nanoukładów w mysich liniach komórkowych AsZ, BsZ, CsZ przy użyciu cytometrii przepływowej.
8. Oznaczenie cytotoksyczności wolnego różu bengalskiego, nanoukładów z różem bengalskim i bez po naświetlaniu oraz bez naświetlania w mysich liniach komórkowych (AsZ, BsZ, CsZ) za pomocą metody MTT.
9. Oznaczenie lokalizacji wewnątrzkomórkowej dendrymersomów z enkapsulowanym różem bengalskim przy użyciu mikroskopii konfokalnej.

4.4. Omówienie wyników

W ramach niniejszej pracy przebadano cztery nanoukłady różniące się strukturą, właściwościami chemicznymi oraz sposobem przenoszenia różu bengalskiego.

Pierwszy etap badań obejmował wykorzystanie komercyjnie dostępnych oraz dobrze scharakteryzowanych kationowych dendrymerów PAMAM oraz PPI trzeciej i czwartej generacji, które są w stanie transportować róż bengalski dzięki tworzeniu niekowalencyjnych kompleksów. Stechiometrię reakcji kompleksowania określono za pomocą pomiaru intensywności fluorescencji oraz potencjału zeta. W pierwszym przypadku podczas miareczkowania różu bengalskiego dendrymerem dochodziło do stopniowego obniżenia intensywności fluorescencji, a następnie przesunięcia długości fali emisji w kierunku fal podczerwonych i ponownego wzrostu intensywności fluorescencji. Takie przesunięcie maksimum emisji jest przypisywane w literaturze wiązaniu cząsteczek do powierzchni dendrymeru¹³. Następnie na podstawie tych danych wyznaczono stosunek intensywności fluorescencji przy pierwotnej oraz przesuniętej w kierunku fal podczerwonych długości fali emisji. Przy użyciu metody Joba¹⁴ określono maksymalne stosunki molowe dendrymer:róż bengalski (D:RB), przy których wszystkie cząsteczki różu są związane przez badany dendrymer. Wyniki te potwierdzono również za pomocą pomiaru potencjału zeta, gdzie podczas miareczkowania dendrymeru różem bengalskim dochodziło do stopniowego obniżenia potencjału zeta, aż do osiągnięcia plateau. Dodatkowo pomiar potencjału zeta wykazał, że przy maksymalnych stosunkach molowych kompleksy posiadały silnie ujemny ładunek powierzchniowy, który mógłby być przeszkodą

¹³ Klajnert, B., Bryszewska, M. (2002) *CMBL*, 7(4), 1087-1094.

¹⁴ Huang, C. Y. (1982) *Methods Enzymol*, 87, 509– 525.

w transporcie dokomórkowym¹⁵, dlatego do dalszych eksperymentów wybrano optymalny stosunek molowy (1:10) czyli taki, przy którym cały układ wykazuje dodatni ładunek powierzchniowy. Analiza tworzenia kompleksów i ocena wpływu kompleksowania na geometrię dendrymerów zostały również przeprowadzone przy użyciu metod *in silico* przez zespół prof. Marco A. Deriu z PolitoMedLab, Politecnico di Torino z Włoch.

Dalsze badania wykazały zwiększoną produkcję tlenu singletowego przez kompleksy dendrymerów generacji trzeciej, a także zwiększoną produkcję wewnątrzkomórkowych reaktywnych form tlenu przez kompleksy obu generacji dendrymerów PPI. Transport dokomórkowy był znacząco zwiększony dla wszystkich kompleksów, a widoczne między nimi różnice można przypisać różnicy potencjałów powierzchniowych określonych na podstawie badań *in silico* (kompleks, który wykazywał najbardziej dodatni ładunek był transportowany do komórek z najwyższą wydajnością). W efekcie została zaobserwowana najwyższa fototoksyczność kompleksów różu bengalskiego i dendrymerów PPI generacji trzeciej.

Kompleksy dendrymerów z różem bengalskim wydajnie przenosiły lek do komórek jednocześnie zwiększając jego aktywność fotodynamiczną. Należy zauważyć jednak, że niekowalencyjne kompleksy dendrymer:lek w mniejszym stopniu niż kowalencyjne koniugaty chronią lek przed biodegradacją w organizmie. Dlatego do kolejnego etapu prac wybrano bardziej stabilne koniugaty dendrymerów fosforowych pierwszej, drugiej oraz trzeciej generacji połączonych z różem bengalskim za pomocą wiązania kowalencyjnego poprzez łącznik na bazie tyraminy. Tyramina jest stabilnym łącznikiem o odpowiedniej długości, pozwalającej wyeksponować róż bengalski na powierzchni dendrymeru. Obecność grup fenolowych umożliwia wytworzenie wiązania kowalencyjnego, mającego za zadanie zwiększyć stabilność nanoukładu i chronić go przed degradacją w organizmie.

Stopniowa modyfikacja chemiczna różu bengalskiego i przyłączanie do niego kolejnych elementów koniugatu za pomocą wiązań kowalencyjnych powodowała spadek intensywności fluorescencji. Warto również zauważyć, że wraz ze zmniejszającą się generacją dendrymeru fosforowego intensywność fluorescencji malała, do tego stopnia, że koniugat dendrymeru fosforowego generacji pierwszej w ogóle jej nie wykazywał.

¹⁵ Honary S, Zahir F. (2013) Trop J Pharm Res. 12(2):255–264.

W związku z tym do dalszej oceny właściwości fotodynamicznych został wybrany koniugat generacji trzeciej oraz róż bengalski połączony z tyraminą jako forma przejściowa między wolnym różem a koniugatem.

Za pomocą DLS oraz pomiaru potencjału zeta określono, że G3-TYR-RB posiada średnicę hydrodynamiczną wynoszącą ok. 18 nm oraz dodatni ładunek powierzchniowy wynoszący 44,5 mV. Za pomocą dializy równowagowej określono, że koniugat jest stabilny zarówno w pH 7,4 jak i pH 5, a róż bengalski jest uwalniany w niewielkiej ilości.

Transport dkomórkowy zbadany za pomocą cytometrii przepływowej wykazał, że nawet niewielka modyfikacja różu bengalskiego przez połączenie go z tyraminą powoduje obniżenie wydajności transportu. Cały koniugat był również transportowany w mniejszym stopniu niż wolny lek.

Modyfikacja różu bengalskiego powodowała obniżenie produkcji tlenu singletowego, a dodatkowo ograniczony transport dkomórkowy przekładał się na zmniejszenie generacji wewnątrzkomórkowych reaktywnych form tlenu. W konsekwencji można było zaobserwować zmniejszony efekt fototoksyczny.

Wyniki drugiego etapu badań wykazały, że modyfikacja kowalencyjna różu bengalskiego umożliwia wytworzenie stabilnego nanoukładu, ale jednocześnie zmniejsza aktywność fotodynamiczną leku. Ponadto koniugaty nie mają zdolności uwolnienia leku w ściśle kontrolowanych warunkach. Takie właściwości natomiast posiadają dendrymersomy oraz polimersomy analizowane podczas kolejnych etapów badań.

Badany polimersom zbudowany jest z amfifilowego kopolimeru blokowego wzbogaconego o element odpowiedzialny za sieciowanie światłem UV oraz element wrażliwy na zmianę pH. Pomiar średnicy hydrodynamicznej w kwaśnym oraz obojętnym środowisku wykazał stabilność polimersomu oraz zdolność do rozluźniania struktury błony w środowisku kwaśnym. Z kolei pomiar potencjału zeta wykazał dodatni ładunek powierzchniowy polimersomu, który obniżał się po enkapsulacji różu bengalskiego. Za pomocą dializy równowagowej potwierdzono również możliwość zatrzymywania różu bengalskiego wewnątrz struktury w pH 7,4 oraz uwalniania w pH 5,5. Badania spektroskopowe wykazały wysoką wydajność enkapsulacji różu bengalskiego w polimersomie wynoszącą około 60%, a dodatkowo przesunięcie maksimum emisji wskazało na oddziaływanie między cząsteczkami różu bengalskiego a polimersomem, co prawdopodobnie dodatkowo stabilizowało cały nanoukład.

W dalszej części pracy zbadano generację tlenu singletowego oraz reaktywnych form tlenu, która okazała się znacząco zwiększona w przypadku rózu bengalskiego enkapsulowanego w polimersomie. To właśnie ten efekt bezpośrednio przełożył się na zwiększoną cytotoksyczność tego nanoukładu, ponieważ transport dokomórkowy był jedynie w niewielkim stopniu zwiększony, prawdopodobnie z powodu niewielkiego dodatniego potencjału powierzchniowego polimersomu.

W ostatnim etapie badań określono zdolność dendrymersomów zbudowanych z amfifilowych, triazynowo-karbokrzemowych dendronów generacji drugiej oraz trzeciej do transportu rózu bengalskiego. Dendrymersomy te są wrażliwe na zamiany pH i ulegają protonacji w środowisku kwaśnym, co prowadzi do rozluźnienia ich struktury i daje możliwość uwolnienia leku w obrębie guza.

Za pomocą badań spektrofluometrycznych stwierdzono wysoką wydajność enkapsulacji fotouczulacza w dendrymersomach. Zaobserwowano również przesunięcie długości fali emisji, co może świadczyć o dodatkowych oddziaływaniach rózu bengalskiego z dendrymersomem. Wysoki, dodatni ładunek powierzchniowy jest dodatkowym atutem tego nanoukładu w kontekście transportu dokomórkowego. Wyniki przeprowadzonej dializy równowagowej wykazały, że róż bengalski jest uwalniany znacznie wolniej z dendrymersomu trzeciej generacji w środowisku kwaśnym. Dalsze badania wykazały zwiększoną produkcję tlenu singletowego przez dendrymersom generacji trzeciej w porównaniu do wolnego leku oraz dendrymersomu generacji drugiej. Wszystkie te wyniki wskazują na występowanie silniejszych oddziaływań między różem bengalskim a dendrymersomem generacji trzeciej niż drugiej.

Za pomocą cytometrii przepływowej oraz mikroskopii konfokalnej wykazano znaczący wzrost dokomórkowego transportu rózu bengalskiego za pomocą dendrymersomów obu generacji. Efekt ten znalazł odzwierciedlenie w zwiększonej produkcji wewnątrzkomórkowych reaktywnych form tlenu, co w konsekwencji spowodowało znacznie zwiększony efekt fototoksyczny.

4.5. Podsumowanie i wnioski

Na podstawie badań przeprowadzonych w ramach niniejszej rozprawy doktorskiej można sformułować następujące obserwacje:

1. Kompleksy dendrymerów PPI z różem bengalskim wykazują zwiększony transport dokomórkowy oraz produkcję tlenu singletowego w stosunku do dendrymerów PAMAM, jednak oba rodzaje dendrymerów kationowych mogą służyć jako wydajne nośniki różu bengalskiego w terapii fotodynamicznej.
2. Modyfikacja kowalencyjna różu bengalskiego wpływa na jego właściwości fluorescencyjne, obniża produkcję tlenu singletowego oraz transport dokomórkowy powodując zmniejszenie potencjału fotodynamicznego.
3. Polimersomy zbudowane z syntetycznego blokopolimeru zdolne są do wydajnej enkapsulacji różu bengalskiego i jego uwalniania w środowisku kwaśnym. Polimersomy wydajnie transportują róż bengalski do wnętrza komórki oraz powodują zwiększoną produkcję tlenu singletowego, co w konsekwencji przekłada się na zwiększony efekt fototoksyczny.
4. Dendrymersomy zbudowane z dendronów triazynowo-karbokrzemowych generacji drugiej oraz trzeciej znacząco zwiększają transport dokomórkowy różu bengalskiego, produkcję tlenu singletowego oraz wewnątrzkomórkowych reaktywnych form tlenu, zwiększając tym samym aktywność fotodynamiczną badanego fotouczulacza.

Wnioski:

1. Przewagę wśród badanych nanonośników różu bengalskiego mają nanoukłady, które nie wymagają chemicznej modyfikacji różu bengalskiego. Optymalne w tym kontekście wydają się nanopęcherzyki zapewniające wydajny transport i wysoką, kontrolowaną stabilność.
2. Spośród przebadanych w niniejszej pracy nanoukładów, najbardziej obiecującym nośnikiem różu bengalskiego w terapii fotodynamicznej raka podstawnocomórkowego skóry jest dendrymersom, który w najwyższym stopniu zwiększał wydajność transportu dokomórkowego, co w konsekwencji przekładało się na zwiększoną aktywność fotodynamiczną.

5. Streszczenie w języku polskim

Terapia fotodynamiczna to alternatywna metoda leczenia m.in. nowotworów skóry, która w znaczący sposób ogranicza skutki uboczne dotychczas stosowanych technik takich jak radioterapia czy chemioterapia. Podstawą jej działania jest jednoczesne zastosowanie fotouczulacza, źródła światła o odpowiedniej dla substancji fotouczulającej długości fali oraz tlenu cząsteczkowego. Naświetlony lek oddziałuje z tlenem cząsteczkowym produkując reaktywne formy tlenu, które powodują śmierć komórek. Jednym z najważniejszych czynników decydujących o powodzeniu terapii jest fotouczulacz, natomiast jego efekt terapeutyczny może być ograniczony przez niską rozpuszczalność i specyficzność leku czy niewystarczającą akumulację w obrębie guza. W związku z tym trwają szeroko zakrojone badania mające na celu opracowanie nośników fotouczulaczy. Do dzisiaj zsyntezowano wiele nanoukładów, z których dendrymery, a także dendrymersomy i polimersomy zasługują na uwagę.

Głównym celem niniejszej pracy była charakterystyka czterech nanoukładów, różniących się budową oraz sposobem przenoszenia obiecującego fotouczulacza, jakim jest róż bengalski, a także ocena możliwości zastosowania tych nanoukładów w terapii fotodynamicznej.

Badania w ramach niniejszej pracy podzielone były na cztery etapy. W każdym został przebadany inny nanoukład pod kątem: (a) właściwości biofizycznych takich jak średnica hydrodynamiczna, potencjał zeta, właściwości spektralne, a także zdolność do tworzenia kompleksów lub enkapsulacji; (b) ocena generacji tlenu singletowego, produkcji wewnątrzkomórkowych reaktywnych form tlenu, transportu dokomórkowego jak i fototoksyczności. Taka dogłębna analiza pozwoliła oszacować potencjał nanoukładów w terapii fotodynamicznej raka podstawnokomórkowego skóry.

Przeprowadzone badania wykazały znaczący wpływ rodzaju oddziaływania różu bengalskiego z nanoukładem na jego potencjał fotodynamiczny. Dzięki temu porównaniu można było stwierdzić, że najwydajniejszą formą przenoszenia tego fotouczulacza jest jego enkapsulacja, która powoduje znaczące zwiększenie generacji tlenu singletowego oraz transportu dokomórkowego, co z kolei prowadzi do poprawienia końcowego efektu fototoksycznego.

6. Streszczenie w języku angielskim

Photodynamic therapy (PDT) is an alternative method for the treatment of skin cancer, which significantly reduces the side effects of commonly used techniques such as radiotherapy or chemotherapy. PDT is based on the simultaneous use of a photosensitizer, a light source of an appropriate wavelength for the photosensitizing agent, and molecular oxygen. The exposed drug interacts with molecular oxygen producing reactive oxygen species that cause cell death. One of the most important factors determining the success of the therapy is a photosensitizer. Its therapeutic effect may be limited by low solubility and specificity of the drug or insufficient accumulation within the tumor. To date, many nanosystems have been developed and synthesized, of which dendrimers as well as dendrimersomes and polymersomes deserve attention.

The main goal of the present work was to characterize four nanosystems, differing in composition and mode of transport of rose bengal, and to evaluate the applicability of these nanosystems in a photodynamic therapy.

The research was divided into four stages. In each, a different nanosystem was evaluated for: (a) biophysical properties such as hydrodynamic diameter, zeta potential, spectral properties and also the ability to form complexes with rose bengal or encapsulate rose bengal; (b) singlet oxygen generation, intracellular reactive oxygen species production, intracellular transport and phototoxic properties. Such in-depth analysis allowed us to estimate the potential of nanocarriers in photodynamic therapy of basal cell skin cancer.

The performed study showed a significant effect of the type of interaction between rose bengal and nanosystems on its photodynamic potential. Through this comparison, it can be determined that the most efficient form of transfer of this photosensitizer is its encapsulation, which results in a significant increase in singlet oxygen generation and intracellular transport, which in turn leads to an improvement in the final phototoxic effect.

7. Dorobek naukowy

7.1. Spis publikacji niewchodzących w skład rozprawy doktorskiej

1. Tomaszewska E., Ranoszek-Soliwoda K., **Sztandera K.**, Błażałek P., Głowacki R., Janaszewska A., Janasik B., Celichowski G., Wąsowicz W., Klajnert-Maculewicz B., Grobelny J. (2021). Systematic studies of gold nanoparticles functionalized with thioglucose and its cytotoxic effect. *ChemistrySelect* (6), 1230-1237 (**IF: 2,109; MEiN: 40 pkt.**)
2. **Sztandera, K.** (2021). Buffer composition affects rose bengal dialysis rate through cellulose membrane. *Acta Universitatis Lodzianis. Folia Biologica et Oecologica*, 17, 32-36. (**MEiN: 20 pkt.**)
3. **Sztandera K.**, Działak P., Marcinkowska M., Stańczyk M., Gorzkiewicz M., Janaszewska A., Klajnert-Maculewicz B. (2019). Sugar modification enhances cytotoxic activity of PAMAM-Doxorubicin conjugate in glucose-deprived MCF-7 cells—possible role of GLUT1 transporter. *Pharmaceutical Research*, 36(10), 140. (**IF: 3,242; MNiSW (stara lista czasopism): 40 pkt.**)
4. **Sztandera, K.**, Gorzkiewicz, M., Klajnert-Maculewicz, B. (2018). Gold nanoparticles in cancer treatment. *Molecular Pharmaceutics*, 16(1), 1-23. (**IF: 4,396; MNiSW (stara lista czasopism): 45 pkt.**)
5. Gorzkiewicz, M., **Sztandera, K.**, Jatczak-Pawlik, I., Zinke, R., Appelhans, D., Klajnert-Maculewicz, B., Pulaski, Ł. (2018). Terminal sugar moiety determines immunomodulatory properties of poly (propyleneimine) glycodendrimers. *Biomacromolecules*, 19(5), 1562-1572. (**IF: 5,667; MNiSW (stara lista czasopism): 45 pkt.**)

Sumaryczny współczynnik wpływu (IF) publikacji stanowiących całkowity dorobek naukowy: 49,706

7.2. Doniesienia konferencyjne

7.2.1. Wystąpienia ustne

1. **Sztandera K.**, Marcinkowska M., Gorzkiewicz M., Bątal M., Janaszewska A., Klajnert-Maculewicz B. *Nanoukłady w terapii fotodynamicznej raka podstawnocomórkowego skóry*, I Interdyscyplinarna Konferencja Doktorantów Uniwersytetu Medycznego w Łodzi, 7 listopada 2020 r., Łódź, Polska
2. **Sztandera, K.**, Działak, P., Gorzkiewicz, M. *Cytotoksyczna aktywność koniugatów PAMAM-doksorubicyna-glukoza wobec komórek nowotworowych pozbawionych źródła glukozy- rola transporterów GLUT*. VII Konferencja Biologii Molekularnej, 12-14 kwietnia 2018, Łódź, Polska

7.2.2. Plakaty

1. **Sztandera K.** *Dendrimersomes as nanocarriers for rose bengal delivery in photodynamic therapy*. Science Polish Perspectives 2021, 7-8 maja 2021 r., Zurich, Szwajcaria
2. **Sztandera K.**, Bątal M., Klajnert-Maculewicz B. *Dendrymersomy jako nośniki rózu bengalskiego w terapii fotodynamicznej*. VI Ogólnopolska Konferencja Doktorantów Nauk o Życiu Bioopen, 15-16 kwietnia 2021 r., Łódź, Polska
3. Zizzi E.A., Pallante L., Micelli M., **Sztandera K.**, Bątal M., Tuszyński J.A., Deriu M.A. *PAMAM and PPI dendrimers as potential anti-cancer drug carriers: A computational investigation*. Cancerto- nanoscience in cancer immunotherapy, 9-11 lutego 2021r., Turyn, Włochy
4. **Sztandera K.**, Marcinkowska M., Gorzkiewicz M., Janaszewska A., Majoral J.P., Klajnert-Maculewicz B. *Phosphorus dendrimers as carriers of rose bengal - a way to increase the efficiency of photodynamic therapy*. Polsko-Francuskie Forum Nauki i Innowacji, 19 listopada 2019 r., Warszawa, Polska
5. **Sztandera K.**, Milczarek M., Majkowska M., Wietrzyk J., Klajnert-Maculewicz B. *Phosphorus dendrimers as carriers for rose bengal in photodynamic therapy*. Eleventh International Dendrimer Symposium, 14-18 lipca 2019, Funchal, Madera, Portugalia
6. **Sztandera K.**, Marcinkowska M., Klajnert-Maculewicz B. *Conjugates of phosphorus dendrimers with rose bengal in photodynamic therapy of the basal cell carcinoma*. FIRST COST ACTION CA17140 Training School, 8-11 kwietnia 2019, Triest, Włochy

7. Gorzkiewicz M., **Sztandera K.** *Właściwości immunomodulacyjne glikodendrymerów poli(propylenoiminowych)*. IV Ogólnopolska Konferencja Doktorantów Nauk o Życiu Bioopen, 24-25 maja 2018 r., Łódź, Polska.

8. Janaszewska A., Gorzkiewicz M., **Sztandera K.**, Studzian M., Jatczak-Pawlik I., Pulaski L., Klajnert-Maculewicz B. *Immunomodulatory properties and drug delivery potential of PPI glycodendrimers*. European Technology Platform on Nanomedicine 2018, 28-30 maja 2018, Berlin, Niemcy

7.3. Działalność naukowa

7.3.1. Projekty

1. Projekt OPUS „Dendrymery fosforowe jako nośniki fotouczulaczy - badania in vivo”, (2017/25/B/NZ7/01304) finansowany przez Narodowe Centrum Nauki - wykonawca.

2. Projekt OPUS “Komórkowe i molekularne mechanizmy działania kompleksów dendrymerów PPI z lekami przeciwnowotworowymi – analogami nukleozydowymi” (2014/13/B/NZ3/04643) finansowany przez Narodowe Centrum Nauki – wykonawca.

3. Projekt „Wykorzystanie polimersomu jako nośnika różu bengalskiego w terapii fotodynamicznej” (B1911000002124.02) finansowany przez Uniwersytet Łódzki - kierownik.

7.3.2. Staże zagraniczne

Leibniz Institute of Polymer Research Dresden, Drezno, Niemcy (20.02-01.04.2022r.)

7.3.3. Zgłoszenie patentowe

Sztandera K., Gorzkiewicz M., Wang X., Appelhans D., Klajnert-Maculewicz B. „Sposób wytwarzania polimersomu zawierającego róż bengalski oraz jego zastosowanie w terapii fotodynamicznej raka podstawnokomórkowego skóry” zgłoszenie patentowe nr P.435870.

Kopie publikacji wchodzących w skład rozprawy doktorskiej

Nanocarriers in photodynamic therapy—in vitro and in vivo studies

Krzysztof Sztandera¹  | Michał Gorzkiewicz¹  | Barbara Klajnert-Maculewicz^{1,2} 

¹Department of General Biophysics, Faculty of Biology and Environmental Protection, University of Lodz, Lodz, Poland

²Leibniz Institute of Polymer Research Dresden, Dresden, Germany

Correspondence

Barbara Klajnert-Maculewicz, Department of General Biophysics, Faculty of Biology and Environmental Protection, University of Lodz, 141/143 Pomorska St., 90-236 Lodz, Poland.

Email: barbara.klajnert@biol.uni.lodz.pl

Funding information

National Science Centre, Poland, Grant/Award Number: UMO-2017/25/B/NZ7/01304

Abstract

Photodynamic therapy (PDT) is a minimally invasive technique which has proven to be successful in the treatment of several types of tumors. This relatively simple method exploits three inseparable elements: phototoxic compound (photosensitizer [PS]), light source, and oxygen. Upon irradiation by light with specified wavelength, PS generates reactive oxygen species, which starts the cascade of reactions leading to cell death. The positive therapeutic outcome of PDT may be limited due to several aspects, including low water solubility of PSs, hampering their effective administration and blood circulation, as well as low tumor specificity, inefficient cellular uptake and activation energies requiring prolonged illumination times. One of the promising approaches to overcome these obstacles involves the use of carrier systems modulating pharmacokinetics and pharmacodynamics of the PSs. In the present review, we summarized current in vitro and in vivo studies regarding the use of nanoparticles as potential delivery devices for PSs to enhance their cellular uptake and cytotoxic properties, and thus—the therapeutic outcome of PDT.

This article is categorized under:

Therapeutic Approaches and Drug Discovery > Emerging Technologies
Nanotechnology Approaches to Biology > Nanoscale Systems in Biology
Therapeutic Approaches and Drug Discovery > Nanomedicine for Oncologic Disease

KEYWORDS

nanocarriers, photodynamic therapy, photosensitizer, singlet oxygen

1 | MAIN ASPECTS OF ANTICANCER PHOTODYNAMIC THERAPY

Population growth, technological development, and lifestyle changes entail more frequent occurrence of civilization diseases, including cancers. Several treatment methods including chemotherapy, radiotherapy, hormone therapy, targeted therapy, and surgery are being used so far (Sztandera et al., 2019). One of the promising strategies of treatment involves photodynamic therapy (PDT), which has its roots in antiquity, when Indians were applying psoralens for repigmentation of vitiliginous skin, and Egyptians were using light to treat vitiligo, rickets, psoriasis, and even skin cancer (Abdel-Kader, 2014; Ackroyd, Kelty, Brown, & Reed, 2001; Daniell & Hill, 1991). However, these methods have been forgotten until 1900s when scientists managed to accurately describe molecular mechanisms of action of phototoxic compounds (Moan & Peng, 2003), hence enabling successful clinical application of PDT nowadays.

PDT is a minimally invasive technique which has proven to be useful for several types of tumors (Phua et al., 2019), such as esophageal cancer (Wu, Minamide, & Yano, 2019), melanoma (Nackiewicz, Kliber-Jasik, & Skonieczna, 2019), and multidrug-resistant breast cancer (Aniogo, Plackal Adimuriyil George, & Abrahamse, 2019). Moreover, it shows antibacterial potential (Oda et al., 2019), and may be successfully used in actinic keratoses, benign skin disease (Spring, Rizvi, & Hasan, 2015) or *Condyloma acuminatum* (S. Hu et al., 2019). This relatively simple technique exploits three inseparable elements: photosensitizer (PS), light source, and oxygen (Figure 1).

In the classic anticancer PDT, the PS is administered to the cancer cells and the area in which the drug is localized is exposed to the light source (Figure 2).

As a result, singlet oxygen and free radicals are generated. This process is associated with the characteristic effect of the PS, which after exposure to the specific wavelength absorbs the quantum of light and goes into an excited singlet state. Upon the absorption, the compound can emit the light (fluorescence), heat, or undergo intersystem crossing leading to excited triplet state, characterized by much longer duration (microseconds) in comparison to the singlet state (nanoseconds). This time is enough for the incidence of phosphorescence returning the PS to its basal state or the occurrence of photochemical reactions of type I or II. During the reaction of type II, the electrons are transferred from PS to molecular oxygen, resulting in the production of singlet oxygen. In the case of type I, the triplet PS directly transfers energy to molecular oxygen in the triplet state, which leads to the formation of free radicals and the oxidation of intracellular structures, causing cell death. The ratio of type I to II reactions varies and depends on the PS used, however, it is postulated that the type II reaction is the basis of PDT (Abrahamse & Hamblin, 2016; MacDonald & Dougherty, 2001; Nishiyama, Morimoto, Jang, & Kataoka, 2009). The process of light absorption together with the following reactions is demonstrated in Figure 3.

These reactions lead to direct cytotoxic effects on tumor (Dabrzalska et al., 2017; Vandenberghe et al., 1997), damage to the tumor vasculature (Chen, Pogue, Hoopes, & Hasan, 2012), or induction of robust inflammatory responses (Castano, Mroz, Wu, & Hamblin, 2008), leading ultimately to cell death. Three main mechanisms of cell death may be triggered (Mroz, Yaroslavsky, Kharkwal, & Hamblin, 2011; Plaetzer, Kiesslich, Verwanger, & Krammer, 2003) (Figure 4). Usually the advantage of one of them is observed.

The best anticancer outcome is achieved through the regulated and highly controlled mechanism of cell death—apoptosis. The apoptosis pathway triggered by PDT has been very well presented and described in 1991 by the Oleinick's group (Agarwal et al., 1991). In this process, chromatin condensation, DNA fragmentation, and the formation of apoptotic bodies

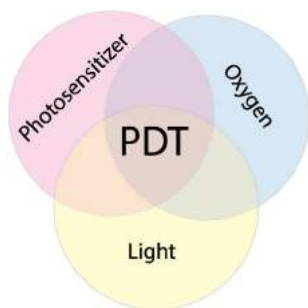


FIGURE 1 Three inseparable elements of photodynamic therapy

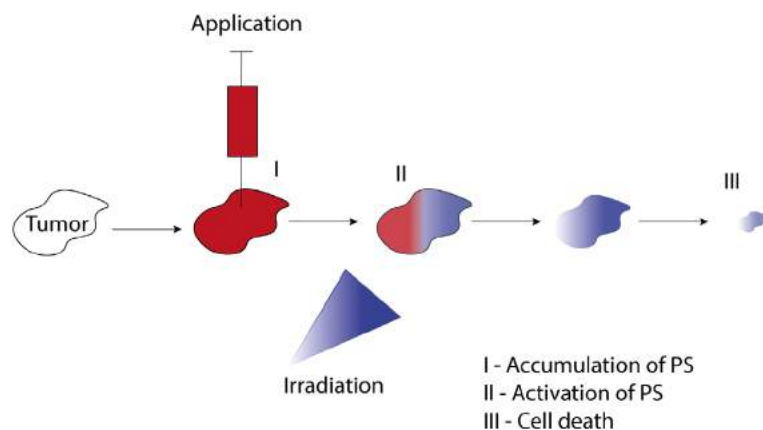


FIGURE 2 The mechanism of photodynamic therapy

FIGURE 3 The scheme of photosensitizer activation

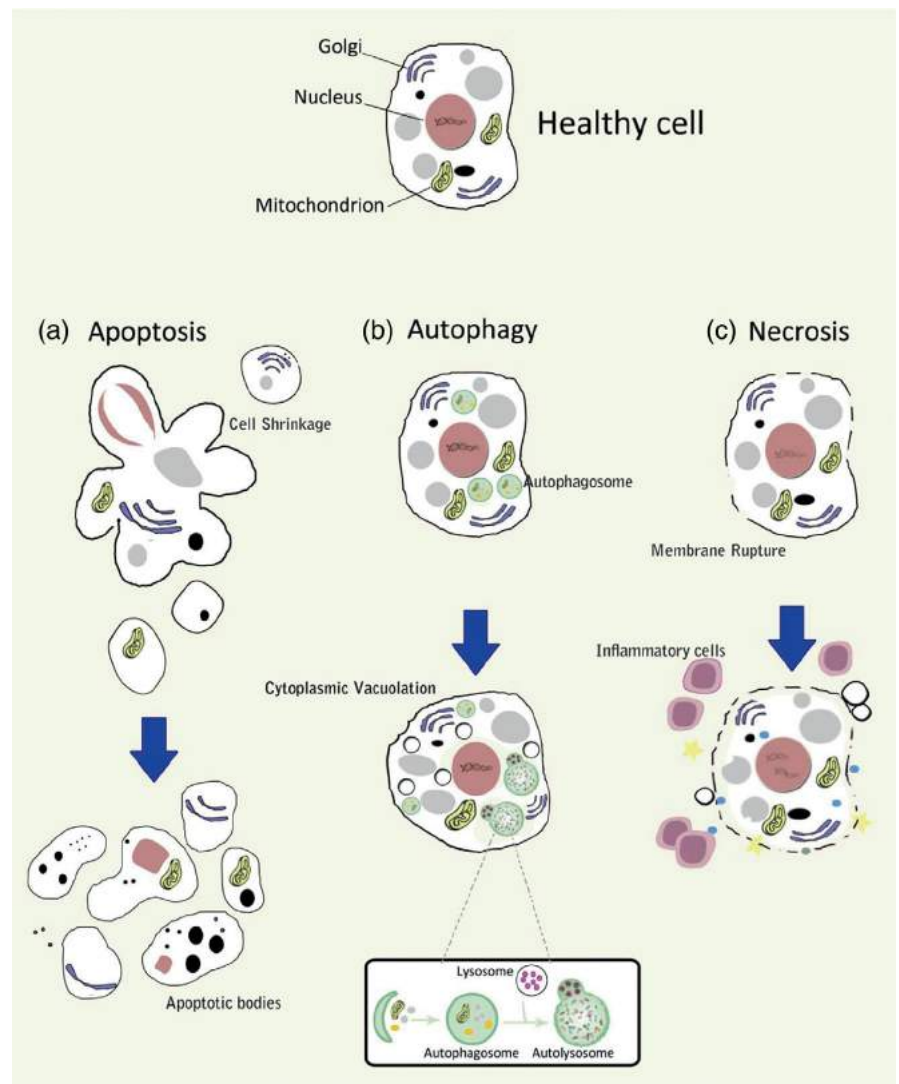
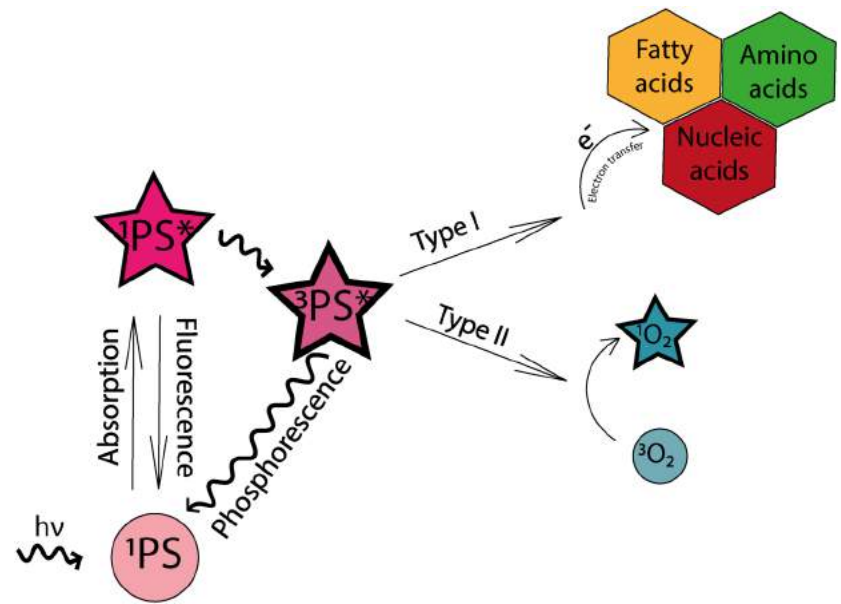


FIGURE 4 Possible pathways of cell death induced during photodynamic therapy. (Reprinted with permission from Carella, Feist, Bignell, and De Vico (2015). Copyright 2019 with permission of Elsevier)

are observed, with the latter being subsequently removed by phagocytes. Numerous novel drugs are developed to interact with cancer cells and specifically trigger apoptotic pathways (C. Lin et al., 2019; Nackiewicz et al., 2019; Qi et al., 2019; Xu et al., 2019). Ali and Olivo showed that the uptake and localization of PS as well as its cellular concentration and light fluence have an impact on induction of apoptosis (Ali & Olivo, 2002). Noteworthy, this mechanism does not lead to the emergence of side effects associated with the other types of cell death, including necrosis. This process is fast, leading to the rapid destruction of cellular organelles and, as a consequence, inflammation (Kim-Campbell, Gomez, & Bayir, 2019). The third possible way of cell death induced by PDT, autophagy (Buytaert, Dewaele, & Agostinis, 2007; Kessel & Oleinick, 2010; Martins et al., 2019), is postulated as the second type of programmed cell death due to its nature (Napoletano, Baron, Vandenabeele, Mollereau, & Fanto, 2019; Yu, Lenardo, & Baehrecke, 2004). Autophagy is based on the closing of the cytoplasm and organelles in autophagosomes, which subsequently combine with lysosomes and their content is degraded. Since this process, similarly to apoptosis, is highly controlled, it is also a desirable way of cell death in PDT (Kessel, Vicente, & Reiners, 2006).

For the development of efficient PDT for the particular type of cancer, it is crucial to select proper PS and light source. PSs are generally divided into several main groups: derivatives of porphyrins (Gomes, Neves, & Cavaleiro, 2018), chlorins (Garcez et al., 2007), or phthalocyanines (Amin, Hauser, Kinzler, Rueck, & Scalfi-Happ, 2012). Each of these groups is characterized by different photophysical properties, primarily with regards to the excitation wavelengths (De Rosa & Bentley, 2000) and the activation of specific cell death mechanisms (Foster et al., 2011). This diversity of PSs and their activities is a huge advantage for the development of successful anticancer therapy. However, the maximum absorption of a potential PS should be in the range between 650 and 850 nm (so-called "therapeutic window"), in which the light has the optimal energy to penetrate tissues and activate PS for reactive oxygen species (ROS) production (Plaetzer, Krammer, Berlanda, Berr, & Kiesslich, 2009). At the same time, PS cannot show any "dark toxicity" in the absence of a light source, exhibit mutagenic properties or cause allergic reactions that could significantly limit the use of PDT.

As for the light source, one of its crucial features involves the ability to generate polarized light with a specific wavelength due to the characteristic of PSs. Nowadays many types of light sources are in use or under development, for example, argon/dye lasers, metal vapor lasers, KTP:YAG/dye lasers, or light-emitting diode (LED) lasers. The second group of light sources includes so-called nonlaser sources in which the light beam can be controlled electronically (Mang, 2004) or by the application of specific filters (Dabrzalska et al., 2017). However, most of the above-mentioned light sources have a serious disadvantage: they are large, which makes them suitable only for external illumination. Fortunately, modern technology enables the use of optical fibers (Mortier et al., 2014), which are much smaller and already widely used in other therapies. Due to their size, it is possible to bring light even to small blood vessels. This technology opens the gate for PDT and its use in the treatment of cancers found in different locations of the body.

2 | PDT—COULD IT BE ANY BETTER?

The advantages of PDT over different types of anticancer chemotherapy undoubtedly include its specificity. Due to the use of PS and an accurate source of light, it is possible to trigger reactions only in a specific place and time. A large number of available compounds exhibiting phototoxic properties enables the choice of proper treatment strategy (Dykman & Khlebtsov, 2011; Robertson, Evans, & Abrahamse, 2009).

However, despite the large number of studies and great effort put in the development and optimization of effective anticancer PDT, in most cases, the positive therapeutic outcome is limited due to several aspects. PSs are usually hydrophobic molecules, which greatly affects their solubility, hampering efficient administration and blood circulation, as well as favorable biodistribution and cellular uptake (Dabrzalska, Zablocka, Mignani, Majoral, & Klajnert-Maculewicz, 2015). Disadvantageous distribution of the PS in the organism may result in long-lasting skin sensitivity to light, forcing patients to stay in subdued light for a significant periods of time (Plaetzer et al., 2009). Further, upon administration, PSs may be subjected to rapid degradation or removal from the organism by the cells of reticuloendothelial system (RES) (Kakde, Jain, Shrivastava, Kakde, & Patil, 2011). Their anticancer activity may be also reduced due to the low tumor specificity and activation energies requiring prolonged illumination times.

3 | NANOTECHNOLOGY FOR ENHANCED EFFICIENCY OF PDT

One of the promising approaches to overcome above-mentioned obstacles involves the use of carrier systems which will increase the solubility of the drugs, protect them from degradation, and provide efficient transport directly to the cancer cells.

TABLE 1 Examples of nanoparticles most suited for drug delivery in photodynamic therapy

| Nanocarrier | Description |
|--|---|
| Liposomes (Allen & Cullis, 2013; Sercombe et al., 2015) | <p>Closed bilayer phospholipid systems, the first nanomedicine delivery vehicles applied clinically. Since they are mimicking natural biological structures, they are nontoxic and highly biocompatible. A liposome has an aqueous solution core surrounded by a hydrophobic membrane composed of lipid bilayer, making them fine candidates for the delivery of both hydrophobic and hydrophilic drugs. Hydrophilic compounds may be entrapped inside the liposome core, while hydrophobic ones associate with the bilayer. The lipid bilayer may fuse with cellular membranes, thus delivering the liposome contents intracellularly. However, this process is complex and may not be spontaneous. Therefore, liposomes are designed to provide triggered release of their content.</p> <p>Their disadvantages include low stability in the biological environment and rapid clearance from the organism. The latter may be overcome with suitable surface modifications, which may additionally ensure targeted delivery.</p> |
| Dendrimers Gorzkiewicz & Klajnert-Maculewicz, 2018; Klajnert, Rozanek, & Bryszewska, 2012) | <p>Highly branched, monodisperse, polyvalent polymers of well-defined, regular, usually spherical structure, which enables the transport of therapeutics either physically entrapped inside the dendritic scaffold or bound to the terminal groups (either covalently or noncovalently). In case of PDT, since photosensitizers do not always have to be released from the nanocarrier, the incorporation of the drug into the internal branches or the core of the dendrimer is also possible. Dendrimers are characterized by high solubility, biopermeability, and high loading capacity. Unfortunately, the use of dendrimers in PDT may be limited due to the reduction of phototoxic properties of the drug caused by the interactions with the polymer. Moreover, cationic dendrimers are featured with significant cytotoxicity, which can be nullified by surface modification of these macromolecules with neutral moieties, additionally providing targeting properties.</p> |
| Gold and silver nanoparticles (AuNPs and AgNPs) (Austin, MacKey, Dreaden, & El-Sayed, 2014; Sztandera, Gorzkiewicz, & Klajnert-Maculewicz, 2019) | <p>Gold/silver nanoparticles are the particles of gold/silver with the size usually between 1 and 100 nm. They have been studied for the drug delivery potential mainly due to their ability to form stable complexes with active compounds and possibility of covalent bonding with therapeutics and targeting molecules.</p> <p>A wide range of possible synthesis methods allows obtaining nanogold and nanosilver particles with specific architecture and characteristics, depending on the intended use. AuNPs and AgNPs have been shown to exhibit size- and shape-dependent biodistribution and cellular uptake. As for their toxicity, the data remain inconsistent, indicating either lack of toxicity or cell type-specific cytotoxic activity.</p> <p>High reactivity and surface area enable their further modifications and functionalization, improving bioavailability and targeting potential. Moreover, gold and silver nanoparticles show significant diagnostic potential due to their tunable optical and physicochemical properties, which distinguish them from other nanoparticles.</p> |
| Metal oxide nanoparticles (Falcaro et al., 2016; Fikai, Oprea, Fikai, & Holban, 2016) | <p>The class of inorganic-based particles with metal oxide core (e.g., ZnO, Fe₃O₄), which may be additionally coated by either inorganic (e.g., silica, gold) or organic materials (phospholipids, polysaccharides, peptides, and surfactants). Although primarily used for visualization techniques (such as magnetic resonance imaging, MRI) due to their paramagnetic properties, they may be used as drug delivery vehicles, providing high loading capacity and controlled release. Based on their inducible magnetization, they can be directed to a defined location and applied for magnetically assisted transfection of cells. They have been shown to be nontoxic and highly biocompatible.</p> |
| Mesoporous silica nanoparticles (Bharti, Gulati, Nagaich, & Pal, 2015; Kwon et al., 2013) | <p>The mesoporous structure of silica allows effective drug loading, homogenous distribution of guest molecules in porous space, and controlled release of therapeutics at their site of action. The characteristics of such nanostructures, including pore size and level of porosity can be altered depending on the application. Additionally, active surface with high area enables functionalization providing targeting properties and stable covalent bonding of the drug molecules.</p> <p>Biodegradable mesoporous silica nanoparticles possess favorable chemical properties, thermal stability, and biocompatibility. They can provide efficient intracellular transport of the drugs and increased solubility of water-insoluble molecules.</p> <p>The major disadvantage of silica nanoparticles is associated with the surface density of silanol groups interacting with phospholipids of cellular membranes, causing, for example, hemolysis.</p> |

(Continues)

TABLE 1 (Continued)

| Nanocarrier | Description |
|---|---|
| | Prolonged retention of silica in the organism may also lead to metabolic changes, and in extreme cases—carcinogenesis. |
| Chitosan (Bernkop-Schnürch & Dünnhaupt, 2012; J. J. Wang et al., 2011) | Chitosan is a natural biopolymer, a linear polysaccharide composed of β -(1 \rightarrow 4)-linked, deacetylated D-glucosamine and acetylated N-acetyl-D-glucosamine. Physicochemical properties of this polymer depend mainly on its molecular weight and degree of acetylation/deacetylation. Chitosan nanoparticles may serve as safe drug carriers due to their good biocompatibility and biodegradability. On the industrial scale, they may be prepared by three techniques (ionic gelation, precipitation with tripolyphosphate, or crosslinking using glutaraldehyde). The choice of appropriate method allows to modify the drug loading efficiency and particle size. It also enables the introduction of modifications to change the polymer's properties. Hydrophilic chitosan nanoparticles have been shown to provide improved solubility and stability, sustained release, and efficient transport of both hydrophilic and hydrophobic drugs across various biological barriers in vivo, including blood–brain barrier. Moreover, chitosan itself shows certain antitumor activity, which may offer additive or synergistic effect with PDT. |
| Polymeric nanoparticles (Andrieux, Nicolas, Moine, & Barratt, 2013; El-Say & El-Sawy, 2017) | These nanoparticles possess favorable characteristics in terms of simple design and preparation, good stability in suspension, good biocompatibility, and a great variety of possible structures enabling bioimitative performance. Due to the well-optimized methods of synthesis, it is possible to efficiently control their superficial features and particle size, adjust solubility, enhance elasticity, and modify drug loading capacity and release patterns. Polymeric nanoparticles have been shown to increase solubility, modulate biodistribution, and prolong blood circulation times of therapeutics. However, since these particles are not natural compounds commonly found in the organism, they may exhibit toxic and immunogenic properties. Moreover, it is difficult to scale up the process of production and to completely remove toxic organic solvents used during the synthesis. |

For this purpose, drug delivery systems must hold an adequate amount of the therapeutic and remove problems such as disadvantageous biodistribution or rapid clearance from the organism. The delivery systems should ensure prolonged blood circulation, accumulation in the tumor area, and efficient uptake of the drugs by cancer cells (Kakde et al., 2011). In the latest clinical applications, lipidic or organic formulations of PSs are being used in order to meet these requirements. However, such compounds may be responsible for unpredictable biodistribution patterns, allergic reactions, hypersensitivity, and systemic toxicity (Master, Livingston, & Sen Gupta, 2013). Thus, the attention of scientists turned to the solutions from the area of nanoscience and nanotechnology. Considering an exceptional growth of research and applications in these fields in the past few decades, it is believed that the introduction of nanoparticles in medicine will improve the diagnosis and treatment of many diseases. Nowadays several nanosized compounds are under investigation for drug delivery, particularly for cancer therapy (A. Z. Wang, Langer, & Farokhzad, 2012).

Nanotechnology is commonly defined as the development of functional systems on the molecular level. Regarding biological and medical aspects, nanotechnology concerns compounds with the structure and function relevant for small sizes (from nanometers to micrometers), similar to those of most fundamental biological macromolecules and cells. At this level, the features, responsible for the specific phenomena in both artificial systems and living organisms, are determined just above the scale of a single atom (Sztandera, Gorzkiewicz, & Klajnert-Maculewicz, 2019). Therefore, nanomaterials with defined properties can be useful for biomedical research and applications both in vivo and in vitro, effectively interacting with cellular components or mimicking various chemical and biological compounds. Bionanotechnology may contribute to the elaboration of diagnostic tools, contrast and drug delivery agents, or drugs per se.

Due to the highly optimized methods of synthesis, it is possible to obtain nanoscale particles with precisely defined features, characterized by monodispersity, high biocompatibility, controllable biodistribution patterns, and specific mechanisms of interaction with biological targets, making them potentially finest tools for modern medicine (I. Y. Wong, Bhatia, & Toner, 2013). Currently there is a growing interest in the production of biodegradable nanomaterials, which would ensure their safe administration and eliminate possible adverse effects associated with prolonged circulation of nanoparticles in the bloodstream.

In case of drug delivery applications, nanoparticles have been shown to protect the drugs from degradation, improve their solubility, prolong blood half-life and modulate pharmacokinetic properties, as well as to provide the targeted delivery and controlled drug release (Bertrand, Wu, Xu, Kamaly, & Farokhzad, 2014). What is more, it has been found that nanoparticles

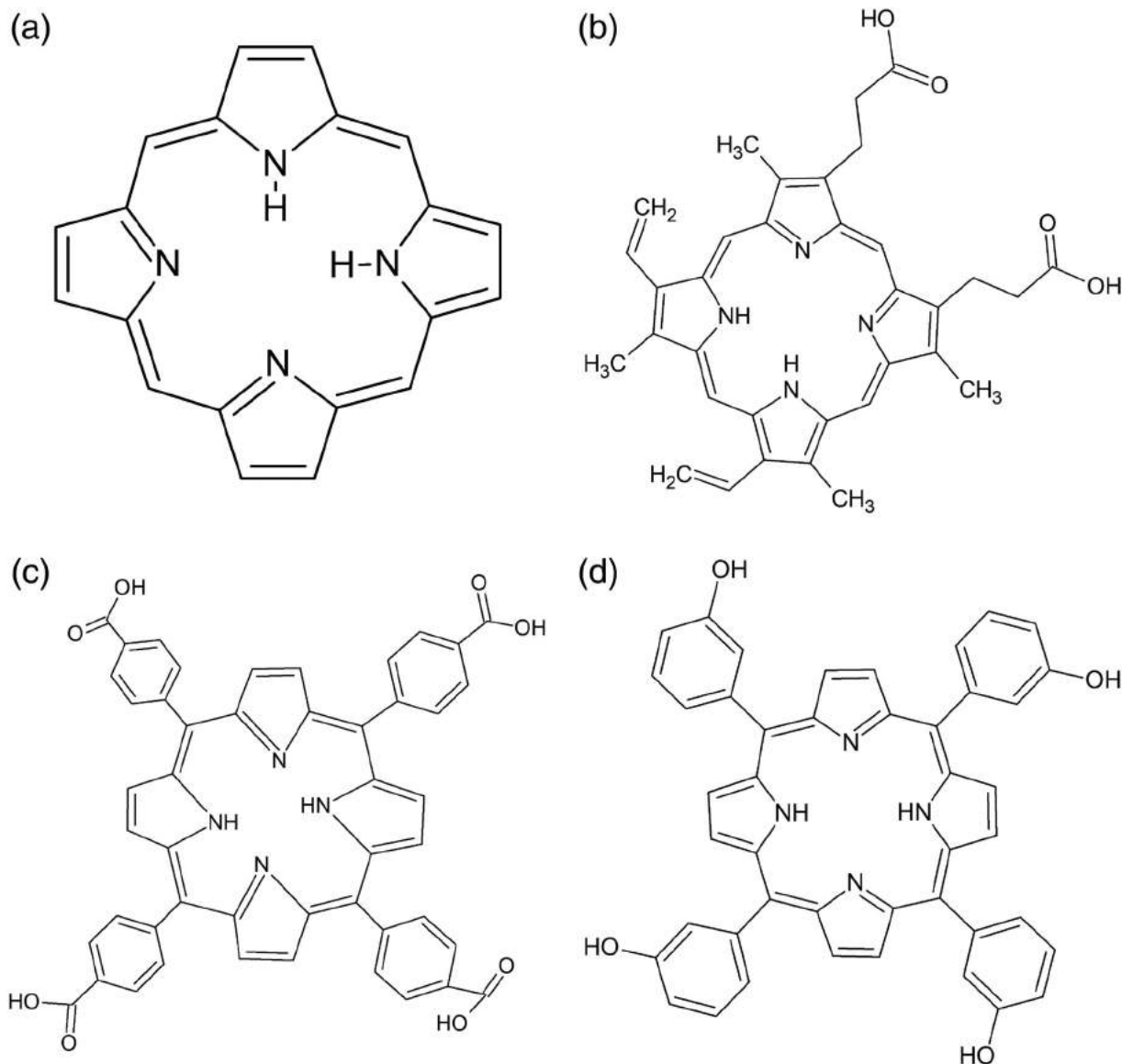


FIGURE 5 The structure of: (a) porphyrin, (b) protoporphyrin IX, (c) mesotetra (carboxyphenyl) porphyrin (TCPP), and (d) 5,10,15,20-Tetrakis(3-hydroxyphenyl) porphyrin (mTHPP)

can accumulate in tumors by passive retention mechanism (so-called enhanced permeability and retention effect, EPR), due to the irregular epithelium, decreased interstitial fluid uptake, and weakened lymphatic drainage of tumor vasculature (Bertrand et al., 2014; H. Li, Jin, Wan, Wu, & Wei, 2018). The possibility of conjugation of nanoparticles with targeting moieties such as peptides, antibodies, carbohydrates, or folic acid can further enhance specific transport of the drugs to their sites of action (Friedman, Claypool, & Liu, 2013). All these features make the drug delivery nanosystems a promising alternative to traditional PDT, enabling the modification of its critical steps, particularly PS transport, location, and intensity of the photodynamic reaction.

Drug molecules may be bound with the nanocarrier in several ways—either encapsulated inside the nanoparticles, conjugated or physically complexed on their surface, or incorporated into their structure. The nanocarrier should provide efficient transport of the therapeutic without its significant loss before reaching the target area. Thus, the physical entrapment of the drug molecules within the vehicle core or covalent bonding may have an advantage over the adsorption of the therapeutic on the surface of the nanoparticle. The latter option is usually based on noncovalent interactions, which may be responsible for premature release of the therapeutic. The drug-nanoparticle binding should be optimized to ensure the protection of the active compound in the bloodstream and its specific release inside the target cells, as it may significantly affect the cytotoxic effect. In the case of PDT, however, the release of the PS from nanocarrier may not be necessary, since the nanoparticle does not

TABLE 2 In vivo and in vitro experiments on porphyrins and porphyrin derivatives as photosensitizer agents in photodynamic therapy. The in vivo studies are italicized

| Photosensitizer | Nanoparticle | Outcome | In vitro | In vivo |
|-------------------|--|--|--|---|
| Photofrin | F3-targeted polymeric nanoparticles | <ul style="list-style-type: none"> High rate of cellular uptake of nanoparticles Significant improvement in survival rate (MDA-MB-435 cell line—breast cancer, rat 9 L gliomas) | (Reddy et al., 2006) | |
| | Nanoporous zinc oxide | <ul style="list-style-type: none"> Enhanced ROS generation Enhanced cytotoxic effect (A549 cell line—lung cancer) | (Fakhar-E-Alam et al., 2012) | |
| | Liposomes | <ul style="list-style-type: none"> Higher phototoxic effect of liposomal photofrin compared to free drug (Athymic, nude rats, strain Cr: NIH-ma with U97 cells) | | (Jiang et al., 1998) |
| Protoporphyrin IX | Gold nanoparticles | <ul style="list-style-type: none"> Increased cytotoxic effect of conjugates (HeLa cell line—cervical cancer) | (Savarimuthu, Gananathan, Rao, Manickam, & Singaravelu, 2014) | |
| | | <ul style="list-style-type: none"> Enhanced apoptosis (HeLa cell line—cervical cancer) | (Juárez, Alvarado, & Gallegos, 2019) | |
| | | <ul style="list-style-type: none"> Enhanced singlet oxygen generation (male neonate National Medical Research Institute [NMRI] mice) | (Ashjari, Dehfily, Fatehi, Shabani, & Koruji, 2015) | |
| | Polyethylenimine nanoparticles | <ul style="list-style-type: none"> Ability to generate singlet oxygen after irradiation with light of 635 nm wavelength | (Ning et al., 2019) | |
| | Carbon dots | <ul style="list-style-type: none"> Enhanced singlet oxygen generation Additional bioluminescence effect Increased phototoxic effect (MMC-7721 cell line—hepatocellular carcinoma) | (Yang et al., 2019) | |
| | | Silver core silica shell nanoparticles | <ul style="list-style-type: none"> Enhanced singlet oxygen generation (U251MG cell line—glioblastoma astrocytoma, HepG2 cell line—hepatocellular carcinoma) | (Lismont, Dreesen, Heinrichs, & Páez, 2016) |
| | Polymersomes | <ul style="list-style-type: none"> Increased cytotoxic effect Selective cytotoxic effect on melanoma cells (A375 cell line—malignant melanoma) | (M. Wang, Geilich, Keidar, & Webster, 2017) | |
| | Poly(ethylene glycol)—polycaprolactone (PEG-PCL) micelles | <ul style="list-style-type: none"> Synergistic activity with erlotinib (MDA-MB-231 cell line—breast cancer) | (L. Yan et al., 2017) | |
| Magnetoliposomes | <ul style="list-style-type: none"> Increased cytotoxic effect (MCF-7 cell line—breast cancer) | (Basoglu, Bilgin, & Demir, 2016) | | |

(Continues)

TABLE 2 (Continued)

| Photosensitizer | Nanoparticle | Outcome | In vitro | In vivo |
|---|--|--|--|---------|
| | Mucin 1-targeted ZnSe/ZnS quantum dots | <ul style="list-style-type: none"> • Selective activity toward cancer cells (HeLa cell line—cervical cancer, RAW cell line—murine macrophages) | (Singh et al., 2016) | |
| Mesotetra (carboxyphenyl) porphyrin (TCPP) | Poly(lactic-co-glycolic acid) (PLGA) nanoparticles | <ul style="list-style-type: none"> • Rapid cellular uptake • Clathrin-dependent endocytosis • High phototoxic effect • <i>Significant tumor-inhibiting efficacy</i> (SW480, HT-29 and LS174T cell lines—colorectal adenocarcinoma, J774 cell line—murine macrophages, <i>athymic mice (athymic nu/nu-)</i>) | (Z. Hu et al., 2009) | |
| 5,10,15,20-Tetrakis (3-hydroxyphenyl) porphyrin (mTHPP) | N-sulfonato-N,O-carboxymethyl chitosan | <ul style="list-style-type: none"> • High efficacy of drug loading • Increased cellular uptake • Increased cytotoxic effect (14C cell line) | (Reza Saboktakin, Tabatabaie, Maharramov, & Ali Ramazanov, 2011) | |
| | Micelles | <ul style="list-style-type: none"> • High loading capacity • Increased phototoxic effect • Low dark cytotoxicity • Increasing intracellular fluorescence (HN5 cell line—head and neck cancer, H2009 cell line—lung cancer) | (Ding, Mora, Gao, & Sumer, 2011) | |

constitute an obstacle for the interaction of the drug with oxygen and generation of ROS, which favors for example the creation of permanent, not-cleavable covalent bondings. Nevertheless, it should be noted that complexation or covalent conjugation of PS with nanocarrier may significantly alter the physicochemical properties of the drug, affecting its phototoxic capacity. Further, although for the standard chemotherapeutics higher drug loading usually translates to enhanced therapeutic outcome, high concentrations of PS may result in self-quenching effect and reduction of phototoxic activity. Thus, it is crucial to find the right balance between the PS loading and photodynamic action of obtained nanoformulation, as well as to comprehensively characterize the novel delivery device upon drug binding before commencing biological research stage (Master et al., 2013).

All these aspects should be considered upon the design of the specific nanocarrier system in order to fully exploit its therapeutic potential and to address challenges of treatment associated with particular clinical target.

So far, a number of nanoparticles have been tested for the potential of the delivery of PSs, the enhancement of their cellular uptake and cytotoxic properties both in vitro and in vivo. The variety of nanosystems gives a huge range of possibilities to develop a specific drug delivery system that would contribute to the circumvention of various limitations of PDT. The most promising nanocarriers of PSs have been briefly described in the Table 1 to outline the topic for the readers and allow them to choose the solution most suited to their purpose.

4 | NANOCARRIERS FOR PHOTSENSITIZERS—IN VITRO AND IN VIVO STUDIES

As mentioned before, PS is one of three inseparable PDT components, which determines all settings such as the time of incubation, light wavelength, light dose, and molecular response of cells to the therapy. To date, many compounds have been tested both in vitro and in vivo for the application in PDT. Comprehensive understanding of the molecular mechanism of a

PS's action, the efficiency of singlet oxygen generation, the cellular uptake and affinity for cell structures as well as the predominant type of triggered cell death is crucial for the development of an effective method of cancer treatment. Well characterized compound may proceed to *in vivo* tests where the parameters such as pharmacokinetics, pharmacodynamics, and biodistribution are examined (Gorzkiwicz, Buczkowski, Pałecz, & Klajnert-Maculewicz, 2019).

4.1 | Porphyrins

Porphyrins (Figure 5) constitute a class of compounds most commonly used as PSs (X. Li, Xiao, Guo, Xiao, & Xiao, 2019). These include macrocyclic molecules with various physicochemical properties such as anion binding, stabilization of metals with unusual oxidation states, electron transfer, and formation of infrequent supramolecular assemblies that enable their use in PDT (Ivanov & Boldyrev, 2014). In nature, they play crucial roles in photosynthesis, oxygen transport, biological oxidation, and reduction reactions (Gouterman, 1961). As positively charged molecules, these compounds are well soluble (Huang, Song, Rieffel, & Lovell, 2015), exhibit high affinity for cell structures (including negatively charged DNA and RNA), and the capacity for production of singlet oxygen in contrast to their negatively charged or neutral analogs (Carneiro et al., 2018). Their first application in modern PDT has been reported in 1913, and the first drug of this class of PSs (Photofrin) has been approved in Canada in 1993 (Dolmans, Fukumura, & Jain, 2003). Most porphyrins are activated in the 400 nm range *in vitro*, and 630 nm *in vivo* due to the presence of several Q-bands (Abrahamse & Hamblin, 2016). Table 2 shows the type of porphyrin used as PS in PDT and the nanoparticle which it is combined with.

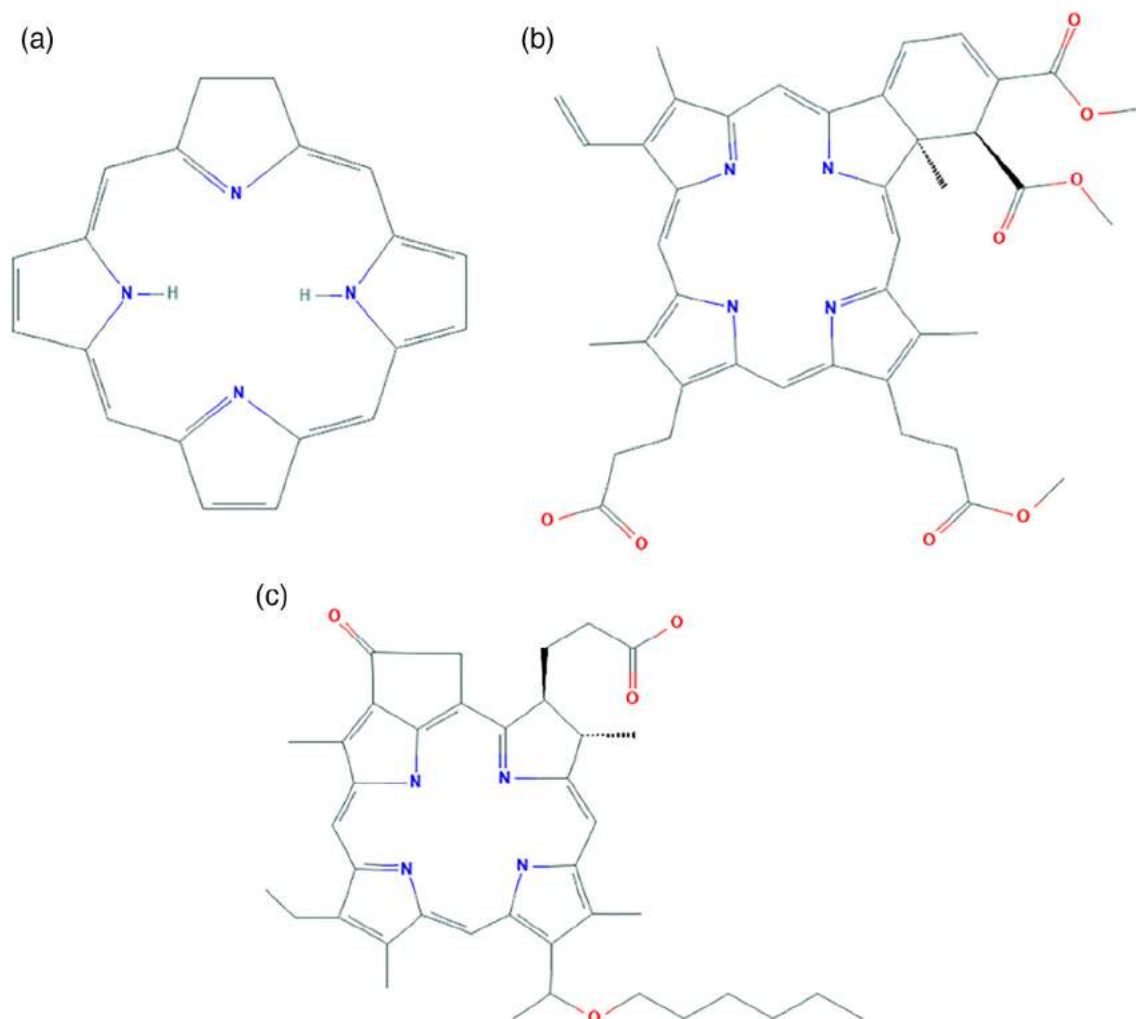


FIGURE 6 The structure of (a) chlorin, (b) verteporfin, and (c) 2-[1-hexyloxyethyl]-2-devinyl pyropheophorbide-a (HPPH)

TABLE 3 In vivo and in vitro experiments on chlorins and chlorin derivatives as photosensitizer agents in photodynamic therapy. The in vivo studies are italicized

| Photosensitizer | Nanoparticle | Outcome | In vitro | In vivo |
|--|--|--|---|---------|
| Chlorin e6 (Ce6) | Lipidots | <ul style="list-style-type: none"> Decreased dark toxicity Preserved phototoxicity (CAL-33 cell line—tongue squamous cell carcinoma) | (Hinger et al., 2016) | |
| | Superparamagnetic iron oxide nanoparticle (SPION) nanoclusters | <ul style="list-style-type: none"> High water solubility Preserved generation of singlet oxygen <i>Significant delay in tumor growth</i> (4T1 cell line—murine breast cancer, <i>athymic nude female mice bearing 4T1</i>) | (Amirshaghghi et al., 2019) | |
| | Methoxy-poly(ethylene glycol)-poly(D,L-lactide) (mPEG-PLA-Ce6) | <ul style="list-style-type: none"> Enhanced singlet oxygen generation Increased cellular internalization (A549 cell line—lung cancer, monolayer and 3D spheroids) | (Kumari, Rompicharla, Bhatt, Ghosh, & Biswas, 2019) | |
| | Mesoporous silica nanoparticles | <ul style="list-style-type: none"> Efficient cellular uptake Enhanced intercellular ROS production (A549R cell line—cisplatin-resistant lung cancer) | (W. Zhang et al., 2016) | |
| | Hyperbranched poly(ether-ester) | <ul style="list-style-type: none"> Enhanced phototoxicity compared to free Ce6 (CAL-27 cell line—oral tongue cancer) | (P. Li et al., 2012) | |
| | Hollow mesoporous silica nanoparticles | <ul style="list-style-type: none"> Dose-dependent cell death <i>Inhibition of tumor growth</i> (4T1 cell line—murine breast cancer, <i>4T1 tumors in Balb/c mice</i>) | (Kamkaew et al., 2016) | |
| | Hydrophobically-modified glycol chitosan nanoparticles | <ul style="list-style-type: none"> Similar size of Ce6-loaded glycol chitosan nanoparticles (HGC-Ce6) and Ce6-conjugated chitosan nanoparticles (GC-Ce6) Similar singlet oxygen generation Rapid cellular uptake profile in case of both nanoparticles <i>Enhanced drug release (HGC-Ce6)</i> <i>Prolonged circulation profile and more efficient tumor accumulation in mice (GC-Ce6)</i> (SCC-7 cell line—squamous cell carcinoma, <i>athymic nude mice</i>) | (Lee et al., 2011) | |
| | Matrix metalloproteinase 2-cleavable polypeptide | <ul style="list-style-type: none"> <i>Enhanced targeting ability</i> <i>Increasing PDT efficacy</i> (A549 tumor-bearing mice) | (Hou et al., 2016) | |
| Verteporfin | Poly(D,L-lactide-co-glycolide) | <ul style="list-style-type: none"> Size-dependent toxicity Increased phototoxic effect in case of smaller nanoparticles <i>Effectively controlled tumor growth by verteporfin-loaded small nanoparticles</i> (EMT-6 cell line—murine breast cancer, <i>female SKH1 hairless mice</i>) | (Koman-Kouakou, Boch, Gurny, & Allémann, 2005) | |
| 2-[1-hexyloxyethyl]-2-devinylpyropheophorbide-a (HPPH) | Functionalized polyacrylamide (AFPAA) | <ul style="list-style-type: none"> Efficient encapsulation, post-loading or conjugation of HPPH The highest phototoxicity and singlet oxygen production for post-loaded form No dark toxicity observed <i>Tumor localization in a mouse colon carcinoma model</i> (PC-3 cell line—prostate cancer, MDA-MB-435S cell line—melanoma, <i>U87MG human glioblastoma—bearing mice</i>) | (Wang et al., 2011) | |

4.2 | Chlorins

Another class of compounds widely used in PDT includes chlorins (Figure 6), derivatives of chlorophyll commonly found in *Spirulina* species. Chemically, they are reduced porphyrins showing improved absorption properties (Spikes & Bommer, 1993), which may be further altered by chelated metal ions (Spikes, 1990). Depending on the structure, they are activated by light with a wavelength of 650–700 nm.

Some of them are already available commercially (e.g., Foscan[®], Verteporfin[®], Bremachlorin[®]) (Abrahamse & Hamblin, 2016), however, several synthetic chlorins such as mesotetrakis (m-hydroxyphenyl) chlorin (m-THPC) or benzoporphyrin derivative BPDMA (Calixto et al., 2016) are still under development. Others are subjected to in vitro and in vivo tests as well as to nanotechnology modifications as presented in Table 3.

4.3 | Phthalocyanines

Initially, due to their properties such as thermal stability, intense color, or high inertness, they were used in the industry as dyes since 1928. Later, their application was extended to other fields such as electronics, photovoltaics, electrophotography, electrocatalysis, or PDT. In PDT, they work as PSs due to their high absorption in the 670–700 nm range, the field of red visible light, which enables deep penetration of tissues, high singlet oxygen generation, and high photostability (R. C. H. Wong, Lo, & Ng, 2019). Moreover, phthalocyanines (Figure 7) possess the ability to coordinate metal ions within their core, which offers numerous options to control or change their physical properties by synthetic modifications. The application of nanotechnology to increase the phototoxic properties of these compounds involves primarily the enhancement of singlet oxygen quantum yield and varied intracellular delivery, since phthalocyanines accumulate mainly in mitochondria (R. C. H. Wong et al., 2019) (Table 4).

4.4 | Synthetic dyes

4.4.1 | Rose bengal

Synthetic dyes constitute the third class of PS agents used in PDT, however, most of them are still underdeveloped. Among these compounds, rose bengal (4,5,6,7-tetrachloro-2',4',5',7'-tetraiodofluorescein, RB) (Figure 8) is the most commonly used both as anticancer and antimicrobial agent, being tested alone as well as in complexes or conjugates with nanoparticles (summarized in Table 5). Rose bengal exhibits strong fluorescence after excitation with light at 520 nm. However, its applicability may be limited due to the hydrophilic nature of RB, leading to its poor cellular uptake (Gianotti et al., 2014). Thus, the main advantage of nanotechnology in this case is based on increased transmembrane transport of the drug.

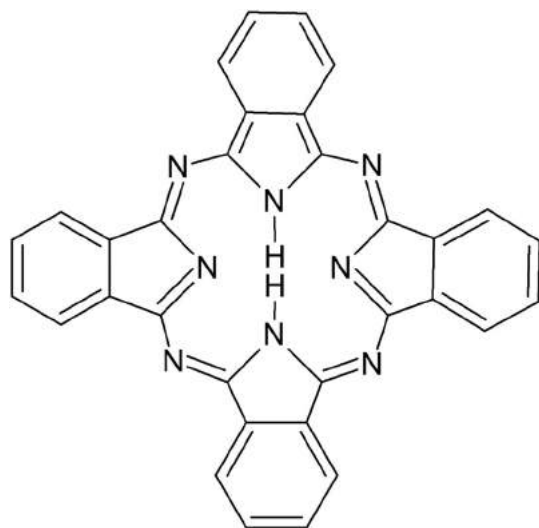


FIGURE 7 The structure of phthalocyanine

TABLE 4 In vivo and in vitro experiments on phthalocyanines as photosensitizer agents in photodynamic therapy. The in vivo studies are italicized

| Nanoparticle | Outcome | In vitro | In vivo |
|---|---|-------------------------------------|------------------------|
| Gold nanoparticles | <ul style="list-style-type: none"> • <i>Biocompatible carrier</i> • <i>Passive targeting to the tumor site</i> • <i>Highly efficient drug delivery (reduced to 2 hr)</i> <i>(Male nude mice)</i> | | (Cheng et al., 2008) |
| Poly(ethylene glycol) (PEG) gold nanoparticles | <ul style="list-style-type: none"> • <i>Enhanced retention in the serum</i> • <i>Increased retention of the nanoparticles in the tumor</i> <i>(C57/BL6 mice bearing a subcutaneously transplanted B78H1 amelanotic melanoma)</i> | | (Camerin et al., 2016) |
| Poly(ethylene glycol) (PEG)- and polyethylenimine (PEI)-functionalized zinc(II) phthalocyanine (ZnPc)-loaded mesoporous silica nanoparticles (MSNs) | <ul style="list-style-type: none"> • Enhanced cytotoxic effect • Significant loss of mitochondrial membrane potential after treatment <i>(H22 cell line—murine ascitic hepatoma, female BALB/c nude mice)</i> | (Tu et al., 2012) | |
| Dendrimer phthalocyanine (DPc)-encapsulated polymeric micelle (DPc/m) | <ul style="list-style-type: none"> • Accumulation in the endolysosomes • Release to the cytoplasm and mitochondria after irradiation • Higher in vivo PDT efficacy than clinically used Photofrin • <i>No skin phototoxicity</i> <i>(A549 cell line—lung cancer, female nude mice (BALB/c nu/nu))</i> | (Nishiyama et al., 2009) | |
| Self-assembled zinc phthalocyanine nanoparticles | <ul style="list-style-type: none"> • Good stability and biocompatibility • Absorption in the appropriate NIR region • High photothermal conversion efficiency <i>(L929 cell line—fibroblasts)</i> | (Z. Wang et al., 2019) | |
| Poly(ethylene glycol) methyl ether-block-poly(lactide-co-glycolide) (PLGA-b-PEG) | <ul style="list-style-type: none"> • The same photochemical properties as free ZnPc • Increased solubility in organic solvents • Efficient drug encapsulation • Increased phototoxicity <i>(A549 cell line—lung cancer)</i> | (Mehraban, Musich, & Freeman, 2019) | |
| Amino-functionalized magnetic nanoparticles (AMNPs) | <ul style="list-style-type: none"> • Increased triplet quantum yields • Increased phototoxic effect • Increase in drug concentration in cells <i>(MCF-7 cell line—breast cancer)</i> | (Matlou, Oluwole, & Nyokong, 2019) | |

4.4.2 | Phenothiazinium salts

Among this class of PSs, two of them are most widely studied: methylene blue and toluidine blue (Figure 9). Methylene blue, characterized by two absorption peaks (635 and 670 nm) (Giannelli & Bani, 2018), is commonly used in medicine due to its low dark toxicity and generation of singlet oxygen together with hydroxyl radicals and induction of apoptosis (Orth, Beck, Genze, & Rück, 2000), and has been subjected to several studies focusing on the application of nanoparticles (Table 6). On the other hand, toluidine blue with absorption peak at 620–660 nm did not acquire much attention as a PS agent in PDT of tumors, although several nanoparticles containing toluidine blue have been developed for this purpose, for example, toluidine blue O-silver nanoparticle (Misba, Kulshrestha, & Khan, 2016) or gold nanoparticle-toluidine blue conjugate (Sherwani, Tufail, Khan, & Owais, 2015).

FIGURE 8 The structure of rose bengal

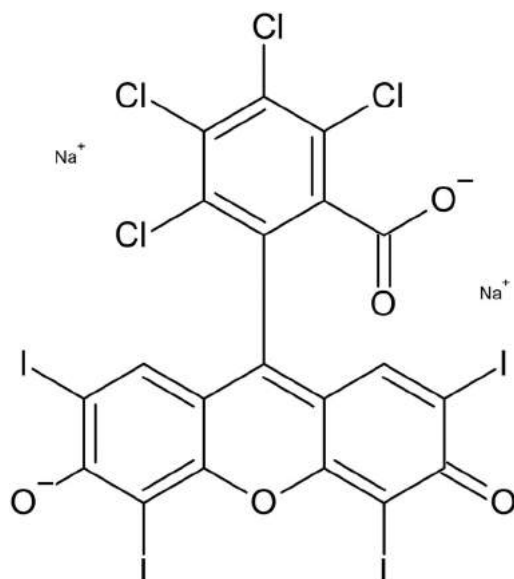
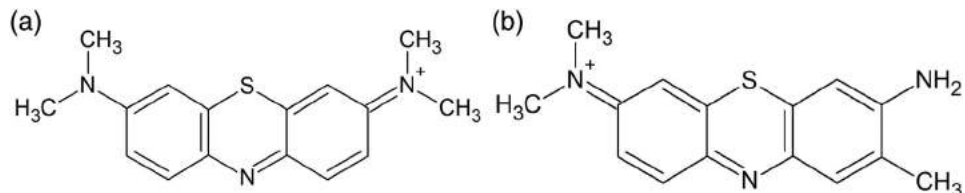


TABLE 5 In vivo and in vitro experiments on rose bengal as a photosensitizer agent in photodynamic therapy. The in vivo studies are italicized

| Nanoparticle | Outcome | In vitro | In vivo |
|---|--|--|---------|
| Fe ₃ O ₄ @Au@mSiO ₂ | <ul style="list-style-type: none"> Enhanced singlet oxygen generation | (Rosa-Pardo et al., 2017) | |
| Gold nanoparticles | <ul style="list-style-type: none"> Enhanced cellular uptake Enhanced PDT effect <i>Enhanced therapeutic effects against oral cancer (Cal-27 cell line—oral squamous cell carcinoma, male Syrian golden hamsters)</i> | (B. Wang et al., 2014) | |
| Silica nanoparticles | <ul style="list-style-type: none"> Enhanced uptake of noncovalent complex Enhanced toxicity compared to free RB (4451 cell line—squamous carcinoma, MCF-7 cell line—breast cancer) | (Uppal, Jain, Gupta, & Das, 2011) | |
| Chitosan | <ul style="list-style-type: none"> Low dark toxicity Enhanced phototoxic effect (MCF-7 cell line—breast cancer) | (X. L. Wang et al., 2011) | |
| Cationic phosphorus dendrimer | <ul style="list-style-type: none"> Enhanced singlet oxygen generation Enhanced phototoxic effect Increased cellular uptake Enhanced PDT activity in case of noncovalent complex (ASZ, BSZ, CSZ cell lines—murine basal cell carcinoma) | (Dabrzalska et al., 2017) | |
| Poly(amidoamine) (PAMAM) dendrimer | <ul style="list-style-type: none"> Decreased dark toxicity Enhanced phototoxic effect (DLA cell line—Dalton's lymphoma ascites) | (Karthikeyan, Babu, Kim, Murugesan, & Jeyasubramanian, 2011) | |
| Mesostructured silica nanoparticles | <ul style="list-style-type: none"> Enhanced singlet oxygen generation | (Martins Estevão et al., 2015) | |
| Barium titanate and rose bengal composite nanoparticles (BT@PAH/RB/PAH) | <ul style="list-style-type: none"> Enhanced singlet oxygen generation Increased PDT effect (Hela cell line—cervical cancer) | (Sun, Ji, & He, 2019) | |
| Carboxymethyl chitosan | <ul style="list-style-type: none"> Enhanced PDT efficacy (Cal-27 cell line—oral cancer) | (X. Zhang et al., 2019) | |
| Rose bengal-loaded surface-modified albumin nanoparticles | <ul style="list-style-type: none"> Controlled drug release Protection against enzymatic degradation | (W. Lin et al., 2001) | |

FIGURE 9 The structures of
(a) methylene blue and
(b) toluidine blue



4.5 | Natural compounds

Among many classes of compounds acting as PSs, one can also distinguish those occurring naturally. Of the most commonly used natural PSs, hypericin, hypocrellins, riboflavin, and curcumin are worth mentioning (Figure 10). All these compounds are featured with very good photochemical and photophysical properties enabling their use for the improvement of PDT.

4.5.1 | Hypericin

Hypericin is a natural pigment extracted from *Hypericum perforatum*. It exhibits low cytotoxicity in the dark and significant anticancer properties in combination with irradiation (Skalkos et al., 2006). A 590 nm light is used for its photoactivation, enabling fluorescence emission at the orange/red wavelength spectrum. The blood half-life equals 2 hr and the complete elimination from the organism takes approximately 38.5 hr (Davids & Maduray, 2011). The compound exhibits a dose-dependent effect and location, being most frequently found intracellularly in the endoplasmic reticulum (ER). Classically after irradiation, it triggers the production of ROS. Moreover, hypericin has been found to cause cellular stress and activation of immune cells upon irradiation, stimulating an increase of interleukin-6 (IL-6) level, correlating with the rate of apoptosis and caspase activity (Sharma & Davids, 2012). The mechanism of action by the p53-independent pathway was also detected (Saw, Heng, & Olivo, 2012). In vivo tests confirmed the effectiveness of this compound, with the final effect depending on its location during exposure. However, hypericin does not remain without flaws, therefore, the scientists focus on the improvement of the efficiency of its action or the protection the drug against enzymatic degradation. For this purpose, they have encapsulated hypericin in P-123 copolymeric micelles (P123-Hyp) (Sakita et al., 2019) and in tetraether liposome conjugates with high specificity toward cancer cells (slow uptake by normal cells) (Davids & Maduray, 2011).

4.5.2 | Hypocrellins

Among this group of compounds, hypocrellin A and B can be used as PSs in PDT thanks to their ability to produce singlet oxygen (Miller et al., 1997). Hypocrellins and their derivatives show strong absorption in the range of 600–900 nm (Y.-Y.

TABLE 6 In vivo and in vitro experiments on methylene blue as a photosensitizer agent in photodynamic therapy. The in vivo studies are italicized

| Nanoparticle | Outcome | In vitro | In vivo |
|---|--|--|---------|
| Silica-coated cobalt ferrite nanoparticles | <ul style="list-style-type: none"> • Singlet oxygen generation similar to free drug • Enhanced effect in photothermal therapy | (Gandhi & Roy, 2019) | |
| Phosphonate-terminated silica nanoparticles | <ul style="list-style-type: none"> • Enhanced singlet oxygen generation • Protection against enzymatic degradation • <i>Induced photodynamic damage (BALB/c [Balb/C-nu] mice)</i> | (X. He, Wu, Wang, Shi, & Hai, 2009) | |
| Calcium phosphate nanoparticles | <ul style="list-style-type: none"> • Protection against enzymatic degradation • Enhanced phototoxic effect with apoptosis as an end point (MCF-7 cell line—breast cancer) | (Seong & Kim, 2015) | |
| Polyacrylamide nanoparticle platforms | <ul style="list-style-type: none"> • Protection against enzymatic degradation (C6 cell line—rat glioma) | (Tang, Xu, Park, Philbert, & Kopelman, 2008) | |
| Supramolecular protein cages | <ul style="list-style-type: none"> • Enhanced singlet oxygen generation • Increased cytotoxic effect (MCF-7 cell line—breast cancer) | (F. Yan, Zhang, Kim, Yuan, & Vo-Dinh, 2010) | |

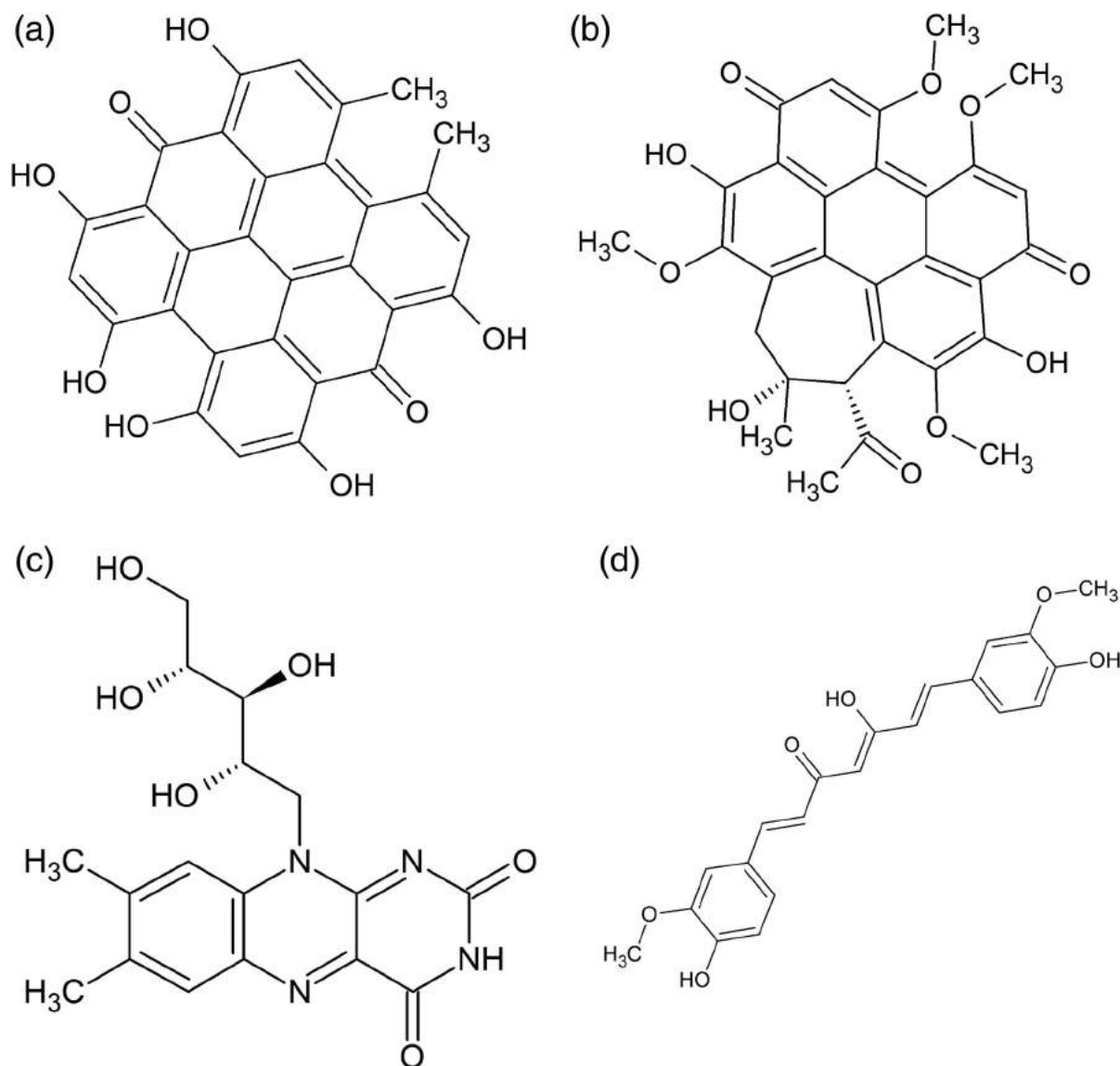


FIGURE 10 Chemical structures of natural photosensitizer (PS): (a) hypericin (ex. 590 nm, em. 640 nm); (b) hypocrellin (ex. 470 nm, em. 650 nm); (c) riboflavin (ex. 440 nm, em. 540 nm); and (d) curcumin (ex. 450 nm, em. 510 nm)

He, Liu, An, Han, & Jiang, 2002). However, they are strongly hydrophobic, which makes it difficult to prepare and administer the solution of the drug. By combining these compounds with ceramic-based nanoparticles, metallic nanoparticles or biodegradable polymer-based nanoparticles improved solubility can be obtained (Zhou et al., 2009). Nanotechnology also allows to create nanoparticles such as poly lactide-co-glycolide nanoparticle formulations with nanosilver (HBS-NPs), increasing the production of singlet oxygen in vitro (Natesan et al., 2017). In addition, liposomes were used as carriers of hypocrellin B (LBH). Low dose of such formulations effectively led to choroidal neovascularization occlusion with minor damage to the collateral retina or retinal pigment epithelium after irradiation. The LHB-treated mice exhibited low skin phototoxicity under simulated sunlight irradiation at 24 hr after dosing (T. Li et al., 2015).

4.5.3 | Riboflavin

Riboflavin (vitamin B₂) is described as a compound with the appropriate photophysical and photochemical properties to act as a PS, having two peaks in UVA at 360 and 440 nm. Riboflavin was coupled with nanoparticles such as pectin-coated silver nanoparticles to increase the production of singlet oxygen (De Melo et al., 2012; Rivas Aiello et al., 2018).

4.5.4 | Curcumin

Curcumin is a polyphenolic compound naturally occurring in *Curcuma longa*. Due to its characteristic color and function (plant dye), it is commonly used as a food additive. Curcumin exhibits many biological features, including antiproliferative, antibacterial, or antioxidant properties (Tao et al., 2019), which enable various medical applications of this compound (e.g., the treatment of wounds, liver diseases, or joint inflammation). However, it has one serious limitation: its poor water solubility, causing serious problems for bioavailability. Thus, curcumin is subjected to modifications aimed at increasing the efficiency of its action. After encapsulation, increased phototoxic activity was obtained for chitosan nanoparticles, while curcumin alone did not show any significant effect (Tsai, Yu, Huang, & Lee, 2018). Further, liposomes (Duse et al., 2018) and lipoproteins (Jutkova, Chorvat, Miskovsky, Jancura, & Datta, 2019) were used as carriers to increase biocompatibility of this compound. The combined therapy of curcumin and 5-aminolevulinic acid (5-ALA) also increased the cytotoxic effect on Caco-2 cells in in vitro studies (Şueki, Ruhi, & Gülsoy, 2019).

5 | FUTURE PERSPECTIVE: NANOPARTICLES FOR TWO-PHOTON PDT

In the nearest future, nanoparticles may serve as carriers for nonclassical, specifically designed PSs. As showed above, the chemical structure of compounds commonly used in PDT is not very diverse, therefore, the elaboration and synthesis of different types of PSs may open new perspectives, especially in the context of nanomedicine. Particularly noteworthy in this matter are compounds with two-photon absorption properties, potentially showing superior phototoxic activities (Bolze, Jenni, Sour, & Heitz, 2017). The idea of application of nanoparticles for two photon PDT is relatively new (Gao, Agayan, Xu, Philbert, & Kopelman, 2006; Sourdon et al., 2019), and has been reviewed elsewhere (Shen, Shuhendler, Ye, Xu, & Chen, 2016).

6 | CONCLUSIONS AND CRITICAL REMARKS

Due to the significant development of nanotechnology and nanoscience over the past few years, numerous compounds of different architectures, shapes, and nanoscale sizes are currently available to scientists. Various methods of synthesis enable the elaboration of nanoparticles with specific structure and properties, depending on the intended application. In most cases, their reactivity allows further modification and functionalization, modulating bioavailability and biodistribution patterns of nanoparticles, and thus broadening the scope of possible biomedical application.

All these aspects contribute to the use of nanosized compounds as drug delivery devices for PSs in PDT. The aim of the present work was to concisely review in vitro and in vivo analysis of drug nanocarriers in PDT. Numerous studies indicate that nanoparticles may improve solubility of PSs, protect them from degradation, modulate their biodistribution, and prolong blood half-life. Nanosized compounds may also provide controlled release, enhanced cellular uptake and improved specificity toward cancer cells, thus eliminating detrimental side effects and systemic toxicity. Moreover, drug-nanoparticle formulations have been shown to modulate phototoxic activity of PSs, providing additive or synergistic effect. These properties bring hope for the development of innovative anticancer PDT that constitute a promising alternative for the most commonly used methods.

However, it may be noticed that only a small number of nanoformulations reported for PDT reached the stage of in vivo tests. This is a huge limitation which must be overcome on the way to clinical application. Nanosystems that provided positive results during in vitro studies on cell line models may turn out to be unstable or ineffective in vivo, exhibiting drastically altered properties and decreased phototoxic activity.

Moreover, it is necessary to develop methods of synthesis and chemical characterization that enable the obtainment of compounds that are reproducible in terms of structure, purity, and properties. Also, there are still many questions concerning biological effects of nanoparticles themselves, primarily due to the differences in in vitro and in vivo models, doses, or experimental procedures presented in currently available scientific data. The insightful evaluation of biocompatibility of nanoparticles, not only at the level of cytotoxicity, but also overall cellular homeostasis is crucial. Several analyzes concerning this aspect indicate its complexity and multilevel nature. Therefore, it is a must to better understand cellular and molecular mechanisms triggered by nanoparticles, including inflammatory processes and impact on epigenetics and various omics. This is particularly important due to the fact that such activities may cause long-lasting effects or toxicity, undermining the biosafety of nanomaterials. Thus, in order to fully exploit the therapeutic potential of nanoparticles, it is crucial to continue and expand the studies both on in vitro cultured cell lines and in more complicated animal models.

Last but not least, it should be noted that complexation or conjugation of PSs with nanoparticles may have a significant impact on physicochemical properties of these drugs, resulting in the decrease of their phototoxicity, and thus—hampering the delivery potential of nanomaterials. Drug-nanoparticle formulations should be subjected to in-depth biophysical characterization before proceeding to biological tests in order to bring positive outcome.

Taking all those aspects into consideration, it can be assumed that the clinical application of nanoparticles as delivery vehicles for therapeutics in PDT still requires a lot of work and can be far from success. Nevertheless, the number of available reports on the biological activities of PS-nanoparticle formulation *in vitro* and *in vivo* allows to hope that in the future we will be able to significantly boost the efficacy of PDT by improved drug delivery.

ACKNOWLEDGMENTS

This work was supported by National Science Centre, Poland (Project UMO-2017/25/B/NZ7/01304 “Phosphorus dendrimers as carriers for photosensitizers—in vivo studies”). The chemical structures have been acquired from PubChem (<https://pubchem.ncbi.nlm.nih.gov>).

CONFLICT OF INTEREST

The authors have declared no conflicts of interest for this article.

AUTHOR CONTRIBUTIONS

Krzysztof Sztandera: Writing-original draft. **Michał Gorzkiewicz:** Writing-original draft. **Barbara Klajnert-Maculewicz:** Writing-original draft.

ORCID

Krzysztof Sztandera  <https://orcid.org/0000-0001-7595-7198>

Michał Gorzkiewicz  <https://orcid.org/0000-0001-9258-3626>

Barbara Klajnert-Maculewicz  <https://orcid.org/0000-0003-3459-8947>

RELATED WIREs ARTICLES

[Recent advances in photodynamic therapy for cancer and infectious diseases](#)

REFERENCES

- Abdel-Kader, M. H. (2014). History of Photodynamic Therapy. In M. H. Abdel-Kader (Ed.), *Photodynamic Therapy* (pp. 3-22). Berlin, Heidelberg, Germany: Springer. https://doi.org/10.1007/978-3-642-39629-8_1
- Abrahamse, H., & Hamblin, M. R. (2016). New photosensitizers for photodynamic therapy. *Biochemical Journal*, *473*(4), 347–364. <https://doi.org/10.1042/BJ20150942>
- Ackroyd, R., Kelty, C., Brown, N., & Reed, M. (2001). The history of photodetection and photodynamic therapy. *Photochemistry and Photobiology*, *74*(5), 656–669. [https://doi.org/10.1562/0031-8655\(2001\)0740656THOPAP2.0.CO2](https://doi.org/10.1562/0031-8655(2001)0740656THOPAP2.0.CO2)
- Agarwal, M. L., Clay, M. E., Harvey, E. J., Evans, H. H., Antunez, A. R., & Oleinick, N. L. (1991). Photodynamic therapy induces rapid cell death by apoptosis in L5178Y mouse lymphoma cells. *Cancer Research*, *51*(21), 5993–5996.
- Ali, S. M., & Olivo, M. (2002). Bio-distribution and subcellular localization of Hypericin and its role in PDT induced apoptosis in cancer cells. *International Journal of Oncology*, *21*(3), 531–540.
- Allen, T. M., & Cullis, P. R. (2013). Liposomal drug delivery systems: From concept to clinical applications. *Advanced Drug Delivery Reviews*, *65*(1), 36–48. <https://doi.org/10.1016/j.addr.2012.09.037>
- Amin, R. M., Hauser, C., Kinzler, I., Rueck, A., & Scalfi-Happ, C. (2012). Evaluation of photodynamic treatment using aluminum phthalocyanine tetrasulfonate chloride as a photosensitizer: New approach. *Photochemical and Photobiological Sciences*, *11*(7), 1156–1163. <https://doi.org/10.1039/c2pp05411f>
- Amirshaghghi, A., Yan, L., Miller, J., Daniel, Y., Stein, J. M., Busch, T. M., ... Tsourkas, A. (2019). Chlorin e6-coated superparamagnetic Iron oxide nanoparticle (SPION) nanoclusters as a Theranostic agent for dual-mode imaging and photodynamic therapy. *Scientific Reports*, *9*(1), 2613. <https://doi.org/10.1038/s41598-019-39036-1>

- Andrieux, K., Nicolas, J., Moine, L., & Barratt, G. (2013). Polymeric nanoparticles for drug delivery. *Polymeric Biomaterials: Medicinal and Pharmaceutical Applications*, 2, 123–152. <https://doi.org/10.1201/b13758>
- Aniogo, E. C., Plackal Adimuriyil George, B., & Abrahamse, H. (2019). The role of photodynamic therapy on multidrug resistant breast cancer. *Cancer Cell International*, 19(1), 91. <https://doi.org/10.1186/s12935-019-0815-0>
- Ashjari, M., Dehfuly, S., Fatehi, D., Shabani, R., & Koruji, M. (2015). Efficient functionalization of gold nanoparticles using cysteine conjugated protoporphyrin IX for singlet oxygen production in vitro. *RSC Advances*, 5(127), 104621–104628. <https://doi.org/10.1039/c5ra15862a>
- Austin, L. A., MacKey, M. A., Dreaden, E. C., & El-Sayed, M. A. (2014). The optical, photothermal, and facile surface chemical properties of gold and silver nanoparticles in biodiagnostics, therapy, and drug delivery. *Archives of Toxicology*, 88(7), 1391–1417. <https://doi.org/10.1007/s00204-014-1245-3>
- Basoglu, H., Bilgin, M. D., & Demir, M. M. (2016). Protoporphyrin IX-loaded magnetoliposomes as a potential drug delivery system for photodynamic therapy: Fabrication, characterization and in vitro study. *Photodiagnosis and Photodynamic Therapy*, 13, 81–90. <https://doi.org/10.1016/j.pdpdt.2015.12.010>
- Bernkop-Schnürch, A., & Dünnhaupt, S. (2012). Chitosan-based drug delivery systems. *European Journal of Pharmaceutics and Biopharmaceutics*, 81(3), 463–469. <https://doi.org/10.1016/j.ejpb.2012.04.007>
- Bertrand, N., Wu, J., Xu, X., Kamaly, N., & Farokhzad, O. C. (2014). Cancer nanotechnology: The impact of passive and active targeting in the era of modern cancer biology. *Advanced Drug Delivery Reviews*, 66(66), 2–25. <https://doi.org/10.1016/j.addr.2013.11.009>
- Bharti, C., Gulati, N., Nagaich, U., & Pal, A. (2015). Mesoporous silica nanoparticles in target drug delivery system: A review. *International Journal of Pharmaceutical Investigation*, 5(3), 124–133. <https://doi.org/10.4103/2230-973X.160844>
- Bolze, F., Jenni, S., Sour, A., & Heitz, V. (2017). Molecular photosensitisers for two-photon photodynamic therapy. *Chemical Communications*, 53(96), 12857–12877. <https://doi.org/10.1039/c7cc06133a>
- Buytaert, E., Dewaele, M., & Agostinis, P. (2007). Molecular effectors of multiple cell death pathways initiated by photodynamic therapy. *Biochimica et Biophysica Acta—Reviews on Cancer*, 1776(1), 86–107. <https://doi.org/10.1016/j.bbcan.2007.07.001>
- Calixto, G. M. F., Bernegossi, J., De Freitas, L. M., Fontana, C. R., Chorilli, M., & Grumezescu, A. M. (2016). Nanotechnology-based drug delivery systems for photodynamic therapy of cancer: A review. *Molecules*, 21(3), 342. <https://doi.org/10.3390/molecules21030342>
- Camerin, M., Moreno, M., Marín, M. J., Schofield, C. L., Chambrier, I., Cook, M. J., ... Russell, D. A. (2016). Delivery of a hydrophobic phthalocyanine photosensitizer using PEGylated gold nanoparticle conjugates for the: in vivo photodynamic therapy of amelanotic melanoma. *Photochemical and Photobiological Sciences*, 15(5), 618–625. <https://doi.org/10.1039/c5pp00463b>
- Campbell, N., Gomez, H., & Bayir, H. (2019). Cell Death Pathways: Apoptosis and Regulated Necrosis. In C. Ronco, R. Bellomo, J. A. Kellum & Z. Ricci (Eds.), *Critical Care Nephrology* (pp. 113–121). Amsterdam, Netherlands: Elsevier. <https://doi.org/10.1016/B978-0-323-44942-7.00020-0>
- Carella, F., Feist, S. W., Bignell, J. P., & De Vico, G. (2015). Comparative pathology in bivalves: Aetiological agents and disease processes. *Journal of Invertebrate Pathology*, 131, 107–120. <https://doi.org/10.1016/j.jip.2015.07.012>
- Carneiro, J., Gonçalves, A., Zhou, Z., Griffin, K. E., Kaufman, N. E. M., & Vicente, M. d. G. H. (2018). Synthesis and in vitro PDT evaluation of new porphyrins containing meso-epoxymethylaryl cationic groups. *Lasers in Surgery and Medicine*, 50(5), 566–575. <https://doi.org/10.1002/lsm.22824>
- Castano, A. P., Mroz, P., Wu, M. X., & Hamblin, M. R. (2008). Photodynamic therapy plus low-dose cyclophosphamide generates antitumor immunity in a mouse model. *Proceedings of the National Academy of Sciences*, 105(14), 5495–5500. <https://doi.org/10.1073/pnas.0709256105>
- Chen, B., Pogue, B. W., Hoopes, P. J., & Hasan, T. (2012). Vascular and cellular targeting for photodynamic therapy. *Critical Reviews™ in Eukaryotic Gene Expression*, 16(4), 279–306. <https://doi.org/10.1615/critrevueukargeneexpr.v16.i4.10>
- Cheng, Y., Samia, A. C., Meyers, J. D., Panagopoulos, I., Fei, B., & Burda, C. (2008). Highly efficient drug delivery with gold nanoparticle vectors for in vivo photodynamic therapy of cancer. *Journal of the American Chemical Society*, 130(32), 10643–10647. <https://doi.org/10.1021/ja801631c>
- Dabrzalska, M., Janaszewska, A., Zablocka, M., Mignani, S., Majoral, J. P., & Klajnert-Maculewicz, B. (2017). Cationic phosphorus dendrimer enhances photodynamic activity of rose bengal against basal cell carcinoma cell lines. *Molecular Pharmaceutics*, 14(5), 1821–1830. <https://doi.org/10.1021/acs.molpharmaceut.7b00108>
- Dabrzalska, M., Zablocka, M., Mignani, S., Majoral, J. P., & Klajnert-Maculewicz, B. (2015). Phosphorus dendrimers and photodynamic therapy. Spectroscopic studies on two dendrimer-photosensitizer complexes: Cationic phosphorus dendrimer with rose bengal and anionic phosphorus dendrimer with methylene blue. *International Journal of Pharmaceutics*, 492(1–2), 266–274. <https://doi.org/10.1016/j.ijpharm.2015.06.014>
- Daniell, M. D., & Hill, J. S. (1991). A history of photodynamic therapy. *ANZ Journal of Surgery*, 61(5), 340–348. <https://doi.org/10.1111/j.1445-2197.1991.tb00230.x>
- Davids, L. M., & Maduray, K. (2011). The anticancer activity of Hypericin in photodynamic therapy. *Journal of Bioanalysis & Biomedicine*, s6(1), 1–3. <https://doi.org/10.4172/1948-593x.s6-004>
- De Melo, L. S. A., Gomes, A. S. L., Saska, S., Nigoghossian, K., Messaddeq, Y., Ribeiro, S. J. L., & De Araujo, R. E. (2012). Singlet oxygen generation enhanced by silver-pectin nanoparticles. *Journal of Fluorescence*, 22(6), 1633–1638. <https://doi.org/10.1007/s10895-012-1107-4>
- De Rosa, F. S., & Bentley, M. V. (2000). Photodynamic therapy of skin cancers: Sensitizers, clinical studies and future directives. *Pharmaceutical Research*, 17(12), 1447–1455. <https://doi.org/10.1023/A:1007612905378>
- Ding, H., Mora, R., Gao, J., & Sumer, B. D. (2011). Characterization and optimization of mTHPP nanoparticles for photodynamic therapy of head and neck cancer. *Otolaryngology- Head and Neck Surgery*, 145(4), 612–617. <https://doi.org/10.1177/0194599811412449>

- Dolmans, D. E. J. G. J., Fukumura, D., & Jain, R. K. (2003). Photodynamic therapy for cancer. *Nature Reviews Cancer*, 3(5), 380–387. <https://doi.org/10.1038/nrc1071>
- Duse, L., Baghdan, E., Pinnapireddy, S. R., Engelhardt, K. H., Jedelská, J., Schaefer, J., ... Bakowsky, U. (2018). Preparation and characterization of curcumin loaded chitosan nanoparticles for photodynamic therapy. *Physica Status Solidi (A) Applications and Materials Science*, 215(15), 1700709. <https://doi.org/10.1002/pssa.201700709>
- Dykman, L. A., & Khlebtsov, N. G. (2011). Gold nanoparticles in biology and medicine: Recent advances and prospects. *Acta Naturae*, 3(2), 34–55. <https://doi.org/10.1039/c0cs00018c>
- El-Say, K. M., & El-Sawy, H. S. (2017). Polymeric nanoparticles: Promising platform for drug delivery. *International Journal of Pharmaceutics*, 528(1–2), 675–691. <https://doi.org/10.1016/J.IJPHARM.2017.06.052>
- Fakhar-E-Alam, M., Ali, S. M. U., Ibutoto, Z. H., Kimleang, K., Atif, M., Kashif, M., ... Willander, M. (2012). Sensitivity of A-549 human lung cancer cells to nanoporous zinc oxide conjugated with Photofrin. *Lasers in Medical Science*, 27(3), 607–614. <https://doi.org/10.1007/s10103-011-0989-8>
- Falcaro, P., Ricco, R., Yazdi, A., Imaz, I., Furukawa, S., Maspoch, D., ... Doonan, C. J. (2016). Application of metal and metal oxide nanoparticles at MOFs. *Coordination Chemistry Reviews*, 307, 237–254. <https://doi.org/10.1016/j.ccr.2015.08.002>
- Ficai, D., Oprea, O., Ficai, A., & Holban, A. (2016). Metal oxide nanoparticles: Potential uses in biomedical applications. *Current Proteomics*, 11(2), 139–149. <https://doi.org/10.2174/157016461102140917122838>
- Foster, T. H., Girotti, A. W., Hahn, S. M., Mroz, P., Hamblin, M. R., Juzeniene, A., ... Berg, K. (2011). Photodynamic therapy of cancer: An update. *CA: A Cancer Journal for Clinicians*, 61(4), 250–281. <https://doi.org/10.3322/caac.20114>
- Friedman, A. D., Claypool, S. E., & Liu, R. (2013). The smart targeting of nanoparticles. *Current Pharmaceutical Design*, 19(35), 6315–6329. <https://doi.org/10.2174/13816128113199990375>
- Gandhi, S., & Roy, I. (2019). Methylene blue loaded, silica coated cobalt ferrite nanoparticles with potential for combination therapy. *Materials Research Express*, 6(7), 074005. <https://doi.org/10.1088/2053-1591/ab187a>
- Gao, D., Agayan, R. R., Xu, H., Philbert, M. A., & Kopelman, R. (2006). Nanoparticles for two-photon photodynamic therapy in living cells. *Nano Letters*, 6(11), 2383–2386. <https://doi.org/10.1021/nl0617179>
- Garcez, A. S., Ribeiro, M. S., Tegos, G. P., Núñez, S. C., Jorge, A. O. C., & Hamblin, M. R. (2007). Antimicrobial photodynamic therapy combined with conventional endodontic treatment to eliminate root canal biofilm infection. *Lasers in Surgery and Medicine*, 39(1), 59–66. <https://doi.org/10.1002/lsm.20415>
- Giannelli, M., & Bani, D. (2018). Appropriate laser wavelengths for photodynamic therapy with methylene blue. *Lasers in Medical Science*, 33(8), 1837–1838. <https://doi.org/10.1007/s10103-018-2566-x>
- Gianotti, E., Martins Estevão, B., Cucinotta, F., Hioka, N., Rizzi, M., Renò, F., & Marchese, L. (2014). An efficient rose bengal based nanoplatform for photodynamic therapy. *Chemistry—A European Journal*, 20(35), 10921–10925. <https://doi.org/10.1002/chem.201404296>
- Gomes, A. T. P. C., Neves, M. G. P. M. S., & Cavaleiro, J. A. S. (2018). Cancer, photodynamic therapy and porphyrin-type derivatives. *Anais Da Academia Brasileira de Ciências*, 90(1), 993–1026. <https://doi.org/10.1590/0001-3765201820170811>
- Gorzkiwicz, M., Buczkowski, A., Pałecz, B., & Klajnert-Maculewicz, B. (2019). *PAMAM and PPI Dendrimers in Biophysical and Thermodynamic Studies on the Delivery of Therapeutic Nucleotides, Nucleosides and Nucleobase Derivatives for Anticancer Applications*. In Demetzos, C., & Pippa, N. (Eds.), *Thermodynamics and Biophysics of Biomedical Nanosystems: Applications and Practical Considerations* (pp. 183–243). Springer, Singapore. https://doi.org/10.1007/978-981-13-0989-2_7
- Gorzkiwicz, M., & Klajnert-Maculewicz, B. (2018). Dendrimers as Nanocarriers for Anticancer Drugs. In A. K. Sharma, & R. K. Keservani (Eds.), *Dendrimers for Drug Delivery* (pp. 327–374). Boca Raton, FL: Apple Academic Press, CRC Press, Taylor & Francis Group.
- Gouterman, M. (1961). Spectra of porphyrins. *Journal of Molecular Spectroscopy*, 6(C), 138–163. [https://doi.org/10.1016/0022-2852\(61\)90236-3](https://doi.org/10.1016/0022-2852(61)90236-3)
- He, X., Wu, X., Wang, K., Shi, B., & Hai, L. (2009). Methylene blue-encapsulated phosphonate-terminated silica nanoparticles for simultaneous in vivo imaging and photodynamic therapy. *Biomaterials*, 30(29), 5601–5609. <https://doi.org/10.1016/j.biomaterials.2009.06.030>
- He, Y.-Y., Liu, H.-Y., An, J.-Y., Han, R., & Jiang, L.-J. (2002). Photodynamic action of hypocrellin dyes: Structure–activity relationships. *Dyes and Pigments*, 44(1), 63–67. [https://doi.org/10.1016/s0143-7208\(99\)00074-1](https://doi.org/10.1016/s0143-7208(99)00074-1)
- Hinger, D., Navarro, F., Käch, A., Thomann, J. S., Mittler, F., Couffin, A. C., & Maake, C. (2016). Photoinduced effects of m-tetrahydroxyphenylchlorin loaded lipid nanoemulsions on multicellular tumor spheroids. *Journal of Nanobiotechnology*, 14(1), 68. <https://doi.org/10.1186/s12951-016-0221-x>
- Hou, W., Xia, F., Alves, C. S., Qian, X., Yang, Y., & Cui, D. (2016). MMP2-targeting and redox-responsive PEGylated Chlorin e6 nanoparticles for Cancer near-infrared imaging and photodynamic therapy. *ACS Applied Materials and Interfaces*, 8(2), 1447–1457. <https://doi.org/10.1021/acsami.5b10772>
- Hu, S., Yang, Y., Jiang, B., Su, D., Zhang, L., Huang, Z., & Zhang, F. (2019). Treatment of *Condyloma acuminatum* using the combination of laser ablation and ALA-PDT. *Photodiagnosis and Photodynamic Therapy*, 25, 193–196. <https://doi.org/10.1016/j.pdpdt.2018.12.006>
- Hu, Z., Pan, Y., Wang, J., Chen, J., Li, J., & Ren, L. (2009). Meso-tetra (carboxyphenyl) porphyrin (TCPP) nanoparticles were internalized by SW480 cells by a clathrin-mediated endocytosis pathway to induce high photocytotoxicity. *Biomedicine and Pharmacotherapy*, 63(2), 155–164. <https://doi.org/10.1016/j.biopha.2008.07.087>
- Huang, H., Song, W., Rieffel, J., & Lovell, J. F. (2015). Emerging applications of porphyrins in photomedicine. *Frontiers in Physics*, 3, 23. <https://doi.org/10.3389/fphy.2015.00023>
- Ivanov, A. S., & Boldyrev, A. I. (2014). Deciphering aromaticity in porphyrinoids via adaptive natural density partitioning. *Organic and Biomolecular Chemistry*, 12(32), 6145–6150. <https://doi.org/10.1039/c4ob01018c>

- Jiang, F., Lilge, L., Grenier, J., Li, Y., Wilson, M. D., & Chopp, M. (1998). Photodynamic therapy of U87 human glioma in nude rat using liposome-delivered photofrin. *Lasers in Surgery and Medicine*, 22(2), 74–80.
- Juárez, A. A. S., Alvarado, E. M., & Gallegos, E. R. (2019). Cell death induced by photodynamic therapy with the conjugate of gold nanoparticles-PpIX in HeLa cell line. In *AIP conference proceedings* (Vol. 2099, p. 040008). <https://doi.org/10.1063/1.5095911>
- Jutkova, A., Chorvat, D., Miskovsky, P., Jancura, D., & Datta, S. (2019). Encapsulation of anticancer drug curcumin and co-loading with photosensitizer hypericin into lipoproteins investigated by fluorescence resonance energy transfer. *International Journal of Pharmaceutics*, 564, 369–378. <https://doi.org/10.1016/j.ijpharm.2019.04.062>
- Kakde, D., Jain, D., Shrivastava, V., Kakde, R., & Patil, A. T. (2011). Cancer therapeutics- opportunities, challenges and advances in drug delivery. *Journal of Applied Pharmaceutical Science*, 1(9), 1–10.
- Kamkaew, A., Cheng, L., Goel, S., Valdovinos, H. F., Barnhart, T. E., Liu, Z., & Cai, W. (2016). Cerenkov radiation induced photodynamic therapy using Chlorin e6-loaded hollow mesoporous silica nanoparticles. *ACS Applied Materials and Interfaces*, 8(40), 26630–26637. <https://doi.org/10.1021/acsami.6b10255>
- Karthikeyan, K., Babu, A., Kim, S. J., Murugesan, R., & Jeyasubramanian, K. (2011). Enhanced photodynamic efficacy and efficient delivery of rose bengal using nanostructured poly(amidoamine) dendrimers: Potential application in photodynamic therapy of cancer. *Cancer Nanotechnology*, 2(1–6), 95–103. <https://doi.org/10.1007/s12645-011-0019-3>
- Kessel, D., & Oleinick, N. L. (2010). Photodynamic therapy and cell death pathways. *Methods in Molecular Biology*, 635, 35–46. https://doi.org/10.1007/978-1-60761-697-9_3
- Kessel, D., Vicente, M. G. H., & Reiners, J. J. (2006). Initiation of apoptosis and autophagy by photodynamic therapy. *Autophagy*, 2(4), 289–290. <https://doi.org/10.4161/auto.2792>
- Klajnert, B., Rozanek, M., & Bryszewska, M. (2012). Dendrimers in photodynamic therapy. *Current Medicinal Chemistry*, 19(29), 4903–4912. <https://doi.org/10.2174/0929867311209024903>
- Konan-Kouakou, Y. N., Boch, R., Gurny, R., & Allémann, E. (2005). In vitro and in vivo activities of verteporfin-loaded nanoparticles. *Journal of Controlled Release*, 103(1), 83–91. <https://doi.org/10.1016/j.jconrel.2004.11.023>
- Kumari, P., Rompicharla, S. V. K., Bhatt, H., Ghosh, B., & Biswas, S. (2019). Development of chlorin e6-conjugated poly(ethylene glycol)-poly(D,L-lactide) nanoparticles for photodynamic therapy. *Nanomedicine*, 14(7), 819–834. <https://doi.org/10.2217/nnm-2018-0255>
- Kwon, S., Singh, R. K., Perez, R. A., Abou Neel, E. A., Kim, H.-W., & Chrzanowski, W. (2013). Silica-based mesoporous nanoparticles for controlled drug delivery. *Journal of Tissue Engineering*, 4, 2041731413503357. <https://doi.org/10.1177/2041731413503357>
- Lee, S. J., Koo, H., Jeong, H., Huh, M. S., Choi, Y., Jeong, S. Y., ... Kwon, I. C. (2011). Comparative study of photosensitizer loaded and conjugated glycol chitosan nanoparticles for cancer therapy. *Journal of Controlled Release*, 152(1), 21–29. <https://doi.org/10.1016/j.jconrel.2011.03.027>
- Li, H., Jin, H., Wan, W., Wu, C., & Wei, L. (2018). Cancer nanomedicine: Mechanisms, obstacles and strategies. *Nanomedicine*, 13(13), 1639–1656. <https://doi.org/10.2217/nnm-2018-0007>
- Li, P., Zhou, G., Zhu, X., Li, G., Yan, P., Shen, L., ... Hamblin, M. R. (2012). Photodynamic therapy with hyperbranched poly(ether-ester) chlorin(e6) nanoparticles on human tongue carcinoma CAL-27 cells. *Photodiagnosis and Photodynamic Therapy*, 9(1), 76–82. <https://doi.org/10.1016/j.pdpdt.2011.08.001>
- Li, T., Hou, X., Deng, H., Zhao, J., Huang, N., Zeng, J., ... Gu, Y. (2015). Liposomal hypocrellin B as a potential photosensitizer for age-related macular degeneration: Pharmacokinetics, photodynamic efficacy, and skin phototoxicity in vivo. *Photochemical and Photobiological Sciences*, 14(5), 972–981. <https://doi.org/10.1039/c4pp00412d>
- Li, X., Xiao, B., Guo, Y., Xiao, Y., & Xiao, S. (2019). Cucurbit[7]uril enhances photosensitization of porphyrins in neuroblastoma cells. *Photodiagnosis and Photodynamic Therapy*, 25, 364–368. <https://doi.org/10.1016/j.pdpdt.2019.01.017>
- Lin, C., Zhang, Y., Zhu, X., Cui, S., Cao, Y., Li, R., & Wang, L. (2019). The study of killing effect and inducing apoptosis of 630-nm laser on lung adenocarcinoma A549 cells mediated by hematoporphyrin derivatives in vitro. *Lasers in Medical Science*. 1–8. <https://doi.org/10.1007/s10103-019-02794-5>
- Lin, W., Garnett, M. C., Davis, S. S., Schacht, E., Ferruti, P., & Illum, L. (2001). Preparation and characterisation of rose bengal-loaded surface-modified albumin nanoparticles. *Journal of Controlled Release*, 71(1), 117–126. [https://doi.org/10.1016/S0168-3659\(01\)00209-7](https://doi.org/10.1016/S0168-3659(01)00209-7)
- Lismont, M., Dreesen, L., Heinrichs, B., & Páez, C. A. (2016). Protoporphyrin IX-functionalized AgSiO₂ Core-Shell nanoparticles: Plasmonic enhancement of fluorescence and singlet oxygen production. *Photochemistry and Photobiology*, 92(2), 247–256. <https://doi.org/10.1111/php.12557>
- MacDonald, I. J., & Dougherty, T. J. (2001). Basic principles of photodynamic therapy. *Journal of porphyrins and Phthalocyanines*, 5(2), 105–129. <https://doi.org/10.1002/jpp.328>
- Mang, T. S. (2004). Lasers and light sources for PDT: Past, present and future. *Photodiagnosis and Photodynamic Therapy*, 1(1), 43–48. [https://doi.org/10.1016/S1572-1000\(04\)00012-2](https://doi.org/10.1016/S1572-1000(04)00012-2)
- Martins Estevão, B., Cucinotta, F., Hioka, N., Cossi, M., Argeri, M., Paul, G., ... Gianotti, E. (2015). Rose bengal incorporated in mesostructured silica nanoparticles: Structural characterization, theoretical modeling and singlet oxygen delivery. *Physical Chemistry Chemical Physics*, 17(40), 26804–26812. <https://doi.org/10.1039/c5cp03564c>
- Martins, W. K., Santos, N. F., Rocha, C. d. S., Bacellar, I. O. L. L., Tsubone, T. M., Viotto, A. C., ... Baptista, M. S. (2019). Parallel damage in mitochondria and lysosomes is an efficient way to photoinduce cell death. *Autophagy*, 15(2), 259–279. <https://doi.org/10.1080/15548627.2018.1515609>
- Master, A., Livingston, M., & Sen Gupta, A. (2013). Photodynamic nanomedicine in the treatment of solid tumors: Perspectives and challenges. *Journal of Controlled Release*, 168(1), 88–102. <https://doi.org/10.1016/j.jconrel.2013.02.020>

- Matlou, G. G., Oluwole, D. O., & Nyokong, T. (2019). Evaluation of the photosensitizing properties of zinc and indium tetra cinnamic acid phthalocyanines linked to magnetic nanoparticles on human breast adenocarcinoma cells. *Journal of Luminescence*, *205*, 385–392. <https://doi.org/10.1016/j.jlumin.2018.09.054>
- Mehraban, N., Musich, P., & Freeman, H. (2019). Synthesis and encapsulation of a new zinc Phthalocyanine photosensitizer into polymeric nanoparticles to enhance cell uptake and Phototoxicity. *Applied Sciences*, *9*(3), 401. <https://doi.org/10.3390/app9030401>
- Miller, G. G., Brown, K., Ballangrud, Å. M., Barajas, O., Xiao, Z., Tulip, J., ... Moore, R. B. (1997). Preclinical assessment of hypocrellin B and hypocrellin B derivatives as sensitizers for photodynamic therapy of cancer: Progress update. *Photochemistry and Photobiology*, *65*(4), 714–722. <https://doi.org/10.1111/j.1751-1097.1997.tb01915.x>
- Misba, L., Kulshrestha, S., & Khan, A. U. (2016). Antibiofilm action of a toluidine blue O-silver nanoparticle conjugate on *Streptococcus mutans*: A mechanism of type I photodynamic therapy. *Biofouling*, *32*(3), 313–328. <https://doi.org/10.1080/08927014.2016.1141899>
- Moan, J., & Peng, Q. (2003). An outline of the hundred-year history of PDT. *Anticancer Research*, *23*(5A), 3591–3600.
- Mortier, L., Tylcz, J. B., Koncar, V., Mordon, S., Cochrane, C., & Betrouni, N. (2014). Light emitting fabric technologies for photodynamic therapy. *Photodiagnosis and Photodynamic Therapy*, *12*(1), 1–8. <https://doi.org/10.1016/j.pdpdt.2014.11.002>
- Mroz, P., Yaroslavsky, A., Kharkwal, G. B., & Hamblin, M. R. (2011). Cell death pathways in photodynamic therapy of cancer. *Cancers*, *3*, 2516–2539. <https://doi.org/10.3390/cancers3022516>
- Nackiewicz, J., Kliber-Jasik, M., & Skonieczna, M. (2019). A novel pro-apoptotic role of zinc octacarboxyphthalocyanine in melanoma me45 cancer cell's photodynamic therapy (PDT). *Journal of Photochemistry and Photobiology B: Biology*, *190*, 146–153. <https://doi.org/10.1016/j.jphotobiol.2018.12.002>
- Napoletano, F., Baron, O., Vandenabeele, P., Mollereau, B., & Fanto, M. (2019). Intersections between regulated cell death and autophagy. *Trends in Cell Biology*, *29*(4), 323–338. <https://doi.org/10.1016/j.tcb.2018.12.007>
- Natesan, S., Krishnaswami, V., Ponnusamy, C., Madiyalakan, M., Woo, T., & Palanisamy, R. (2017). Hypocrellin B and nano silver loaded polymeric nanoparticles: Enhanced generation of singlet oxygen for improved photodynamic therapy. *Materials Science and Engineering C*, *77*, 935–946. <https://doi.org/10.1016/j.msec.2017.03.179>
- Ning, L. G., Liu, P., Wang, B., Li, C. M., Kang, E. T., Lu, Z. S., ... Xu, L. Q. (2019). Hydrothermal derived protoporphyrin IX nanoparticles for inactivation and imaging of bacteria strains. *Journal of Colloid and Interface Science*, *549*, 72–79. <https://doi.org/10.1016/j.jcis.2019.04.050>
- Nishiyama, N., Morimoto, Y., Jang, W. D., & Kataoka, K. (2009). Design and development of dendrimer photosensitizer-incorporated polymeric micelles for enhanced photodynamic therapy. *Advanced Drug Delivery Reviews*, *61*(4), 327–338. <https://doi.org/10.1016/j.addr.2009.01.004>
- Nishiyama, N., Nakagishi, Y., Morimoto, Y., Lai, P. S., Miyazaki, K., Urano, K., ... Kataoka, K. (2009). Enhanced photodynamic cancer treatment by supramolecular nanocarriers charged with dendrimer phthalocyanine. *Journal of Controlled Release*, *133*(3), 245–251. <https://doi.org/10.1016/j.jconrel.2008.10.010>
- Oda, D. F., Duarte, M. A. H., Andrade, F. B., Moriyama, L. T., Bagnato, V. S., & de Moraes, I. G. (2019). Antimicrobial action of photodynamic therapy in root canals using LED curing light, curcumin and carbopol gel. *International Endodontic Journal*, *13092*, 1010–1019. <https://doi.org/10.1111/iej.13092>
- Orth, K., Beck, G., Genze, F., & Rück, A. (2000). Methylene blue mediated photodynamic therapy in experimental colorectal tumors in mice. *Journal of Photochemistry and Photobiology B: Biology*, *57*(2–3), 186–192. [https://doi.org/10.1016/S1011-1344\(00\)00105-6](https://doi.org/10.1016/S1011-1344(00)00105-6)
- Phua, S. Z. F., Xue, C., Lim, W. Q., Yang, G., Chen, H., Zhang, Y., ... Zhao, Y. (2019). Light-responsive prodrug-based supramolecular Nanosystems for site-specific combination therapy of Cancer. *Chemistry of Materials*, *acs.chemmater.9b00439*, *31*, 3349–3358. <https://doi.org/10.1021/acs.chemmater.9b00439>
- Plaetzer, K., Kiesslich, T., Verwanger, T., & Krammer, B. (2003). The modes of cell death induced by PDT: An overview. *Medical Laser Application*, *18*(1), 7–19. <https://doi.org/10.1078/1615-1615-00082>
- Plaetzer, K., Krammer, B., Berlanda, J., Berr, F., & Kiesslich, T. (2009). Photophysics and photochemistry of photodynamic therapy: Fundamental aspects. *Lasers in Medical Science*, *24*(2), 259–268. <https://doi.org/10.1007/s10103-008-0539-1>
- Qi, S., Guo, L., Yan, S., Lee, R. J., Yu, S., & Chen, S. (2019). Hypocrellin A-based photodynamic action induces apoptosis in A549 cells through ROS-mediated mitochondrial signaling pathway. *Acta Pharmaceutica Sinica B*, *9*(2), 279–293. <https://doi.org/10.1016/j.apsb.2018.12.004>
- Reddy, G. R., Bhojani, M. S., McConville, P., Moody, J., Moffat, B. A., Hall, D. E., ... Ross, B. D. (2006). Vascular targeted nanoparticles for imaging and treatment of brain tumors. *Clinical Cancer Research*, *12*(22), 6677–6686. <https://doi.org/10.1158/1078-0432.CCR-06-0946>
- Reza Saboktakin, M., Tabatabaie, R. M., Maharramov, A., & Ali Ramazanov, M. (2011). Synthesis and in vitro studies of biodegradable modified chitosan nanoparticles for photodynamic treatment of cancer. *International Journal of Biological Macromolecules*, *49*(5), 1059–1065. <https://doi.org/10.1016/j.ijbiomac.2011.08.031>
- Rivas Aiello, M. B., Castrogiovanni, D., Parisi, J., Azcárate, J. C., García Einschlag, F. S., Gensch, T., ... Mártire, D. O. (2018). Photodynamic therapy in HeLa cells incubated with riboflavin and pectin-coated silver nanoparticles. *Photochemistry and Photobiology*, *94*(6), 1159–1166. <https://doi.org/10.1111/php.12974>
- Robertson, C. A., Evans, D. H., & Abrahamse, H. (2009). Photodynamic therapy (PDT): A short review on cellular mechanisms and cancer research applications for PDT. *Journal of Photochemistry and Photobiology B: Biology*, *96*(1), 1–8. <https://doi.org/10.1016/j.jphotobiol.2009.04.001>
- Rosa-Pardo, I., Roig-Pons, M., Heredia, A. A., Usagre, J. V., Ribera, A., Galian, R. E., & Pérez-Prieto, J. (2017). Fe₃O₄@Au@mSiO₂ as an enhancing nanoplatform for rose bengal photodynamic activity. *Nanoscale*, *9*(29), 10388–10396. <https://doi.org/10.1039/c7nr00449d>
- Sakita, K. M., Conrado, P. C., Faria, D. R., Arita, G. S., Capoci, I. R., Rodrigues-Vendramini, F. A., ... Bonfim-Mendonça, P. S. (2019). Copolymeric micelles as efficient inert nanocarrier for hypericin in the photodynamic inactivation of *Candida* species. *Future Microbiology*, *14*(6), 519–531. <https://doi.org/10.2217/fmb-2018-0304>

- Savarimuthu, W. P., Ganathan, P., Rao, A. P., Manickam, E., & Singaravelu, G. (2014). Protoporphyrin IX-gold nanoparticle conjugates for targeted photodynamic therapy—An in-vitro study. *Journal of Nanoscience and Nanotechnology*, *15*(8), 5577–5584. <https://doi.org/10.1166/jnn.2015.10302>
- Saw, C. L. L., Heng, P. W. S., & Olivo, M. (2012). Potentiation of the photodynamic action of Hypericin. *Journal of Environmental Pathology, Toxicology and Oncology*, *27*(1), 23–33.
- Seong, D. Y., & Kim, Y. J. (2015). Enhanced photodynamic therapy efficacy of methylene blue-loaded calcium phosphate nanoparticles. *Journal of Photochemistry and Photobiology B: Biology*, *146*, 34–43. <https://doi.org/10.1016/j.jphotobiol.2015.02.022>
- Sercombe, L., Veerati, T., Moheimani, F., Wu, S. Y., Sood, A. K., & Hua, S. (2015). Advances and challenges of liposome assisted drug delivery. *Frontiers in Pharmacology*, *6*(DEC), 286. <https://doi.org/10.3389/fphar.2015.00286>
- Sharma, K. V., & Davids, L. M. (2012). Hypericin-PDT-induced rapid necrotic death in human squamous cell carcinoma cultures after multiple treatment. *Cell Biology International*, *36*(12), 1261–1266. <https://doi.org/10.1042/cbi20120108>
- Shen, Y., Shuhendler, A. J., Ye, D., Xu, J. J., & Chen, H. Y. (2016). Two-photon excitation nanoparticles for photodynamic therapy. *Chemical Society Reviews*, *45*(24), 6725–6741. <https://doi.org/10.1039/c6cs00442c>
- Sherwani, M. A., Tufail, S., Khan, A. A., & Owais, M. (2015). Gold nanoparticle-photosensitizer conjugate based photodynamic inactivation of bio-film producing cells: Potential for treatment of *C. albicans* infection in BALB/c mice. *PLoS One*, *10*(7), e0131684. <https://doi.org/10.1371/journal.pone.0131684>
- Singh, S., Jha, P., Singh, V., Sinha, K., Hussain, S., Singh, M. K., & Das, P. (2016). A quantum dot-MUC1 aptamer conjugate for targeted delivery of protoporphyrin IX and specific photokilling of cancer cells through ROS generation. *Integrative Biology*, *8*(10), 1040–1048. <https://doi.org/10.1039/c6ib00092d>
- Skalkos, D., Gioti, E., Stalikas, C. D., Meyer, H., Papazoglou, T. G., & Filippidis, G. (2006). Photophysical properties of *Hypericum perforatum* L. extracts—Novel photosensitizers for PDT. *Journal of Photochemistry and Photobiology B: Biology*, *82*(2), 146–151. <https://doi.org/10.1016/j.jphotobiol.2005.11.001>
- Sourdon, A., Gary-Bobo, M., Maynadier, M., Garcia, M., Majoral, J. P., Caminade, A. M., ... Blanchard-Desce, M. (2019). Dendrimeric nanoparticles for two-photon photodynamic therapy and imaging: Synthesis, Photophysical properties, innocuousness in daylight and cytotoxicity under two-photon irradiation in the NIR. *Chemistry—A European Journal*, *25*(14), 3637–3649. <https://doi.org/10.1002/chem.201805617>
- Spikes, J. D. (1990). New trends in photobiology. *Journal of Photochemistry and Photobiology B: Biology*, *6*(3), 259–274. [https://doi.org/10.1016/1011-1344\(90\)85096-f](https://doi.org/10.1016/1011-1344(90)85096-f)
- Spikes, J. D., & Bommer, J. C. (1993). Photosensitizing properties of mono-l-aspartyl chlorin e6 (NPe6): A candidate sensitizer for the photodynamic therapy of tumors. *Journal of Photochemistry and Photobiology B: Biology*, *17*(2), 135–143. [https://doi.org/10.1016/1011-1344\(93\)80006-U](https://doi.org/10.1016/1011-1344(93)80006-U)
- Spring, B. Q., Rizvi, I., & Hasan, T. (2015). The role of photodynamic therapy in overcoming. *Photochemical & Photobiological Sciences*, *14*(8), 1476–1491. <https://doi.org/10.1039/c4pp00495g>
- Şueki, F., Ruhi, M. K., & Gülsoy, M. (2019). The effect of curcumin in antitumor photodynamic therapy: in vitro experiments with Caco-2 and PC-3 Cancer lines. *Photodiagnosis and Photodynamic Therapy*, *27*, 95–99. <https://doi.org/10.1016/j.pdpdt.2019.05.012>
- Sun, X., Ji, Z., & He, S. (2019). SHG-enhanced NIR-excited in vitro photodynamic therapy using composite nanoparticles of barium titanate and rose bengal. *RSC Advances*, *9*(14), 8056–8064. <https://doi.org/10.1039/C9RA00432G>
- Sztandera, K., Działak, P., Marcinkowska, M., Stańczyk, M., Gorzkiewicz, M., Janaszewska, A., & Klajnert-Maculewicz, B. (2019). Sugar modification enhances cytotoxic activity of PAMAM-doxorubicin conjugate in glucose-deprived MCF-7 cells—Possible role of GLUT1 transporter. *Pharmaceutical Research*, *36*, 140. <https://doi.org/10.1007/s11095-019-2673-9>
- Sztandera, K., Gorzkiewicz, M., & Klajnert-Maculewicz, B. (2019). Gold nanoparticles in Cancer treatment. *Molecular Pharmaceutics*, *16*(1), 1–23. <https://doi.org/10.1021/acs.molpharmaceut.8b00810>
- Tang, W., Xu, H., Park, E. J., Philbert, M. A., & Kopelman, R. (2008). Encapsulation of methylene blue in polyacrylamide nanoparticle platforms protects its photodynamic effectiveness. *Biochemical and Biophysical Research Communications*, *369*(2), 579–583. <https://doi.org/10.1016/j.bbrc.2008.02.066>
- Tao, R., Zhang, F., Tang, Q. j., Xu, C. s., Ni, Z. J., & Meng, X. h. (2019). Effects of curcumin-based photodynamic treatment on the storage quality of fresh-cut apples. *Food Chemistry*, *274*, 415–421. <https://doi.org/10.1016/j.foodchem.2018.08.042>
- Tsai, W. H., Yu, K. H., Huang, Y. C., & Lee, C. I. (2018). EGFR-targeted photodynamic therapy by curcumin-encapsulated chitosan/TPP nanoparticles. *International Journal of Nanomedicine*, *13*, 903–916. <https://doi.org/10.2147/IJN.S148305>
- Tu, J., Wang, T., Shi, W., Wu, G., Tian, X., Wang, Y., ... Ren, L. (2012). Multifunctional ZnPc-loaded mesoporous silica nanoparticles for enhancement of photodynamic therapy efficacy by endolysosomal escape. *Biomaterials*, *33*(31), 7903–7914. <https://doi.org/10.1016/j.biomaterials.2012.07.025>
- Uppal, A., Jain, B., Gupta, P. K., & Das, K. (2011). Photodynamic action of rose bengal silica nanoparticle complex on breast and oral cancer cell lines. *Photochemistry and Photobiology*, *87*(5), 1146–1151. <https://doi.org/10.1111/j.1751-1097.2011.00967.x>
- Vandenbogaerde, A. L., Cuveele, J. F., Proot, P., Himpens, B. E., Merlevede, W. J., & De Witte, P. A. (1997). Differential cytotoxic effects induced after photosensitization by hypericin. *Journal of Photochemistry and Photobiology B: Biology*, *38*(2–3), 136–142. [https://doi.org/10.1016/S1011-1344\(96\)07446-5](https://doi.org/10.1016/S1011-1344(96)07446-5)
- Wang, A. Z., Langer, R., & Farokhzad, O. C. (2012). Nanoparticle delivery of Cancer drugs. *Annual Review of Medicine*, *63*(1), 185–198. <https://doi.org/10.1146/annurev-med-040210-162544>
- Wang, B., Wang, J. H., Liu, Q., Huang, H., Chen, M., Li, K., ... Chu, P. K. (2014). Rose-Bengal-conjugated gold nanorods for in vivo photodynamic and photothermal oral cancer therapies. *Biomaterials*, *35*(6), 1954–1966. <https://doi.org/10.1016/j.biomaterials.2013.11.066>

- Wang, J. J., Zeng, Z. W., Xiao, R. Z., Xie, T., Zhou, G. L., Zhan, X. R., & Wang, S. L. (2011). Recent advances of chitosan nanoparticles as drug carriers. *International Journal of Nanomedicine*, *6*, 765–774. <https://doi.org/10.2147/IJN.S17296>
- Wang, M., Geilich, B. M., Keidar, M., & Webster, T. J. (2017). Killing malignant melanoma cells with protoporphyrin IX-loaded polymersome-mediated photodynamic therapy and cold atmospheric plasma. *International Journal of Nanomedicine*, *12*, 4117–4127. <https://doi.org/10.2147/IJN.S129266>
- Wang, S., Fan, W., Kim, G., Hah, H. J., Lee, Y. E. K., Kopelman, R., ... Pandey, R. K. (2011). Novel methods to incorporate photosensitizers into nanocarriers for cancer treatment by photodynamic therapy. *Lasers in Surgery and Medicine*, *43*(7), 686–695. <https://doi.org/10.1002/lsm.21113>
- Wang, X. L., Zeng, Y., Zheng, Y. Z., Chen, J. F., Tao, X., Wang, L. X., & Teng, Y. (2011). Rose bengal-grafted biodegradable microcapsules: Singlet-oxygen generation and cancer-cell incapacitation. *Chemistry—A European Journal*, *17*(40), 11223–11229. <https://doi.org/10.1002/chem.201100975>
- Wang, Z., Gai, S., Wang, C., Yang, G., Zhong, C., Dai, Y., ... Yang, P. (2019). Self-assembled zinc phthalocyanine nanoparticles as excellent photothermal/photodynamic synergistic agent for antitumor treatment. *Chemical Engineering Journal*, *361*, 117–128. <https://doi.org/10.1016/j.cej.2018.12.007>
- Wong, I. Y., Bhatia, S. N., & Toner, M. (2013). Nanotechnology: Emerging tools for biology and medicine. *Genes and Development*, *27*(22), 2397–2408. <https://doi.org/10.1101/gad.226837.113>
- Wong, R. C. H., Lo, P. C., & Ng, D. K. P. (2019). Stimuli responsive phthalocyanine-based fluorescent probes and photosensitizers. *Coordination Chemistry Reviews*, *379*, 30–46. <https://doi.org/10.1016/j.ccr.2017.10.006>
- Wu, H., Minamide, T., & Yano, T. (2019). Role of photodynamic therapy in the treatment of esophageal cancer. *Digestive Endoscopy*, *31*, 508–516. <https://doi.org/10.1111/den.13353>
- Xu, L., Zhang, X., Cheng, W., Wang, Y., Yi, K., Wang, Z., ... Zhao, T. (2019). Hypericin-photodynamic therapy inhibits the growth of adult T-cell leukemia cells through induction of apoptosis and suppression of viral transcription. *Retrovirology*, *16*(1), 5. <https://doi.org/10.1186/s12977-019-0467-0>
- Yan, F., Zhang, Y., Kim, K. S., Yuan, H. K., & Vo-Dinh, T. (2010). Cellular uptake and photodynamic activity of protein nanocages containing methylene blue photosensitizing drug. *Photochemistry and Photobiology*, *86*(3), 662–666. <https://doi.org/10.1111/j.1751-1097.2009.00696.x>
- Yan, L., Miller, J., Yuan, M., Liu, J. F., Busch, T. M., Tsourkas, A., & Cheng, Z. (2017). Improved photodynamic therapy efficacy of Protoporphyrin IX-loaded polymeric micelles using Erlotinib pretreatment. *Biomacromolecules*, *18*(6), 1836–1844. <https://doi.org/10.1021/acs.biomac.7b00274>
- Yang, K., Wang, C., Liu, C., Ding, S., Tian, F., & Li, F. (2019). Bioluminescence-initiated photodynamic therapy bridged on high-luminescent carbon dots-conjugated protoporphyrin IX. *Journal of Materials Science*, *54*(4), 3383–3391. <https://doi.org/10.1007/s10853-018-3038-1>
- Yu, L., Lenardo, M. J., & Baehrecke, E. H. (2004). Autophagy and caspases: A new cell death program. *Cell Cycle*, *3*(9), 1124–1126. <https://doi.org/10.4161/cc.3.9.1097>
- Zhang, W., Shen, J., Su, H., Mu, G., Sun, J. H., Tan, C. P., ... Mao, Z. W. (2016). Co-delivery of cisplatin prodrug and Chlorin e6 by mesoporous silica nanoparticles for chemo-photodynamic combination therapy to combat drug resistance. *ACS Applied Materials and Interfaces*, *8*(21), 13332–13340. <https://doi.org/10.1021/acsami.6b03881>
- Zhang, X., Li, L., Liu, Q., Wang, Y., Yang, J. G., Qiu, T., & Zhou, G. (2019). Co-delivery of rose bengal and doxorubicin nanoparticles for combination photodynamic and chemo-therapy. *Journal of Biomedical Nanotechnology*, *15*(1), 184–195. <https://doi.org/10.1166/jbn.2019.2674>
- Zhou, L., Zhou, J. H., Dong, C., Ma, F., Wei, S. H., & Shen, J. (2009). Water-soluble hypocrellin a nanoparticles as a photodynamic therapy delivery system. *Dyes and Pigments*, *82*(1), 90–94. <https://doi.org/10.1016/j.dyepig.2008.11.009>

How to cite this article: Sztandera K, Gorzkiewicz M, Klajnert-Maculewicz B. Nanocarriers in photodynamic therapy—in vitro and in vivo studies. *WIREs Nanomed Nanobiotechnol*. 2019;e1509. <https://doi.org/10.1002/wnan.1599>



Article

In Search of a Phosphorus Dendrimer-Based Carrier of Rose Bengal: Tyramine Linker Limits Fluorescent and Phototoxic Properties of a Photosensitizer

Krzysztof Sztandera ¹, Monika Marcinkowska ¹ , Michał Gorzkiewicz ¹ , Anna Janaszewska ¹, Regis Laurent ^{2,3}, Maria Zabłocka ⁴, Serge Mignani ^{5,6}, Jean Pierre Majoral ^{2,3,*} and Barbara Klajnert-Maculewicz ^{1,7,*}

¹ Department of General Biophysics, Faculty of Biology and Environmental Protection, University of Lodz, 141/143 Pomorska St., 90-236 Lodz, Poland; krzysztof.sztandera@unilodz.eu (K.S.); monika.marcinkowska@biol.uni.lodz.pl (M.M.); michal.gorzkiwicz@biol.uni.lodz.pl (M.G.); anna.janaszewska@biol.uni.lodz.pl (A.J.)

² Laboratoire de Chimie de Coordination, CNRS, 205 Route de Narbonne, BP44099, 31077 Toulouse CEDEX 4, France; regis.laurent@lcc-toulouse.fr

³ LCC-CNRS, Université de Toulouse, CNRS, 31077 Toulouse, France

⁴ Centre of Molecular and Macromolecular Studies, Polish Academy of Sciences, 112 Sienkiewicza St., 90-363 Lodz, Poland; zabloc@cbmm.lodz.pl

⁵ CQM-Centro de Quimica da Madeira, Universidade da Madeira, Campus da Penteada, 9020-105 Funchal, Portugal; serge_mignani@orange.fr

⁶ Laboratoire de Chimie et de Biochimie Pharmacologiques et Toxicologiques, Université Paris Descartes, PRES Sorbonne Paris Cité, CNRS UMR 860, 45 rue des Saints Peres, 75006 Paris, France

⁷ Leibniz-Institut für Polymerforschung Dresden e.V., 6 Hohe St., 01069 Dresden, Germany

* Correspondence: jean-pierre.majoral@lcc-toulouse.fr (J.P.M.); barbara.klajnert@biol.uni.lodz.pl (B.K.-M.)

Received: 9 May 2020; Accepted: 19 June 2020; Published: 23 June 2020



Abstract: Photodynamic therapy (PDT) is a skin cancer treatment alternative to chemotherapy and radiotherapy. This method exploits three elements: a phototoxic compound (photosensitizer), light source and oxygen. Upon irradiation by light of a specific wavelength, the photosensitizer generates reactive oxygen species triggering the cascade of reactions leading to cell death. The positive therapeutic effect of PDT may be limited due to low solubility, low tumor specificity and inefficient cellular uptake of photosensitizers. A promising approach to overcome these obstacles involves the use of nanocarrier systems. The aim of this initial study was to determine the potential of the application of phosphorus dendrimers as carriers of a photosensitizer—rose bengal (RB). The primary goal involved the synthesis and in vitro studies of covalent drug–dendrimer conjugates. Our approach allowed us to obtain RB–dendrimer conjugates with the use of tyramine as an aromatic linker between the carrier and the drug. The compounds were characterized by FT-IR, ¹H NMR, ¹³C NMR, ³¹P NMR, size and zeta potential measurements and spectrofluorimetric analysis. The dialysis to check the drug release from the conjugate, flow cytometry to specify intracellular uptake, and singlet oxygen generation assay were also applied. Finally, we used MTT assay to determine the biological activity of the tested compounds. The results of our experiments indicate that the conjugation of RB to phosphorus dendrimers via the tyramine linker decreases photodynamic activity of RB.

Keywords: skin cancer; photodynamic therapy; phosphorus dendrimers; rose bengal (RB)

1. Introduction

According to World Health Organization (WHO), the incidence of both non-melanoma and melanoma skin cancers has been increasing over the past decades. Currently, between two and three million non-melanoma skin cancers and 132,000 melanoma skin cancers occur globally each year [1]. Chemotherapy and radiotherapy are used successfully in the treatment of these types of cancer, but cause many complications and side effects [2,3]. Limited specificity of those therapies provokes the search for safer and more effective treatment strategies [4]. Photodynamic therapy (PDT) is a very interesting alternative method of skin cancer therapy [5]. In particular, the effectiveness of PDT depends on three factors: the presence of molecular oxygen, a specific wavelength of light, and the use of special particles called photosensitizers or photosensitizing agents (PSs) [6].

In the first step of PDT, photosensitizer absorbs the quantum of light and goes into the singlet excited state. Then, due to the non-radiant intercrossing transition, the PS reaches the excited triplet state. This form is capable of exciting biomolecules around it. The excess of energy is transferred to oxygen which triggers the production of reactive oxygen species (ROS), causing tissue damage. The result of such mechanism involves the accumulation of superoxide anion radicals. However, another mechanism seems to be more significant in photodynamic therapy. After the occurrence of the excited triplet state of the photosensitizer, there is a direct transfer (without participation of biomolecules) of energy to the oxygen, which leads to the formation of singlet oxygen. Singlet oxygen belongs to very strong oxidizers, so its life in tissue is very short. Both mechanisms (Figure 1) take place in photosensitization and they share the resultant outcome of toxicity, which depends on the concentration of oxygen in the tissue, the pH, the dielectric constant of the tissue and other factors [7–9].

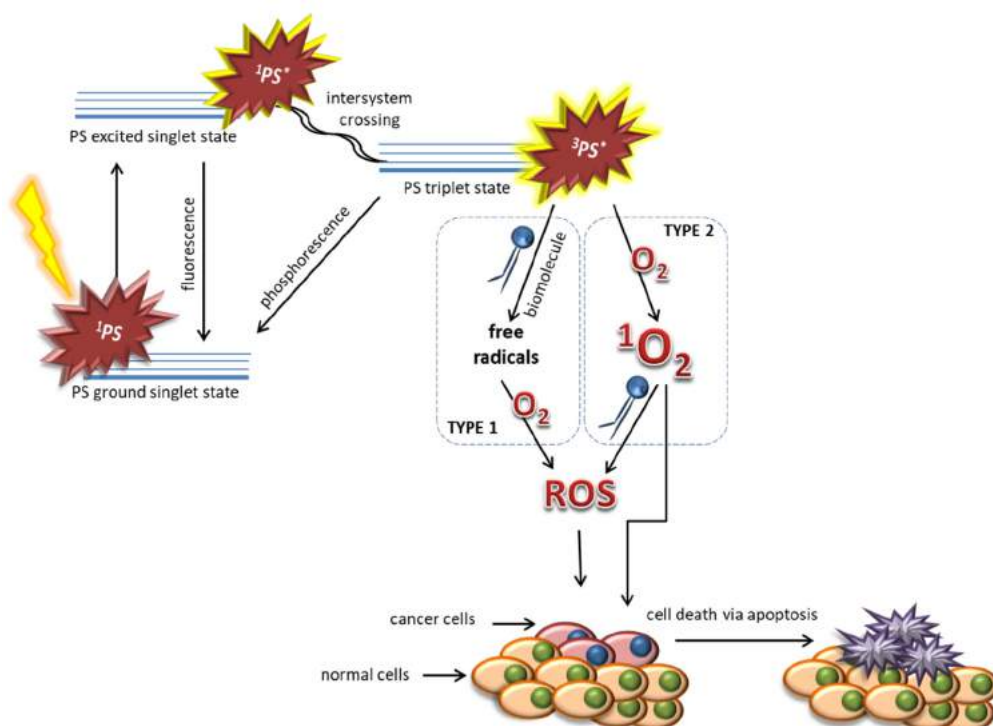


Figure 1. Two possible mechanisms of the photodynamic effect.

Some recent studies proved that covalent attachment of photosensitizers to nanomaterials can increase phototherapy outcome and reduce their side effects [10,11]. Metal nanoparticles [12], polymeric micelles [13], and ceramic-based nanoparticles [14] were recognized as potential carriers of photosensitizers. Moreover, it was previously demonstrated that the use of nanoparticles avoids the transfer of the photosensitizer to healthy tissues [15,16].

Phosphorus dendrimers are very promising carriers, e.g., for therapeutic siRNA [17]. Polycationic phosphorus dendrimers [18] are also able to transport negatively charged molecules, such as rose bengal (RB) [19]. Combining cationic charges present on the surface of phosphorus dendrimers and anionic charges of the RB allows to obtain complexes in which the photosensitizer retains its properties in vitro [20]. However, the complexes can show a very serious disadvantage—low stability in vivo.

Therefore, in the initial study, we decided to design more stable conjugates containing RB and polycationic phosphorus dendrimers using a linker—a small particle working as a bridge between RB and phosphorus dendrimers.

The aim of our work was to chemically modify rose bengal in order to graft it on the surface of phosphorus dendrimers and to investigate the influence of the resulting conjugates on the effectiveness of phototherapy in vitro.

2. Results

2.1. Synthesis and Characterization of Conjugates

Our approach allowed to obtain rose bengal–phosphorus dendrimer conjugates using tyramine as a linker. The compounds were characterized by FT-IR, ^1H NMR, ^{13}C NMR and ^{31}P NMR. Synthesis of rose bengal–phenol (RB-TYR) required a two-step reaction. The first step involves the conversion of the carboxylic group of rose bengal to an acid chloride group which in turn reacts with tyramine, forming an amide bond. The progress of reactions was confirmed by TLC, MALDI-TOF, ^1H NMR and FT-IR spectroscopy (Figure 2). For example, the reaction was monitored by FT-IR: we observed the disappearance of the band at 1780 cm^{-1} (for acid chloride) on behalf of a new one at 1614 cm^{-1} (for amide group), which confirmed the conversion of acid chloride into the corresponding phenol (Figure 2C).

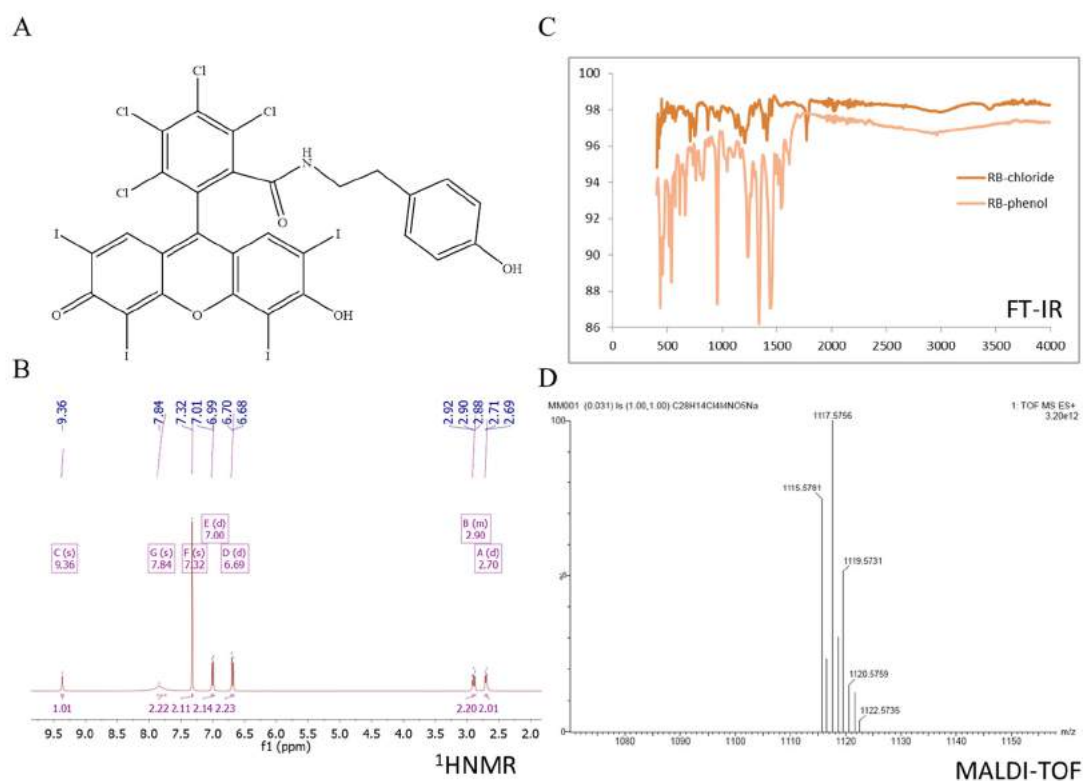


Figure 2. Results for rose bengal–phenol: (A) chemical formula; (B) ^1H NMR spectra (DMSO- d_6 ; ppm), (C) FT-IR spectra (neat), (D) MALDI-TOF spectrum of obtained rose bengal–phenol at $m/z = 1117.57$. The calculated molecular weight is M: 1116.

The second step of the reaction concerns the partial grafting of such a modified RB derivative (65 μmol) onto the surface of phosphorus dendrimers (21 μmol). For this purpose we prepared phosphorus dendrimers of generation 1 to 3 (G1, G2 and G3) with P(S)Cl₂-terminal groups according to the synthesis pathway previously described [21]. The third step involved the addition of amino groups on the remaining P-Cl bonds on the outer shell of the phosphorus dendrimers followed by protonation of the grafted amino groups with HCl.

³¹P NMR spectra for G1-3RB (A) and G1-3RB-9 amine (B) are presented in the Figure 3. On the upper panel (A), we observed the presence of a signal at 73.13 ppm characteristic for the P(S)CIRB group occurring on the surface of modified phosphorus dendrimer and a signal at 61.99 ppm characteristic for unmodified P(S)Cl₂ groups. The signals at 8.09 ppm (6A) and 8.07 ppm (6B) correspond to the core (P₃N₃). On the lower panel (B), after the grafting of amino groups, we observed the disappearance of both chemical shifts (73.13 and 61.99 ppm), on behalf of two new signals at 68.45 ppm (-P(S)RB-pyrrolidine) and 68.80 ppm (-P(S)(pyrrolidine)₂). ¹H NMR values were in agreement with the presence of three molecules of RB and nine molecules of pyrrolidine on the surface of the dendrimer.

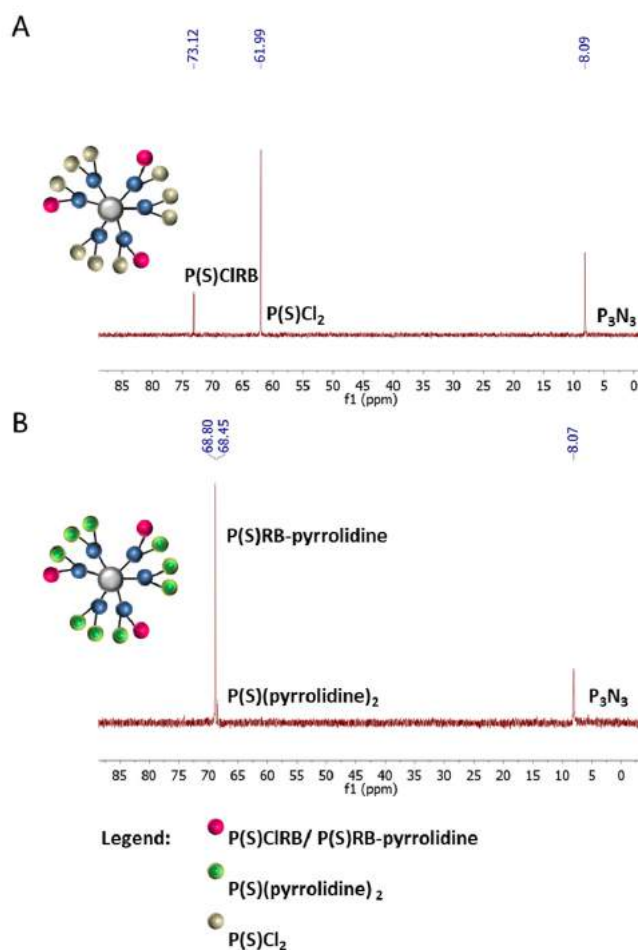


Figure 3. ³¹P NMR spectra for: (A) G1-3RB (THF-d₈; ppm), (B) G1-3RB-9 pyrrolidine (G1-3RB-pyrro) (CDCl₃; ppm).

Using the same technique, we modified the surface of the G2 phosphorus dendrimer containing 12P(S)Cl₂-terminal groups with 3 equivalents of RB derivative and 21 equivalents of amine. In Figure 4, ³¹P NMR spectra for G2-3RB (A) and G2-3RB-21 amine (B) are presented. On the upper panel (A) we observed a chemical shift at 73.26 ppm characteristic for the P(S)CIRB group occurring on the surface of the modified phosphorus dendrimer and signals at 8.39 (core), 62.40 (-P(S)Cl₂) and 62.24 (P₁) ppm. The signal at 8.39 ppm corresponds to the core (P₃N₃). On the lower panel (B), after the addition of pyrrolidine, we observed the appearance of new signals at the 68.76 (-P(S)RB-pyrrolidine) and 69.40 ppm (-P(S)(pyrrolidine)₂). ¹H NMR values were in agreement with the presence of 3 molecules of RB and 21 molecules of pyrrolidine on the surface of the dendrimer.

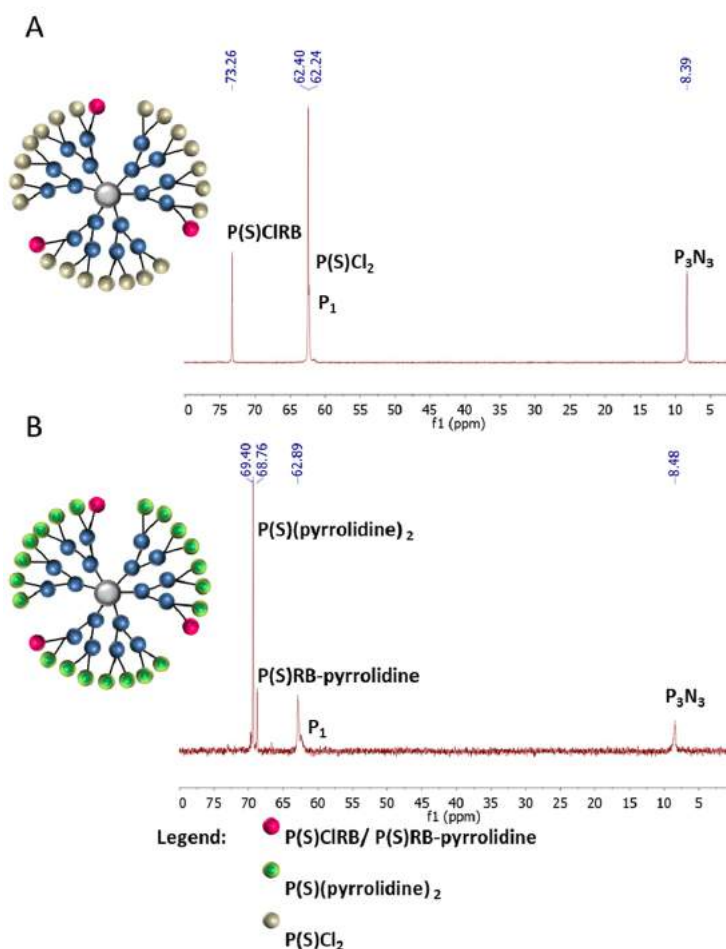


Figure 4. ³¹P NMR spectra for: (A) G2-3RB (THF-d₈; ppm), (B) G2-3RB-21 pyrrolidine (G2-3RB-pyrro) (CDCl₃; ppm).

Finally, we modified the surface of the G3 phosphorus dendrimer containing 24 P(S)Cl₂-terminal groups with three equivalents of RB derivative and 45 equivalents of amine. In Figure 5, ³¹P NMR spectra for G3-3RB (A) and G3-3RB-45 pyrrolidine (B) are presented. On the upper panel (A) we observed new chemical shift at 72.55 ppm characteristic for the P(S)CIRB group occurring on the surface of the modified phosphorus dendrimer and other signals at 8.30 (core), 61.90 (P₂), 62.24 (P₁), 62.78 (P₃) ppm. On the lower panel (B), after the addition of pyrrolidine, we observed the appearance of new signals at 67.69 (-P(S)RB-pyrrolidine) and 68.38 ppm (-P(S)(pyrrolidine)₂). ¹H NMR values were in agreement with the presence of 3 molecules of RB and 45 molecules of pyrrolidine on the surface of the dendrimer.

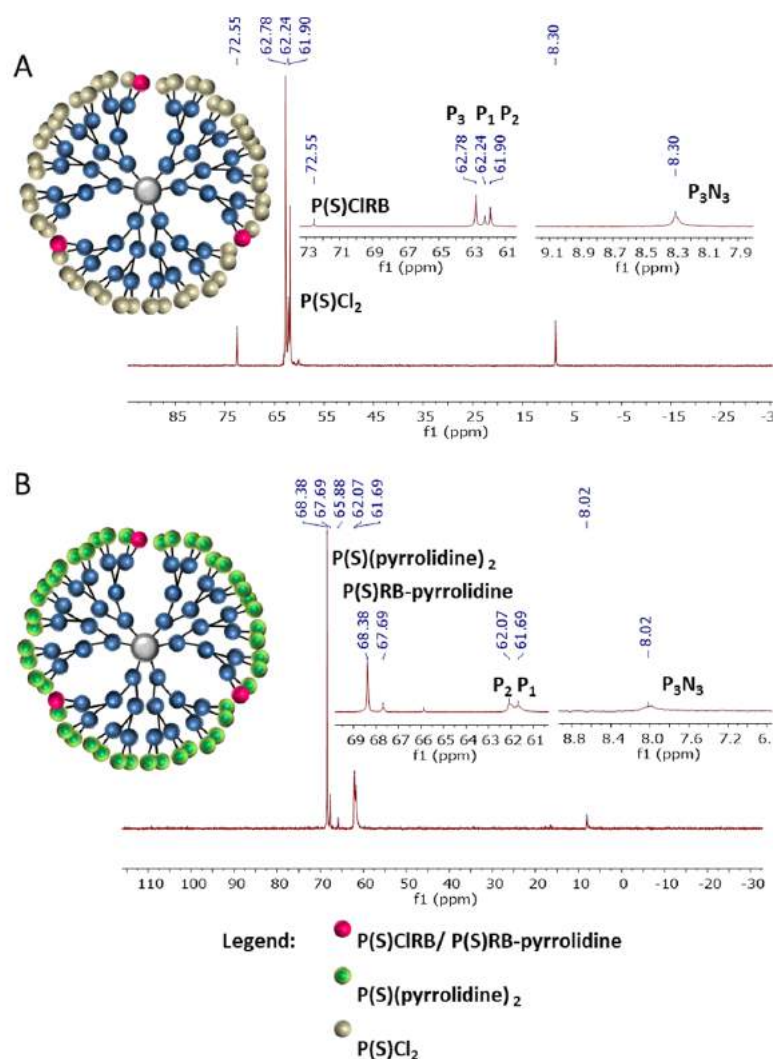


Figure 5. ^{31}P NMR spectra for: (A) G3-3RB (CDCl_3 ; ppm); (B) G3-3RB-45 pyrrolidine (G3-3RB-pyrro) (CDCl_3 ; ppm).

2.2. Spectroscopy Studies

Spectrofluorimetric analysis showed drastic changes of the spectral properties of RB upon modification with tyramine and subsequent conjugation to phosphorus dendrimers (Figure 6). The attachment of tyramine to RB caused a two-fold decrease in fluorescence intensity. Furthermore, the fluorescence of all conjugates was extremely low: G1-3RB-pyrro was non-fluorescent, the fluorescence of G2-3RB-pyrro and G3-3RB-pyrro was only slightly higher, and the fluorescence of G3 conjugate was sufficient for the next experiments. Moreover, the results showed the emission wavelength shift from 565 for RB and RB-TYR, to 575 and 580 nm for G3-3RB-pyrro and G2-3RB-pyrro, respectively.

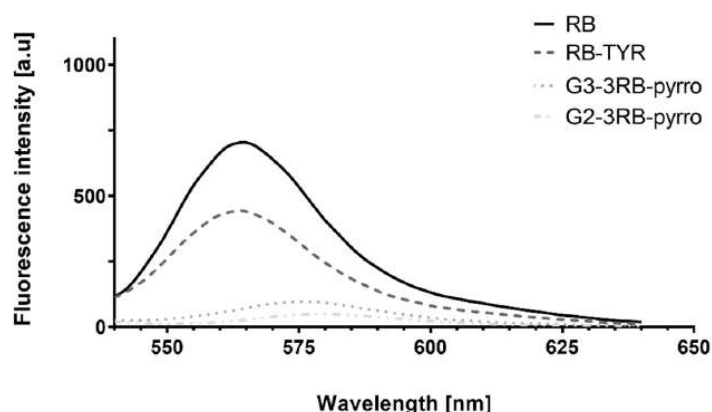


Figure 6. Fluorescence of rose bengal (RB), rose bengal modified with tyramine (RB-TYR) and conjugates of phosphorus dendrimers of the second and the third generation with three molecules of RB (G2-3RB-pyrro and G3-3RB-pyrro, respectively), dissolved in distilled water. Concentration of all compounds was calculated for RB and equaled 2.5 μ M. Due to the lack of fluorescence activity of the G1-3RB-pyrro conjugate, data are not shown. Excitation wavelength: 525 nm.

2.3. Size and Zeta Potential Measurements

It was shown that the G3-3RB-pyrro conjugate retained the nanometric size and significant surface positive charge (Table 1), potentially favoring efficient endocytosis and cell entry [22]. However, when compared with our previous research [23], the size of the tested conjugate was enlarged, suggesting the possibility of aggregation.

Table 1. Size and zeta potential of the G3-3RB-pyrro conjugate. Data presented as mean \pm SD.

| | Hydrodynamic Diameter (nm) | Zeta Potential (mV) |
|--------|----------------------------|---------------------|
| G3-3RB | 18.17 \pm 4.96 | 44.54 \pm 2.42 |

2.4. Drug Release Studies

The release of RB from the G3-3RB-pyrro conjugate was evaluated under two pH conditions (pH 5 and pH 7.4) (Figure 7). The results showed that in both cases, the release of RB is extremely low, plateauing after 8 h at 15% release. Furthermore, there was no significant difference between the release rates under both pH conditions.

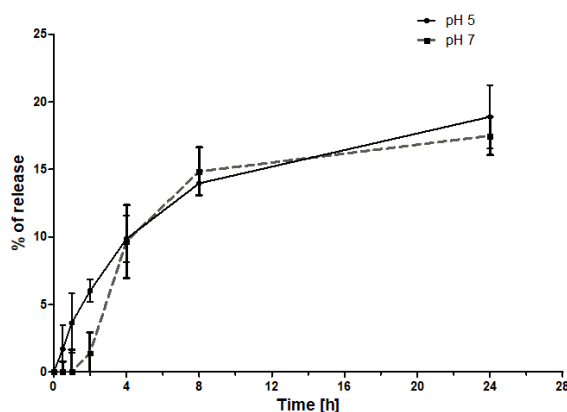


Figure 7. Release of RB from the G3-3RB-pyrro conjugate under different pH conditions. Data presented as mean \pm SD.

2.5. Cellular Uptake Assay

Uptake experiments showed significant differences in cell uptake rates between both compounds tested and cell lines (Figure 8). First, in all cell lines, RB showed similar potential to enter the cells, with its cellular uptake being the most efficient in comparison to other compounds. The modification of RB with tyramine decreased uptake level approximately by half, independently of cell line. Finally, the G3-3RB conjugate was characterized by moderate but slowed down cellular transport compared to free RB in the AsZ cell line, while for the BsZ and CsZ lines, cellular uptake was similar to RB-TYR.

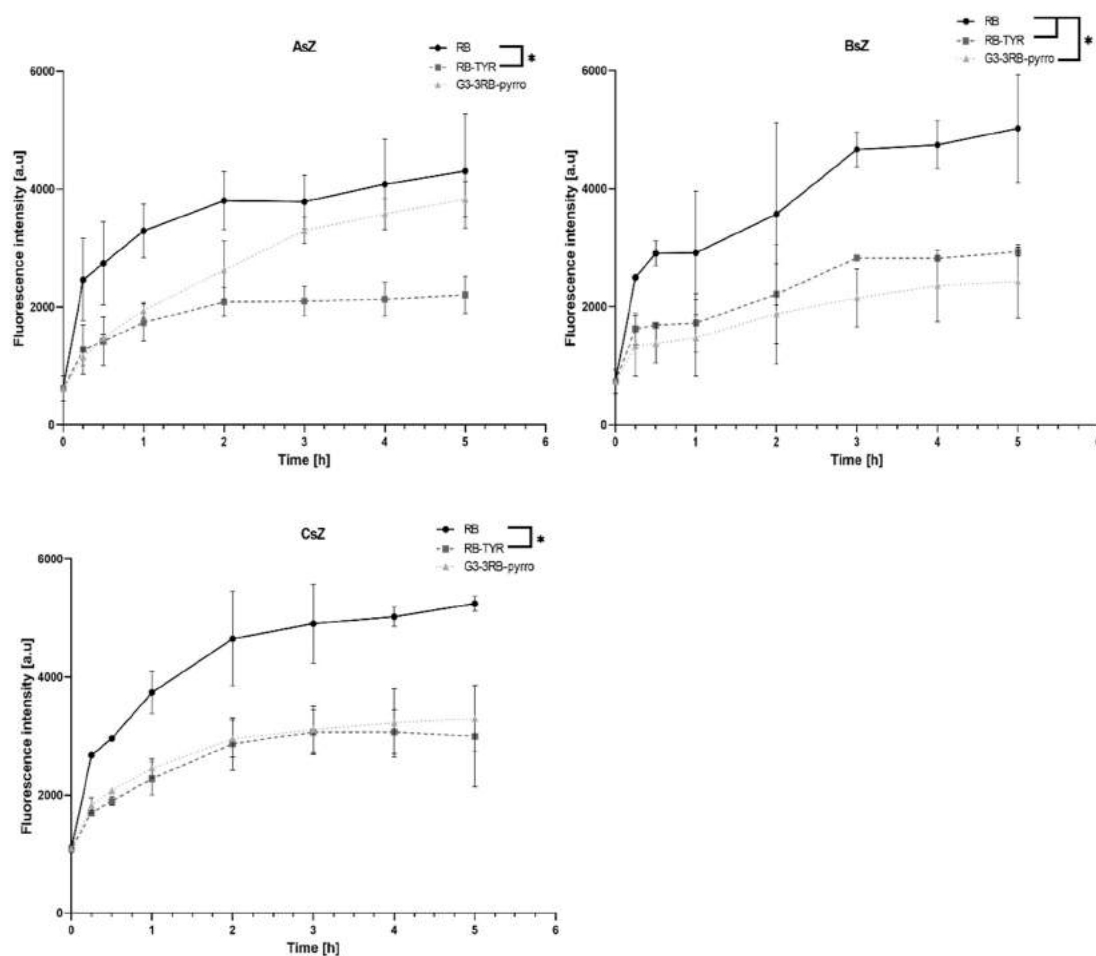


Figure 8. Cellular uptake of tested compounds (RB, RB-TYR, G3-3RB-pyrro at 5 μ M final concentration of RB) by AsZ, BsZ and CsZ cell lines. Data presented as mean \pm SD. * $p < 0.05$.

2.6. Singlet Oxygen Generation

Singlet oxygen generation by the compounds under evaluation was assessed with the use of a highly selective Singlet Oxygen Green Sensor (SOSG) probe. It was found that the modification of RB with tyramine and subsequent attachment of such construct to the G3 dendrimer gradually reduced singlet oxygen production (Figure 9). The RB-tyramine conjugation caused a decrease in singlet oxygen generation in comparison with free RB, and the covalent binding of RB-TYR to the dendrimer further reduced the level of fluorescence.

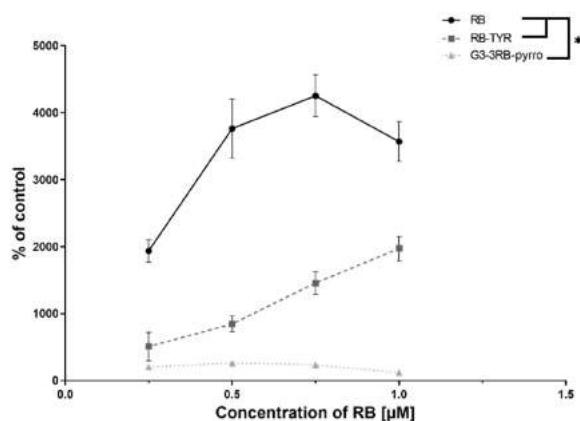


Figure 9. Comparison of singlet oxygen generation by free rose bengal (RB), rose bengal modified with tyramine (RB-TYR) and conjugate of phosphorus dendrimer of the third generation with rose bengal (G3-3RB-pyrro). Data presented as mean \pm SD. * $p < 0.05$.

2.7. Phototoxicity

Cytotoxicity studies performed with the use of MTT assay allowed to demonstrate an evident decrease in phototoxic activity with increasing modification of RB. In all cell lines, free RB showed the highest toxicity after irradiation, with RB-TYR being less toxic and G3-3RB-pyrro being almost non-toxic in the tested concentration range (Figure 10). Additionally, tested compounds were completely non-toxic without irradiation.

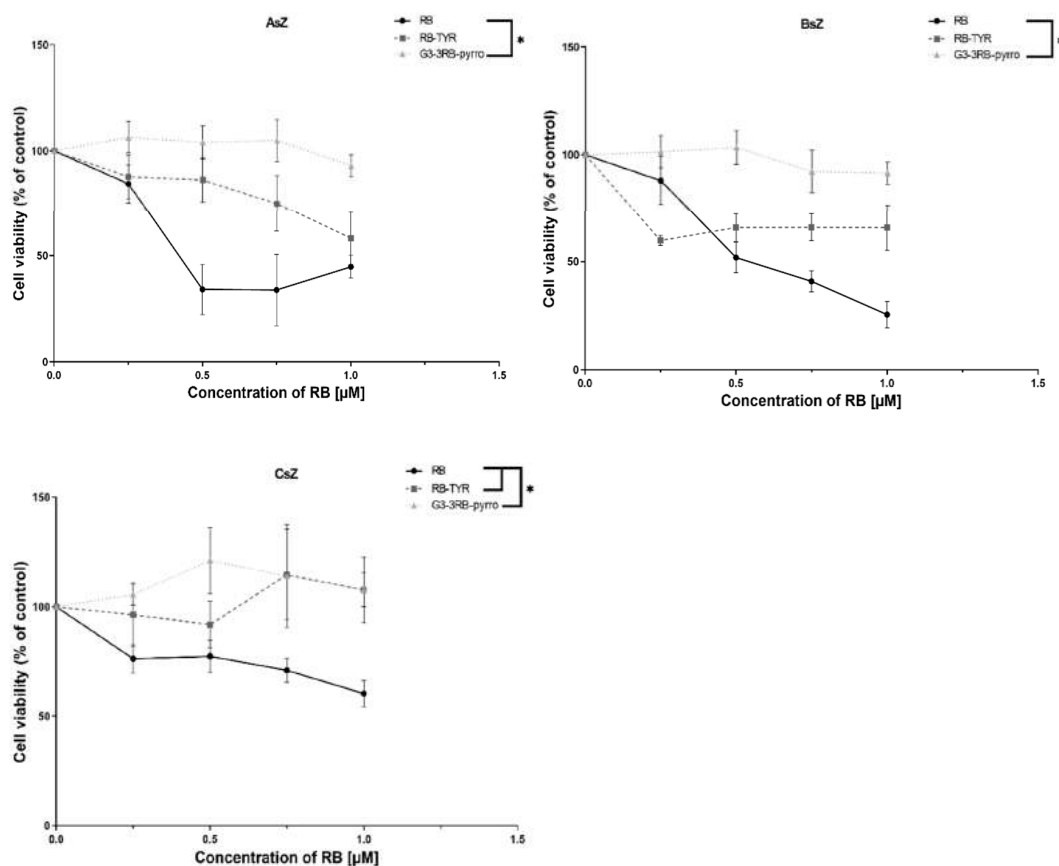


Figure 10. Phototoxic activity of rose bengal (RB), rose bengal modified with tyramine (RB-TYR) and conjugate of phosphorus dendrimer of the third generation with rose bengal (G3-3RB-pyrro). Data presented as mean \pm SD. * $p < 0.05$.

3. Discussion

Photodynamic therapy is based on the application of a photosensitizer that, upon irradiation by light of a specified wavelength, produces reactive oxygen species and singlet oxygen [24], the generation of which starts a cascade of reactions ultimately leading to cell death [25]. The ideal photosensitizer is characterized by the following: maximum absorbance between 650 and 850 nm, high efficiency of free radical production, fluorescence emission, low photodegradation, non-toxicity in the dark, lack of allergic reactions and other side effects [26]. Unfortunately, despite many years of research on photosensitizers, so far, no drug has been developed that would be characterized by all of these features. Therefore, photosensitizers are being subjected to chemical modifications, e.g., being combined with nanoparticles. Major benefits of using nanoparticles in PDT include protection of the drugs from degradation, improvement of their solubility, prolongation of blood half-life, modulation of pharmacokinetic properties and targeted delivery [11,27]. Modern techniques of nanotechnology allow to synthesize numerous nanoparticles with various shapes, sizes and properties. Among them, dendrimers deserve special attention. These highly branched, monodisperse, polyvalent polymers of well-defined, regular structure are characterized by high solubility, biopermeability, and high loading capacity. Dendrimers, due to their shape, structure and nanometric size, may also efficiently penetrate into the tumor environment and retain in tumor interstitium, which is described as enhanced permeability and retention (EPR) effect [28]. Due to their three-dimensional architecture, they provide the possibility of covalent conjugation of the drug to the functional surface groups or encapsulation inside the dendritic structure [29].

In order to create covalent bonding between the drug and the dendrimers, the choice of appropriate linker is crucial. Linkers are molecules possessing two functional sides that can be used for joining chemical compounds together. Capability to design different kinds of linkers enable their application in drug development, proteomics, imaging and DNA sequencing. Nowadays it is possible to manufacture linker with strictly defined chemical composition and properties, including high stability in changeable environment or, on the other hand, the possibility of specific cleavage. By using different linkers, it is possible to release the therapeutic compound in a specified place and time, which can contribute to the reduction of side effects of classical drug application. This includes linkers that are sensitive to the change of pH or temperature, enzymatic or redox reactions, light irradiation, and hypoxia [30,31]. However, it has been shown that in case of PDT, the drug does not have to be released due to the specificity of its anticancer activity [11,32].

Previously, non-covalent complexes based on a phosphorus dendrimer and RB have been evaluated *in vitro*. The formation of non-covalent complexes [19,33] and their promising application in PDT [20] have been described. In the present paper, we focused on the evaluation of the ability of phosphorous dendrimers of different generations covalently modified with RB to act as efficient carriers for this drug. Thus, we used tyramine as a stable linker with suitable length to ensure proper exposition of RB on the surface of the dendrimer [34]. The presence of the phenol group allows for the formation of stable O-P bonds in the framework of the phosphorus dendrimer, as demonstrated previously [35]. Our main goal involved the increase in the stability of the delivery system, which may be vital in the case of *in vivo* experiments in comparison to non-covalent complexes. In the initial *in vitro* studies, we examined the properties and stability of conjugates of phosphorus dendrimers with RB-TYR, as well as their ability to generate singlet oxygen and exert phototoxic effect *in vitro*.

Three conjugates of phosphorus dendrimers of different generations with RB (G1-, 2-, 3-3RB-pyrro) were successfully synthesized and characterized. Interestingly, the spectrofluorimetric studies revealed that even a small chemical modification of RB by the attachment of tyramine reduces its fluorescence two-fold in comparison to free RB. The conjugation of RB to phosphorus dendrimers using a tyramine linker caused further reduction of fluorescence. This effect is not unexpected and was previously described by Li et al. [36]. In general, we observed a decrease in fluorescence intensity with a decreasing generation of phosphorus dendrimers to such an extent that the G1 dendrimer did not show any fluorescence. Thus, in the next experiments we used RB, RB-TYR as an intermediate form,

and G3–3RB–pyrro as the conjugate with the highest fluorescence, which is important for effective PDT [37]. This conjugate retained its nano-size and positive surface electrostatic potential, which is important for efficient cellular uptake [22]. Furthermore, G3–3RB–pyrro was stable both in pH conditions of the bloodstream (pH 7.4) and the tumor environment (pH 5)—only a small amount of the drug was released from the conjugate, even after 24 h.

Since RB is a hydrophilic compound, it cannot penetrate the cell membrane by passive diffusion and most probably require specific membrane transporters. Repeated administration of the drug may lead to down-regulated of expression of those transporters, subsequently leading to drug resistance [38]. Therefore, we evaluated the cellular uptake of the tested compounds in order to check if the conjugation can improve intracellular delivery of the photosensitizer. First, we observed that the uptake level of RB–TYR was decreased approximately two-fold in comparison with free RB in all tested cell lines. This result may be caused by a reduced affinity of the chemically modified drug to membrane protein transporters. However, the conjugate in the AsZ cell line was uptaken as efficiently as the free drug, which indicated that the tested phosphorus dendrimer could act as an efficient nanocarrier. On the other hand, the uptake in the BsZ and CsZ cell lines was decreased to the level of RB–TYR. This phenomenon can be caused by differences in endocytosis processes in different cell lines, which was previously shown, e.g., for poly(propyleneimine) (PPI) glycodendrimers [39,40].

Since one of the most important feature of a photosensitizer is the generation of singlet oxygen, which is the basic mechanism responsible for death of cancer cells [41,42], we evaluated this process under the influence of the tested compounds. However, the results showed that RB–TYR exhibits decreased production of singlet oxygen in comparison to free RB, while G3–3RB–pyrro practically does not show this ability. These observations were consistent with the results of the analysis of fluorescence properties of the tested compounds and, moreover, they translated into the results of cytotoxicity tests, which showed that free RB has the highest phototoxicity, and with its progressive modification (attachment of tyramine and then the G3 dendrimer), the reduction of toxic effect occurs.

4. Materials and Methods

4.1. Materials

Phosphorus dendrimers (and their conjugates with RB) of the first, second and third generation were synthesized in the Laboratoire de Chimie de Coordination, CNRS (Figure 11).

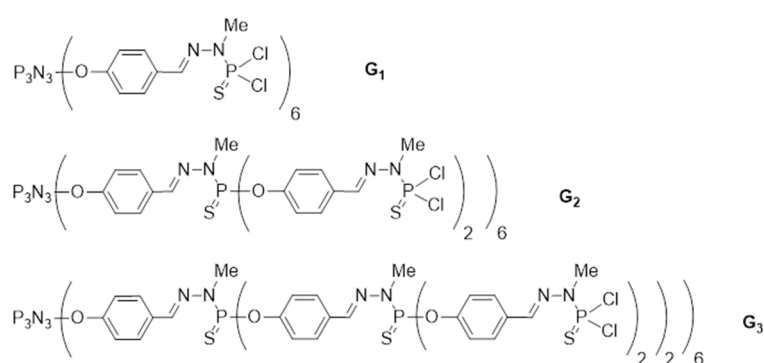


Figure 11. The schemes of G1, G2, G3 phosphorus dendrimers.

Rose bengal, tyramine, cesium carbonate, thionyl chloride, 1-(2-aminoethyl)pyrrolidine, triethylamine (TEA), N,N-diisopropylethylamine (DIPEA), fetal bovine serum, penicillin/streptomycin solution, trypsin–EDTA solution, and MTT (3-(4,5-dimethyl-2-thiazolyl)-2,5-diphenyl-2H-tetrazolium bromide) were purchased from Sigma-Aldrich, Taufkirchen, Germany and TCI, Zwijndrecht, Belgium. Dulbecco’s phosphate buffered saline with no calcium and no magnesium (DPBS) was purchased from Biowest, France. 154 CF culture medium was obtained from Gibco, Thermo Fisher Scientific,

Waltham, MA, USA. Chelex 100 Resin was obtained from Bio-Rad. Singlet oxygen sensor green (SOSG) was purchased from Molecular Probes, ThermoFisher, Waltham, MA, USA. Dimethyl sulfoxide (DMSO) was purchased from POCH (Gliwice, Poland). Snake-Skin™ Dialysis Tubing, 3.5K MWCO, 22 mm was obtained from ThermoFisher, Waltham, MA, USA. Murine basal cell carcinoma lines (AsZ, BsZ, CsZ) were kindly provided by Dr. Ervin Epstein (Children's Oakland Research Institute, Oakland, CA, USA).

4.2. Methods

4.2.1. Preparation of Drug–Dendrimer Conjugates—General Information

All reactions were carried out in organic solvents using standard high vacuum and dry-argon techniques. All purchased chemicals were used without further purification. All solvents were dried and purified with the MBraun SPS 800 solvent purification system before use. ^1H , ^{13}C , and ^{31}P NMR spectra were recorded with DPX300 and AV400 spectrometers (Bruker, Billerica, MA, USA). All ^{13}C NMR and ^{31}P NMR spectra were generally recorded decoupled $\{^1\text{H}\}$. The signal of the nondeuterated solvent served as an internal standard.

IR spectra were recorded with Perkin Elmer Frontier (Waltham, MA, USA) and MALDI-TOF spectra with MALDI TOF MICROMASS WATERS (Milford, MA, USA).

4.2.2. Synthesis of the Rose Bengal Acid Chloride

Rose bengal disodium salt (2 g; 2 mmol) was dried, dissolved in 20 mL of chloroform and cooled to 0 °C. Thionyl chloride (10 mL) was added and the resulting solution was stirred for 2 h at 60 °C under reflux and then stirred overnight at room temperature (RT). The reaction was carried out in an argon atmosphere. After completion of the reaction (checked by TLC), the solvent was removed under vacuum line at 50 °C. Solid residue was characterized by IR with appearance of a band at 1780 cm^{-1} corresponding to acid chloride. Crude solid residue was carried forward as such for next step, because purification leads to the conversion of chloride into acid.

4.2.3. Synthesis of Rose Bengal–Tyramine

RB acid chloride (0.5 g, 0.5 mmol) was mixed with tyramine (0.1 g; 0.65 mmol), dried and kept in THF (30 mL). In the next step TEA (0.65 mmol) was added. The resulting mixture was stirred for 24 h. After completion of the reaction (checked by TLC), the solvent was evaporated under vacuum. Crude residue was purified on silica column using ethyl acetate and methanol as a mobile phase (20% of methanol and 80% of ethyl acetate). The scheme of the rose bengal modification is presented in Figure 12.

The rose bengal modified with tyramine was characterized by NMR (^1H and ^{13}C NMR). ^1H NMR (DMSO- d_6 ; ppm): δ 9.36 (s, 1H, NHCO), 7.84 (s, 2H, OH), 7.32 (s, 2H, ArH_{RB}), 7.00 (d, $J = 8.4$ Hz, ^2H , CHAr_{TYR}), 6.69 (d, $J = 8.4$ Hz, ^2H , CHAr_{TYR}), 2.90 (t, $J = 8.6$ Hz, 2H, CH_2NHCO), 2.70 (t, $J = 8.6$ Hz, 2H, $\text{CH}_2\text{Ar}_{\text{TYR}}$). ^{13}C NMR (DMSO- d_6 ; ppm): δ 172.09 ($\text{Ar}_{\text{RB}}=\text{O}$, $\text{Ar}_{\text{RB}}-\text{O}^-$), 162.09 (NCO), 157.88 ($\text{Ar}_{\text{RB}}-\text{O}$), 156.63 ($\text{Ar}-\text{C}-\text{Cl}$), 137.37 ($\text{Ar}_{\text{RB}}-\text{Cl}$, $\text{C}_{\text{TYR}}-\text{CH}_2$), 130.91 (Ar_{TYR}), 130.26 ($\text{Ar}_{\text{RB}}-\text{Cl}$), 115.81 (Ar_{TYR}), 111.61, 97.12 ($\text{Ar}_{\text{RB}}-\text{I}$), 97.07 ($\text{Ar}_{\text{RB}}-\text{I}$), 76.18 (C-CONH), 44.09 (CH_2TYR), 34.01 (CH_2TYR). IR spectra (neat) show the disappearance of the band at 1780 cm^{-1} and the appearance of a new band at 1614 cm^{-1} , which confirms the conversion of acid chloride into the corresponding phenol. Mass spectra corroborate the formation of the desired RB–tyramine derivative (Figure 13).

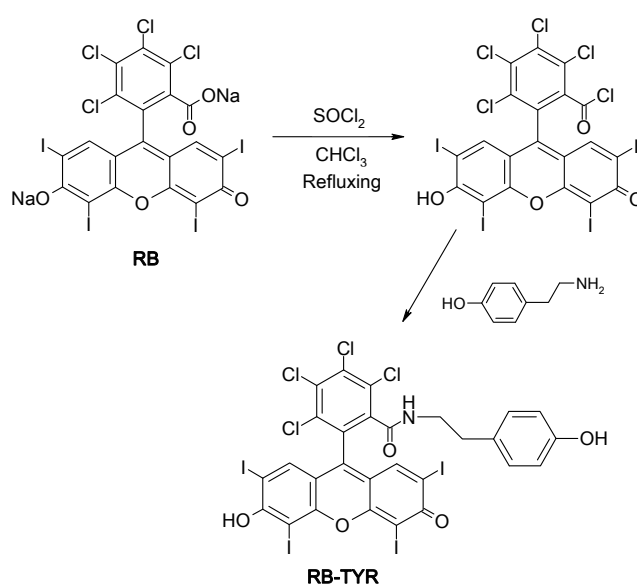


Figure 12. The scheme of the RB–TYR synthesis.

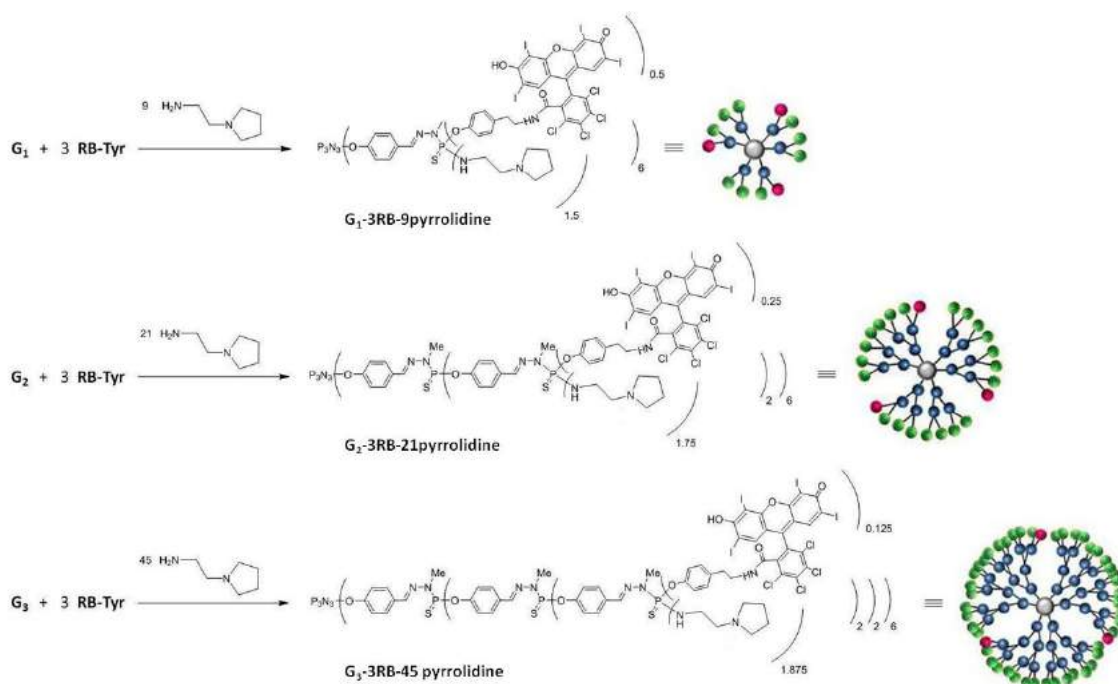


Figure 13. The scheme of the synthesis of the G₁–, 2–, 3–RB–pyrrolidine conjugates.

4.2.4. Synthesis of Rose Bengal–G₁, G₂, G₃ Phosphorus Dendrimers—Pyrrolidine Conjugates

Preparation of the PS-Cl₂ G₁, G₂, G₃ Dendrimer Conjugates Containing Three Molecules of Rose Bengal

RB–TYR (65 μmol) and cesium carbonate (65 μmol) were dried under vacuum, dissolved in 20 mL of THF and kept in dark at RT. A total of 21 μmol of PS-Cl₂ G₁ or PS-Cl₂ G₂, or PS-Cl₂ G₃ dendrimer were added. The resulting mixtures were stirred for 72 h in an argon atmosphere. After completion of the reaction, the solvent was evaporated under reduced pressure. The residue was dissolved in 10 mL THF and precipitated in 100 mL pentane.

The structure of the G₁–3RB conjugate was controlled by ³¹P NMR, ¹H NMR, ¹³C NMR in THF-d₈. ³¹P NMR: δ 8.09 (s, P₀), 61.99 (s, P₁), 73.13 (s, P₁-tyramine) ppm; ¹H NMR: 7.60 (m, 18H,

ArH_{Den} and CH=N), 7.24–6.99 (m, 24H, ArH_{Den}, ArH_{RB}, ArH_{TYR}), 6.68 (d, J = 7.2 Hz, 6H, ArH_{TYR}), 3.52–3.38 (m, 18H, P-N-CH₃), 3.10 (s, 6H, CH₂-NH), 2.94 (s, 6H, CH₂-Ar_{TYR}); ¹³C NMR: δ 162.37 (NCO), 158.39 (C_{Ar}O), 156.32 (Ar_{TYR}-O), 152.34 (C_{Ar}-Den), 139.44 (CH=N), 139.22 (C_{RB}-Cl), 137.18 (C=C-I), 136.65 (C_{RB}-CO), 135.81 (Ar_{TYR}), 131.04 (C_{Ar}-Den), 129.49 (Ar_{TYR}), 129.06 (C_{RB}-Cl), 129.03 (C_{Ar}-Den), 128.11 (C_{RB}-Cl), 127.74 (C_{RB}-Cl), 124.53 (C_{Ar}-RB), 120.94 (C_{Ar}-Den), 115.16 (Ar_{TYR}), 94.49 (C_{RB}-I), 78.20 (C_{RB}), 44.09 (CH₂_{TYR}), 34.01 (CH₂_{TYR}), 29.72 (br.s., P-N-CH₃).

The structure of the G2–3RB conjugate was controlled by ³¹P NMR, ¹H NMR, ¹³C NMR in THF-d₈. ³¹P NMR: δ 8.39 (s, P₀), 62.24 (s, P₁), 62.40 (s, P₂), 73.26 (s, P₂-tyramine) ppm; ¹H NMR: δ 7.76–7.55 (m, 54H, ArH_{Den} and CH=N), 7.27 (d, J = 16.8, d, J = 8.8 Hz, 36H, ArH_{Den}), 7.09–7.06 (m, 6H, ArH_{TYR}), 7.02–7.00 (m, 6H, ArH_{RB}), 6.68 (d, J = 2.6 Hz, 6H, ArH_{TYR}), 3.46 (d, J = 14.0 Hz, 36H, P-N-CH₃), 3.34 (d, J = 10.4 Hz, 18H, P-N-CH₃), 2.88–2.63 (m, 12H, CH₂-NH, CH₂-Ar); ¹³C NMR: δ 162.42 (NCO), 158.39 (C_{Ar}O), 156.27 (Ar_{TYR}), 151.92 (C_{Ar}-Den), 151.36 (C_{Ar}-Den), 148.13 (C_{RB}-Cl), 141.88 (CH=N), 139.48 (CH=N), 136.66 (C_{RB}-Cl), 135.86 (Ar_{TYR}), 132.38 (C_{RB}-Cl), 131.85 (C_{Ar}-Den), 131.07 (C_{Ar}-Den), 129.55 (Ar_{TYR}), 128.51 (C_{RB}-Cl), 128.10 (C_{Ar}-Den), 127.76 (C_{Ar}-Den), 124.90 (C_{RB}-Cl), 123.93 (C_{Ar}-RB), 121.64 (C_{Ar}-Den), 121.10 (C_{Ar}-Den), 115.19 (C_{Ar}-RB-OH), 78.82 (C_{RB}-I), 78.26 (C_{RB}), 44.00 (CH₂_{TYR}), 34.11 (CH₂_{TYR}), 31.30 (br.s. P-N-CH₃).

The structure of the G3–3RB conjugate was controlled by ³¹P NMR, ¹H NMR, ¹³C NMR in CDCl₃. ³¹P NMR: δ 8.30 (s, P₀), 61.90 (s, P₂), 62.24 (s, P₁), 62.78 (s, P₃), 72.55 (s, P₃-tyramine) ppm; ¹H NMR: δ 7.97–7.35 (m, 116H, ArH_{Den} and CH=N), 7.21 (m, 72H, ArH_{Den}), 7.02–6.90 (m, 6H, ArH_{TYR}), 6.90 (s, 6H, ArH_{RB}), 6.70 (d, J = 6.8 Hz, 6H, ArH_{TYR}), 3.46–3.18 (m, 126H, P-N-CH₃), 2.84 (d, J = 11.4 Hz, 6H, CH₂-NH, CH₂-Ar), 2.72 (s, 6H, CH₂-Ar_{TYR}); ¹³C NMR: δ 156.81 (NCO), 155.22 (C_{Ar}O), 151.79 (Ar_{TYR}), 151.79 (Ar-CCl), 151.73 (C_{Ar}-Den), 151.35 (C_{Ar}-Den), 140.86 (C_{RB}-Cl), 140.68 (CH=N), 139.10 (CH=N), 136.24 (Ar_{TYR}), 132.21 (C_{RB}-Cl), 131.52 (C_{Ar}-Den), 130.05 (C_{Ar}-Den), 129.42 (Ar_{TYR}), 128.75 (C_{Ar}-Den, C_{RB}-Cl), 128.35 (C_{Ar}-Den), 121.81 (C_{Ar}-Den), 121.28 (C_{Ar}-Den, Ar_{RB}), 115.72 (C_{Ar}-RB-OH), 77.33 (C_{RB}-I), 74.08 (C_{RB}-I), 68.57 (C_{RB}), 42.84 (CH₂_{TYR}), 33.14 (CH₂_{TYR}), 30.62 (br.s. P-N-CH₃).

Preparation of the PS-Cl₂ G1, G2, G3 Dendrimer Conjugates Containing Three Molecules of Rose Bengal and 9, 21 and 45 Molecules of Pyrrolidine, Respectively

The conjugates (16 μmol) bearing 3 RB units on their surface and 9, 21 or 45 terminal P-Cl bonds in 20 mL of THF were mixed with the excess of anhydrous sodium sulphate. The solution was cooled to 0 °C. (DIPEA) (144, 336 and 730 μmol, respectively) was added, followed by the slow addition of 1-(2-aminoethyl)pyrrolidine (144, 336 and 730 μmol, respectively), and then the solution was stirred for 6h. After completion of the reaction controlled by ³¹P NMR, the solvent was evaporated under reduced pressure. The residue was extracted with dichloromethane (DCM) (20 mL) and 10% K₂CO₃ in water (10 mL). The organic layer was dried over magnesium. The residue was again dissolved in 10 mL THF and precipitated in 100 mL pentane. The last step involved the protonation of the grafted amino groups with HCl, subsequently leading to the formation of charged phosphorus dendrimers G1–3RB–9 pyrrolidinium, G2–3RB–21 pyrrolidinium and G3–3RB–45 pyrrolidinium (Figure 14).

The structure of the G1–RB–pyrrolidine conjugate was controlled by ³¹P NMR, ¹H NMR, ¹³C NMR in CDCl₃. ³¹P NMR: δ 8.07 (s, P₀), 68.45 (s, P₁-RB), 68.80 ppm (s, P₁-pyrrolidine); ¹H NMR: δ 7.46 (d, J = 10.6 Hz, 18H, ArH_{Den} and CH=N), 7.18–6.50 (m, 30H, ArH_{Den}, ArH_{RB}, ArH_{TYR}), 3.15 (d, J = 9.4 Hz, 18H, P-N-CH₃), 3.07–2.97 (m, 30H, CH₂-Ar, CH₂NH), 2.58–2.52 (m, 54H, CH₂N, NCH₂), 1.79–1.76 (m, 36H, CH₂); ¹³C NMR of G1–RB–pyrrolidine: δ 158.19 (C_{Ar}O), 156.80 (NCO), 156.32 (Ar_{TYR}), 152.34 (C_{Ar}-Den), 151.79 (Ar-CCl), 139.44 (CH=N), 139.22 (C-Cl), 137.18 (C-I), 136.60 (C_{RB}-CO), 135.75 (Ar_{TYR}), 131.04 (C_{Ar}-Den), 129.49 (Ar_{TYR}), 129.06 (C_{RB}-Cl), 129.03 (C_{Ar}-Den), 128.11 (C-Cl), 127.74 (C_{Ar}-Den), 127.51 (Ar_{TYR}, Ar_{RB}), 121.12 (Ar_{TYR}), 121.05 (C_{Ar}-Den), 84.88 (C_{RB}-I), 56.44 (CH₂), 39.81 (N-CH₂), 39.81 (CH₂-N), 37.07 (CH₂_{TYR}-NH), 36.56 (CH₂_{TYR}), 31.91 (P-N-CH₃), 25.59 (CH₂).

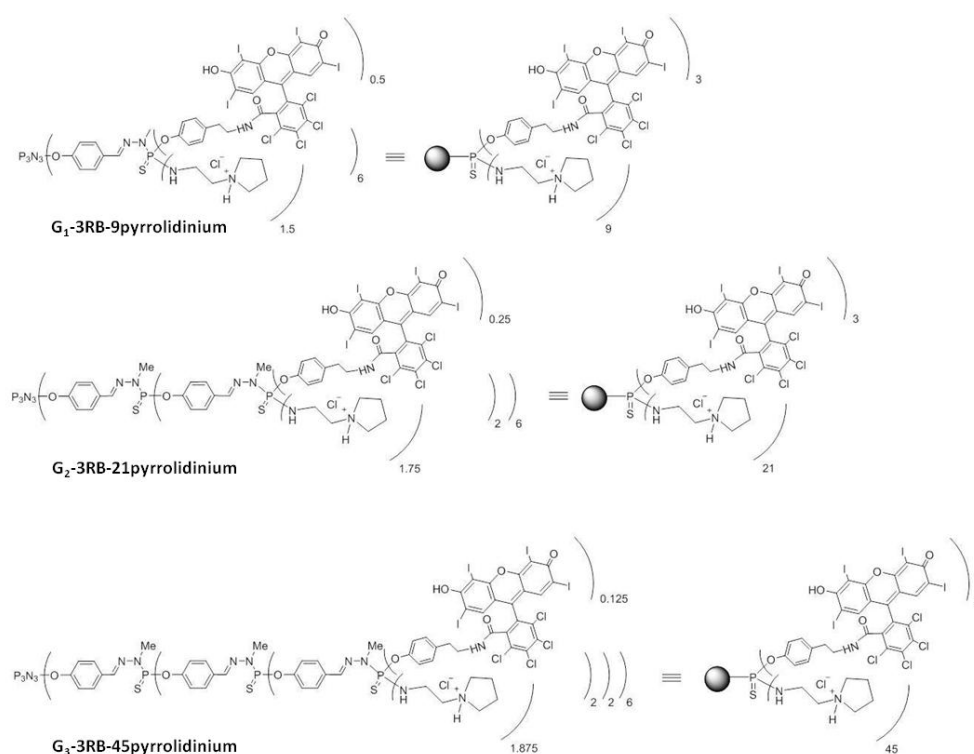


Figure 14. The structures of the G1-, 2-, 3-RB-pyrrolidinium conjugates. Black spheres are graphical representation of non-modified phosphorus dendrimer.

The structure of the G2-RB-pyrrolidine conjugate was controlled by ^{31}P NMR, ^1H NMR, ^{13}C NMR in CDCl_3 . ^{31}P NMR: δ 8.48 (s, P_0), 62.89 (s, P_1), 68.76 (s, P_2 -RB), 69.40 (s, P_2 -pyrrolidine) ppm; ^1H NMR: δ (m, 54H, ArH_{Den} and $\text{CH}=\text{N}$), 7.18 (s, 36H, ArH_{Den}), 7.10 (d, $J = 6.8$ Hz, 6H, ArH_{TYR}), 7.04 (s, 6H, ArH_{RB}), 6.7 (d, $J = 6.8$ Hz, 6H, ArH_{TYR}), 3.40–3.27 (m, 36H, P-N- CH_3), 3.26 (d, $J = 5.8$ Hz, 18H, P-N- CH_3), 3.19 (d, $J = 6.2$ Hz, 6H, CH_2 -NHPS), 3.15–3.07 (m, 48H, CH_2 NHCO, CH_2 - Ar_{TYR}), 2.53–2.48 (m, 126H, CH_2 N, N CH_2); ^{13}C NMR: δ 171.96 (NCO), 164.85 (C_{ArO}), 137.21 ($\text{C}_{\text{Ar-Den}}$, $\text{C}_{\text{RB-Cl}}$), 129.16 ($\text{C}_{\text{Ar-Den}}$, CH_{TYR}), 127.80 ($\text{C}_{\text{Ar-Den}}$), 127.15 ($\text{C}_{\text{Ar-Den}}$, $\text{C}_{\text{RB-Cl}}$), 124.86 ($\text{C}_{\text{Ar-Den}}$), 121.30 ($\text{C}_{\text{Ar-Den}}$), 115.03 (Ar-C-OH), 84.18 ($\text{C}_{\text{RB-I}}$), 53.67 (CH_2 - NH_2), 39.75 (CH_2 TYR), 39.73 (CH_2 -N, N- CH_2), 39.04 (CH_2 TYR), 32.60 (P-N- CH_3), 29.72 (P-N- CH_3), 26.96 (CH_2).

The structure of the G3-RB-pyrrolidine conjugate was controlled by ^{31}P NMR, ^1H NMR, ^{13}C NMR in CDCl_3 . ^{31}P NMR: δ 8.02 (s, P_0), 61.69 (s, P_2), 62.07 (s, P_1), 67.69 (s, P_3 -RB), 68.38 (s, P_3 -pyrrolidine) ppm; ^1H NMR: δ 7.69–7.40 (m, 116H, ArH_{Den} and $\text{CH}=\text{N}$), 7.25–6.51 (m, 102H, ArH_{Den} , ArH_{RB} , ArH_{TYR}), 3.17–3.02 (m, 90H, CH_2 -NHPS), 3.14–3.00 (m, 126H, P_1 -N- CH_3), 2.67–2.52 (m, 12H, CH_2 -NH, CH_2 - Ar_{TYR}), 2.50–2.41 (m, 270H, CH_2 -N, N- CH_2), 1.89–1.69 (m, 180H, CH_2); ^{13}C NMR: δ 156.80 (NCO), 156.32 (Ar_{TYR}), 152.34 ($\text{C}_{\text{Ar-Den}}$), 151.69 (Ar-CCl), 136.60 ($\text{C}_{\text{RB-CO}}$, 135.40 ($\text{CH}=\text{N}$), 133.12 (C-Cl), 132.18 (C-I), 135.75 (Ar_{TYR}), 131.04 ($\text{C}_{\text{Ar-Den}}$), 129.49 (Ar_{TYR}), 129.06 ($\text{C}_{\text{RB-Cl}}$), 129.03 ($\text{C}_{\text{Ar-Den}}$), 128.11 (C-Cl), 127.74 ($\text{C}_{\text{Ar-Den}}$), 127.51 (Ar_{TYR} , Ar_{RB}), 121.12 (Ar_{TYR}), 121.05 ($\text{C}_{\text{Ar-Den}}$), 84.88 ($\text{C}_{\text{RB-I}}$), 56.44 (CH_2), 39.81 (N- CH_2), 39.81 (CH_2 -N), 37.07 (CH_2 TYR -NH), 36.56 (CH_2 TYR), 30.98 (P-N- CH_3), 23.58 (CH_2).

4.2.5. Spectroscopy Studies

Fluorescence spectra were acquired using a PerkinElmer LS-50B spectrofluorometer (Waltham, MA, USA). All measurements were performed in distilled water, at RT. The excitation wavelength was set to 525 nm and spectra were collected in a wavelength range from 540 nm to 640 nm. Excitation and emission slits were 5 nm and 7 nm, respectively. The measurements were carried out for tested compounds: RB, RB-TYR, and G1-, 2-, 3-RB-pyrrolidinium (G1-, 2-, 3-RB-pyrro) conjugates (Figure 14) at 2.5 μM concentration of RB.

4.2.6. Size and Zeta Potential Measurements

Measurements of size and zeta potential were performed with the use of Zetasizer Nano ZS (Malvern Instruments Ltd., Malvern, UK). Water solutions containing the studied compound at the final dendrimer concentration of 10 μM were placed in the low volume sizing cuvettes (ZEN0112, Malvern) for size determination or in the folded capillary cells (DTS 1070, Malvern) for zeta potential measurements and measured at 25 °C. The data were analyzed using the Malvern software.

4.2.7. Drug Release Studies

In order to evaluate the rate of photosensitizer release from the conjugate (G3-3RB-pyrro) under different pH conditions, a 50 μM solution of G3-3RB-pyrro in DPBS was enclosed in a dialysis membrane tubing (SnakeSkin™ Dialysis Tubing, 3.5K MWCO, 22 mm, ThermoFisher, Waltham, MA, USA) and immersed in DPBS at a pH of 5 or 7.4 at RT. Samples from the internal phase were collected at subsequent intervals (0.5, 1, 2, 4, 8, 24 h) and the RB-TYR fluorescence similarly to spectroscopy studies. Percentage of release was determined with regards to the first sample, where the drug was not released from the conjugate (100% of initial fluorescence). The experiment was performed three times.

4.2.8. Cell Culture

Murine basal cell carcinoma lines were cultured in 154-CF medium with 5% penicillin/streptomycin, 0.05 mM calcium, and 2% chelexed, heat-inactivated fetal bovine serum (FBS). Cells were cultured in T-75 culture flasks at 37 °C, 5% CO₂ and subcultured every 2 or 3 days. The number of viable cells was determined by trypan blue exclusion assay with the use of Countess Automated Cell Counter (Invitrogen, Carlsbad, CA, USA). For the harvesting of the cells, a 0.25% (*w/v*) trypsin–0.03% (*w/v*) EDTA solution was used.

4.2.9. Cellular Uptake Determination

To define cellular uptake of tested compounds, AsZ, BsZ and CsZ cells were seeded into 12-well plates at a density of 2×10^5 cells per well. After 24 h incubation (37 °C, 5% CO₂) cells were treated with selected compounds (RB, RB-TYR, G1-3-3RB-pyrro) at 5 μM of the final concentration of RB up to 5 h. Following the incubation, cells were collected using the trypsin–EDTA solution, washed with DPBS and suspended in fresh medium. To estimate the cellular uptake, fluorescence of the samples was measured using flow cytometer (LSRII, Becton Dickinson, BD Biosciences, city, if any state, San Jose, CA, USA). The excitation and the emission filters were 520 and 570 nm, respectively.

4.2.10. Singlet Oxygen Generation Assay

To determine singlet oxygen production, Singlet Oxygen Sensor Green (SOSG) probe at 1 μM concentration was used. The solutions of RB, RB-TYR and G3-3RB-pyrro were prepared in DPBS. The samples were prepared at 0.25, 0.5, 0.75 and 1 μM concentration of RB. Upon sample preparation, 100 μL of each solution was transferred to the 96-well black plate. All measurements were recorded using fluorescence microplate reader (Fluoroscan Ascent FL, ThermoFisher, Waltham, MA, USA). The excitation wavelength was 500 nm, and the emission wavelength was 538 nm. Samples were shaken before every measurement. The first measurement was recorded with no SOSG probe to determine whether RB, RB-TYR or G3-3RB-pyrro emit fluorescence in this range. Following the first measurement, SOSG was added to each well, and the fluorescence of the probe without irradiation was checked. Next, the plate was immediately placed under the Q.Light Pro Unit lamp equipped with a filter emitting visible light in the range of 385–780 nm (Q.Light, Rorschach, Switzerland). The plate was irradiated, and the fluorescence of the probe was measured in the course of irradiation time (5–60 min). Then, the slopes of the fluorescence curves were considered for the measurement of singlet oxygen generation. The results were presented as percentage of singlet oxygen generation in control (PBS).

4.2.11. Cytotoxicity Studies

To measure the cytotoxicity, AsZ, BsZ and CsZ cells were seeded into 96-well plates at a density of 3×10^4 cells per well. After 24 h incubation, the culture medium was aspirated from the wells. Then, 100 μ L of the free photosensitizer (RB, RB-TYR or G3-3RB-pyrro) was added to the cells at final RB concentrations of 0.25, 0.5, 0.75 and 1 μ M in fresh culture medium. Cells were incubated with tested compounds for 5 h (37 °C, 5% CO₂). Then, the medium was replaced with fresh DPBS buffer, and cells were irradiated with visible light using a lamp (Q.Light Pro Unit Q.Light, Rorschach, Switzerland). The time of irradiation was 30 min. Immediately after irradiation, DPBS was replaced with fresh culture medium, and cells were incubated for 24 h as post PDT incubation. Additionally, the “dark” toxicity (without irradiation) was evaluated. Then, cell viability was measured using MTT assay. MTT was added to the wells at a concentration of 0.5 mg/mL and the plates were incubated for 3 h (37 °C, 5% CO₂). After incubation, formazan crystals were dissolved in DMSO and the absorbance was read at 570 nm using the PowerWave HT Microplate Spectrophotometer (BioTek, Winooski, VT, USA)

4.2.12. Statistical Analysis

For statistical significance testing, one-way ANOVA for concentration series and post hoc Tukey’s test for pairwise difference testing were used. In all tests, *p*-values < 0.05 were considered to be statistically significant. Data are presented as arithmetic mean \pm SD.

5. Conclusions

The present work demonstrates that it was possible to (1) modify the structure of rose bengal—a well-known photosensitizer used for photodynamic therapy studies—with a linker in the form of tyramine; (2) to graft selectively three modified rose bengal units onto the surface of phosphorus dendrimers of generation 1, 2 and 3 used as nanocarriers; (3) to modify these new nanoobjects via the grafting with pyrrolidino groups, followed by their protonation; (4) to study in depth their physicochemical and biological properties; (5) to point out the key role of the linker between phosphorus dendrimers and rose bengal in limiting fluorescence and phototoxic properties of the photosensitizer.

Investigations are underway with the aim of preparing similar conjugates in order to examine the impact of the nature of the linker, the generation of the dendrimers, the nature of the amino groups, and the number of grafted rose bengal units (or other photosensitizers) on the *in vitro* and *in vivo* properties of these macromolecules.

Dendrimers are chemically well-designed drug nanocarriers, and the application of an appropriate linker allows to prepare stable compounds for *in vitro* tests. However, we observed a weakened photodynamic effect of RB upon conjugation of the drug to phosphorus dendrimers via the tyramine linker, which excludes this type of linker from further studies on dendrimer-based carriers for this photosensitizer. The most promising strategy in this case would be the selection of a linker that ensures stability in systemic circulation and specific release of the unmodified drug inside the tumor cells, thus ensuring its unchanged structure and phototoxic properties. In subsequent studies, we plan to screen different linkers and types of drug–dendrimer bonding in order to choose the best solution for the preparation of a RB–phosphorus dendrimer conjugate.

Author Contributions: Conceptualization, J.P.M., B.K.-M.; synthesis and characterization of conjugates, M.M., J.P.M.; methodology, K.S., M.M., M.G., A.J., R.L., M.Z., S.M., J.P.M., B.K.-M.; formal analysis, K.S., M.M., M.G., A.J.; investigation, K.S., M.M., M.G.; data curation, K.S., M.M., M.G., R.L., M.Z., S.M., J.P.M.; writing—original draft preparation, K.S., M.M., M.G.; writing—review and editing, K.S., M.M., M.G., J.P.M.; visualization, K.S., M.M.; supervision, J.P.M., B.K.-M.; funding acquisition, B.K.-M. All authors have read and agreed to the published version of the manuscript.

Funding: This work was supported by National Science Centre, Poland (Project UMO-2017/25/B/NZ7/01304 “Phosphorus dendrimers as carriers for photosensitizers-*in vivo* studies”)

Acknowledgments: Based upon work from COST Action “Nano2Clinic. Cancer Nanomedicine-from the bench to the bedside” CA17140 supported by COST (European Cooperation in Science and Technology).

Conflicts of Interest: The authors declare no conflict of interest.

References

1. WHO. Skin Cancers. Available online: <https://www.who.int/uv/faq/skincancer/en/index1.html> (accessed on 4 February 2020).
2. Kirby, J.S.; Miller, C.J. Intralesional chemotherapy for nonmelanoma skin cancer: A practical review. *J. Am. Acad. Dermatol.* **2010**, *63*, 689–702. [CrossRef] [PubMed]
3. Neville, J.A.; Welch, E.; Leffell, D.J. Management of nonmelanoma skin cancer in 2007. *Nat. Clin. Pract. Oncol.* **2007**, *4*, 462–469. [CrossRef] [PubMed]
4. Szeimies, R.M.; Karrer, S. Towards a more specific therapy: Targeting nonmelanoma skin cancer cells. *Br. J. Dermatol.* **2006**, *154*, 16–21. [CrossRef] [PubMed]
5. Vianna Lopez, R.F.; Lange, N.; Guy, R.; Bentley, M.V.L.B. Photodynamic therapy of skin cancer: Controlled drug delivery of 5-ALA and its esters. *Adv. Drug Deliv. Rev.* **2004**, *56*, 77–94. [CrossRef]
6. Ochsner, M. Photophysical and photobiological processes in the photodynamic therapy of tumours. *J. Photochem. Photobiol. B Biol.* **1997**, *39*, 1–18. [CrossRef]
7. Kwiatkowski, S.; Knap, B.; Przystupski, D.; Saczko, J.; Kędzińska, E.; Knap-Czop, K.; Kotlińska, J.; Michel, O.; Kotowski, K.; Kulbacka, J. Photodynamic therapy – mechanisms, photosensitizers and combinations. *Biomed. Pharmacother.* **2018**, *106*, 1098–1107. [CrossRef]
8. Granville, D.J.; McManus, B.M.; Hunt, D.W.C. Photodynamic therapy: Shedding light on the biochemical pathways regulating porphyrin-mediated cell death. *Histol. Histopathol.* **2001**, *16*, 309–317. [PubMed]
9. Castano, A.P.; Demidova, T.N.; Hamblin, M.R. Mechanisms in photodynamic therapy: Part one—Photosensitizers, photochemistry and cellular localization. *Photodiagnosis Photodyn. Ther.* **2004**, *1*, 279–293. [CrossRef]
10. Marcucci, F.; Lefoulon, F. Active targeting with particulate drug carriers in tumor therapy: Fundamentals and recent progress. *Drug Discov. Today* **2004**, *9*, 219–228. [CrossRef]
11. Sztandera, K.; Gorzkiewicz, M.; Klajnert-Maculewicz, B. Nanocarriers in photodynamic therapy—In vitro and in vivo studies. *Wiley Interdiscip. Rev. Nanomed. Nanobiotechnology* **2020**, *12*, 1–24. [CrossRef]
12. Wieder, M.E.; Hone, D.C.; Cook, M.J.; Handsley, M.M.; Gavrilovic, J.; Russell, D.A. Intracellular photodynamic therapy with photosensitizer-nanoparticle conjugates: Cancer therapy using a ‘Trojan horse’. *Photochem. Photobiol. Sci.* **2006**, *5*, 727–734. [CrossRef] [PubMed]
13. Rijcken, C.J.F.; Hofman, J.W.; van Zeeland, F.; Hennink, W.E.; van Nostrum, C.F. Photosensitizer-loaded biodegradable polymeric micelles: Preparation, characterisation and in vitro PDT efficacy. *J. Control. Release* **2007**, *124*, 144–153. [CrossRef] [PubMed]
14. Roy, I.; Ohulchanskyy, T.Y.; Pudavar, H.E.; Bergey, E.J.; Oseroff, A.R.; Morgan, J.; Dougherty, T.J.; Prasad, P.N. Ceramic-based nanoparticles entrapping water-insoluble photosensitizing anticancer drugs: A novel drug-carrier system for photodynamic therapy. *J. Am. Chem. Soc.* **2003**, *125*, 7860–7865. [CrossRef]
15. Pucińska, J.; Podbielska, H. Nanomateriały we wspomaganiu terapii fotodynamicznej. *Acta Bio-Optica Inform. Medica. Inżynieria Biomed.* **2009**, *15*, 178–189.
16. Wilk, K.A.; Zielińska, K.; Pietkiewicz, J.; Skońska, N.; Choromańska, A.; Rossowska, J.; Garbiec, A.; Saczko, J. Photo-oxidative action in MCF-7 cancer cells induced by hydrophobic cyanines loaded in biodegradable microemulsion-templated nanocapsules. *Int. J. Oncol.* **2012**, *41*, 105–116. [PubMed]
17. Ferenc, M.; Pedziwiatr-Werbicka, E.; Nowak, K.E.; Klajnert, B.; Majoral, J.P.; Bryszewska, M. Phosphorus dendrimers as carriers of siRNA—characterisation of dendriplexes. *Molecules* **2013**, *18*, 4451–4466. [CrossRef]
18. Loup, C.; Zanta, M.A.; Caminade, A.M.; Majoral, J.P.; Meunier, B. Preparation of Water-Soluble Cationic Phosphorus-Containing Dendrimers as DNA Transfecting Agents. *Chem.-A Eur. J.* **1999**, *5*, 3644–3650. [CrossRef]
19. Dabrzalska, M.; Zablocka, M.; Mignani, S.; Majoral, J.P.; Klajnert-Maculewicz, B. Phosphorus dendrimers and photodynamic therapy. Spectroscopic studies on two dendrimer-photosensitizer complexes: Cationic phosphorus dendrimer with rose bengal and anionic phosphorus dendrimer with methylene blue. *Int. J. Pharm.* **2015**, *492*, 266–274. [CrossRef] [PubMed]

20. Dabrzalska, M.; Janaszewska, A.; Zablocka, M.; Mignani, S.; Majoral, J.P.; Klajnert-Maculewicz, B. Cationic Phosphorus Dendrimer Enhances Photodynamic Activity of Rose Bengal against Basal Cell Carcinoma Cell Lines. *Mol. Pharm.* **2017**, *14*, 1821–1830. [[CrossRef](#)]
21. Launay, N.; Caminade, A.M.; Majoral, J.P. Synthesis of bowl-shaped dendrimers from generation 1 to generation 8. *J. Organomet. Chem.* **1997**, *529*, 51–58. [[CrossRef](#)]
22. Honary, S.; Zahir, F. Effect of zeta potential on the properties of nano-drug delivery systems—A review (Part 1 and 2). *Trop. J. Pharm. Res.* **2013**, *12*, 255–273.
23. Posadas, I.; Romero-Castillo, L.; El Brahm, N.; Manzanares, D.; Mignani, S.; Majoral, J.P.; Ceña, V. Neutral high-generation phosphorus dendrimers inhibit macrophage-mediated inflammatory response in vitro and in vivo. *Proc. Natl. Acad. Sci. USA* **2017**, *114*, E7660–E7669. [[CrossRef](#)] [[PubMed](#)]
24. Juarranz, Á.; Jaén, P.; Sanz-Rodríguez, F.; Cuevas, J.; González, S. Photodynamic therapy of cancer. Basic principles and applications. *Clin. Transl. Oncol.* **2008**, *10*, 148–154. [[CrossRef](#)]
25. Robertson, C.A.; Evans, D.H.; Abrahamse, H. Photodynamic therapy (PDT): A short review on cellular mechanisms and cancer research applications for PDT. *J. Photochem. Photobiol. B Biol.* **2009**, *96*, 1–8. [[CrossRef](#)] [[PubMed](#)]
26. Allison, R.R.; Moghissi, K. Photodynamic therapy (PDT): PDT mechanisms. *Clin. Endosc.* **2013**, *46*, 24–29. [[CrossRef](#)]
27. Bertrand, N.; Wu, J.; Xu, X.; Kamaly, N.; Farokhzad, O.C. Cancer nanotechnology: The impact of passive and active targeting in the era of modern cancer biology. *Adv. Drug Deliv. Rev.* **2014**, *66*, 2–25. [[CrossRef](#)]
28. Agarwal, A.; Gupta, U.; Asthana, A.; Jain, N.K. Dextran conjugated dendritic nanoconstructs as potential vectors for anti-cancer agent. *Biomaterials* **2009**, *30*, 3588–3596. [[CrossRef](#)] [[PubMed](#)]
29. Patri, A.K.; Kukowska-Latallo, J.F.; Baker, J.R. Targeted drug delivery with dendrimers: Comparison of the release kinetics of covalently conjugated drug and non-covalent drug inclusion complex. *Adv. Drug Deliv. Rev.* **2005**, *57*, 2203–2214. [[CrossRef](#)]
30. Leriche, G.; Chisholm, L.; Wagner, A. Cleavable linkers in chemical biology. *Bioorganic Med. Chem.* **2012**, *20*, 571–582. [[CrossRef](#)]
31. Ding, C.; Li, Z. A review of drug release mechanisms from nanocarrier systems. *Mater. Sci. Eng. C* **2017**, *76*, 1440–1453. [[CrossRef](#)]
32. Gorzkiewicz, M.; Klajnert-Maculewicz, B. Chapter X in Dendrimers for Drug Delivery. In *Dendrimers as Nanocarriers for Anticancer Drugs*; Sharma, A., Keservan, R., Eds.; Apple Academic Press: Palm Bay, Brevard, FL, USA, 2018; pp. 327–374.
33. Dabrzalska, M.; Benseny-Cases, N.; Barnadas-Rodríguez, R.; Mignani, S.; Zablocka, M.; Majoral, J.P.; Bryszewska, M.; Klajnert-Maculewicz, B.; Cladera, J. Fourier transform infrared spectroscopy (FTIR) characterization of the interaction of anti-cancer photosensitizers with dendrimers. *Anal. Bioanal. Chem.* **2016**, *408*, 535–544. [[CrossRef](#)] [[PubMed](#)]
34. Caminade, A.M.; Fruchon, S.; Turrin, C.O.; Poupot, M.; Ouali, A.; Maraval, A.; Garzoni, M.; Maly, M.; Furer, V.L.; Kovalenko, V.; et al. The key role of the scaffold on the efficiency of dendrimer nanodrugs. *Nat. Commun.* **2015**, *6*, 1–11. [[CrossRef](#)]
35. Griffe, L.; Poupot, M.; Marchand, P.; Maraval, A.; Turrin, C.O.; Rolland, O.; Métivier, P.; Bacquet, G.; Fournié, J.J.; Caminade, A.M.; et al. Multiplication of human natural killer cells by nanosized phosphonate-capped dendrimers. *Angew. Chemie-Int. Ed.* **2007**, *46*, 2523–2526. [[CrossRef](#)] [[PubMed](#)]
36. Li, N.; Than, A.; Wang, X.; Xu, S.; Sun, L.; Duan, H.; Xu, C.; Chen, P. Ultrasensitive Profiling of Metabolites Using Tyramine-Functionalized Graphene Quantum Dots. *ACS Nano* **2016**, *10*, 3622–3629. [[CrossRef](#)]
37. MacDonald, I.J.; Dougherty, T.J. Basic principles of photodynamic therapy. *J. Porphyr. Phthalocyanines* **2001**, *5*, 105–129. [[CrossRef](#)]
38. Hoffmann, E.K.; Lambe, I.H. Ion channels and transporters in the development of drug resistance in cancer cells. *Philos. Trans. R. Soc. B Biol. Sci.* **2014**, *369*, 20130109. [[CrossRef](#)]
39. Studzian, M.; Szulc, A.; Janaszewska, A.; Appelhans, D.; Pułaski, Ł.; Klajnert-Maculewicz, B. Mechanisms of Internalization of Maltose-Modified Poly(propyleneimine) Glycodendrimers into Leukemic Cell Lines. *Biomacromolecules* **2017**, *18*, 1509–1520. [[CrossRef](#)] [[PubMed](#)]
40. Filimon, A.; Sima, L.E.; Appelhans, D.; Voit, B.; Negroiu, G. Internalization and Intracellular Trafficking of Poly(propylene imine) Glycodendrimers with Maltose Shell in Melanoma Cells. *Curr. Med. Chem.* **2012**, *19*, 4955–4968. [[CrossRef](#)]

41. Abrahamse, H.; Hamblin, M.R. New photosensitizers for photodynamic therapy. *Biochem. J.* **2016**, *473*, 347–364. [[CrossRef](#)]
42. Wang, B.; Wang, J.-H.H.; Liu, Q.; Huang, H.; Chen, M.; Li, K.; Li, C.; Yu, X.-F.F.; Chu, P.K. Rose-bengal-conjugated gold nanorods for in vivo photodynamic and photothermal oral cancer therapies. *Biomaterials* **2014**, *35*, 1954–1966. [[CrossRef](#)]



© 2020 by the authors. Licensee MDPI, Basel, Switzerland. This article is an open access article distributed under the terms and conditions of the Creative Commons Attribution (CC BY) license (<http://creativecommons.org/licenses/by/4.0/>).

Noncovalent Interactions with PAMAM and PPI Dendrimers Promote the Cellular Uptake and Photodynamic Activity of Rose Bengal: The Role of the Dendrimer Structure

Krzysztof Sztandera,* Michał Gorzkiewicz, Ana Sofia Dias Martins, Lorenzo Pallante, Eric Adriano Zizzi, Marcello Miceli, Mateusz Bątal, Catarina Pinto Reis, Marco A. Deriu, and Barbara Klajnert-Maculewicz*



Cite This: <https://doi.org/10.1021/acs.jmedchem.1c01080>



Read Online

ACCESS |



Metrics & More



Article Recommendations



Supporting Information

ABSTRACT: Rose bengal is an anionic dye considered as a potential photosensitizer for anticancer photodynamic therapy. The clinical utility of rose bengal is hampered by its short half-life, limited transmembrane transport, aggregation, and self-quenching; consequently, efficient drug carriers that overcome these obstacles are urgently required. In this study, we performed multilevel *in vitro* and *in silico* characterization of interactions between rose bengal and cationic poly(amidoamine) (PAMAM) and poly(propyleneimine) (PPI) dendrimers of the third and fourth generation and assessed the ability of the resultant complexes to modulate the photosensitizing properties of the drug. We focused on explaining the molecular basis of this phenomenon and proved that the generation- and structure-dependent binding of the dye by the dendrimers increases the cellular uptake and production of singlet oxygen and intracellular reactive oxygen species, leading to an increase in phototoxicity. We conclude that the application of dendrimer carriers could enable the design of efficient photodynamic therapies based on rose bengal.



1. INTRODUCTION

Photodynamic therapy (PDT) is one of the most promising methods for the treatment of basal cell carcinoma and different types of skin cancer.¹ This highly specific approach is primarily based on the application of a light-sensitive compound (so-called photosensitizer, PS), which, upon excitation with light of a certain wavelength, generates reactive oxygen species (ROS). This, in turn, leads to the oxidation of cellular nucleic acids, lipids, and proteins, disrupting cell signaling cascades or gene regulation and ultimately activating several cell death pathways.² Such a specific mechanism enables treatment to be targeted precisely to the area of a neoplastic lesion upon direct application of PS and light.³ Thus, the benefits of PDT are its noninvasiveness and lack of adverse side effects. However, the level of damage and the mechanisms of cell death depend not only on the clinical setup (e.g., time of irradiation and light intensity) but also on the properties, concentration, and subcellular localization of PS.⁴ Consequently, to take full advantage of the potential of PDT, it is essential to select the appropriate phototoxic drug.

The ideal PS should have the following properties: maximum absorbance between 650 and 850 nm, high efficiency of free radical production, low photodegradation, and nontoxicity in the dark. Additionally, PSs should have long half-lives and efficient cellular uptake, enabling sufficient intracellular

accumulation to trigger a toxic effect.^{4,5} Despite many years of research, clinically used PSs remain far from perfect.

Rose bengal (4,5,6,7-tetrachloro-2',4',5',7'-tetraiodofluorescein; RB) is a dianionic fluorescent dye belonging to the class of xanthenes. RB is currently approved as an ocular diagnostic tool and has been designated by the Food and Drug Administration (FDA) for the treatment of several types of cancers and skin conditions.⁵ Due to its high efficiency of singlet oxygen generation,⁶ RB is considered a good candidate to serve as a PS in anticancer PDT. However, the potential use of RB in the photodynamic therapy of neoplasms is limited mainly by its short half-life, hydrophilic nature, and tendency to aggregate. RB is negatively charged at physiological pH, hindering transmembrane transport and preventing the accumulation of clinically relevant intracellular concentrations. Its half-life (~30 min) further limits distribution and tissue accumulation; consequently, multiple dosing may be needed to reach the

Received: June 15, 2021

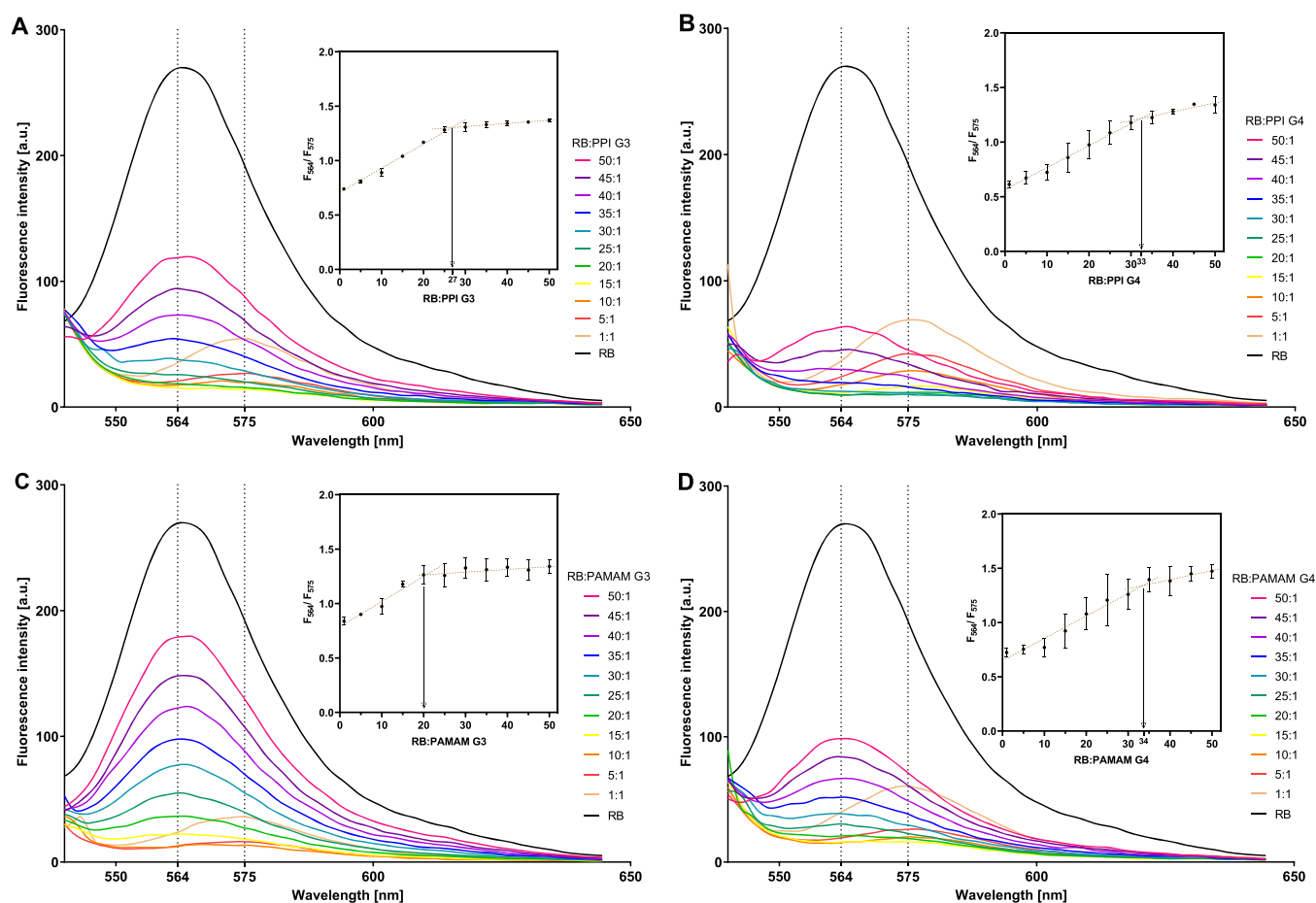


Figure 1. Changes in the fluorescence spectrum of RB ($1 \mu\text{M}$) upon titration with (A) PPI G3, (B) PPI G4, (C) PAMAM G3, and (D) PAMAM G4, maintaining a dendrimer:RB molar ratio of 1:50 to 1:1. The insets show the determination of the stoichiometry of complexes fully saturated with RB using Job's method based on the plots of F_{564}/F_{575} vs RB:dendrimer molar ratio. Data are presented as means \pm SD; $n = 3$.

optimal therapeutic effect. In addition, RB forms aggregates in solutions, which affect the spectral properties of the dye and cause a decrease in its photodynamic activity, including the ability to generate singlet oxygen and other ROS.⁵

To overcome the limitations associated with photo-instability, poor biodistribution, and cellular uptake, the use of the appropriate RB formulation or delivery system may be a promising approach. Clinically used lipidic and organic formulations of PSs may yield unpredictable distribution patterns, allergic reactions, hypersensitivity, and systemic toxicity.⁷ To overcome these problems, researchers have turned to the field of nanotechnology, which has the potential to generate nanoscale particles with precisely defined features.^{8,9} Here, dendrimers are a class of nanoparticles that has been studied comprehensively both *in vitro* and *in vivo* in the context of anticancer drug delivery.^{10–12} These sphere-shaped, water-soluble polymers of symmetrical, well-defined structure protect drugs from degradation, extend their half-life, promote intracellular transport,¹³ and provide semispecific accumulation in tumor regions; the latter phenomenon is referred to as the enhanced permeability and retention (EPR) effect.¹⁴

The three-dimensional architecture and chemical composition of dendrimers offer several options for the attachment of drugs. In particular, therapeutics can be physically entrapped inside the dendritic scaffold or linked by noncovalent interactions or covalent bonds, both on the surface and within the dendrimer structure.¹⁵ In the context of PDT, an additional

advantage is that optimized release of PS from the carrier at the target site is not required for the cytotoxic effect so long as the nanocarrier does not limit the diffusion of molecular oxygen.⁸ However, although dendrimer/drug conjugates are generally more stable in solutions and *in vivo*, the use of covalent linkers can drastically alter the photosensitive properties of PS, thus decreasing its phototoxicity.¹ Therefore, numerous studies on the use of nanoparticles, including dendrimers, as RB carriers have focused on noncovalent interactions,⁵ demonstrating the efficient intracellular uptake and superior photodynamic properties of such formulations.^{16–18} Because complex formation is usually based on ionic interactions, the process itself, as well as the physicochemical and biological properties of dendrimer/drug complexes, is greatly influenced by pH; ionic strength; buffer composition; and, most importantly, the structure of the dendritic carriers.^{19,20}

In this study, we focused on well-characterized and commercially available cationic poly(amidoamine) (PAMAM) and poly(propyleneimine) (PPI) dendrimers of the third (G3) and fourth (G4) generation. We took a holistic approach, performing an in-depth characterization of dendrimer:RB interactions both *in vitro* and *in silico*, and performed further assessment of the multilevel biophysical and biological activity of the resultant complexes: singlet oxygen generation, cellular uptake, intracellular ROS production, and phototoxicity. To the best of our knowledge, this is the first attempt to compare the ability of cationic dendrimers of different types and generations

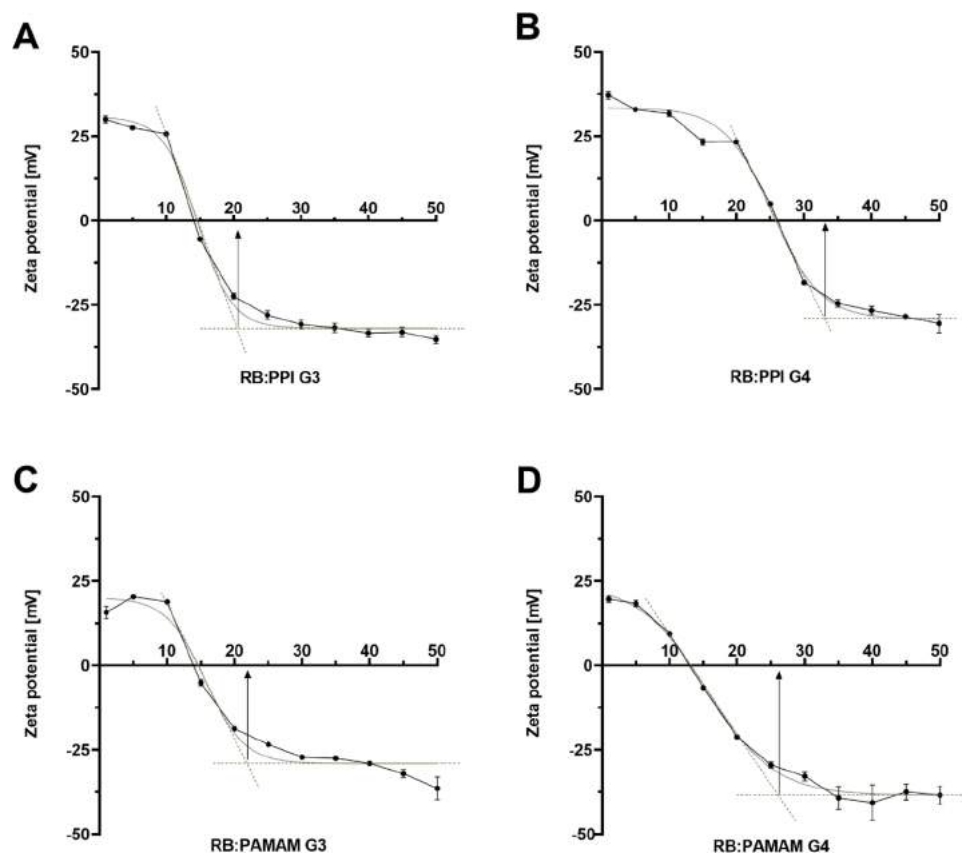


Figure 2. Titration curves for the measurements of zeta potential: effects of titration of 10 μM solutions of (A) PPI G3, (B) PPI G4, (C) PAMAM G3, and (D) PAMAM G4 with RB, maintaining the dendrimer:RB molar ratio of 1:1 to 1:50. Analysis of the course of titration curves allowed us to use Job's method to determine the stoichiometry of complexes fully saturated with RB. Data are presented as means \pm SD; $n = 3$.

to serve as carriers for anionic RB, and to link the dendrimer structure to the activity of complexes.

2. RESULTS

2.1. In Vitro Evaluation of Dendrimer:RB Complexation. To characterize the complex formation between the tested dendrimers and RB, we exploited their characteristic properties, i.e., dye fluorescence and the zeta potential of nanoparticles in solutions. Spectrofluorimetric studies revealed that the addition of a dendrimer to an RB solution caused a sharp reduction in dye fluorescence. Subsequent titration caused a progressive quenching of RB fluorescence until a red shift of the emission wavelength from 564 to 575 nm was observed, with a subsequent increase in the fluorescence signal (Figure 1), indicating polarity changes in the vicinity of the chromophore molecule.²¹ Based on this phenomenon, the F_{564}/F_{575} ratio was calculated and plotted vs the RB:dendrimer molar ratio. Using Job's method,²² we approximated the stoichiometry of binding in fully saturated complexes as 1:27 for PPI G3:RB, 1:33 for PPI G4:RB, 1:20 for PAMAM G3:RB, and 1:34 for PAMAM G4:RB (Figure 1, insets). This outcome was confirmed by the measurement of changes in the zeta potential of dendrimers during titration with RB. Upon the addition of subsequent portions of RB to the solution, the initial positive zeta potential of the dendrimers began to decrease until it reached a plateau at approximately -30 mV, indicating the full saturation of the polymers with PS. Based on the titration curves, we determined the stoichiometry of the formed complexes; the resultant values were similar to those obtained by spectrofluorimetric analyses:

1:21 for PPI G3:RB, 1:33 for PPI G4:RB, 1:22 for PAMAM G3:RB, and 1:26 for PAMAM G4:RB (Figure 2).

For the following experiments, the 1:10 dendrimer:RB molar ratio was used to ensure the stability of the complex and to maintain its positive surface potential, as positively charged nanoparticles have a greater ability to cross the barrier of biological membranes.^{23,24}

2.2. In Vitro Photodynamic and Phototoxic Properties of RB and Dendrimer:RB Complexes. Singlet oxygen generation assays using the ABDA probe showed that the tested compounds were able to increase the singlet oxygen levels. At the highest concentration tested, free RB caused a ~ 3 -fold increase in singlet oxygen generation relative to the control, slightly less than for the case of complexes with dendrimers of the fourth generation (~ 4 -fold for PAMAM G4 and ~ 6 -fold for PPI G4). On the other hand, complexes of RB with dendrimers of the third generation caused a greater increase in the generation of singlet oxygen (~ 16 -fold for PAMAM G3 and ~ 19 -fold for PPI G3), significantly exceeding the effect observed with free PS (Figure 3). Free dendrimers did not generate singlet oxygen (data not shown).

The cytotoxicity of tested compounds was evaluated in three basal cell carcinoma cell line models, as basal cell carcinoma is the most common form of skin cancer and the most frequently occurring form of cancer overall.^{25,26} The complexes revealed a higher phototoxicity relative to free RB (Figure 4A and Figure S1), and this trend was maintained in all tested cell lines: RB in complex with PPI dendrimers was more toxic than RB in complex with PAMAM dendrimers, regardless of the generation. Cells treated with the free RB solution exhibited the highest

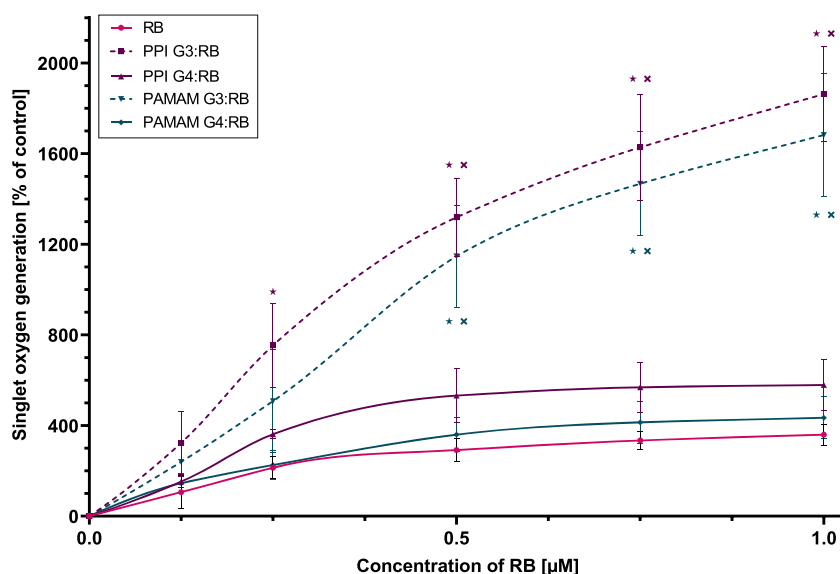


Figure 3. Singlet oxygen generation by RB and dendrimer:RB complexes in a 1:10 molar ratio. The singlet oxygen generation assay was performed using the ABDA probe as an indicator. Data are presented as the percentage of the singlet oxygen generation in the control sample containing only the ABDA probe; means \pm SD; $n = 4$. *Statistically significant difference vs free RB ($p < 0.05$). \times Statistically significant difference between generations of dendrimers of the same type ($p < 0.05$).

viability. We did not observe cytotoxicity of free dendrimers or dark toxicity of RB and dendrimer:RB complexes (data not shown). The cell lines exhibited a range of susceptibilities to all treatments, with AsZ cells being the most susceptible [e.g., PPI:RB complexes with the highest RB concentration reduced the viability of AsZ cells to $\sim 20\%$; in the case of BsZ cells, viability was $\sim 30\%$, and for CsZ cells, viability was $\sim 50\%$ (Figure 4A and Figure S1)]. Accordingly, we used AsZ for intracellular ROS production and cellular uptake assays.

The outcome of the intracellular ROS production assay coincided with the results of the cytotoxicity evaluation (Figure 4B). The tested compounds induced the production of ROS, with PPI:RB complexes exerting the greatest effect. The activity of the PAMAM:RB complexes was significantly lower but still exceeded the effect observed for free PS. The phenomenon was independent of the generation of dendrimers. Free dendrimers did not generate ROS (data not shown).

Complexation of RB with the tested dendrimers significantly increased the intracellular concentration of PS (Figure 4C). The PPI G4 dendrimer turned out to be the most effective carrier, with PAMAM G3 being the least efficient, but even in the latter case, the uptake of RB was almost 2-fold higher than when AsZ cells were treated with free PS. The effects of the PPI G3 and PAMAM G4 dendrimers were similar and intermediate between the PPI G4 and PAMAM G3. Overall, when comparing dendrimers of the same type, fourth-generation dendrimers had a greater ability to transport RB intracellularly than third-generation dendrimers. When comparing dendrimers of the same generation, PPI dendrimers were more efficient carriers than PAMAM dendrimers.

2.3. Molecular Modeling. **2.3.1. Single-Dendrimer Conformational Dynamics.** We assessed the geometrical properties of dendrimers over the last 50 ns of two independent 200 ns MD simulations. The RoG, which represents a reliable metric for assessing the overall size of a dendrimer, and shape descriptors aspect ratio and asphericity (δ) were calculated as described in the Experimental Section. Geometrical properties of the two MD replicas were averaged over the last 50 ns of simulation, with

snapshots taken every 2 ps (Table 1). The data obtained were in close agreement with *in silico* and experimental data from the previous literature for all the simulated systems (as reported in detail in Table S2), confirming that the dendrimer structures were well equilibrated.

Figure 5 shows the probability density function (PDF) of the RoG during the last 50 ns of MD replicas, highlighting the greater flexibility of PAMAM dendrimers relative to PPI dendrimers. Time series of the RoG during the entire simulations are reported in Figure S2.

2.3.2. Dendrimer:RB Complexation and Interaction Dynamics. To assess the structural effects of RB on each dendrimer type and analyze the mode of dendrimer/drug interaction, dendrimer structures from the previous equilibration were simulated in the presence of 10 RB molecules (maintaining a 1:10 dendrimer:RB stoichiometry). MD trajectories showed the early and stable complexation of all 10 RB molecules after ≤ 16 ns, with no unbinding events observed throughout the 200 ns simulations (see also Figures S3–S5 and Videos S1–S4).

We assessed the structural effects of RB on the dendrimers again using RoG, aspect ratios, and asphericity measures, but we observed no remarkable effects upon ligand complexation (see Figure S6 and Figure S7). Similarly, the particle density of dendrimers with respect to the dendrimer central core was not remarkably altered in the presence of RB molecules (see Figure S8).

The radial distribution function (RDF) of the RB with respect to the dendrimer core (Figure 6) revealed that PPI dendrimers had a greater ability to internalize RB molecules. On the other hand, drug molecules were more exposed to the external solvent when bound to PAMAM dendrimers. It is worth mentioning that, despite this difference in ligand internalization, we observed no marked differences in the dendrimer:RB interaction surface among the dendrimers examined (see Figure S9).

The RDFs for the external amino groups, water molecules, and chlorine and sodium ions are shown in Figure 7, in the presence and absence of RB, to compare the effects of the drug

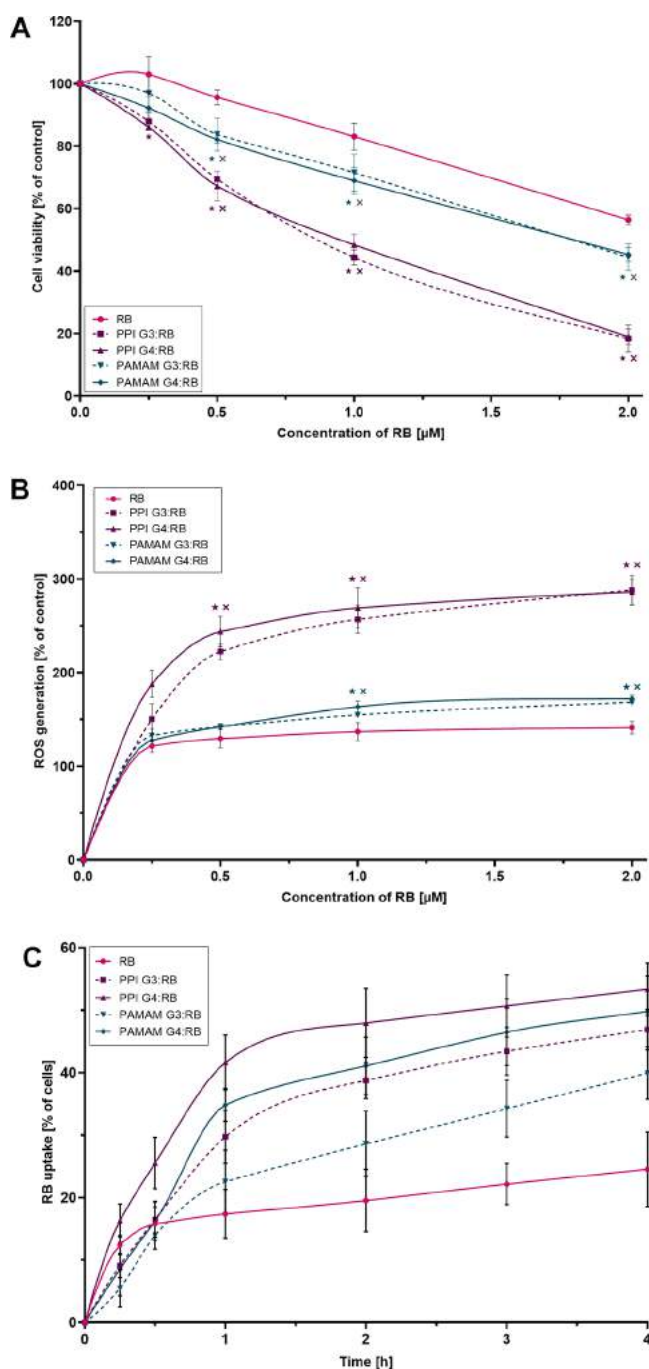


Figure 4. (A) Phototoxic effect of RB and dendrimer:RB complexes in 1:10 molar ratio in AsZ cells. Cell viability was determined using MTT assay. Data are presented as percentages of the viability of control (untreated) cells; means \pm SD; $n = 6$. *Statistically significant difference vs free RB; $p < 0.05$. \times Statistically significant difference vs dendrimers of different type, regardless of generation; $p < 0.05$. (B) ROS production in AsZ cells triggered by RB and dendrimer:RB complexes in 1:10 molar ratio upon irradiation determined by the use of the 2',7'-dichlorodihydrofluorescein diacetate (H_2DCFDA) probe. Data are presented as percentages of intracellular ROS generation in control (untreated) cells; means \pm SD; $n = 4$. *Statistically significant difference vs free RB; $p < 0.05$. \times Statistically significant difference vs dendrimers of different type, regardless of generation; $p < 0.05$. (C) Uptake of RB and dendrimer:RB complexes in 1:10 molar ratio by AsZ cells as determined by flow cytometry assay. Data are presented as the percentage of cells in the population exhibiting RB-associated fluorescence; means \pm SD; $n = 5$. For statistical analysis, see Table S1.

inclusion. The RDF trends of the external amines were unaltered in the presence of the RB for PPI dendrimers, confirming the more rigid behavior of these dendrimers (green and blue lines in Figure 7A,E). On the other hand, the RDF peaks of external amines of PAMAM dendrimers changed markedly upon drug complexation (black and red lines in Figure 7A,E), suggesting a major conformational change in the dendrimer structure. The reduced values of water molecules RDF in the internal layers are also indicative of the fact that these molecules are forced out by the entrance of RB, especially in the case of PPI dendrimers (Figure 7B,F). Similarly, the presence of RB leads to the ejection of chlorine ions from the internal layers of the dendrimers of the third generation (Figure 7C,G). The positively charged sodium ions on the other hand were not noticeably displaced with respect to the dendrimer core in the presence of RB if compared to the neat systems (Figure 7D,H).

We further assessed the structural characteristics of both the free dendrimers and their complexes with RB molecules by analyzing hydrogen bonds (H-bonds). As highlighted in Figure 8A, PAMAM dendrimers of both G3 and G4 are able to form an intramolecular network of H-bonds, mainly due to the presence of acceptor oxygen atoms within their underlying chemical structure.²⁷ No intramolecular network of hydrogen bonds was observed for PPI dendrimers. Interestingly, the number of intramolecular H-bonds in PAMAM dendrimers did not seem to be influenced by the presence of RB. H-bonding between dendrimers and the surrounding water was more prominent in PAMAM dendrimers than in PPI dendrimers, with only a marginal decrease caused by RB complexation (Figure 8B).

Overall, PPI dendrimers formed fewer H-bonds with the solvent than PAMAM dendrimers, whereas fourth-generation dendrimers formed more H-bonds with the solvent, as expected from the increase in the number of surface amino groups. Finally, PAMAM dendrimers formed significantly more H-bonds with RB than PPI dendrimers, with no difference between dendrimer generations (Figure 8C). Overall, PAMAM dendrimers formed the largest number of H-bonds internally, with both the solvent and RB molecules.

Void volume analysis revealed that the presence of RB reduces the internal volumes of PAMAM dendrimers, whereas internal cavities of PPI dendrimers were not altered by the drug (Figure 9; see also Figure S10). Specifically, the ratios between the void volumes in the presence and absence of RB were 0.82 for PAMAM G3, 0.77 for PAMAM G4, 0.98 for PPI G3, and 0.97 for PPI G4.

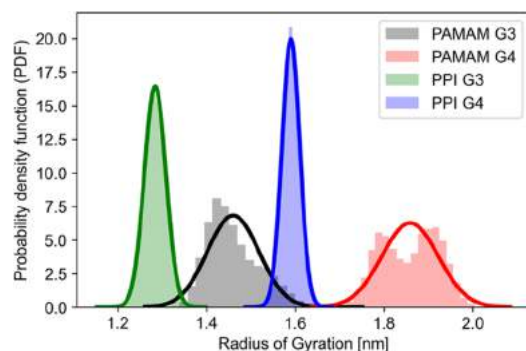
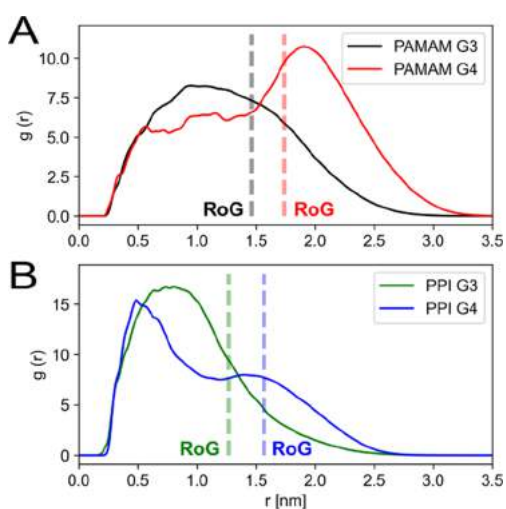
Finally, we investigated the surface electrostatic potential of the complexes by extracting frames from the dendrimer:RB simulations and evaluating the dendrimer electrostatic potential in the presence of RB (Figure 10). We observed predominantly positive potential up to 5 kT/e on the dendrimer surface for all simulated systems; only PAMAM G3 had a prominent number of neutral surface patches (Figure 10A), indicating the ability of RB to locally neutralize the surface electrostatic potential of this specific dendrimer more effectively than for other systems. Overall, dendrimers of the fourth generation (Figure 10B,D) were characterized by a more positive surface potential even in the presence of bound RB, whereas third-generation dendrimers (Figure 10A,C) had a more neutral surface potential resulting from the shielding effect of bound RB.

3. DISCUSSION AND CONCLUSIONS

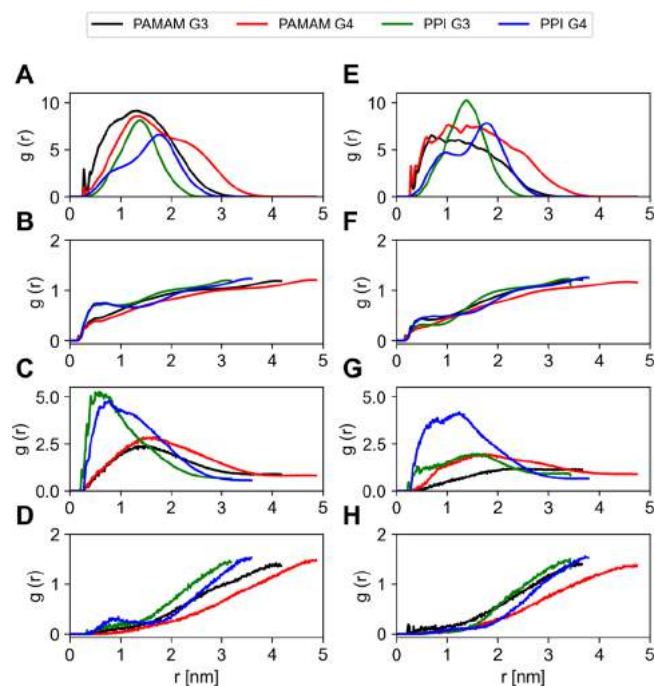
Photodynamic therapy (PDT), which relies on the use of a PS and a light source to induce singlet oxygen and ROS formation

Table 1. Radius of Gyration (RoG), Aspect Ratios, and Asphericity Values for the Simulated Dendrimers, Presented as Means \pm SD

| | RoG [nm] | I_x/I_y | I_x/I_z | δ |
|----------|-------------------|-------------------|-------------------|-------------------|
| PAMAM G3 | 1.460 \pm 0.058 | 0.708 \pm 0.128 | 0.581 \pm 0.087 | 0.026 \pm 0.012 |
| PAMAM G4 | 1.859 \pm 0.064 | 0.839 \pm 0.086 | 0.705 \pm 0.069 | 0.012 \pm 0.006 |
| PPI G3 | 1.284 \pm 0.024 | 0.792 \pm 0.080 | 0.685 \pm 0.068 | 0.013 \pm 0.006 |
| PPI G4 | 1.590 \pm 0.020 | 0.826 \pm 0.050 | 0.746 \pm 0.042 | 0.008 \pm 0.003 |

**Figure 5.** Probability density function (PDF) of the radius of gyration during the last 50 ns of two independent MD simulations.**Figure 6.** Radial distribution function (RDF) of RB with respect to the dendrimer central core for (A) PAMAM and (B) PPI dendrimers; dotted lines represent the radius of gyration for each dendrimer.

in the presence of molecular oxygen, is a promising therapeutic strategy against basal cell carcinoma. The use of dendrimers as drug carriers has the potential to overcome the known drawbacks of currently investigated PSs, such as self-quenching, short half-life, and suboptimal cellular uptake. In this work, we performed an in-depth characterization of the complexes of cationic poly(amidoamine) (PAMAM) and poly(propyleneimine) (PPI) dendrimers of the third and fourth generation with anionic rose bengal. A combined *in vitro* and *in silico* approach allowed for a complementary characterization of the effects of the dendrimers' physical and chemical properties on their interactions with RB and ultimately on the phototoxic activity of the latter. Interestingly, most previous research concentrated on RB as a model molecule, which, due to its spectral properties, was used to study interactions with dendrimers (usually PAMAM; less often PPI and other types of macromolecules).^{18,28–33} Significantly fewer studies have

**Figure 7.** Radial distribution functions of external amines (A, E), TIP3P water (B, F), chlorine ions (C, G), and sodium ions (D, H) with respect to the dendrimer core from the concatenated trajectory of the last 50 ns of simulation of two independent MD replicas in the absence (A–D) and presence (E–H) of RB.

analyzed the phototoxic activity of the dendrimer:RB complexes.^{16–18}

The PAMAM and PPI dendrimers used in this study were inspected at atomic resolution at the single-dendrimer level. The analysis of neat dendrimer trajectories yielded geometrical shape descriptors consistent with the existing literature^{34–50} in terms of RoG, asphericity, and aspect ratios, implying well-converged simulations. Both types of dendrimers are spherical in shape. In general, G3 dendrimers have a smaller radius and smaller internal cavities than G4 macromolecules. When comparing dendrimers of the same generation, PPIs are smaller, more rigid, and more compact than PAMAMs. PAMAM dendrimers form intramolecular H-bonds (more in the case of the fourth generation), whereas PPI dendrimers do not; moreover, PAMAM dendrimers form more hydrogen bonds with water than PPI dendrimers.

In our initial studies of the formation of dendrimer:RB complexes and the determination of their stoichiometry, we analyzed the changes in the spectral properties of the dye upon complexation. As a result of the titration of the RB solution with dendrimers, the fluorescence intensity of RB decreased followed by a red shift of the spectral peak and subsequent increase in fluorescence. A similar red shift of both RB absorbance³¹ and fluorescence³² most often indicates the binding of the dye to the dendrimer surface.²¹ We exploited this phenomenon to

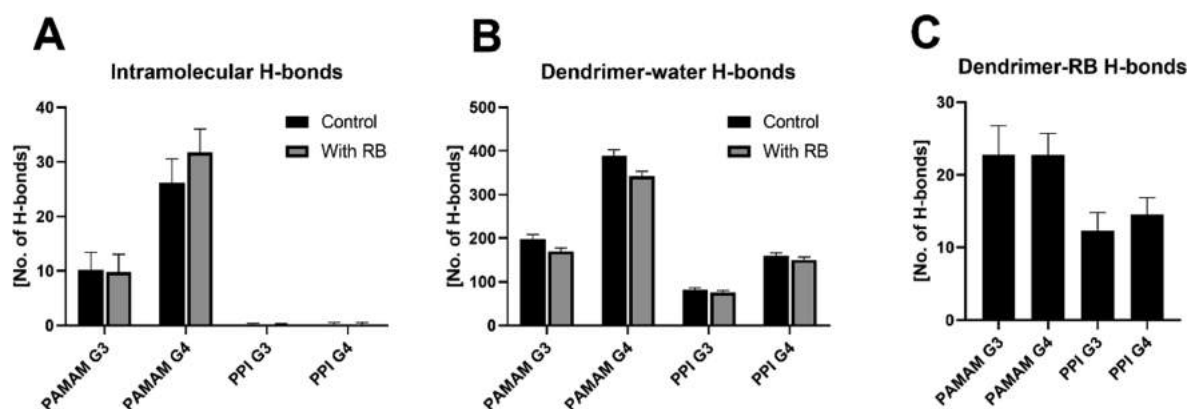


Figure 8. (A) Number of internal H-bonds in each dendrimer investigated. (B) Number of H-bonds between dendrimers and surrounding water molecules. (C) Number of H-bonds between dendrimers and RB. Data are presented as means \pm SD across the last 50 ns of two 200 ns replicas.

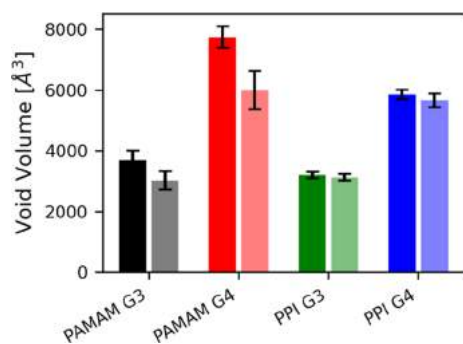


Figure 9. Volumes of dendrimers' internal cavities. Solid colors refer to simulations of the free dendrimer systems, whereas shaded colors refer to simulations of the dendrimer:RB complexes.

determine binding stoichiometry. As we expected, G4 dendrimers could bind more RB molecules (approx. 35 per dendrimer molecule) than G3 dendrimers (20–25 RB molecules per dendrimer molecule), likely due to differences in the dendrimers' volume and the level of protonation.^{38,51,52} The interactions of RB with the cationic phosphorus dendrimer

were analyzed in an analogous manner, but the binding stoichiometry was significantly lower. This is probably due to the use of a different buffer (HEPES vs PBS) since it has been shown that the buffer composition has a significant influence on the formation of the complex^{32,51} Furthermore, stoichiometry was affected by NaCl concentration; consistent with our hypothesis, this indicates the essential role of electrostatic interactions in the formation of complexes between anionic RB and cationic dendrimers.³² These results were confirmed by Fourier transform infrared spectroscopy (FTIR). Additionally, RB does not form complexes with anionic phosphorus dendrimers.³³ Other research groups also identified electrostatic interactions as the main driving force for the formation of complexes between RB and surface-modified PAMAM and PPI dendrimers^{18,31} and also reported a strong influence of the type of solvent on the binding stoichiometry.¹⁸

The determined stoichiometry of the PAMAM:RB and PPI:RB complexes was confirmed by titration of the dendrimer solutions with RB with the accompanying measurement of the zeta potential. The findings roughly coincided with those of the spectrofluorimetric method, with minor variations attributable to differences in the specificities of the two techniques. The

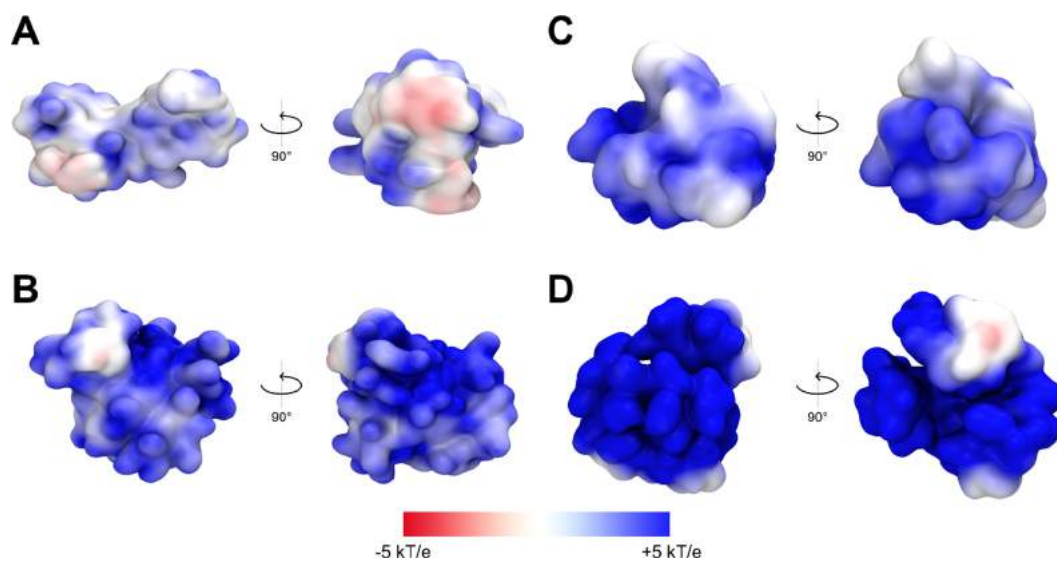


Figure 10. Front and side electrostatic maps for dendrimer:RB complexes (1:10): (A) PAMAM G3, (B) PAMAM G4, (C) PPI G3, and (D) PPI G4. Potential isocontours (obtained by the solution of the NLPBE at 150 mM ionic strength with a solute dielectric of 4 and solvent dielectric of 78.4) in the range from +5 kT/e (blue) to -5 kT/e (red).

results indicated that complexes fully saturated with RB exhibit negative zeta potential values. Assuming a surface binding mechanism, we can conclude that, in the final stages of titration, anionic RB molecules completely covered the outer layer of positively charged dendrimers.²⁰ In light of these observations, in subsequent investigations, we set a subsaturating concentration of RB (namely, 1:10 dendrimer:RB molar ratio), which retained a residual positive surface charge for increased cellular uptake and decreased aggregation of complexes.²⁴

Our molecular investigation of 1:10 dendrimer:RB complexes was carried out *in silico*, allowing the characterization of the binding mechanism and its effect on dendrimer geometry. Previous computational investigations of PPI:RB complexes clearly demonstrated the potential of atomistic simulations to complement experimental analyses by elucidating dendrimer:RB interaction dynamics.⁵³ Herein, we extended the computational approach to substantially longer timescales, as well as to different dendrimer types and generations, and expanded the analysis by including a higher number of ligands as well as by randomizing their initial placement in the solvent. Although these differences hinder a direct comparison of the present and earlier results, the strong complexation of RB with positively charged dendrimers is confirmed. Indeed, MD simulations revealed short complexation times, below 16 ns, and the ability of the investigated dendrimers to carry all 10 RB molecules, with no subsequent unbinding event detected over 200 ns in each MD replica, suggesting binding energies significantly exceeding thermal fluctuation (kT) and a strong tendency of RB to bind to each type of dendrimer. This behavior was primarily driven by electrostatics (see also Figure S11), consistent with previous observations. Interestingly, despite the predominant role of electrostatic interactions, we also observed the formation of H-bonds between dendrimers and RB, more strongly in the case of PAMAM than PPI.

The binding of RB did not significantly affect the geometrical characteristics of the dendrimers, and the estimated dendrimer:RB interaction areas were similar in all investigated systems. The volumes of the internal cavities decreased in the case of PAMAM dendrimers while remaining unchanged for PPI dendrimers. This was also reflected in the arrangement of the surface amino groups, which was influenced by RB binding only for PAMAM dendrimers. The attachment of RB also caused the displacement of water molecules (more evident in case of PPI dendrimers) and negatively charged chlorine ions (in the case of G3 dendrimers) from the inside of the dendritic scaffolds.

Notably, we found that RB has the ability to penetrate the structure of dendrimers, positioning itself preferentially inside the scaffold rather than on the surface. Comparison of these findings with the previously discussed fluorescence red shift indicates that the dendrimer:RB binding mechanism is more complex than indicated solely by spectrofluorimetric studies. Overall, the *in silico* investigation highlighted the greater ability of PPI dendrimers to internalize RB molecules within the inner dendrimer branches (see RDF data, Figure 6B). The size of the dendrimers and the specific arrangement of the RB molecules also influenced the surface potential of the complexes, which was significantly reduced (to values close to neutral) in the case of G3 dendrimers. Given the characteristics of the surface potential, it is plausible that interactions among multiple dendrimers occur in the presence of RB. This idea is consistent with preliminary data concerning interacting systems consisting of two dendrimers and 20 RB molecules, in which G3 complexes exhibited a marked tendency to engage in dendrimer–

dendrimer interactions (see Figure S12 and Videos S5 and S6). Interestingly, the complexes with PPI G4 also showed a tendency to aggregate during longer measurement times, which was consistent with the results of the analysis of the hydrodynamic diameter of the complexes by dynamic light scattering (DLS) (Table S3).

Our approach allowed us to highlight significant differences in complex formation and interaction patterns as a function of dendrimer type and generation. Because the photodynamic properties of RB are determined by several factors, including the chemical environment, it seems reasonable that these observed differences could significantly influence the ultimate cytotoxic effect.

Because the level of singlet oxygen generation is thought to be directly related to the efficacy of photodynamic therapy,⁵⁴ we assessed the activity of tested compounds in this regard. RB complexes with G3 dendrimers exhibited a significantly higher production of singlet oxygen, whereas the effect of G4 dendrimers was only slightly higher than that of free RB. At the same time, free dendrimers did not generate singlet oxygen. A similar effect was previously observed for supramolecular complexes of PSs and various polymers,⁵⁵ including RB and cationic dendrimers.¹⁶ On the other hand, no increase in singlet oxygen production was observed in the case of RB complexed with anionic half-generation PAMAM dendrimers;¹⁷ for PEG2000-modified PPI and PAMAM G4 dendrimers, the singlet oxygen level was reduced upon encapsulation of RB. In the latter case, however, the effect was attributed to RB aggregation and quenching due to the high local concentration of PS inside dendrimers (approx. 180 RB molecules per dendrimer).¹⁸ Such complexes exhibited no increase in phototoxic activity (relative to free RB) in HeLa cells. These observations underlie the influence of both the dendrimer:RB interaction and their molar ratio on the ultimate photodynamic effect.

The increase in singlet oxygen production can be explained by the immobilization of RB by the nanoparticle in more than one dimension, translating into a change in optical properties. Analysis of the Jablonski diagram reveals that excited RB can return to the ground state through photon emission or the transition to the triplet excited state responsible for singlet oxygen generation.¹ Considering the decrease in fluorescence during RB binding by the tested dendrimers, it is likely that, in this case, the second process is favored.⁵⁶ Nanoparticles can affect the fluorescence of the dye in the solution in several ways, including the internal fluorescence filter effect, dynamic quenching, static quenching, surface enhancement, and modulation of the quantum yield of the fluorophore. These phenomena are related to the binding-induced conformational changes in the structure of PS.^{57,58} Furthermore, the patterns of interaction between the dye, nanoparticle, and solvent can significantly affect aggregation, causing changes in the behavior and properties of PS in the vicinity of different nanoparticles suspended in the same solvent.

Indeed, the effect of dendrimer binding on RB-triggered singlet oxygen generation might be directly linked to the fact that RB tends to aggregate under physiological conditions⁵⁹ due to π -stacking and that PS aggregation has a detrimental effect on singlet oxygen generation due to the self-quenching of excited states.⁶⁰ Hence, better encapsulation of individual RB molecules by dendrimers would lead to a reduction in RB–RB aggregation and thus of self-quenching, yielding more efficient generation of singlet oxygen.

From this standpoint, the difference in the generation of singlet oxygen by G3 and G4 complexes is worth noting and remains difficult to explain at this stage of our research. The difference may be associated with the better prevention of RB aggregation and improved stabilization of the excited state by G3 dendrimers. Further stabilization of the transition state might also be achieved through complex–complex interactions. In addition, given the observed displacement of anions from inside the G3 dendrimers caused by RB, we can assume that anions play an active thermodynamic role in RB binding; thus, the latter might be more favored for G3 than G4 dendrimers. Such a binding strength- and mode-dependent production of singlet oxygen by PSs has already been observed during interactions with DNA.⁶¹ These observations highlight the need for further biophysical analyses, including confirmation using more direct, probe-independent methods of singlet oxygen detection; such techniques are currently under development in our laboratory.

Surprisingly, the results of the singlet oxygen generation assay were not reflected in our studies of cellular models. In these analyses, we observed the highest phototoxic activity in basal cell carcinoma models using PPI:RB complexes, regardless of generation. A similar lack of dependence on generation was observed in the case of PAMAM:RB complexes, whose cytotoxicity was intermediate between the action of PPI:RB complexes and free RB. It should be emphasized that, in the tested concentration range, free dendrimers did not exhibit phototoxicity, and no dark toxicity was observed for any of the compounds examined. Similar results were obtained when analyzing the production of intracellular ROS. Because the cellular factor is the most important difference between the singlet oxygen generation assay and subsequent studies, we hypothesized that the differences observed in cellular models are related to another crucial aspect of RB application: cellular uptake and subcellular localization. Indeed, dendrimer:RB complexes were able to deliver PS intracellularly much more effectively than intracellular transport of free RB.¹⁶

The efficiency of the intracellular transport of complexes perfectly matched the differences in their surface potential, evaluated based on the APBS electrostatic map analysis (Figure 10) of dendrimer:RB MD simulations: the PAMAM G3:RB complex with the surface electrostatic potential closest to neutral was the least efficient carrier, whereas the most cationic PPI G4:RB complex had the greatest intracellular transport capacity. These observations are consistent with reports of the efficient crossing of cell membranes by positively charged nanoparticles and allow us to predict the behavior of complexes depending on their surface potential.^{23,24,62,63}

The different delivery capacities of the investigated dendrimers may also be related to their chemical composition, as well as mechanical and structural properties. In this regard, PAMAM and PPI dendrimers exhibited differences in flexibility throughout the MD simulations, with PPIs exhibiting higher rigidity than PAMAMs. This behavior was emphasized by (i) the RDF, which showed that external amines of PPI dendrimers were not affected by the presence of RB; (ii) the RoG, which indicated that PAMAM dendrimers were more flexible; and (iii) the void volume, which revealed that the volumes of PPI internal cavities were not affected by the inclusion of the drug. Thus, the rigid and compact structure of PPI dendrimers may favor the intracellular delivery of RB.

On its own, the more efficient singlet oxygen generation is insufficient to explain the ultimate effects on cell viability, as the efficacy of PDT also depends on the cellular uptake and

subcellular location of PS.⁶⁴ Indeed, because the generation of singlet oxygen outside the cell is unlikely to significantly affect cell viability due to the limited lifespan of singlet oxygen molecules,⁶⁴ the ability of dendrimers to efficiently cross the cell membrane might be a decisive factor. Therefore, the observed cytotoxic effect, likely related to the production of intracellular ROS, may be the result of an increase in the cellular RB uptake and production of singlet oxygen. The latter effect, in turn, may differ significantly between cellular and extracellular systems due to the difference in light penetration and the changes in properties of the complexes upon transfer from a buffer with a limited composition into the culture medium and subsequently into the cell interior.

The joint effects of dendrimer structural and mechanical properties, the tendency of RB to penetrate the dendrimer, and the dendrimer surface electrostatics are thus crucial factors determining the ability of complexes to induce cell death. Based on our results, we conclude that cationic PAMAM and PPI dendrimers can serve as efficient carriers of RB in photodynamic therapy. Due to their structural properties, the patterns of interaction with RB, and the characteristic features of the dendrimer:RB complexes, PPI dendrimers outperform PAMAM dendrimers, providing the most efficient uptake in the case of PPI G4 and significantly increasing generation of singlet oxygen in the case of PPI G3. Particular attention should be paid to the selection of appropriate drug and dendrimer concentrations, ensuring a uniform distribution of RB within the structure of the dendrimer, thus preventing the aggregation of the PS and allowing the maintenance of a positive surface charge of the delivery system.

4. EXPERIMENTAL SECTION

4.1. Materials. The RB, fetal bovine serum (FBS), penicillin/streptomycin solution, trypsin–EDTA solution, ABDA probe [9,10-antherachenediyl-bis(methylene) dimalonate], MTT [3-(4,5-dimethyl-2-thiazolyl)-2,5-diphenyl-2H-tetrazolium bromide], and HEPES (4-(2-hydroxyethyl)-1-piperazineethanesulfonic acid) were purchased from Sigma-Aldrich (Taufkirchen, Germany). Dulbecco's phosphate-buffered saline without calcium and magnesium (DPBS) was purchased from Biowest (Nuaille, France). HBSS (Hanks' balanced salt solution) and the 154 CF culture medium were obtained from Gibco/ThermoFisher Scientific (Waltham, MA, USA). Chelex 100 Resin was obtained from Bio-Rad (Hercules, CA, USA). H₂DCFDA (2',7'-dichlorodihydrofluorescein diacetate) was purchased from Invitrogen/ThermoFisher Scientific. Dimethyl sulfoxide (DMSO) was purchased from POCH (Gliwice, Poland). Murine basal cell carcinoma lines (AsZ, BsZ, and CsZ) were provided by Dr. Ervin Epstein (Children's Oakland Research Institute, Oakland, CA, USA).

Poly(propyleneimine) (PPI) dendrimers of the third and fourth generation^a with 32 or 64 primary amino surface groups, respectively, were obtained from Symo-Chem (Eindhoven, the Netherlands). Poly(amidoamine) (PAMAM) dendrimers of the third and fourth generation with 32 and 64 primary amino surface groups, respectively, were obtained from Sigma-Aldrich.

4.2. Methods. **4.2.1. Spectrofluorimetric and Zeta Potential Studies on the Interaction between PAMAM or PPI Dendrimers and RB.** Fluorescence (F) emission spectra were obtained on an LS 55 fluorescence spectrometer (PerkinElmer, Waltham, MA, USA) at a constant temperature of 25 °C. All samples were prepared in HEPES buffer (10 mM, pH 7.4) and measured in quartz cuvettes. The excitation wavelength was set to 525 nm, and spectra were recorded between 540 and 650 nm. Excitation and emission slits were 5 and 7.5 nm, respectively. The RB solution in a constant concentration of 1 μM was titrated with dendrimer solutions in concentrations ranging from 0.02 to 1 μM to maintain the molar ratio of dendrimer:RB complexes between 1:50 and 1:1. The experiments were performed in three

independent replicates. To determine the stoichiometry of the polymer/dye complexes, plots of F_{364}/F_{375} vs the RB:dendrimer molar ratio were evaluated using Job's method.

Zeta potential measurements were performed using electrophoretic mobility assays on a Zetasizer Nano ZS (Malvern Instruments Ltd., Malvern, UK) at a constant temperature of 25 °C. All samples were prepared in a HEPES buffer (10 mM, pH 7.4). Dendrimer solutions of constant concentration (10 μ M) were placed in DTS 1070 folded capillary cells, and their zeta potentials were measured. The solutions were subsequently titrated with RB solution to obtain final RB concentrations ranging from 10 to 500 μ M, corresponding to dendrimer:RB molar ratios of 1:1 to 1:50. The experiments were performed in three independent replicates. Analysis of the titration curves for all studied systems enabled the evaluation of the stoichiometry of complexes as follows: the decreasing dependence of dendrimer zeta potential on dendrimer:RB mixture stoichiometry was extrapolated to the intersection with the eventual zeta potential value of the fully saturated dendrimer, and binding stoichiometry was determined from the intersection point (Job's method).

4.2.2. Preparation of Complexes for Further In Vitro Studies. Dendrimers were dissolved in double-distilled water to a final concentration of 40 μ M. Dendrimer solutions were prepared fresh and used on the same day. RB (dissolved in double-distilled water) was added to the dendrimer solutions in a dendrimer:RB molar ratio of 1:10 (to a final RB concentration of 400 μ M). This molar ratio ensures the complete complexation of RB molecules by all tested dendrimers. The mixtures were stirred for 0.5 h at the ambient temperature. Stock solutions were prepared just before the experiments.

4.2.3. Singlet Oxygen Generation Assay. The singlet oxygen generation was studied using the ABDA probe (final concentration: 5 μ M) as an indicator. Solutions of RB, PAMAM G3:RB, PAMAM G4:RB, PPI G3:RB, PPI G4:RB, and free dendrimers in the highest concentration used for complex formation (0.1 μ M) were prepared in 10 mM HEPES. The complexes were prepared at RB concentrations of 0.125, 0.25, 0.5, 0.75, and 1 μ M. Upon sample preparation, 100 μ L of each solution was transferred to a 96-well black plate. All measurements were performed on a fluorescence microplate reader (Fluoroskan Ascent FL, ThermoFisher Scientific) at an excitation wavelength of 355 nm and an emission wavelength of 430 nm. Samples were mixed before each measurement. The first measurement was recorded without the ABDA probe to determine whether RB, dendrimers, or their complexes exhibit any fluorescence in this range. Following the first measurement, ABDA was added to each well, and the fluorescence of the probe without irradiation was measured. Next, the plate was immediately placed under a Q.Light Pro Unit lamp (Q.Light, Rorschach, Switzerland) equipped with a filter emitting visible light in the wavelength range 385–780 nm. Fluorescence was measured in 5 min intervals during irradiation for 5–60 min. The experiments were performed in four independent replicates. The slopes of the fluorescence curves were considered to be a measurement of singlet oxygen generation. The results were presented as percentages of the singlet oxygen generation in the control sample (HEPES buffer irradiated with probe).

4.2.4. Cell Culture. AsZ, BsZ, and CsZ (murine basal cell carcinoma) cell lines were cultured in the 154 CF medium with 5% penicillin/streptomycin, 0.05 mM calcium, and 2% Chelex-purified, heat-inactivated FBS. Cells were cultured in T-75 culture flasks at 37 °C/5% CO₂ and subcultured every 2 or 3 days. Cells were harvested using 0.25% (w/v) trypsin/0.03% (w/v) EDTA. The number of viable cells was determined by Trypan blue exclusion assay on a Countess Automated Cell Counter (Invitrogen, Carlsbad, CA, USA).

4.2.5. Cytotoxicity Studies. AsZ, BsZ, and CsZ cells were seeded in 96-well transparent plates at a density of 3×10^4 cells per well in 90 μ L of the medium and incubated for 24 h before experiments. Then, using stock solutions (according to 4.2.2), the samples (PAMAM G3:RB, PAMAM G4:RB, PPI G3:RB PPI G4:RB, and free RB solutions) were prepared in the HEPES buffer and added to the cells to obtain final RB concentrations of 0.25, 0.5, 0.75, and 1 μ M. The cytotoxicity of free dendrimers was also evaluated at the highest concentration used for the preparation of complexes. Cells were incubated with tested compounds

for 5 h (37 °C, 5% CO₂). The medium was replaced with DPBS, and the cells were irradiated with visible light using the Q.Light Pro Unit lamp for 30 min. Immediately after irradiation, DPBS was replaced with the fresh culture medium, and the cells were incubated for 24 h (post-PDT incubation). The so-called "dark" toxicity (without irradiation) was evaluated in parallel.

The cell viability was measured by the MTT assay. MTT was added to the wells at a final concentration of 0.5 mg/mL, and the plates were incubated for 2 h (37 °C, 5% CO₂). After incubation, formazan crystals were dissolved in DMSO, and the absorbance was read at 570 nm using a PowerWave HT Microplate Spectrophotometer (BioTek, Winooski, VT, USA). Experiments were performed in six independent replicates. Cell viabilities are presented as percentages of the viability in the untreated control.

4.2.6. ROS Generation Assay. An H₂DCFDA probe was used to investigate the intracellular production of ROS. For this purpose, AsZ cells were seeded in 96-well black plates at a density of 1×10^4 cells per well in 90 μ L of the medium. After incubation for 24 h, the samples (PAMAM G3:RB, PAMAM G4:RB, PPI G3:RB PPI G4:RB, and free RB solutions) were prepared in the HEPES buffer and added to the cells to obtain final RB concentrations of 0.25, 0.50, 1, or 2 μ M. The ROS-generating activity of free dendrimers was also evaluated at the highest concentration used for the preparation of complexes. Cells were incubated with tested compounds for 5 h (37 °C, 5% CO₂). The medium containing the tested compounds was removed, a 2 μ M solution of H₂DCFDA in HBSS was added to each well, and the plates were incubated for the next 20 min in the dark (37 °C, 5% CO₂). Next, the cells were washed with HBSS, and the background fluorescence (excitation: 485 nm; emission: 530 nm) of nonirradiated cells submerged in 100 μ L HBSS was measured on a PowerWave HT Microplate reader (BioTek). The cells were then irradiated using Q.Light Pro Unit lamp for 30 min, and 2',7'-dichlorofluorescein (DCF) fluorescence was measured. The experiments were performed in four independent replicates. The ROS level was calculated as the DCF fluorescence intensity and was presented as a percentage of the ROS production in control samples (without treatment). Each measurement was corrected by subtraction of the background fluorescence intensity (before irradiation).

4.2.7. Cellular Uptake Assay. AsZ cells were seeded into 24-well plates at a density of 1×10^5 cells per well and incubated for 24 h (37 °C, 5% CO₂). Next, RB, PAMAM G3:RB, PAMAM G4:RB, PPI G3:RB, and PPI G4:RB (5 μ M final concentration of RB) were added to each well, and the cells were incubated with the compounds for up to 4 h. Following incubation, the compounds were removed, and the cells were washed with DPBS and detached using the trypsin–EDTA solution. The fresh culture medium was added to the cells, and the samples were gently mixed and collected for measurements. To estimate cellular uptake, the fluorescence of the samples was measured using flow cytometry (LSRII, Becton Dickinson, Franklin Lakes, NJ, USA). The excitation and emission filters were 520 and 570 nm, respectively. The experiments were performed in five independent replicates. The results are presented as the percentage of cells in the population that internalized RB.

4.2.8. Statistical Analysis. Statistical significance was tested using two-way ANOVA for concentrations and compound series followed by *post hoc* Tukey's test for pairwise difference testing. In all tests, *p* values <0.05 were considered statistically significant. Data were collected from at least three independent experiments and presented as arithmetic means \pm SD.

4.2.9. In Silico Studies.
4.2.9.1. System Setup. Initial configurations for PAMAM and PPI dendrimers were built using the Dendrimer Builder Toolkit (DBT)³⁴ and the General Amber Force Field (GAFF).⁶⁶ The protonation state was chosen based on neutral pH, as reported previously.^{34,35,43,67} Under these conditions, the amine groups in the external layers of PAMAM dendrimers were fully protonated, whereas all the primary amines present at the periphery and the tertiary amines in alternating layers of the PPI dendrimers were protonated, resulting in 2/3 protonation according to the Ising model.^{52,68} The assigned protonation states resulted in a total charge of +32, +64, +42, and +84 for PAMAM G3, PAMAM G4, PPI G3, and PPI

G4, respectively. RB was described by the GAFF force field, and partial charges were assigned using the AM1-BCC charge method (see also Figure S13).⁶⁹ Topology and parametrization were constructed using antechamber and GROMACS tools.^{70,71}

4.2.9.2. Single-Dendrimer Conformational Dynamics. Each dendrimer was positioned in a dodecahedral box filled with TIP3P (transferable intermolecular potential 3P) water molecules⁷² and ions to neutralize the system charge at a physiological NaCl concentration (0.15 M). Each system was energy-minimized using the steepest descent energy minimization algorithm (2000 steps). After randomly initializing atom velocities following a Maxwell–Boltzmann distribution, a 100 ps position-restrained molecular dynamics (MD) was performed in the canonical ensemble (NVT) at 300 K using the v-rescale algorithm⁷³ for temperature coupling. Then, an NPT position-restrained MD was executed for 500 ps using a v-rescale thermostat⁷³ and a Berendsen barostat⁷⁴ to equilibrate temperature (300 K) and pressure (1 atm), respectively. Finally, an unrestrained 200 ns MD simulation was performed in the isothermal–isobaric ensemble (NPT) at 300 K and 1 atm using the v-rescale and Parrinello–Rahman coupling algorithms.^{73,75} The GROMACS 2020 package was used for all MD simulations.⁷⁶ Long-range electrostatic interactions were calculated at every step with the particle mesh Ewald method⁷⁷ with a cutoff radius of 1.2 nm; the same cutoff was also applied to Lennard–Jones interactions. The simulation time step was 2 fs using the LINCS (LINear Constraint Solver) algorithm.⁷⁸ To ensure the reproducibility of the data, a second replicate was performed after re-initializing velocities after the minimization step and following the same simulation protocol as described above. The final 50 ns of MD simulations was considered as a single ensemble trajectory representing the structural stability of each treated system.

4.2.9.3. Dendrimer:RB Complexation and Interaction Dynamics. The final configuration from the aforementioned equilibrium ensembles was extracted for each dendrimer type. The structure was again inserted into a dodecahedral box, and 10 RB molecules were added in random positions around the dendrimer to obtain a 1:10 molar concentration ratio. The box was filled with TIP3P water molecules and NaCl at a physiological concentration (0.15 M) to neutralize the system charge. The systems were then simulated using the same simulation protocol described in the previous section. Two replicates were performed to ensure data reproducibility, and the last 50 ns of these MD simulations was considered as a single ensemble trajectory representing the structural stability of each investigated system.

4.2.9.4. Simulation Analysis. As reported previously,^{34,35,43,48} the geometrical characterization of the investigated dendrimers was evaluated using the radius of gyration (RoG), which measures the size of the dendrimers, and three main geometrical descriptors (I_x/I_y , I_x/I_z , and δ) that evaluate the shape of the dendrimers. In more detail, we calculated the three principal moments of inertia (I_x , I_y , and I_z) and derived two aspect ratios (I_x/I_y and I_x/I_z) and asphericity (δ) as defined by Rudnick and Gaspari:⁷⁹

$$\delta = 1 - 3 \frac{\langle I_2 \rangle}{\langle I_1^2 \rangle} \quad (1)$$

where $I_1 = I_x + I_y + I_z$, $I_2 = I_x I_y + I_y I_z + I_x I_z$, and angle brackets denote time averaging. In this formulation, the closer to zero the value of δ is, the more spherical the molecule is.

The volumes of dendrimer internal cavities were calculated as described previously.^{80,81} First, volumes associated with accessible surface areas (V_{sasa}) were calculated at different probe radii. Then, a linear fitting on the cubic root values of V_{sasa} was performed at different probe radii, starting from 0.4 nm. The deviation of the calculated volume from the aforementioned fitting line, at a probe radius of 0.3 nm, provides an estimate of the volumes of internal voids. Internal cavities have been evaluated both for the neat dendrimer systems and for the dendrimer:RB complexes. In the latter case, to ensure a consistent comparison, the volumes of dendrimer cavities were evaluated after removing RB molecules from the complex snapshots, thus excluding the volume occupied by RB molecules from the

calculations. This ensures that we evaluated the actual structural effects on the dendrimer itself rather than the volume occupancy of RB.

We also analyzed the dendrimer:RB complexes by comparing electrostatic potentials in the absence and presence of bound RB using the APBS package.⁸² Specifically, the nonlinear Poisson–Boltzmann equation was applied using single Debye–Hückel sphere boundary conditions on a $200 \times 200 \times 200$ grid with a spacing of 1 Å centered at the center of mass (CoM) of the molecular system. The relative dielectric constants of the solute and the solvent were set to 4 and 78.4,^{82,83} respectively. The ionic strength was set to 150 mM, and the temperature was fixed at 300 K.

The visual inspection of simulations and all molecular renderings was carried out with the Visual Molecular Dynamics (VMD) package.⁸⁴

■ ASSOCIATED CONTENT

Supporting Information

The Supporting Information is available free of charge at <https://pubs.acs.org/doi/10.1021/acs.jmedchem.1c01080>.

Additional figures and tables illustrating the cytotoxicity, cellular uptake, and further results of *in silico* studies (PDF)

MD trajectories showing the early and stable complexation of all 10 RB molecules (MP4)

MD trajectories showing the early and stable complexation of all 10 RB molecules (MP4)

MD trajectories showing the early and stable complexation of all 10 RB molecules (MP4)

MD trajectories showing the early and stable complexation of all 10 RB molecules (MP4)

G3 complexes exhibiting a marked tendency to engage in dendrimer–dendrimer interactions (MP4)

G3 complexes exhibiting a marked tendency to engage in dendrimer–dendrimer interactions (MP4)

Molecular formula strings (CSV)

PDB submission (ZIP)

■ AUTHOR INFORMATION

Corresponding Authors

Krzysztof Sztandera – Department of General Biophysics, Faculty of Biology and Environmental Protection, University of Lodz, 90-236 Lodz, Poland; orcid.org/0000-0001-7595-7198; Email: krzysztof.sztandera@edu.uni.lodz.pl

Barbara Klajnert-Maculewicz – Department of General Biophysics, Faculty of Biology and Environmental Protection, University of Lodz, 90-236 Lodz, Poland; orcid.org/0000-0003-3459-8947; Email: barbara.klajnert@biol.uni.lodz.pl

Authors

Michał Gorzkiewicz – Department of General Biophysics, Faculty of Biology and Environmental Protection, University of Lodz, 90-236 Lodz, Poland; orcid.org/0000-0001-9258-3626

Ana Sofia Dias Martins – iMed.Ulisboa—Research Institute for Medicines, Faculdade de Farmácia, Universidade de Lisboa, 1649-003 Lisboa, Portugal

Lorenzo Pallante – Polito^{BIO}MedLab, Department of Mechanical and Aerospace Engineering, Politecnico di Torino, 10129 Turin, Italy; orcid.org/0000-0001-9969-6519

Eric Adriano Zizzi – Polito^{BIO}MedLab, Department of Mechanical and Aerospace Engineering, Politecnico di Torino, 10129 Turin, Italy

Marcello Miceli – Polito^{BIO}MedLab, Department of Mechanical and Aerospace Engineering, Politecnico di Torino, 10129 Turin, Italy

Mateusz Bątal – Department of General Biophysics, Faculty of Biology and Environmental Protection, University of Lodz, 90-236 Lodz, Poland

Catarina Pinto Reis – iMed.Ulisboa—Research Institute for Medicines, Faculdade de Farmácia, Universidade de Lisboa, 1649-003 Lisboa, Portugal; Instituto de Biofísica e Engenharia Biomédica, Faculdade de Ciências, Universidade de Lisboa, 1749-016 Lisboa, Portugal

Marco A. Deriu – Polito^{BIO}MedLab, Department of Mechanical and Aerospace Engineering, Politecnico di Torino, 10129 Turin, Italy

Complete contact information is available at:

<https://pubs.acs.org/10.1021/acs.jmedchem.1c01080>

Notes

The authors declare no competing financial interest.

ACKNOWLEDGMENTS

This work was supported by the National Science Centre, Poland (Project UMO-2017/25/B/NZ7/01304 "Phosphorus dendrimers as carriers for photosensitizers—in vivo studies"), and based upon work from COST Action "Nano2Clinic. Cancer Nanomedicine—from the bench to the bedside" CA17140 supported by COST (European Cooperation in Science and Technology). The authors would also like to thank Prof. Prabal Maiti, Mr. Vishal Maingi, and Mr. Vaibhav Jain for their precious help in the dendrimer modeling.

ABBREVIATIONS

DCF, 2',7'-dichlorofluorescein; DLS, dynamic light scattering; H₂DCFDA, 2',7'-dichlorodihydrofluorescein diacetate; LINCS, LINear Constraint Solver; MD, molecular dynamics; NPT, isothermal–isobaric ensemble; NVT, canonical ensemble; PAMAM G3:RB, complex of PAMAM dendrimer third generation with rose bengal; PAMAM G4:RB, complex of PAMAM dendrimer fourth generation with rose bengal; PDF, probability density function; PPI G3:RB, complex of PPI dendrimer third generation with rose bengal; PPI G4:RB, complex of PPI dendrimer fourth generation with rose bengal; PS, photosensitizer; RB, rose bengal; RDF, radial distribution function; RoG, radius of gyration; TIP3P, transferable intermolecular potential 3P

ADDITIONAL NOTE

^aAccording to ref 65, the nomenclature for Tomalia-type PAMAM dendrimers can be used for PPI dendrimers. Hence, we adopted the suggested classification, describing the commercially available PPI dendrimer of the fifth generation (DAB-Am-64) as fourth generation, and fourth generation (DAB-Am-32) as third generation.

REFERENCES

- (1) Sztandera, K.; Marcinkowska, M.; Gorzkiewicz, M.; Janaszewska, A.; Laurent, R.; Zablocka, M.; Mignani, S.; Majoral, J. P.; Klajnert-Maculewicz, B. In Search of a Phosphorus Dendrimer-Based Carrier of Rose Bengal: Tyramine Linker Limits Fluorescent and Phototoxic Properties of a Photosensitizer. *Int. J. Mol. Sci.* **2020**, *21*, 4456.
- (2) Kucinska, M.; Skupin-Mrugalska, P.; Szczolko, W.; Sobotta, L.; Sciepora, M.; Tykarska, E.; Wierzchowski, M.; Teubert, A.; Fedoruk-Wyszomirska, A.; Wyszko, E.; Gdaniec, M.; Kaczmarek, M.; Goslinski, T.; Mielcarek, J.; Murias, M. Phthalocyanine Derivatives Possessing 2-(Morpholin-4-yl)ethoxy Groups as Potential Agents for Photodynamic Therapy. *J. Med. Chem.* **2015**, *58*, 2240–2255.

- (3) Olivo, M.; Bhuvanewari, R.; Lucky, S. S.; Dendukuri, N.; Thong, P. S.-P. Targeted Therapy of Cancer Using Photodynamic Therapy in Combination with Multi-Faceted Anti-Tumor Modalities. *Pharmaceuticals* **2010**, *3*, 1507–1529.

- (4) Dos Santos, A. F.; De Almeida, D. R. Q.; Terra, L. F.; Baptista, M. S.; Labriola, L. Photodynamic Therapy in Cancer Treatment - an Update Review. *J. Cancer Metastasis Treat.* **2019**, *5*, 25.

- (5) Demartis, S.; Obinu, A.; Gavini, E.; Giunchedi, P.; Rassa, G. Nanotechnology-Based Rose Bengal: A Broad-Spectrum Biomedical Tool. *Dyes Pigm.* **2021**, *188*, 109236.

- (6) Redmond, R. W.; Gamlin, J. N. A Compilation of Singlet Oxygen Yields from Biologically Relevant Molecules. *Photochem. Photobiol.* **1999**, *70*, 391–475.

- (7) Master, A.; Livingston, M.; Sen Gupta, A. Photodynamic Nanomedicine in the Treatment of Solid Tumors: Perspectives and Challenges. *J. Controlled Release* **2013**, *168*, 88–102.

- (8) Sztandera, K.; Gorzkiewicz, M.; Klajnert-Maculewicz, B. Nano-carriers in Photodynamic Therapy—in Vitro and in Vivo Studies. *Wiley Interdiscip. Rev.: Nanomed. Nanobiotechnol.* **2020**, *12*, 1–24.

- (9) Qjdwai, A.; Annu, N.; Nabi, B.; Kotta, S.; Narang, J. K.; Baboota, S.; Ali, J. Role of Nanocarriers in Photodynamic Therapy. *Photodiagn. Photodyn. Ther.* **2020**, *30*, 101782.

- (10) Ghaffari, M.; Dehghan, G.; Baradaran, B.; Zarebkohan, A.; Mansoori, B.; Soleymani, J.; Dolatabadi, J. E. N.; Hamblin, M. R. Co-Delivery of Curcumin and Bcl-2 siRNA by PAMAM Dendrimers for Enhancement of the Therapeutic Efficacy in HeLa Cancer Cells. *Colloids Surf., B* **2020**, *188*, 110762.

- (11) Duncan, R.; Izzo, L. Dendrimer Biocompatibility and Toxicity. *Adv. Drug Delivery Rev.* **2005**, *57*, 2215–2237.

- (12) Tripathi, P. K.; Tripathi, S. Dendrimers for Anticancer Drug Delivery. *Pharm. Appl. Dendrimers* **2019**, 131–150.

- (13) Gorzkiewicz, M.; Klajnert-Maculewicz, B. Chapter 10 in Dendrimers for Drug Delivery. In *Dendrimers as Nanocarriers for Anticancer Drugs*; Sharma, A., Keservan, R., Eds.; Apple Academic Press, 2018; pp. 327–374.

- (14) Agarwal, A.; Gupta, U.; Asthana, A.; Jain, N. K. Dextran Conjugated Dendritic Nanoconstructs as Potential Vectors for Anti-Cancer Agent. *Biomaterials* **2009**, *30*, 3588–3596.

- (15) Patri, A. K.; Kukowska-Latallo, J. F.; Baker, J. R., Jr. Targeted Drug Delivery with Dendrimers: Comparison of the Release Kinetics of Covalently Conjugated Drug and Non-Covalent Drug Inclusion Complex. *Adv. Drug Delivery Rev.* **2005**, *57*, 2203–2214.

- (16) Dabrzalska, M.; Janaszewska, A.; Zablocka, M.; Mignani, S.; Majoral, J. P.; Klajnert-Maculewicz, B. Cationic Phosphorus Dendrimer Enhances Photodynamic Activity of Rose Bengal against Basal Cell Carcinoma Cell Lines. *Mol. Pharmaceutics* **2017**, *14*, 1821–1830.

- (17) Karthikeyan, K.; Babu, A.; Kim, S. J.; Murugesan, R.; Jayasubramanian, K. Enhanced Photodynamic Efficacy and Efficient Delivery of Rose Bengal Using Nanostructured Poly(Amidoamine) Dendrimers: Potential Application in Photodynamic Therapy of Cancer. *Cancer Nanotechnol.* **2011**, *2*, 95–103.

- (18) Kojima, C.; Toi, Y.; Harada, A.; Kono, K. Preparation of Poly(ethylene glycol)-Attached Dendrimers Encapsulating Photosensitizers for Application to Photodynamic Therapy. *Bioconjugate Chem.* **2007**, *18*, 663–670.

- (19) Gorzkiewicz, M.; Appelhans, D.; Boye, S.; Lederer, A.; Voit, B.; Klajnert-Maculewicz, B. Effect of the Structure of Therapeutic Adenosine Analogues on Stability and Surface Electrostatic Potential of Their Complexes with Poly(Propyleneimine) Dendrimers. *Macromol. Rapid Commun.* **2019**, *40*, 1900181.

- (20) Gorzkiewicz, M.; Buczkowski, A.; Appelhans, D.; Voit, B.; Pułaski, L.; Pałecz, B.; Klajnert-Maculewicz, B. Poly(Propyleneimine) Glycodendrimers Non-Covalently Bind ATP in a PH- and Salt-Dependent Manner – Model Studies for Adenosine Analogue Drug Delivery. *Int. J. Pharm.* **2018**, *544*, 83–90.

- (21) Klajnert, B.; Bryszewska, M. The Interaction of Tryptophan and ANS with PAMAM Dendrimers. *Cell. Mol. Biol. Lett.* **2002**, *7*, 1087–1094.

- (22) Huang, C. Y. Determination of Binding Stoichiometry by the Continuous Variation Method: The Job Plot. *Methods Enzymol.* **1982**, *87*, 509–525.
- (23) Hong, S.; Leroueil, P. R.; Janus, E. K.; Peters, J. L.; Kober, M.-M.; Islam, M. T.; Orr, B. G.; Baker, J. R., Jr.; Banaszak Holl, M. M. Interaction of Polycationic Polymers with Supported Lipid Bilayers and Cells: Nanoscale Hole Formation and Enhanced Membrane Permeability. *Bioconjugate Chem.* **2006**, *17*, 728–734.
- (24) Honary, S.; Zahir, F. Effect of Zeta Potential on the Properties of Nano-Drug Delivery Systems - A Review (Part 1 and 2). *Trop. J. Pharm. Res.* **2013**, *12*, 255–264.
- (25) Basset-Seguín, N.; Herms, F. Update on the Management of Basal Cell Carcinoma. *Acta Derm.-Venereol.* **2020**, 284–290.
- (26) Di Stefani, A.; Chimenti, S. Basal Cell Carcinoma: Clinical and Pathological Features. *G. Ital. di Dermatologia e Venereol.* **2015**, *150*, 385–391.
- (27) Tanis, I.; Karatasos, K. Molecular Dynamics Simulations of Polyamidoamine Dendrimers and Their Complexes with Linear Poly(Ethylene Oxide) at Different PH Conditions: Static Properties and Hydrogen Bonding. *Phys. Chem. Chem. Phys.* **2009**, *11*, 10017–10028.
- (28) Kono, K.; Miyoshi, T.; Haba, Y.; Murakami, E.; Kojima, C.; Harada, A. Temperature Sensitivity Control of Alkylamide-Terminated Poly(Amidoamine) Dendrimers Induced by Guest Molecule Binding. *J. Am. Chem. Soc.* **2007**, *129*, 7222–7223.
- (29) Jansen, J. F. G. A.; Meijer, E. W.; de Brabander-van den Berg, E. M. M. The Dendritic Box: Shape-Selective Liberation of Encapsulated Guests. *J. Am. Chem. Soc.* **1995**, *117*, 4417–4418.
- (30) Tamaki, M.; Fukushima, D.; Kojima, C. Dual PH-Sensitive and UCST-Type Thermosensitive Dendrimers: Phenylalanine-Modified Polyamidoamine Dendrimers with Carboxyl Termini. *RSC Adv.* **2018**, *8*, 28147–28151.
- (31) Haba, Y.; Harada, A.; Takagishi, T.; Kono, K. Synthesis of Biocompatible Dendrimers with a Peripheral Network Formed by Linking of Polymerizable Groups. *Polymer (Guildf).* **2005**, *46*, 1813–1820.
- (32) Dabrzalska, M.; Zablocka, M.; Mignani, S.; Majoral, J. P.; Klajnert-Maculewicz, B. Phosphorus Dendrimers and Photodynamic Therapy. Spectroscopic Studies on Two Dendrimer-Photosensitizer Complexes: Cationic Phosphorus Dendrimer with Rose Bengal and Anionic Phosphorus Dendrimer with Methylene Blue. *Int. J. Pharm.* **2015**, *492*, 266–274.
- (33) Dabrzalska, M.; Benseny-Cases, N.; Barnadas-Rodríguez, R.; Mignani, S.; Zablocka, M.; Majoral, J. P.; Bryszewska, M.; Klajnert-Maculewicz, B.; Cladera, J. Fourier Transform Infrared Spectroscopy (FTIR) Characterization of the Interaction of Anti-Cancer Photosensitizers with Dendrimers. *Anal. Bioanal. Chem.* **2016**, *408*, 535–544.
- (34) Maingi, V.; Jain, V.; Bharatam, P. V.; Maiti, P. K. Dendrimer Building Toolkit: Model Building and Characterization of Various Dendrimer Architectures. *J. Comput. Chem.* **2012**, *33*, 1997–2011.
- (35) Jain, V.; Maingi, V.; Maiti, P. K.; Bharatam, P. V. Molecular Dynamics Simulations of PPI Dendrimer-Drug Complexes. *Soft Matter* **2013**, *9*, 6482–6496.
- (36) Rathgeber, S.; Monkenbusch, M.; Kreitschmann, M.; Urban, V.; Brulet, A. Dynamics of Star-Burst Dendrimers in Solution in Relation to Their Structural Properties. *J. Chem. Phys.* **2002**, *117*, 4047–4062.
- (37) Liu, Y.; Bryantsev, V. S.; Diallo, M. S.; Goddard, W. A., II PAMAM Dendrimers Undergo PH Responsive Conformational Changes Without Swelling. *J. Am. Chem. Soc.* **2009**, *131*, 2798–2799.
- (38) Maiti, P. K.; Çağın, T.; Lin, S.-T.; Goddard, W. A. Effect of Solvent and PH on the Structure of PAMAM Dendrimers. *Macromolecules* **2005**, *38*, 979–991.
- (39) Topp, A.; Bauer, B. J.; Tomalia, D. A.; Amis, E. J. Effect of Solvent Quality on the Molecular Dimensions of PAMAM Dendrimers. *Macromolecules* **1999**, *32*, 7232–7237.
- (40) Scherrenber, R.; Coussens, B.; Van Vliet, P.; Edouard, G.; Brackman, J.; De Brabander, E.; Mortensen, K. The Molecular Characteristics of Poly(Propyleneimine) Dendrimers as Studied with Small-Angle Neutron Scattering, Viscosimetry, and Molecular Dynamics. *Macromolecules* **1998**, *31*, 456–461.
- (41) Prosa, T. J.; Bauer, B. J.; Amis, E. J.; Tomalia, D. A.; Scherrenber, R. A SAXS Study of the Internal Structure of Dendritic Polymer Systems. *J. Polym. Sci., Part B: Polym. Phys.* **1997**, *35*, 2913–2924.
- (42) Wu, C. PH Response of Conformation of Poly(Propylene Imine) Dendrimer in Water: A Molecular Simulation Study. *Mol. Simul.* **2010**, *36*, 1164–1172.
- (43) Ramos, M. C.; Horta, V. A. C.; Horta, B. A. C. Molecular Dynamics Simulations of PAMAM and PPI Dendrimers Using the GROMOS-Compatible 2016H66 Force Field. *J. Chem. Inf. Model.* **2019**, *59*, 1444–1457.
- (44) Opitz, A. W.; Wagner, N. J. Structural Investigations of Poly(Amido Amine) Dendrimers in Methanol Using Molecular Dynamics. *J. Polym. Sci., Part B: Polym. Phys.* **2006**, *44*, 3062–3077.
- (45) Barraza, L. F.; Zuñiga, M.; Alderete, J. B.; Arbeloa, E. M.; Jiménez, V. A. Effect of PH on Eosin Y/PAMAM Interactions Studied from Absorption Spectroscopy and Molecular Dynamics Simulations. *J. Lumin.* **2018**, *199*, 258–265.
- (46) Caballero, J.; Poblete, H.; Navarro, C.; Alzate-Morales, J. H. Association of Nicotinic Acid with a Poly(Amidoamine) Dendrimer Studied by Molecular Dynamics Simulations. *J. Mol. Graphics Modell.* **2013**, *39*, 71–78.
- (47) Kanchi, S.; Gosika, M.; Ayappa, K. G.; Maiti, P. K. Dendrimer Interactions with Lipid Bilayer: Comparison of Force Field and Effect of Implicit vs Explicit Solvation. *J. Chem. Theory Comput.* **2018**, *14*, 3825–3839.
- (48) Kavyani, S.; Amjad-Iranagh, S.; Dadvar, M.; Modarress, H. Hybrid Dendrimers of PPI(Core)-PAMAM(Shell): A Molecular Dynamics Simulation Study. *J. Phys. Chem. B* **2016**, *120*, 9564–9575.
- (49) Lee, I.; Athey, B. D.; Wetzel, A. W.; Meixner, W.; Baker, J. R. Structural Molecular Dynamics Studies on Polyamidoamine Dendrimers for a Therapeutic Application: Effects of PH and Generation. *Macromolecules* **2002**, *35*, 4510–4520.
- (50) Porcar, L.; Liu, Y.; Verduzco, R.; Hong, K.; Butler, P. D.; Magid, L. J.; Smith, G. S.; Chen, W.-R. Structural Investigation of PAMAM Dendrimers in Aqueous Solutions Using Small-Angle Neutron Scattering: Effect of Generation. *J. Phys. Chem. B* **2008**, *112*, 14772–14778.
- (51) Gorzkiewicz, M.; Buczkowski, A.; Palecz, B.; Klajnert-Maculewicz, B. PAMAM and PPI Dendrimers in Biophysical and Thermodynamic Studies on the Delivery of Therapeutic Nucleotides, Nucleosides and Nucleobase Derivatives for Anticancer Applications. In *Thermodynamics and Biophysics of Biomedical Nanosystems*; Springer, 2019; pp 183–243, DOI: 10.1007/978-981-13-0989-2_7.
- (52) Koper, G. J. M.; Van Genderen, M. H. P.; Elissen-Román, C.; Baars, M. W. P. L.; Meijer, E. W.; Borkovec, M. Protonation Mechanism of Poly(Propylene Imine) Dendrimers and Some Associated Oligo Amines. *J. Am. Chem. Soc.* **1997**, *119*, 6512–6521.
- (53) Miklis, P.; Çağın, T.; Goddard, W. A. Dynamics of Bengal Rose Encapsulated in the Meijer Dendrimer Box. *J. Am. Chem. Soc.* **1997**, *119*, 7458–7462.
- (54) Liang, X.; Wang, K. K.; Zhu, T. C. Singlet Oxygen Dosimetry Modeling for Photodynamic Therapy. In *Optical Methods for Tumor Treatment and Detection: Mechanisms and Techniques in Photodynamic Therapy XXI*; 2012; Vol. 8210, p 82100T.
- (55) Kashyap, A.; Ramasamy, E.; Ramalingam, V.; Pattabiraman, M. Supramolecular Control of Singlet Oxygen Generation. *Molecules* **2021**, *26*, 2673.
- (56) Allison, R. R.; Downie, G. H.; Cuenca, R.; Hu, X.-H.; Childs, C. J. H.; Sibata, C. H. Photosensitizers in Clinical PDT. *Photodiagn. Photodyn. Ther.* **2004**, *1*, 27–42.
- (57) Zhang, D.; Nettles, C. B., II A Generalized Model on the Effects of Nanoparticles on Fluorophore Fluorescence in Solution. *J. Phys. Chem. C* **2015**, *119*, 7941–7948.
- (58) Zhai, W.; Wang, C.; Yu, P.; Wang, Y.; Mao, L. Single-Layer MnO₂ Nanosheets Suppressed Fluorescence of 7-Hydroxycoumarin: Mechanistic Study and Application for Sensitive Sensing of Ascorbic Acid in Vivo. *Anal. Chem.* **2014**, *86*, 12206–12213.

- (59) Killig, F.; Stark, G.; Apell, H. J. Photodynamic Inactivation of the Na,K-ATPase Occurs via Different Pathways. *J. Membr. Biol.* **2004**, *200*, 133–144.
- (60) Nishiyama, N.; Morimoto, Y.; Jang, W. D.; Kataoka, K. Design and Development of Dendrimer Photosensitizer-Incorporated Polymeric Micelles for Enhanced Photodynamic Therapy. *Adv. Drug Delivery Rev.* **2009**, *61*, 327–338.
- (61) Hirakawa, K.; Hirano, T.; Nishimura, Y.; Arai, T.; Nosaka, Y. Dynamics of Singlet Oxygen Generation by DNA-Binding Photosensitizers. *J. Phys. Chem. B* **2012**, *116*, 3037–3044.
- (62) Gorzkiewicz, M.; Deriu, M. A.; Studzian, M.; Janaszewska, A.; Grasso, G.; Pułaski, Ł.; Appelhans, D.; Danani, A.; Klajnert-Maculewicz, B. Fludarabine-Specific Molecular Interactions with Maltose-Modified Poly(Propyleneimine) Dendrimer Enable Effective Cell Entry of the Active Drug Form: Comparison with Clofarabine. *Biomacromolecules* **2019**, *20*, 1429–1442.
- (63) Fox, L. J.; Richardson, R. M.; Briscoe, W. H. PAMAM Dendrimer - Cell Membrane Interactions. *Adv. Colloid Interface Sci.* **2018**, 1–18.
- (64) Kochevar, I. E.; Redmond, R. W. [2] Photosensitized Production of Singlet Oxygen. *Methods Enzymol.* **2000**, *319*, 20–28.
- (65) Tomalia, D. A.; Rookmaker, M. The Polymer Data Handbook. Poly(1,3-Trimethyleneimine) Dendrimers. In *Polymer Data Handbook*; 2nd edition, Mark, J., Ed.; Oxford University Press, 2009; pp. 979–982.
- (66) Wang, J.; Wolf, R. M.; Caldwell, J. W.; Kollman, P. A.; Case, D. A. Development and Testing of a General Amber Force Field. *J. Comput. Chem.* **2004**, *25*, 1157–1174.
- (67) Gupta, S.; Biswas, P. Effect of PH on Size and Internal Structure of Poly(Propylene Imine) Dendrimers: A Molecular Dynamics Simulation Study. *J. Phys. Chem. B* **2018**, *122*, 9250–9263.
- (68) Van Duijvenbode, R. C.; Borkovec, M.; Koper, G. J. M. Acid-Base Properties of Poly(Propylene Imine) Dendrimers. *Polymer (Guildf)*. **1998**, *39*, 2657–2664.
- (69) Jakalian, A.; Jack, D. B.; Bayly, C. I. Fast, Efficient Generation of High-Quality Atomic Charges. AM1-BCC Model: II. Parameterization and Validation. *J. Comput. Chem.* **2002**, *23*, 1623–1641.
- (70) Wang, J.; Wang, W.; Kollman, P. A.; Case, D. A. Automatic Atom Type and Bond Type Perception in Molecular Mechanical Calculations. *J. Mol. Graphics Modell.* **2006**, *25*, 247–260.
- (71) Da Silva, A. W. S.; Vranken, W. F. ACPYPE - AnteChamber PYthon Parser Interface. *BMC Res. Notes* **2012**, *5*, 367.
- (72) Mark, P.; Nilsson, L. Structure and Dynamics of the TIP3P, SPC, and SPC/E Water Models at 298 K. *J. Phys. Chem. A* **2001**, *105*, 9954–9960.
- (73) Bussi, G.; Donadio, D.; Parrinello, M. Canonical Sampling through Velocity Rescaling. *J. Chem. Phys.* **2007**, *126*, No. 014101.
- (74) Berendsen, H. J. C.; Postma, J. P. M.; Van Gunsteren, W. F.; Dinola, A.; Haak, J. R. Molecular Dynamics with Coupling to an External Bath. *J. Chem. Phys.* **1984**, *81*, 3684–3690.
- (75) Parrinello, M.; Rahman, A. Polymorphic Transitions in Single Crystals: A New Molecular Dynamics Method. *J. Appl. Phys.* **1981**, *52*, 7182–7190.
- (76) Abraham, M. J.; Murtola, T.; Schulz, R.; Páll, S.; Smith, J. C.; Hess, B.; Lindah, E. Gromacs: High Performance Molecular Simulations through Multi-Level Parallelism from Laptops to Supercomputers. *SoftwareX* **2015**, *1–2*, 19–25.
- (77) Darden, T.; York, D.; Pedersen, L. Particle Mesh Ewald: An N·log(N) Method for Ewald Sums in Large Systems. *J. Chem. Phys.* **1993**, *98*, 10089–10092.
- (78) Hess, B.; Bekker, H.; Berendsen, H. J. C.; Fraaije, J. G. E. M. LINCS: A Linear Constraint Solver for Molecular Simulations. *J. Comput. Chem.* **1997**, *18*, 1463–1472.
- (79) Rudnick, J.; Gaspari, G. The Aspharity of Random Walks. *J. Phys. A: Math. Gen.* **1986**, *19*, L191–L193.
- (80) Maiti, P. K.; Çağın, T.; Wang, G.; Goddard, W. A. Structure of PAMAM Dendrimers: Generations 1 through 11. *Macromolecules* **2004**, *37*, 6236–6254.
- (81) Deriu, M. A.; Popescu, L. M.; Ottaviani, M. F.; Danani, A.; Piticescu, R. M. Iron Oxide/PAMAM Nanostructured Hybrids: Combined Computational and Experimental Studies. *J. Mater. Sci.* **2016**, *51*, 1996–2007.
- (82) Baker, N. A.; Sept, D.; Joseph, S.; Holst, M. J.; McCammon, J. A. Electrostatics of Nanosystems: Application to Microtubules and the Ribosome. *Proc. Natl. Acad. Sci. U. S. A.* **2001**, *98*, 10037–10041.
- (83) Chen, C.; Pettitt, B. M. The Binding Process of a Nonspecific Enzyme with DNA. *Biophys. J.* **2011**, *101*, 1139–1147.
- (84) Humphrey, W.; Dalke, A.; Schulten, K. VMD: Visual Molecular Dynamics. *J. Mol. Graphics* **1996**, *14*, 33–38.

Triazine–Carbosilane Dendrimersomes Enhance Cellular Uptake and Phototoxic Activity of Rose Bengal in Basal Cell Skin Carcinoma Cells

Krzysztof Sztandera¹, Michał Gorzkiewicz^{1,2}, Mateusz Bątał¹, Valeria Arkhipova^{3,4}, Nadezhda Knauer^{3,5,6}, Javier Sánchez-Nieves^{7,8}, Fco Javier de la Mata⁷⁻⁹, Rafael Gómez⁷⁻⁹, Evgeny Apartsin^{3,4,10}, Barbara Klajnert-Maculewicz¹

¹Department of General Biophysics, Faculty of Biology and Environmental Protection, University of Lodz, Lodz, 90-236, Poland; ²Department of Molecular Medicine II, Medical Faculty, Heinrich Heine University Düsseldorf, Düsseldorf, 40225, Germany; ³Institute of Chemical Biology and Fundamental Medicine SB RAS, Novosibirsk, 630090, Russia; ⁴Department of Natural Sciences, Novosibirsk State University, Novosibirsk, 630090, Russia; ⁵Research Institute of Fundamental and Clinical Immunology, Novosibirsk, 630099, Russia; ⁶Clinic for Neurosurgery, Medical Faculty, Heinrich Heine University Düsseldorf, Düsseldorf, 40225, Germany; ⁷Departamento de Química Orgánica y Química Inorgánica, UAH-IQAR, Alcalá de Henares, 28805, Spain; ⁸Networking Research Center on Bioengineering, Biomaterials and Nanomedicine (CIBER-BBN), Madrid, 28029, Spain; ⁹Instituto Ramón y Cajal de Investigación Sanitaria, IRYCIS, Madrid, 28034, Spain; ¹⁰Laboratoire de Chimie de Coordination CNRS, Toulouse, 31077, France

Correspondence: Barbara Klajnert-Maculewicz, Department of General Biophysics, Pomorska 141/143, Łódź, 90-236, Poland, Tel +48 42 635 44 29, Fax +48 42 635 4474, Email barbara.klajnert@biol.uni.lodz.pl

Background: The search for new formulations for photodynamic therapy is intended to improve the outcome of skin cancer treatment using significantly reduced doses of photosensitizer, thereby avoiding side effects. The incorporation of photosensitizers into nanoassemblies is a versatile way to increase the efficiency and specificity of drug delivery into target cells. Herein, we report the loading of rose bengal into vesicle-like constructs of amphiphilic triazine-carbosilane dendrons (dendrimersomes) as well as biophysical and in vitro characterization of this novel nanosystem.

Methods: Using established protocol and analytical and spectroscopy techniques we were able to synthesized dendrons with strictly designed properties. Engaging biophysical methods (hydrodynamic diameter and zeta potential measurements, analysis of spectral properties, transmission electron microscopy) we confirmed assembling of our nanosystem. A set of in vitro techniques was used for determination ROS generation, (ABDA and H₂DCFDA probes), cell viability (MTT assay) and cellular uptake (flow cytometry and confocal microscopy).

Results: Encapsulation of rose bengal inside dendrimersomes enhances cellular uptake, intracellular ROS production and consequently, the phototoxicity of this photosensitizer.

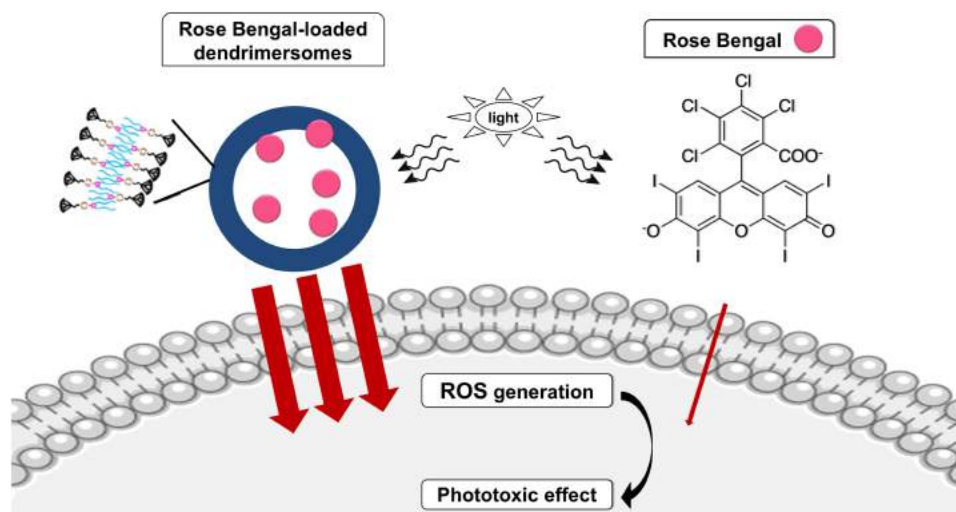
Conclusion: Triazine-carbosilane dendrimersomes show high capacity as drug carriers for anticancer photodynamic therapy.

Keywords: dendrons, amphiphiles, carbosilane, photodynamic therapy, rose bengal, dendrimersomes

Introduction

As the incidence of basal cell carcinoma continues to rise, novel methods of treatment are urgently required.¹ One of the most promising approaches for treating these cancers is photodynamic therapy, which is based on the interplay between molecular oxygen, photosensitizer (PS), and light.² This technique is non-invasive and has high efficacy with relatively few side effects. The photodynamic reaction starts with absorption of a light quantum (photon) by the photosensitizer, which then enters an excited singlet state. Because the singlet form is unstable, it is transformed into the triplet state, which triggers a cascade of reactions leading to formation of singlet oxygen and other reactive oxygen species (ROS). This, in turn, leads to uncontrolled oxidation of intracellular structures and ultimately to cell death. Because PS plays a

Graphical Abstract



pivotal role in this technique,^{3,4} it is important to choose a compound with relevant photodynamic properties, significant half-life, and accumulation inside cancer cells.⁵ Rose bengal (RB), an anionic, water-soluble fluorescein derivative that generates singlet oxygen after irradiation with light of 520 nm wavelength, is one of the most extensively tested photosensitizers and holds great promise for medical applications.^{6,7} However, the anionic nature of RB limits its use in PDT due to low cellular uptake,⁸ necessitating the use of appropriate drug delivery systems. Modern nanotechnology methods can overcome this obstacle, yielding nanoparticles with strictly defined properties that can act as carriers for drugs in various therapies, including PDT.^{4,9} A number of PS nanocarriers has been reported so far,¹⁰ including liposomes,¹¹ dendrimers^{12–15} and polymersomes¹⁶ as well as dendrimersomes.^{17–19}

Dendrimersomes are three-dimensional structures built of self-assembling amphiphilic dendrons.²⁰ The final properties of dendrimersomes are dependent on the number of hydrophilic branches, which decide about dendrimersomes generation, the distribution of chemical groups inside or outside the branches, as well as appropriately selected pH-responsive or hydrophobic elements. Optimized synthesis of dendrons from carefully adjusted elements results in properties that enable the formation of a bilayers, similar to the liposomes, wherein drugs can be loaded.^{21,22} The present work focus on triazine-carbosilane dendrimersomes of the second (G2) and third (G3) generation. These compounds have a branched hydrophobic part, a triazine cycle (the protonation of which, depending on the pH of the environment, allows the structure of the dendrimersome to loosen or shorten), a piperazine ring (which plays the role of the linker), and the hydrophilic part. The obtained dendrimersomes have a compact (closed) structure in a neutral pH, opening in an acidic environment.²⁰ This allows for a selective delivery and release of the cargo only in the tumor environment.²³ In this study, we report the assembly of triazine-carbosilane dendron-based dendrimersomes loaded with rose bengal, as well as proof-of-concept studies of their efficacy in PDT.

Materials and Methods

Materials

RB, fetal bovine serum (FBS), penicillin/streptomycin solution, trypsin-EDTA solution, ABDA probe [9,10-antherachenediyl-bis(methylene) dimalonic acid], MTT [3-(4,5-dimethyl-2-thiazolyl)-2,5-diphenyl-2H-tetrazolium bromide], and HEPES (4-(2-hydroxyethyl)-1-piperazineethanesulfonic acid) were purchased from Sigma-Aldrich (Taufkirchen, Germany). Dulbecco's phosphate buffered saline without calcium and magnesium (DPBS) was purchased from Biowest (Nuaille, France). HBSS (Hanks' Balanced Salt Solution) and 154 CF culture medium were obtained from

Gibco/ThermoFisher Scientific (Waltham, MA, USA). Chelex 100 Resin was obtained from Bio-Rad (Hercules, CA, USA). H₂DCFDA (2',7'-dichlorodihydrofluorescein diacetate) was purchased from Invitrogen/ThermoFisher Scientific (Waltham, MA, USA). Dimethyl sulfoxide (DMSO) was purchased from POCH (Gliwice, Poland). Murine basal cell carcinoma lines (AsZ, BsZ, CsZ) were provided by Dr. Ervin Epstein (Children's Oakland Research Institute, Oakland, CA, USA).

Organic solvents were dried and freshly distilled under argon prior to use. Chemicals were obtained from commercial sources and used as received. Water solutions of chemicals, amphiphiles and buffer solutions were prepared using milliQ[®] deionized water. Sonication of amphiphile solutions was done in a Sonorex Super RK 31 H ultrasonic bath (Bandelin Electronic, Berlin, Germany).

Methods

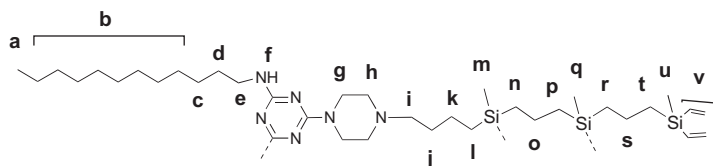
Analytical and Spectroscopic Techniques

¹H and ¹³C spectra were recorded on Varian Unity VXR-300 (Varian Inc., Palo Alto, CA) and Bruker AV400 (Bruker, Karlsruhe, Germany) instruments. Chemical shifts (δ , ppm) were measured relative to residual ¹H and ¹³C resonances for CDCl₃ used as solvent. ESI-TOF analysis was carried out in an Agilent 6210 TOF LC/MS mass spectrometer (Agilent, Santa Clara, CA). UV-vis absorbance spectra were acquired using a Jasco V-650 spectrophotometer (Jasco, Cremella, Italy). Fluorescence emission spectra were obtained on an LS 55 fluorescence spectrometer (PerkinElmer, Waltham, MA, USA) at 25°C.

Synthesis of Dendritic Amphiphiles

Vinyl-terminated dendron precursors G2, G3 bearing bromine in the focal point were obtained as described elsewhere.²⁴ 2,4-dodecylamino-6-chloro-1,3,5-triazine, 2,4-dodecylamino-6-piperazino-1,3,5-triazine, vinyl-terminated dendron G2 and amphiphilic dendron G2 were synthesized as previously described.²⁰ Only the synthesis of new compounds is described herein.

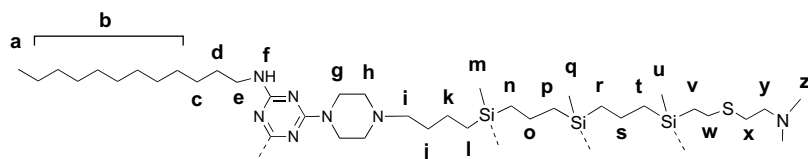
Vinyl-Terminated Dendron G3



2,4-didodecylamino-6-piperazino-1,3,5-triazine (350 mg, 0.66 mmol), vinyl-terminated carbosilane dendron BrG₃V₈ (544 mg, 0.6 mmol), K₂CO₃ (124 mg, 0.9 mmol) were mixed in 30 mL acetone in a sealed ampule with catalytic amounts of 18-crown-6 and KI added. The reaction mixture was stirred for 24 h at 90 °C. The reaction completion was monitored by TOCSY ¹H NMR following the disappearance of BrCH₂ protons. When the reaction was over, the solvent was removed under vacuum, the residue was dissolved in ethyl acetate and washed with brine. The organic phase was dried over Na₂SO₄, and the solvent was removed. The crude product was purified by silica gel column chromatography (eluent: ethyl acetate:hexane 1:1) to yield functionalized dendron as light-yellow oil (590 mg, 72%).

¹H NMR (400 MHz, CDCl₃) δ -0.11 (s, 6H, H_q), -0.10 (s, 3H, H_m), 0.11 (s, 12H, H_u), 0.45 (m, 2H, H_i), 0.51 (m, 6H, H_n, H_p, H_r), 0.69 (m, 8H, H_l), 0.86 (t, J = 6.7 Hz, 6H, H_a), 1.21–1.38 (m, 50H, H_b, H_c, H_k, H_o, H_s), 1.51 (t, J = 7.3 Hz, 6H, H_d, H_j), 2.34 (t, J = 7.9 Hz, 2H, H_i), 2.43 (m, 4H, H_h), 3.31 (m, 4H, H_g), 3.77 (s, 4H, H_e), 4.81 (s, 2H, H_f), 5.63–6.19 (m, 24H, H_v). ¹³C NMR (101 MHz, CDCl₃) δ -5.2, -5.1, -5.0, 13.9, 14.1, 18.3, 18.5, 18.7 (m), 18.9, 22.1, 22.7, 26.9, 29.1–29.9 (m), 30.7, 30.9, 31.9, 40.7, 42.9, 53.2, 58.7, 132.6, 137.2, 164.7, 166.1. MS: [M+H]⁺ 1357.03 amu (calcd 1357.67 amu).

Amphiphilic Dendron G3



Functionalized vinyl-terminated dendron (400 mg, 0.3 mmol), 2-(dimethylamino) ethanethiol hydrochloride (340 mg, 2.4 mmol) and dimethoxyphenylacetophenone (DMPA) (16 mg, 0.06 mmol) were dissolved in 5 mL of mixture THF: CH₃OH (1:2). The reaction mixture was deoxygenated by bubbling argon and irradiated by UV for 2 h (365 nm, 120W). Then, another 16 mg (0.06 mmol) of DMPA was added, and the reaction mixture was irradiated for another 2 h. The reaction completion was monitored by ¹H NMR. After the reaction was completed, the solvents were removed under vacuum and then the residue was dissolved in methanol. Afterward, it was precipitated in diethyl ether, and after the solvent was separated, the solid was dried under vacuum to afford the desired dendron as light-yellow solid (500 mg, 68%). For characterization, the dendron was deprotonated with K₂CO₃.

¹H NMR (400 MHz, CDCl₃) δ -0.11 (m, 9H, H_m, H_q), -0.02 (s, 6H, H_u), 0.50 (m, 16H, H_l, H_n, H_p, H_r), 0.58 (m, 8H, H_t), 0.86 (s, 22H, H_a, H_v), 1.18–1.33 (m, 50H, H_b, H_c, H_k, H_o, H_s), 1.49 (m, 6H, H_d, H_j), 2.23 (s, 24H, H_z), 2.32 (m, 2H, H_i), 2.39 (m, 4H, H_h), 2.46 (m, 16H, H_y), 2.53 (m, 16H, H_w), 2.60 (m, 16H, H_x), 3.30 (s, 4H, H_g), 3.73 (s, 4H, H_e), 4.70 (s, 2H, H_f). ¹³C NMR (101 MHz, CDCl₃) δ -5.3, -5.1, -5.0, 14.0, 14.1, 14.6, 18.3, 18.4, 18.7, 22.1, 22.6, 27.0, 27.8, 29.3–30.0 (m), 30.9, 31.9, 37.0, 40.6, 42.9, 45.4, 53.3, 59.3, 127.7, 128.5, 165.0, 166.2.

Preparation of Rose Bengal-Loaded Dendrimersomes

Solutions of rose bengal (5 μL, 10 mM) and dendron (G2 or G3, 10 μL, 10 mM) were quickly mixed in 1 mL of deionized water (mQ). The mixture was sonicated for 30 min and then incubated for 48 h at room temperature (RT). Empty dendrimersomes were prepared analogously. A UV-vis spectrum of the mixture was recorded (before dialysis). In the next step dendrimersomes loaded with RB (G2-RB and G3-RB) were purified by dialysis in SnakeSkin™ Dialysis Tubing (3.5K MWCO, 22 mm, ThermoFisher, Waltham, Massachusetts, USA) against deionized water (mQ) for 6 h, changing water three times during this time. A UV-vis spectrum of the mixture was recorded (after dialysis). The percentage of encapsulated drug (encapsulation efficiency) was estimated from the ratio of absorbance values at 565 nm (before and after dialysis).

Hydrodynamic Diameter

The water solution of RB-loaded dendrimersomes (G2-RB or G3-RB, 400 μL) was mixed with 20 μL phosphate buffer (200 mM, pH 7) and incubated in RT for 2 h. The solutions were subsequently placed in the low volume sizing cuvettes (ZEN0112, Malvern). Measurements of hydrodynamic diameter were performed with the use Dynamic Light Scattering (DLS) on Zetasizer Nano ZS (Malvern Instruments Ltd., Malvern, UK) at 25°C. The data were analyzed using the Malvern software.

Zeta Potential

For zeta potential measurements, 50 μL of G2-RB or G3-RB was added to 1 mL of deionized water (mQ). Then the solutions were placed in the folded capillary cells (DTS 1070, Malvern) and the zeta potential was measured with the use of Zetasizer Nano ZS (Malvern Instruments Ltd., Malvern, UK) at 25°C. The data were analyzed using the Malvern software.

Transmission Electron Microscopy

Transmission electron microscopy (TEM) images were obtained using a Veleta digital camera (EM SIS, Muenster, Germany) mounted on a JEM 1400 transmission electron microscope (JEOL, Japan) at the accelerating voltage of 80 kV. Samples were stained with 0.1% uranyl acetate.

Spectroscopy Studies

Absorbance MeasurementAll measurements were performed in mQ water at RT on a Jasco V-650 spectrophotometer. Spectra were recorded in a wavelength range from 300 to 650 nm. Optical path length was 1 cm. The measurements were carried out for tested compounds at 5 μM concentration of RB. Deionized water (mQ) was used as a reference for all measurements.

Fluorescence MeasurementAll samples were prepared in mQ water and measured in quartz cuvettes on LS 55 fluorescence spectrophotometer (PerkinElmer, Waltham, MA, USA). The excitation wavelength was set to 525 nm, and spectra were recorded between 540 and 650 nm. Excitation and emission slits were 5 and 7.5 nm, respectively. The measurements were carried out for tested compounds at 1 μM concentration of RB.

Release Studies

To evaluate the rate of RB release from the dendrimersomes, 1 mL solution of G2-RB or G3-RB (50 μM of RB) dissolved in distilled water was enclosed in a dialysis membrane tube (SnakeSkin™ Dialysis Tubing, 3.5K MWCO, 22 mm, ThermoFisher, Waltham, Massachusetts, USA) and dialyzed against phosphate buffer (pH 5.5) at RT, changing buffer after each two hours of dialysis. Aliquots from the internal phase were collected after 0, 0.25, 0.5, 1, 2, 4, 6 and 24 h, and the RB absorbance was analyzed similarly to spectroscopy studies. The percentage of release was determined regarding the first sample (0 h, 100% of initial absorbance). The experiment was performed in triplicates.

Singlet Oxygen Generation

The singlet oxygen generation assay was performed with use of ABDA probe. The solution of free photosensitizer (RB), G2 and G3 empty dendrimersomes, G2-RB and G3-RB were prepared in DPBS at 0.25, 0.5, 1, 2 μM final concentration of RB. Then 100 μL of each solution was transferred to the 96-well black plate. All measurements were recorded using fluorescence microplate reader (Fluoroskan Ascent FL, ThermoFisher, Waltham, MA, USA). The excitation and emission wavelength were set to 355 and 430 nm, respectively. First measurement was recorded without probe in order to verify whether compounds under study exhibit fluorescence in this range. Then, 20 μL of 30 μM ABDA was added to each sample and the fluorescence intensity of samples with ABDA was measured. Subsequently, the plate was irradiated for 5 min with the lamp equipped with a filter emitting visible light in the range of 385–780 nm and the light dose of 2.4 J/cm^2 per minute (Q. Light Pro Unit, Q. Products AG, Switzerland). Fluorescence intensity of probe was measured after each 5 minutes of irradiation up to 1 h. Then, the slopes of the fluorescence intensity curves were considered for the measurement of singlet oxygen generation, and the results were presented as percentage of singlet oxygen generation in control (DPBS irradiated with probe).

Cell Cultures

Murine basal cell carcinoma lines (AsZ, BsZ and CsZ) were cultured in 154-CF medium with 5% penicillin/streptomycin, 0.05 mM calcium, and 2% chelexed, heat-inactivated fetal bovine serum (FBS). Cells were cultured in T-75 culture flasks at 37 °C, 5% CO_2 and subcultured every 2 or 3 days. The number of viable cells was determined by trypan blue exclusion assay with the use of Countess Automated Cell Counter (Invitrogen, Carlsbad, California, USA). For harvesting the cells, 0.25% (w/v) trypsin–0.03% (w/v) EDTA solution was used.

ROS Generation Assay

AsZ, BsZ, CsZ cells were seeded into 96-well plates at a density of 1×10^4 cells per well. After 24 h of incubation (37 °C, 5% CO_2), 100 μL of free photosensitizer (RB), G2 or G3 empty dendrimersomes, G2-RB or G3-RB dissolved in fresh culture medium was added to the cells at final RB concentrations of 0.25, 0.5, 1, 2 μM . Cells were incubated with tested compounds for 5 h (37 °C, 5% CO_2). Then the medium was replaced with 100 μL fresh Hank's Balanced Salt Solution (HBSS). The 20 μL of H_2DCFDA solution (final concentration: 2 μM) was added to each sample and cells were incubated for 20 min in dark (37 °C, 5% CO_2). Cells were subsequently washed with 100 μL of HBSS and fluorescence intensity of non-irradiated cells was measured using fluorescence microplate reader PowerWave HT Microplate Spectrophotometer (BioTek, USA). Then the cells were irradiated for 30 min (2.4 J/cm^2 per minute) with use of Q. Light Pro Unit lamp and the fluorescence intensity of DCF was measured. The ROS level was calculated as DCF

fluorescence intensity increase and presented as a percentage of ROS production in control samples (without tested compounds). Every measurement was corrected by subtraction of the background fluorescence intensity.

Cellular Uptake

AsZ, BsZ, CsZ cells were seeded into 24-well plates at a density of 1×10^5 cells per well and incubated for 24 h (37 °C, 5% CO₂). Next, 300 µL of free photosensitizer (RB), G2-RB or G3-RB was added to the cells in fresh culture medium at the final RB concentration of 5 µM. The cells were incubated with compounds up to 4 h. Following the incubation, the compounds were discarded, and cells were washed with DPBS. Next, the cells were detached from the plates using trypsin-EDTA solution. Then the fresh culture medium was added to the cells, the samples were gently mixed and collected for measurements. For estimation of the cellular uptake, the fluorescence of the samples was measured using flow cytometry (LSRII, Becton Dickinson). The excitation and the emission filters were 520 and 570 nm, respectively.

Confocal Microscopy

AsZ, BsZ, CsZ cells were seeded into 96-well black plate with transparent glass bottom at a density of 1×10^4 cells per well. After 24 h of incubation in standard conditions, medium was replaced with 100 µL of free photosensitizer (RB), G2-RB or G3-RB dissolved in fresh culture medium at the final RB concentration of 5 µM. The plates were incubated for 4 h in the dark (37 °C, 5% CO₂). Cells were subsequently washed with PBS and fixed with 4% formaldehyde solution for 15 min. Then the solution of Phalloidin–Atto 633 (1:400) was added to each well for 20 minutes to stain F-actin in cell membrane. The cells were washed with DPBS and the solution of 5 µM Hoechst 33342 was added to the cells for additional 15 min to stain DNA in cell nucleus. Following the incubation, cells were washed with DPBS and submerged in 100 µL of fresh DPBS. The images were taken with Leica TCS SP8 confocal microscope.

Cytotoxicity Studies

AsZ, BsZ, CsZ cells were seeded into 96-well plates at a density of 2.5×10^4 cells per well. After 24 h of incubation (37 °C, 5% CO₂) 100 µL of free photosensitizer (RB), G2 or G3 empty dendrimersomes, G2-RB or G3-RB dissolved in fresh culture medium were added to the cells at 0.25, 0.5, 1, 2 µM final concentrations of RB. Cells were incubated with tested compounds for 5 h (37 °C, 5% CO₂). Then the medium was replaced with DPBS buffer and cells were irradiated for 30 min (2.4 J/cm² per minute) with Q. Light Pro Unit lamp. Immediately after irradiation, DPBS was replaced with fresh culture medium, and cells were incubated for 24 h as post-PDT incubation. Additionally, the “dark” toxicity (without irradiation) was evaluated. The cell viability was measured using MTT assay. MTT was added to the wells at a final concentration of 0.5 mg/mL and the plates were incubated for 2 h (37 °C, 5% CO₂). After incubation, formazan crystals were dissolved in DMSO, and the absorbance was read at 570 nm using the PowerWave HT Microplate Spectrophotometer (BioTek, USA).

Statistical Analysis

Mann–Whitney test was used for testing statistical significance in release studies. For the rest of the experiments, two-way ANOVA for concentration series and compounds followed by post-hoc Tukey’s test for pairwise difference testing were used. In all tests, p-values < 0.05 were considered statistically significant. Data were collected from at least three independent experiments and presented as arithmetic mean ±SD.

Results

Amphiphilic triazine–carbosilane dendrons (Figures 1 and 2) were synthesized in a convergent way by a conjugation of hydrophobic triazine block and vinyl-terminated dendrons G2 and G3 by a piperazine linker followed by the functionalization of dendron periphery with cationic groups via a thiol-ene reaction. Amphiphilic dendron G2 was reported recently,²⁰ the dendron G3 has been obtained herein for the first time. Features of the architecture, such as combination of hydrophobic and hydrophilic fragments in the structure, allow for the self-association of dendrons into supramolecular constructions – dendrimersomes.

Dendrimersomes formed at neutral pH have mean diameter of 40–50 nm and in the acidic conditions they reorganize into larger particles (100–150 nm diameter) (Figure 3).

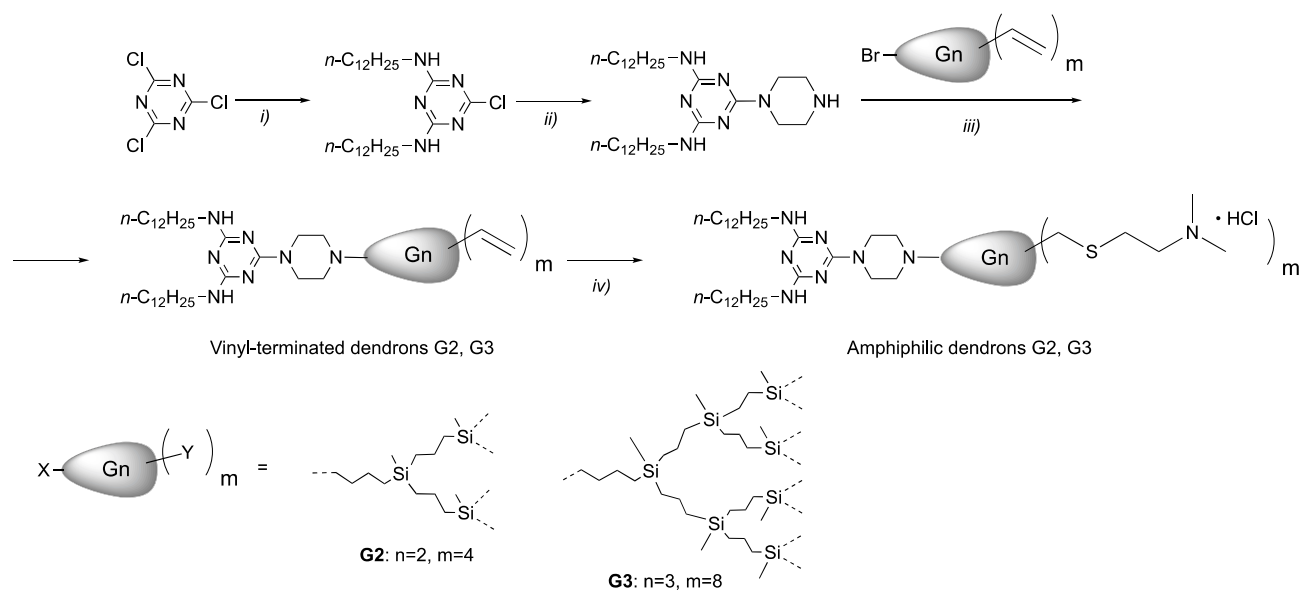


Figure 1 Synthesis of the amphiphilic dendron: (i) $n\text{-C}_{12}\text{H}_{25}\text{NH}_2$, CHCl_3 , NaOH (aq); (ii) piperazine, CHCl_3 ; (iii) BrG_nV_m , K_2CO_3 , 18-crown-6, KI, acetone; (iv) $\text{HS}(\text{CH}_2)_2\text{NH}(\text{CH}_2)_2\text{NH}_2 \cdot \text{HCl}$, DMPA, 365 nm UV, $\text{THF}:\text{CH}_3\text{OH}$.

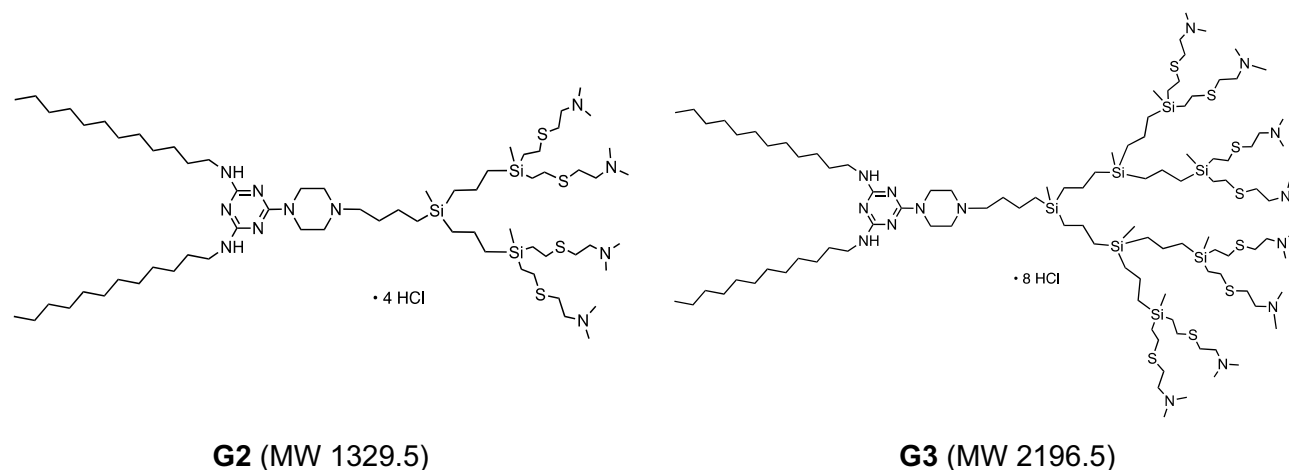


Figure 2 Structures of amphiphilic triazine-carbosilane dendrons of 2nd and 3rd generation.

The zeta potential as well as hydrodynamic diameter of evaluated compounds is similar, regardless generation of dendrimersomes (Table 1).

Both absorbance and fluorescence emission spectra of RB-loaded dendrimersomes showed a red shift of the maximum and a decrease in the intensity compared with free RB. After purification by dialysis, absorbance (Figure 4) and fluorescence intensities (Figure 4 inset) were further decreased. Based on changes in absorbance, the estimated percentage of RB encapsulation was 76% for G2 and 89% for G3.

Because the structures of both G2 and G3 dendrimersomes were compact (“closed”) at neutral pH and more loose (“open”) in slightly acidic pH (Figure 3), we monitored release of RB from the dendrimersomes at pH 5.5.²⁰ The RB release rate differed significantly between the two generations of dendrimersomes (G2-RB and G3-RB). RB release from G3-RB was much slower during dialysis, although the release of RB from the two types of dendrimersomes was similar after 24 h of dialysis (Figure 5). Generation of singlet oxygen by RB and G2-RB at the highest concentration of PS was approx. 3-fold higher than in the control, with no significant differences between the two compounds. We observed a

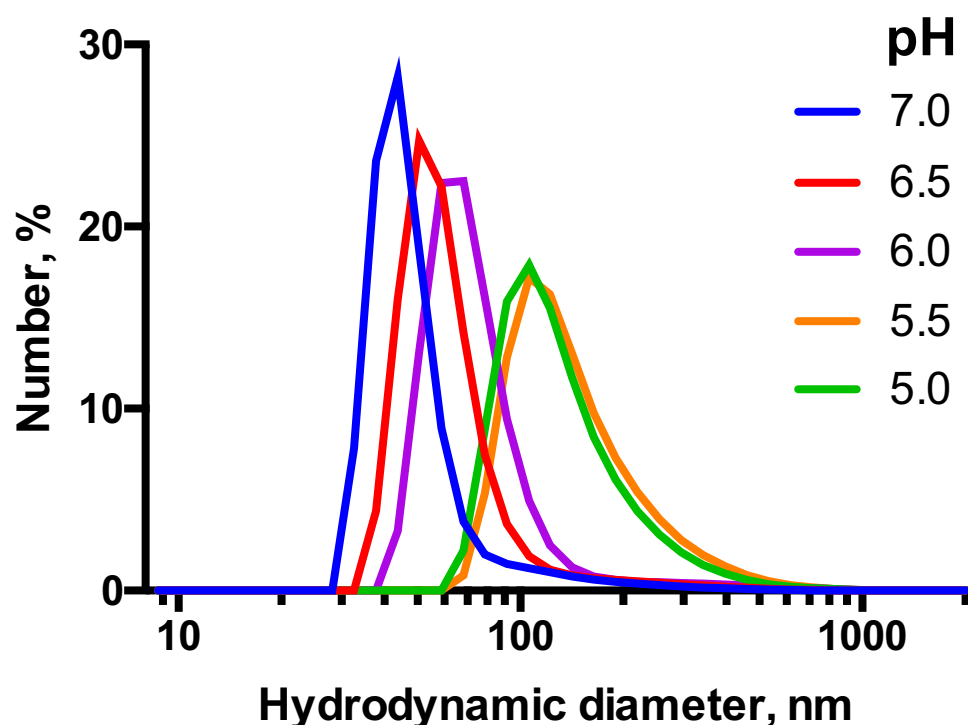


Figure 3 DLS profiles for supramolecular associates of the amphiphilic dendron G3 (100 μM) exposed to different pH in 10 mM Na-phosphate buffer.

statistically significant difference between free RB and G3-RB; in the case of the latter, the level of singlet oxygen was 5-fold higher than in the unstimulated control (Figure 6).

Cellular uptake of G2-RB and G3-RB was significantly higher in comparison to free RB. In all cell lines almost 80% of tested cells absorbed RB encapsulated in dendrimersomes. Moreover, the percentage of RB-positive cells reached a plateau after 0.5 h from the start of the experiment (Figure 7A and Figure S1). Consistent with the results of flow cytometry experiments, confocal micrographs of the AsZ (Figure 7B), BsZ (Figure S2), and CsZ (Figure S3) cell lines revealed that both G2-RB and G3-RB were taken up to a greater extent than free RB.

Encapsulation of RB in both dendrimersomes caused a significant increase in ROS production in all cell lines to a similar degree. Figure 8A shows representative results from AsZ cell lines, and ROS production in BsZ and CsZ cell lines is shown in Figure S4. At RB concentrations of 1 and 2 μM , we observed statistically significant differences between free RB and G2-RB or G3-RB. At the highest concentration, fluorescence intensity of the probe increased 10-fold for both RB-loaded dendrimersomes relative to the untreated control. The phototoxic effect was observed in all cell lines under study (AsZ, BsZ, and CsZ) (Figures 8B and S5). Both RB-loaded dendrimersomes (G2-RB and G3-RB) exerted significantly higher cytotoxic effects after irradiation, and this trend was maintained in all cell lines. At the

Table 1 Size and Zeta Potential of Rose Bengal-Loaded Dendrimersomes (G2-RB and G3-RB) as Well as Free Dendrimersomes (G2 and G3).

| | G2-RB | G3-RB | G2 | G3 |
|-----------------------------------|-------------------|-------------------|-------------------|-------------------|
| PDI | 0.38 \pm 0.14 | 0.31 \pm 0.10 | 0.27 \pm 0.007 | 0.31 \pm 0.012 |
| Hydrodynamic diameter [nm] | 55.47 \pm 23.97 | 72.64 \pm 36.49 | 36.68 \pm 7.933 | 55.75 \pm 9.696 |
| Zeta potential [mV] | 39.17 \pm 3.17 | 39.50 \pm 3.59 | 37.25 \pm 2.60 | 44.24 \pm 2.26 |
| Drug loading capacity [%] | >22.5 | >17.6 | | |

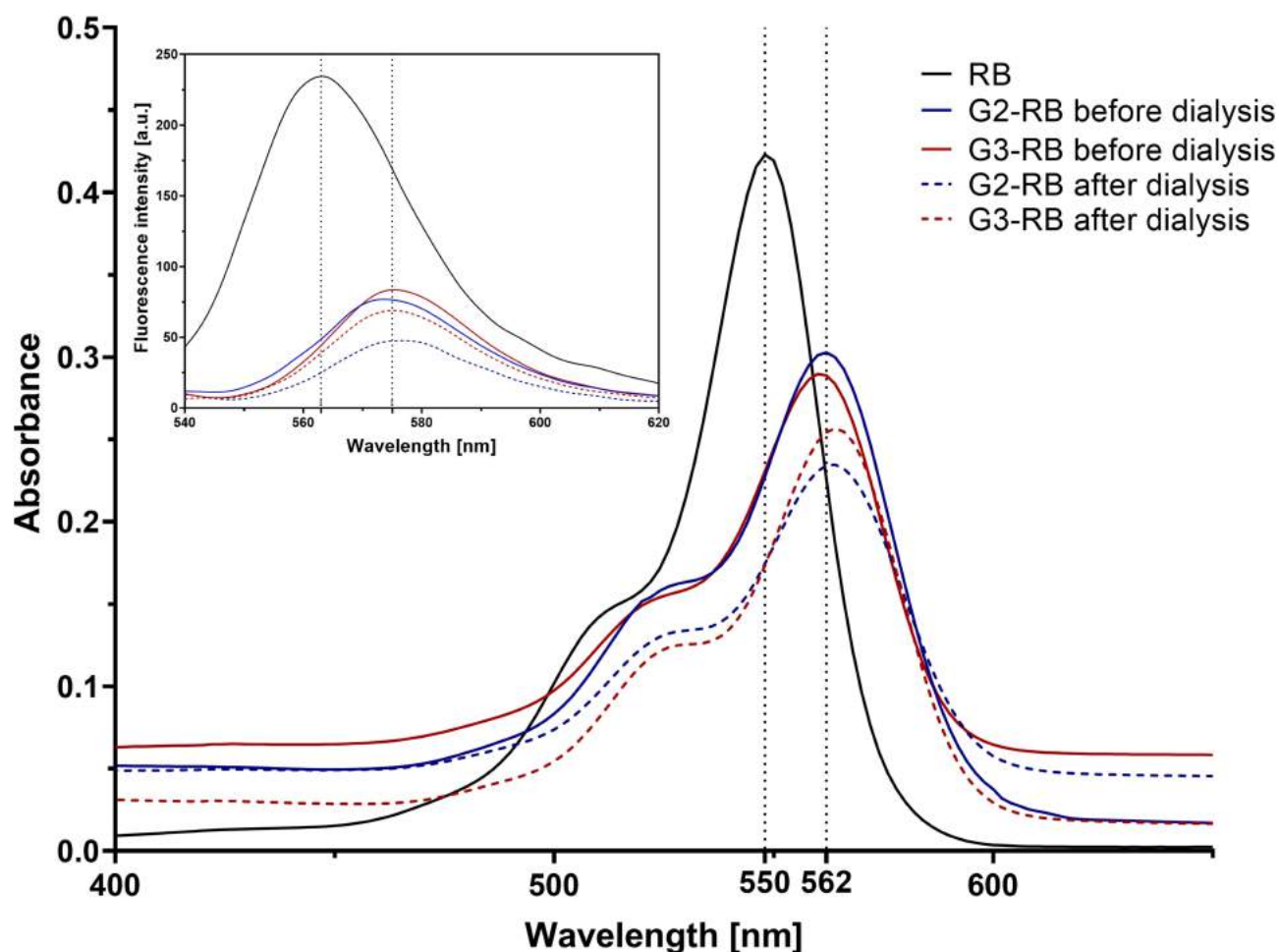


Figure 4 Changes in fluorescence and absorbance spectra of RB after encapsulation within dendrimersomes. The measurements of absorbance and fluorescence intensity were carried out for the tested compounds at RB concentrations of 5 and 1 μM , respectively.

highest concentration, the viability of cells decreased to approx. 25%, whereas free RB decreased cell viability only to approx. 75%. IC_{50} values are presented in [Table S1](#). We also observed a lack of dark toxicity of the tested compounds in all cell lines ([Figure S6](#)). Moreover, empty dendrimersomes exerted neither phototoxicity nor dark toxicity ([Figure S7](#)).

Discussion

Basal cell carcinoma is the most frequently diagnosed type of skin cancer in humans, but accurate estimation of the number of cases is difficult due to the fact that only a small fraction of the cancers is correctly diagnosed. However, we do know that over a lifetime, the likelihood of developing this type of cancer is as high as 30%, irrespective of genetic aspects and environmental factors. Currently, basal cell carcinoma is treated using several conventional techniques: surgery, chemotherapy, and radiotherapy; however, all of these approaches are associated with numerous side effects.^{1,25} Accordingly, highly efficient novel treatment methods are urgently required.

Photodynamic therapy (PDT) is a noninvasive alternative to the aforementioned techniques. PDT exploits three inseparable elements (photosensitizer, oxygen, and light) that act together and start a cascade of reactions generating singlet oxygen (II type of PDT reactions) and/or reactive oxygen species, and the oxidation of intracellular structures such as fatty acids, nucleic acids, and proteins (type I PDT reactions).⁴ Rose bengal (RB) deserves special attention because it generates singlet oxygen with higher efficiency than other photosensitizers.^{26,27} However, free RB has a tendency to aggregate in aqueous solutions and is characterized by limited cell membrane penetration.⁸ Hence, the search for an appropriate carrier for RB is still ongoing. A promising way to increase bioavailability of RB is to deliver it in

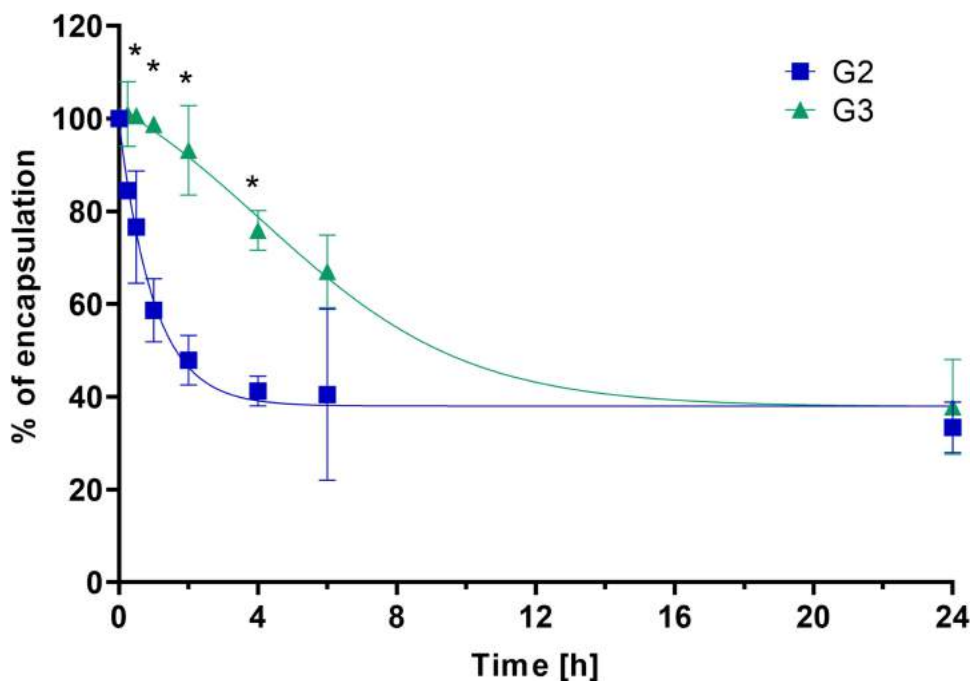


Figure 5 Release of RB from G2-RB and G3-RB dendrimersomes at pH 5.5. Percentage of release was determined relative to the first sample (0 h, 100% of initial absorbance). *Statistically significant difference at $p < 0.05$ between the two generations of dendrimersomes. Data are presented as means \pm SD, $n=3$.

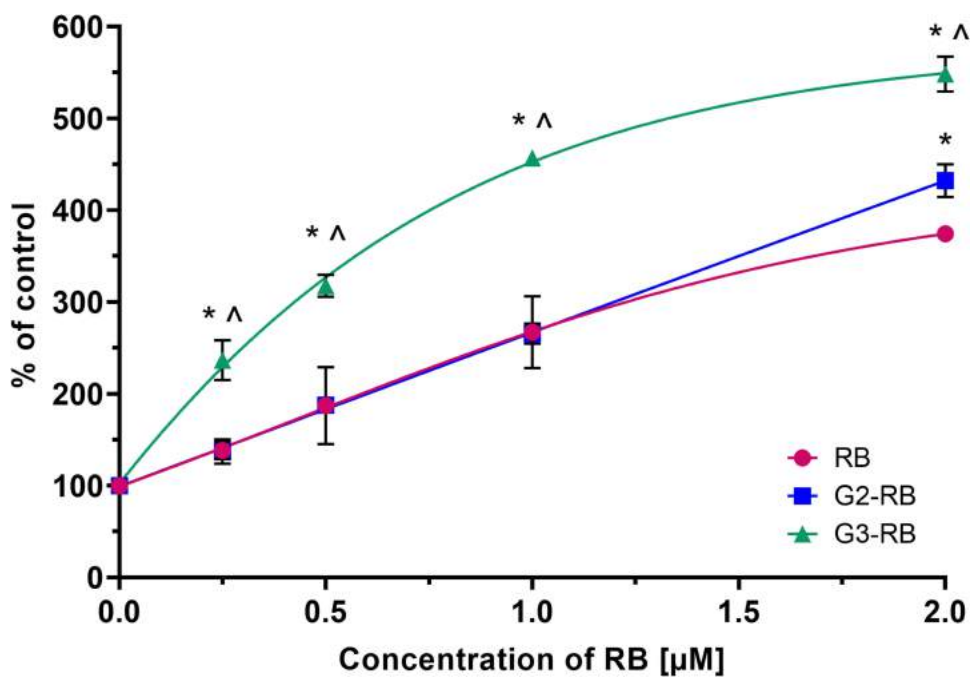


Figure 6 Singlet oxygen generation by free RB and dendrimersomes loaded with RB (G2-RB and G3-RB), determined using an ABDA probe. *Statistically significant difference at $p < 0.05$ between G3-RB or G2-RB and RB. ^ Statistically significant difference at $p < 0.05$ between G2-RB and G3-RB. Data are presented as means \pm SD, $n=3$.

nanoformulations.⁸ To date, various types of RB-loaded nanocarriers have been designed for skin cancer PDT in vitro and in vivo, including lipid-based formulations^{28–30} polymeric nanoparticles,^{31–33} upconversion nanoparticles,^{34,35} inorganic nanoparticles³⁶ and so on.

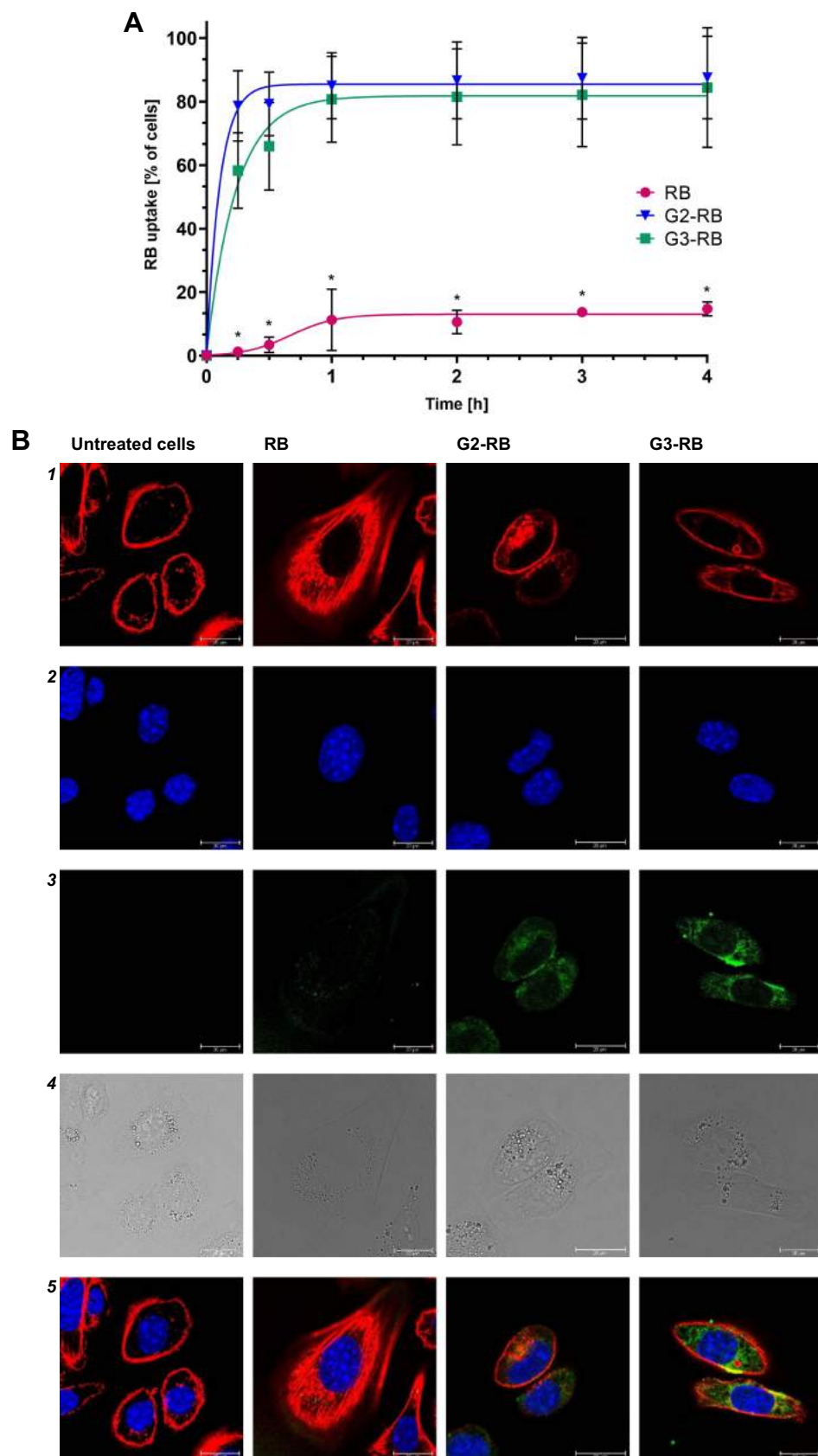


Figure 7 (A) Uptake of free RB and dendrimersomes loaded with RB (G2-RB and G3-RB) by AsZ cells. Data are presented as means \pm SD, $n=3$. *Statistically significant difference at $p<0.05$ between evaluated compounds and RB. **(B)** Confocal micrographs: (1) Phalloidin-Atto 633; (2) Hoechst 33342; (3) rose bengal; (4) bright field image; (5) merge of channels 1, 2, and 3. Scale bar represents 20 μ m.

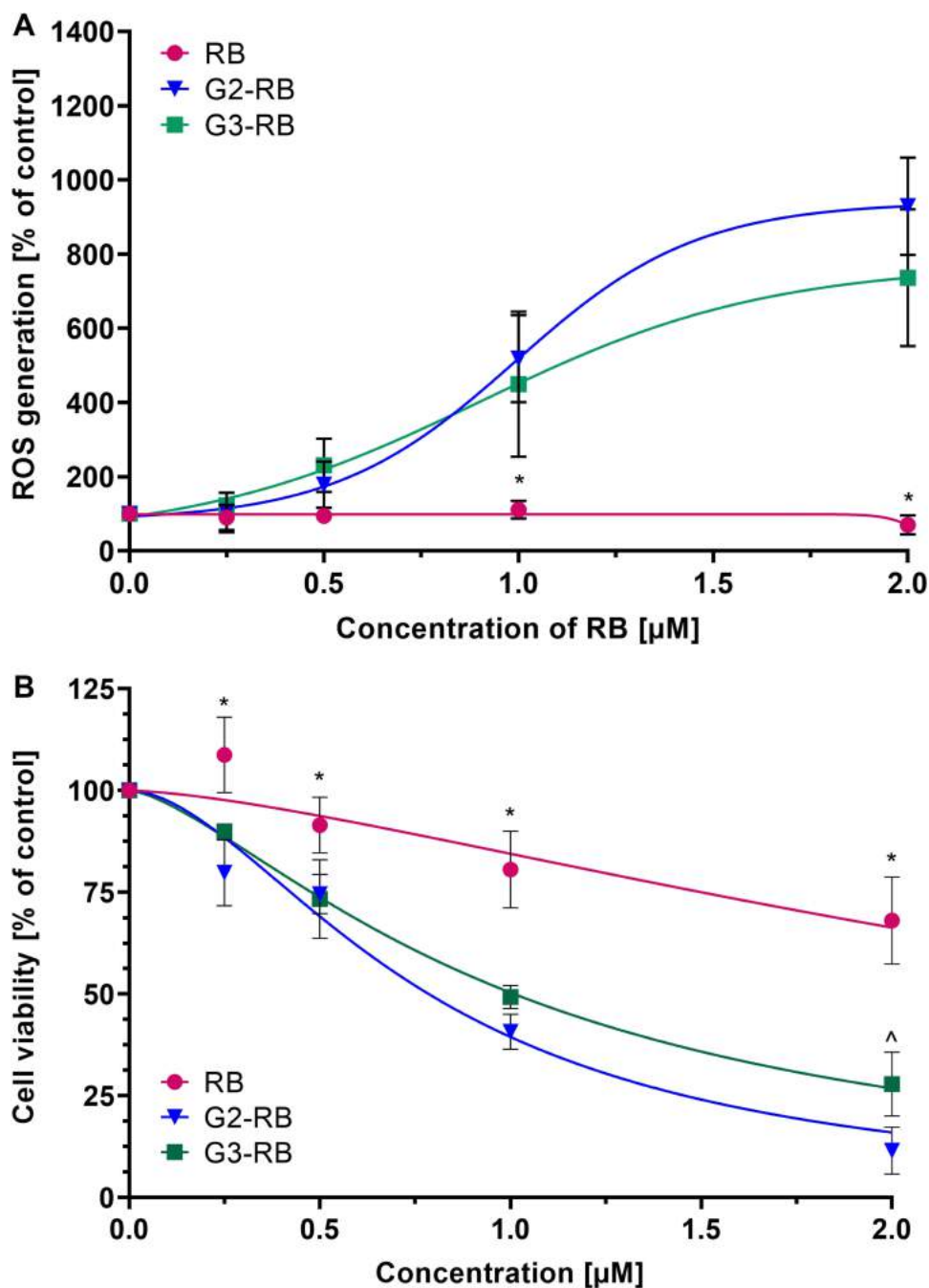


Figure 8 (A) ROS generation and **(B)** phototoxic activity of free RB and RB-loaded dendrimersomes (G2-RB and G3-RB) on AsZ cells. Data are presented as means \pm SD, $n=3$. *Statistically significant difference at $p < 0.05$ between RB and G2-RB or G3-RB. ^ Statistically significant difference at $p < 0.05$ between G2-RB and G3-RB.

A promising approach for the design of therapeutic formulations is based on hyperbranched molecules - dendrimers and dendrons. Their advantages include monodisperse and reproducible molecular structure, combined with inherent multivalency.^{37,38} Such a feature provides dendritic molecules with considerable activity at nano-bio interface, both as drug carriers and therapeutic entities themselves. Nanoformulations based on dendrimers and dendrons have been used to deliver low-molecular bioactive compounds,^{39,40} therapeutic nucleic acids,^{41,42} peptides and proteins⁴³ into target cells.

In particular, using amphiphilic dendrons as building blocks, it is possible to obtain supramolecular formulations with micellar or vesicular architecture.^{21,44,45} The properties and morphology of dendritic assemblies depend on the size and topology of the dendron scaffold, the arrangement of chemical moieties within the dendron structure, and specifically selected hydrophilic and hydrophobic elements. Upon assembly, low-molecular weight drugs can be encapsulated either in the inner cavity or in the bilayer and can also be retained on the vesicle surface through complexation. Encapsulation protects a drug from degradation en route to the tumor.²² Carbosilane dendritic architecture is versatile for designing functional systems for therapy,^{46–49} imaging⁵⁰ and nanoparticle decoration.^{51–53} Furthermore, the chemical structure of carbosilane dendrons containing two orthogonal functionalities favors the synthesis of amphiphilic derivatives self-organizing into micelles^{54–56} or dendrimersomes.²⁰

In this study, we examined the performance of triazine–carbosilane dendrimersomes as nanocarriers for RB in PDT. A previous study showed that due to the presence of protonatable triazine fragments inside the scaffold, dendrimersomes are pH-sensitive. Under slightly acidic conditions, reorganization of the vesicular structure occurs, as evidenced by the change in hydrodynamic diameter of dendrimersomes (Figure 3) and shrinkage of a hydrophobic bilayer observed in TEM images (Figure S8). This behavior can be exploited to achieve drug delivery directly into the tumor acidic environment.^{20,57} In the first part of the research, we studied the loading of RB into dendrimersomes of triazine–carbosilane dendrons of the second and third generation. We observed wavelength shifts of maximum absorbance or fluorescence of the RB–dendrimersome formulations in comparison to free RB. This finding indicates interaction between anionic RB and protonated dendrons, as described in the literature,^{58,59} providing evidence for the formation of stable RB–dendrimersome formulations. Moreover, we observed visible changes in the absorbance and fluorescence intensity before and after dialysis used to purify RB-loaded dendrimersomes from the non-bound RB in solution. These changes could be used to determine the encapsulation efficiency and drug loading capacity (Table 1), as reported previously.²⁰ Zeta potential measurements revealed highly positive surface potential, which may be beneficial for cellular uptake.⁶⁰ Because these dendrimersomes formed at neutral pH, and the structure of dendrimersomes reorganizes at acidic conditions to enable drug release, we tested the release of RB from dendrimersomes of both generations at pH 5.5. Release was much slower for G3, which may explain why singlet oxygen generation was significantly higher for G3–RB. Because interactions with cationic polymers increase singlet oxygen production by RB, we believe the slower release is due to the fact that RB interacts with G3 more strongly than with G2 dendrimersomes.⁶¹ The specific activities of different generations of dendrons/dendrimersomes require further study. However, for photodynamic therapy, PS does not need to be released from the carrier if the carrier allows diffusion of molecular oxygen.^{4,62}

In an *in vitro* model using basal cell carcinoma cell lines, both flow cytometry and confocal microscopy revealed that cellular uptake of RB encapsulated in dendrimersomes was significantly greater than uptake of RB. This dramatic increase is likely due to the shielding of negatively charged groups in the RB structure by the positive surface charge of dendrimersomes. Nanoparticles with positive surface charges exhibit much more efficient intracellular transport. This phenomenon has been widely described in the literature and allows us to predict the behavior of nanosystems.^{63–66} In the case of RB, increased cellular uptake seems to be critical for phototoxic activity: regardless of the level of singlet oxygen generation, RB-loaded dendrimersomes generate significantly higher levels of intracellular ROS, which translates into a stronger phototoxic effect. The IC₅₀ values for RB-loaded dendrimersomes *in vitro* are remarkably low (~1 μM RB for both formulations), considerably lower than those for most formulations mentioned above (for instance^{28,30,32,36}). Importantly, the dark toxicity of RB-loaded dendrimersomes is negligible in the concentration range used. It should be also noted that under the same conditions, empty dendrimersomes did not exert cytotoxic or phototoxic activity, so the observed results should not be attributed to additive or synergistic effects.

Conclusion

Our findings suggest that dendrimersomes built of amphiphilic triazine–carbosilane dendrons are robust vehicles for delivering RB into basal skin cancer cells, increasing the therapeutic performance of the PS through increased cellular uptake and intracellular ROS generation. This highly encouraging outcome sheds new light on PDT of skin cancers. However, further research is needed to answer the fundamental questions: how does RB interact with the carrier? How strong are these interactions? What is the localization of RB in the dendrimersome? What influences the difference in the

interactions of G2 and G3 with RB? Further studies on this system are also needed in term of intracellular localization of RB-loaded dendrimersomes and possibility of lysosomal escape, as well as in vivo activity.

Acknowledgments

The authors thank Dr. Julia Poletaeva and Prof. Elena Ryabchikova (ICBFM) for the TEM study of dendrimersomes and Dr. Ervin Epstein (Children's Oakland Research Institute, Oakland, CA, USA) for providing murine basal cell carcinoma lines (AsZ, BsZ, CsZ). This work was supported by National Science Centre, Poland (Project UMO-2017/25/B/NZ7/01304 "Phosphorus dendrimers as carriers for photosensitizers - in vivo studies"), by RFBR grant No. 18-33-20109, and based upon work from COST Action CA17140 NANO2CLINIC "Cancer Nanomedicine - from the bench to the bedside" supported by COST (European Cooperation in Science and Technology). The project received funding from the European Union's Horizon 2020 research and innovation programme under the Marie Skłodowska-Curie grant agreement No 844217. This work was also supported by PID2020-112924RB-I00 (Ministry of Science and Innovation), Consortium IMMUNOTHERCAN-CM B2017/BMD-3733 (CAM), NANODENDMED II-CM ref B2017/BMD-3703 and project SBPLY/17/180501/000358 JCCM and PIE14/00061 (CIBER-BBN).

Disclosure

The authors report no conflicts of interest in this work.

References

1. Basset-Seguín N, Herms F. Update on the management of basal cell carcinoma. *Acta Derm Venereol.* 2020;100(11):284–290. doi:10.2340/00015555-3495
2. Olivo M, Bhuvaneshwari R, Lucky SS, Dendukuri N, Thong PSP. Targeted therapy of cancer using photodynamic therapy in combination with multi-faceted anti-tumor modalities. *Pharmaceuticals.* 2010;3(5):1507–1529. doi:10.3390/ph3051507
3. Kucinska M, Skupin-Mrugalska P, Szczolko W, et al. Phthalocyanine derivatives possessing 2-(morpholin-4-yl) ethoxy groups as potential agents for photodynamic therapy. *J Med Chem.* 2015;58(5):2240–2255. doi:10.1021/acs.jmedchem.5b00052
4. Sztandera K, Gorzkiewicz M, Klajnert-Maculewicz B. Nanocarriers in photodynamic therapy—in vitro and in vivo studies. *Wiley Interdiscip Rev Nanomed Nanobiotechnol.* 2020;12(3):1–24. doi:10.1002/wnan.1599
5. Pham TC, Nguyen VN, Choi Y, Lee S, Yoon J. Recent strategies to develop innovative photosensitizers for enhanced photodynamic therapy. *Chem Rev.* 2021;121(21):13454–13619. doi:10.1021/acs.chemrev.1c00381
6. Redmond RW, Gamlin JN. A compilation of singlet oxygen yields from biologically relevant molecules. *Photochem Photobiol.* 1999;70(4):391–475. doi:10.1111/j.1751-1097.1999.tb08240.x
7. Vanerio N, Stijnen M, De Mol BAJM, Kock LM. Biomedical applications of photo- and sono-activated rose bengal: a review. *Photobiomodulation Photomed Laser Surg.* 2019;37(7):383–394. doi:10.1089/photob.2018.4604
8. Demartis S, Obinu A, Gavini E, Giunchedi P, Rasso G. Nanotechnology-based rose Bengal: a broad-spectrum biomedical tool. *Dye Pigment.* 2021;188:109236. doi:10.1016/j.dyepig.2021.109236
9. Qidwai A, Annu NB. Role of nanocarriers in photodynamic therapy. *Photodiagnosis Photodyn Ther.* 2020;30:101782. doi:10.1016/j.pdpdt.2020.101782
10. Xie J, Wang Y, Choi W, et al. Overcoming barriers in photodynamic therapy harnessing nano-formulation strategies. *Chem Soc Rev.* 2021;50(16):9152–9201. doi:10.1039/d0cs01370f
11. Antimisiaris SG, Marazioti A, Kannavou M, et al. Overcoming barriers by local drug delivery with liposomes. *Adv Drug Deliv Rev.* 2021;174:53–86. doi:10.1016/j.addr.2021.01.019
12. Ghaffari M, Dehghan G, Baradaran B, et al. Co-delivery of curcumin and Bcl-2 siRNA by PAMAM dendrimers for enhancement of the therapeutic efficacy in HeLa cancer cells. *Colloids Surf B Biointerfaces.* 2020;188:110762. doi:10.1016/j.colsurfb.2019.110762
13. Duncan R, Izzo L. Dendrimer biocompatibility and toxicity. *Adv Drug Deliv Rev.* 2005;57(15):2215–2237. doi:10.1016/j.addr.2005.09.019
14. Tripathi PK, Tripathi S. Dendrimers for anticancer drug delivery. *Pharm Appl Dendrimers.* 2019;4:131–150.
15. Sztandera K, Gorzkiewicz M, Dias Martins AS, et al. Noncovalent interactions with PAMAM and PPI dendrimers promote the cellular uptake and photodynamic activity of rose bengal: the role of the dendrimer structure. *J Med Chem.* 2021;64(21):15758–15771. doi:10.1021/acs.jmedchem.1c01080
16. Zhou D, Fei Z, Jin L, et al. Dual-responsive polymersomes as anticancer drug carriers for the co-delivery of doxorubicin and paclitaxel. *J Mater Chem B.* 2021;9(3):801–808. doi:10.1039/D0TB02462G
17. Laskar P, Dufès C. Emergence of cationic polyamine dendrimersomes: design, stimuli sensitivity and potential biomedical applications. *Nanoscale Adv.* 2021;3(21):6007–6026. doi:10.1039/D1NA00536G
18. Laskar P, Somani S, Campbell SJ, et al. Camptothecin-based dendrimersomes for gene delivery and redox-responsive drug delivery to cancer cells. *Nanoscale.* 2019;11(42):20058–20071. doi:10.1039/C9NR07254C
19. Laskar P, Somani S, Altwaijry N, et al. Redox-sensitive, cholesterol-bearing PEGylated poly(propylene imine)-based dendrimersomes for drug and gene delivery to cancer cells. *Nanoscale.* 2018;10(48):22830–22847. doi:10.1039/C8NR08141G
20. Apartsin E, Knauer N, Arkhipova V, et al. pH-sensitive dendrimersomes of hybrid triazine-carbosilane dendritic amphiphiles-smart vehicles for drug delivery. *Nanomaterials.* 2020;10(10):1899. doi:10.3390/nano10101899

21. Percec V, Wilson DA, Leowanawat P, et al. Self-assembly of janus dendrimers into uniform dendrimersomes and other complex architectures. *Science (80-)*. 2010;328(5981):1009–1014. doi:10.1126/science.1185547
22. Hu FF, Sun YW, Zhu YL, Huang YN, Li ZW, Sun ZY. Enthalpy-driven self-assembly of amphiphilic Janus dendrimers into onion-like vesicles: a Janus particle model. *Nanoscale*. 2019;11(37):17350–17356. doi:10.1039/C9NR05885K
23. Estrella V, Chen T, Lloyd M, et al. Acidity generated by the tumor microenvironment drives local invasion. *Cancer Res*. 2013;73(5):1524–1535. doi:10.1158/0008-5472.CAN-12-2796
24. Fuentes-Paniagua E, Peña-González CE, Galán M, Gómez R, De La Mata FJ, Sánchez-Nieves J. Thiol-ene synthesis of cationic carbosilane dendrons: a new family of synthons. *Organometallics*. 2013;32(6):1789–1796. doi:10.1021/om301217g
25. Jones OT, Ranmuthu CKI, Hall PN, Funston G, Walter FM. Recognising skin cancer in primary care. *Adv Ther*. 2020;37(1):603–616. doi:10.1007/s12325-019-01130-1
26. Dabrzalska M, Janaszewska A, Zablocka M, Mignani S, Majoral JP, Klajnert-Maculewicz B. Complexing methylene blue with phosphorus dendrimers to increase photodynamic activity. *Molecules*. 2017;22(3). doi:10.3390/molecules22030345
27. Lutkus LV, Rickenbach SS, McCormick TM. Singlet oxygen quantum yields determined by oxygen consumption. *J Photochem Photobiol a Chem*. 2019;378:131–135. doi:10.1016/j.jphotochem.2019.04.029
28. Demartis S, Rasso G, Murgia S, Casula L, Giunchedi P, Gavini E. Improving dermal delivery of rose bengal by deformable lipid nanovesicles for topical treatment of melanoma. *Mol Pharm*. 2021;18(11):4046–4057. doi:10.1021/acs.molpharmaceut.1c00468
29. Ali MFM. Topical delivery and photodynamic evaluation of a multivesicular liposomal Rose Bengal. *Lasers Med Sci*. 2011;26(2):267–275. doi:10.1007/s10103-010-0859-9
30. Forouz F, Dabbaghi M, Namjoshi S, Mohammed Y, Roberts MS, Grice JE. Development of an oil-in-water self-emulsifying microemulsion for cutaneous delivery of rose Bengal: investigation of anti-melanoma properties. *Pharmaceutics*. 2020;12(10):1–17. doi:10.3390/pharmaceutics12100947
31. Torres-Martínez A, Bedrina B, Falomir E, et al. Non-polymeric nanogels as versatile nanocarriers: intracellular transport of the photosensitizers rose bengal and hypericin for photodynamic therapy. *ACS Appl Bio Mater*. 2021;4(4):3658–3669. doi:10.1021/acsabm.1c00139
32. Yeh HP, Del Valle AC, Syu MC, Qian Y, Chang YC, Huang YF. A new photosensitized oxidation-responsive nanoplatfor for controlled drug release and photodynamic cancer therapy. *ACS Appl Mater Interfaces*. 2018;10(25):21160–21172. doi:10.1021/acsami.8b05205
33. Yan Y, Li J, Zheng J, et al. Poly (L-lysine)-based star-block copolymers as pH-responsive nanocarriers for anionic drugs. *Colloids Surf B Biointerfaces*. 2012;95:137–143. doi:10.1016/j.colsurfb.2012.02.034
34. Wang HY, Hou L, Li HL, et al. A nanosystem loaded with perfluorohexane and rose bengal coupled upconversion nanoparticles for multimodal imaging and synergetic chemo-photodynamic therapy of cancer. *Biomater Sci*. 2020;8(9):2488–2506. doi:10.1039/C9BM02081K
35. Han S, Hwang BW, Jeon EY, et al. Upconversion nanoparticles/hyaluronate-rose bengal conjugate complex for noninvasive photochemical tissue bonding. *ACS Nano*. 2017;11(10):9979–9988. doi:10.1021/acsnano.7b04153
36. Chen K, Chang C, Liu Z, et al. Hyaluronic acid targeted and pH-responsive nanocarriers based on hollow mesoporous silica nanoparticles for chemo-photodynamic combination therapy. *Colloids Surf B Biointerfaces*. 2020;194:111166. doi:10.1016/j.colsurfb.2020.111166
37. Mignani S, Rodrigues J, Roy R, et al. Exploration of biomedical dendrimer space based on in-vivo physicochemical parameters: key factor analysis (Part 2). *Drug Discov Today*. 2019;24(5):1184–1192. doi:10.1016/j.drudis.2019.03.001
38. Dias AP, da Silva Santos S, da Silva JV, et al. Dendrimers in the context of nanoMedicine. *Int J Pharm*. 2020;5:573.
39. Sandoval-Yañez C, Rodriguez CC. Dendrimers: amazing platforms for bioactive molecule delivery systems. *Materials*. 2020;13(3):570. doi:10.3390/ma13030570
40. Bolu BS, Sanyal R, Sanyal A. Drug delivery systems from self-assembly of dendron-polymer conjugates. *Molecules*. 2018;23(7):1570. doi:10.3390/molecules23071570
41. Mendes LP, Pan J, Torchilin VP. Dendrimers as nanocarriers for nucleic acid and drug delivery in cancer therapy. *Molecules*. 2017;22(9):1401. doi:10.3390/molecules22091401
42. Dzmirutuk V, Apartsin E, Ihnatsyeyu-Kachan A, Abashkin V, Shcharbin D, Bryszewska M. Dendrimers show promise for siRNA and microRNA therapeutics. *Pharmaceutics*. 2018;10(3):126. doi:10.3390/pharmaceutics10030126
43. Knauer N, Pashkina E, Apartsin E. Topological aspects of the design of nanocarriers for therapeutic peptides and proteins. *Pharmaceutics*. 2019;11(2):91. doi:10.3390/pharmaceutics11020091
44. Peterca M, Percec V, Leowanawat P, Bertin A. Predicting the size and properties of dendrimersomes from the lamellar structure of their amphiphilic janus dendrimers. *J Am Chem Soc*. 2011;133(50):20507–20520. doi:10.1021/ja208762u
45. Apartsin E, Caminade AM. Supramolecular self-associations of amphiphilic dendrons and their properties. *Chem – a Eur J*. 2021;27(72):17976–17998. doi:10.1002/chem.202102589
46. Fernandez J, Acosta G, Pulido D, et al. Carbosilane dendron-peptide nanoconjugates as antimicrobial agents. *Mol Pharm*. 2019;16(6):2661–2674. doi:10.1021/acs.molpharmaceut.9b00222
47. Sepúlveda-Crespo D, De La Mata FJ, Gómez R, Muñoz-Fernández MA. Sulfonate-ended carbosilane dendrimers with a flexible scaffold cause inactivation of HIV-1 virions and gp120 shedding. *Nanoscale*. 2018;10(19):8998–9011. doi:10.1039/C8NR01664J
48. Krasheninina OA, Apartsin EK, Fuentes E, et al. Complexes of pro-apoptotic siRNAs and carbosilane dendrimers: formation and effect on cancer cells. *Pharmaceutics*. 2019;11(1):25. doi:10.3390/pharmaceutics11010025
49. Sánchez-Milla M, Muñoz-Moreno L, Sánchez-Nieves J, et al. Anticancer activity of dendriplexes against advanced prostate cancer from protumoral peptides and cationic carbosilane dendrimers. *Biomacromolecules*. 2019;20(3):1224–1234. doi:10.1021/acs.biomac.8b01632
50. Carloni R, Del Olmo NS, Ortega P, et al. Exploring the interactions of ruthenium (II) carbosilane metallodendrimers and precursors with model cell membranes through a dual spin-label spin-probe technique using EPR. *Biomolecules*. 2019;9(10):540. doi:10.3390/biom9100540
51. Gutiérrez-Ulloa CE, Buyanova MY, Apartsin EK, Venyaminova AG, de la Mata FJ, Gómez R. Carbon nanotubes decorated with cationic carbosilane dendrons and their hybrids with nucleic acids. *ChemNanoMat*. 2018;4(2):220–230. doi:10.1002/cnma.201700351
52. Pędziwiatr-Werbicka E, Gorzkiewicz M, Horodecka K, et al. Silver nanoparticles surface-modified with carbosilane dendrons as carriers of anticancer siRNA. *Int J Mol Sci*. 2020;21(13):1–17. doi:10.3390/ijms21134647
53. González-García E, Gutiérrez Ulloa CE, de la Mata FJ, Marina ML, García MC. Sulfonate-terminated carbosilane dendron-coated nanotubes: a greener point of view in protein sample preparation. *Anal Bioanal Chem*. 2017;409(22):5337–5348. doi:10.1007/s00216-017-0479-3

54. Gutierrez-Ulloa CE, Buyanova MY, Apartsin EK, et al. Amphiphilic carbosilane dendrons as a novel synthetic platform toward micelle formation. *Org Biomol Chem*. 2017;15(35):7352–7364. doi:10.1039/C7OB01331K
55. Mencía G, Lozano-Cruz T, Valiente M, de la Mata J, Cano J, Gómez R. New ionic carbosilane dendrons possessing fluorinated tails at different locations on the skeleton. *Molecules*. 2020;25(4):807. doi:10.3390/molecules25040807
56. Mencía G, Lozano-Cruz T, Valiente M, et al. Evaluation of pH-dependent amphiphilic carbosilane dendrons in micelle formation, drug loading and HIV-1 infection. *Org Biomol Chem*. 2020;18(47):9639–9652. doi:10.1039/D0OB01867H
57. Filippi M, Catanzaro V, Patrucco D, Botta M, Tei L, Terreno E. First in vivo MRI study on theranostic dendrimersomes. *J Control Release*. 2017;248:45–52. doi:10.1016/j.jconrel.2017.01.010
58. Haba Y, Harada A, Takagishi T, Kono K. Synthesis of biocompatible dendrimers with a peripheral network formed by linking of polymerizable groups. *Polymer*. 2005;46(6):1813–1820. doi:10.1016/j.polymer.2005.01.004
59. Dabrzalska M, Zablocka M, Mignani S, Majoral JP, Klajnert-Maculewicz B. Phosphorus dendrimers and photodynamic therapy. Spectroscopic studies on two dendrimer-photosensitizer complexes: cationic phosphorus dendrimer with rose bengal and anionic phosphorus dendrimer with methylene blue. *Int J Pharm*. 2015;492(1–2):266–274. doi:10.1016/j.ijpharm.2015.06.014
60. Fröhlich E. The role of surface charge in cellular uptake and cytotoxicity of medical nanoparticles. *Int J Nanomedicine*. 2012;7:5577–5591. doi:10.2147/IJN.S36111
61. Dabrzalska M, Janaszewska A, Zablocka M, Mignani S, Majoral JP, Klajnert-Maculewicz B. Cationic phosphorus dendrimer enhances photodynamic activity of rose bengal against basal cell carcinoma cell lines. *Mol Pharm*. 2017;14(5):1821–1830. doi:10.1021/acs.molpharmaceut.7b00108
62. Gorzkiewicz M, Klajnert-Maculewicz B. Chapter 10 in dendrimers for drug delivery. In: Sharma A, Keservan R, editors. *Dendrimers as Nanocarriers for Anticancer Drugs*. Apple Academic Press; 2018:327–374.
63. Honary S, Zahir F. Effect of zeta potential on the properties of nano-drug delivery systems - A review (Part 1 and 2). *Trop J Pharm Res*. 2013;12(2):255–264.
64. Gorzkiewicz M, Deriu MA, Studzian M, et al. Fludarabine-specific molecular interactions with maltose-modified poly (propyleneimine) dendrimer enable effective cell entry of the active drug form: comparison with clofarabine. *Biomacromolecules*. 2019;20(3):1429–1442. doi:10.1021/acs.biomac.9b00010
65. Fox LJ, Richardson RM, Briscoe WH. PAMAM dendrimer - cell membrane interactions. *Adv Colloid Interface Sci*. 2018;257:1–18. doi:10.1016/j.cis.2018.06.005
66. Hong S, Leroueil PR, Janus EK, et al. Interaction of polycationic polymers with supported lipid bilayers and cells: nanoscale hole formation and enhanced membrane permeability. *Bioconjug Chem*. 2006;17(3):728–734. doi:10.1021/bc060077y

International Journal of Nanomedicine

Dovepress

Publish your work in this journal

The International Journal of Nanomedicine is an international, peer-reviewed journal focusing on the application of nanotechnology in diagnostics, therapeutics, and drug delivery systems throughout the biomedical field. This journal is indexed on PubMed Central, MedLine, CAS, SciSearch®, Current Contents®/Clinical Medicine, Journal Citation Reports/Science Edition, EMBASE, Scopus and the Elsevier Bibliographic databases. The manuscript management system is completely online and includes a very quick and fair peer-review system, which is all easy to use. Visit <http://www.dovepress.com/testimonials.php> to read real quotes from published authors.

Submit your manuscript here: <https://www.dovepress.com/international-journal-of-nanomedicine-journal>

pH-stable polymersome as nanocarrier for post-loaded rose bengal in photodynamic therapy

K. Sztandera¹, M. Gorzkiewicz^{1,2}, X. Wang³, S. Boye⁴, D. Appelhans⁴, B. Klajnert-Maculewicz¹

¹ *Department of General Biophysics, Faculty of Biology and Environmental Protection, University of Lodz, 141/143 Pomorska St., 90-236 Lodz, Poland.*

² *Department of Molecular Medicine II, Medical Faculty, Heinrich Heine University Düsseldorf, Universitätsstr. 1, 40225 Düsseldorf, Germany*

³ *Dongguan Hospital, Southern Medical University, Dongguan 523059, P. R. China.*

⁴ *Leibniz Institute for Polymer Research Dresden, 6 Hohe St., 01069 Dresden, Germany*

*Corresponding author: krzysztof.sztandera@edu.uni.lodz.pl

Total number of words: 6754

Number of tables: 1

Number of figures: 7

Abstract:

Photodynamic therapy is one of the best alternatives to chemo-, radio- or surgical therapy, as it is noninvasive and causes no severe side effects. The mechanism of photodynamic therapy involves activation of the drug (photosensitizer) with light of appropriate wavelength, which combined with molecular oxygen, leads to production of reactive oxygen species. This starts a cascade of reactions leading to cell death. Thus, the efficiency of this therapy is based mainly on the properties of a photosensitizer, including singlet oxygen yield and accumulation in the tumor area. Current research is aimed at applying nanosystems for the improvement of availability and photodynamic properties of photosensitizers. In order to improve the activity and increase photodynamic potential of rose bengal, one of the most promising drugs in anticancer photodynamic therapy, several drug delivery systems were developed. Among them, polymersomes represent a group of innovative polymeric vesicles mimicking membranous cell structures. Polymersomes are nanosystems made of amphiphilic block copolymers, possessing a spherical, liposome-like architecture. Within this study we present biophysical and in vitro biological characterization of this novel pH-stable nanosystem, which due to the improvement of singlet oxygen and ROS production by rose bengal is a good candidate for nanocarrier in photodynamic therapy.

Key words: Rose bengal, photodynamic therapy, polymersome, skin cancer

1. Introduction

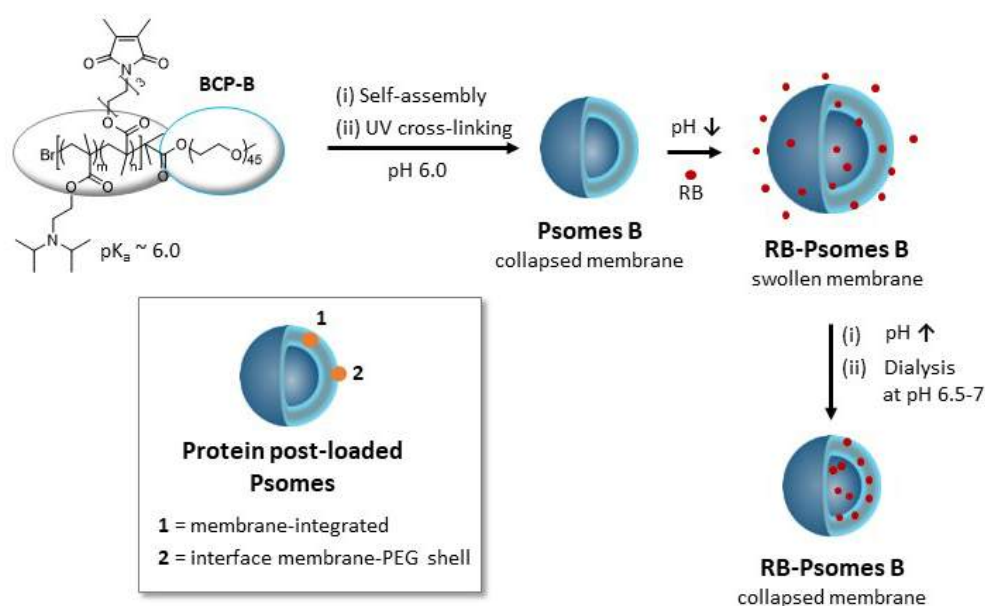
Due to the undoubted advantages such as non-invasiveness and lack of severe side effects, photodynamic therapy (PDT) is gaining more and more popularity (Karges, 2022), providing a promising alternative to traditional methods of cancer treatment, such as chemo-, radio-, or surgical therapy. It encompasses three fundamental elements: a photosensitizer (PS), a light source, and molecular oxygen. The mechanism of PDT involves activation of the photosensitizer with light of appropriate wavelength, which combined with molecular oxygen, leads to production of reactive oxygen species. The products of this reaction initiate a cascade of effects leading to cell death (Sztandera et al.,

2020a). Such a specific mechanism, with the activation of the photosensitizer only in the irradiated area, gives PDT the hallmarks of targeted therapy (Hong et al., 2016). The ideal PS should exhibit absorbance in a range of 650-850 nm, efficiently produce reactive oxygen species, resist photodegradation and show lack of toxicity in the absence of light. PS should be also characterized by efficient cellular uptake and significant half-life (Allison et al., 2004).

One of the most promising photosensitizers for anticancer therapy is rose bengal (RB), an anionic, water-soluble fluorescein derivative that generates singlet oxygen after irradiation with light of 525 nm wavelength (Dabrzalska et al., 2017; Sztandera et al., 2021, 2020b). This compound has been already approved for use in PDT (Dees et al., 2015; Dees and Scott, 2001; Prokopovich and Perni, 2017), which proves its great application potential. Current research is aimed at applying innovative nanosystems for the improvement of availability and photodynamic properties of RB (Demartis et al., 2021; Sztandera et al., 2020a, 2020b). Nanocarriers are meant to protect photosensitizer from degradation and rapid clearance from the organism, improve solubility and transport the drug directly to its site of action. The delivery systems should ensure prolonged blood circulation, accumulation in the tumor area and efficient uptake of the drugs by cancer cells (Kakde et al., 2011).

In order to improve the activity of RB and increase its photodynamic potential, several drug delivery systems were developed (Dabrzalska et al., 2017; Sztandera et al., 2020b; Thambi and Lee, 2018) and a few of them were already patented (Bottiroli et al., 1996; Hasan, 2006; Pouge et al., 2005). Among them, polymersomes (Psomes) represent a group of innovative polymeric vesicles (Kyropoulou et al., 2020; Sood, 2014; Wang et al., 2017) made of amphiphilic block copolymers (Discher et al., 1999; Gaitzsch et al., 2016, 2011; Moreno et al., 2020b; Peters et al., 2014; Tu et al., 2016), possessing a spherical, liposome-like architecture (Discher et al., 1999). To develop new Psome nanosystem for intra- and extracellular matrix applications, it is desirable to establish pH-stable structures with swelling and shrinking membrane characteristics upon transition from physiological to slightly acidic pH. This is preventing any disassembly processes when nanosystem is guided through different environments. Our own established, photo-crosslinked and pH-responsive Psomes have been used for the design and fabrication of enzymatic nanoreactors, artificial organelles, protein targeted therapeutics and extracellular matrix therapeutics (Gaitzsch et al., 2012; Geervliet et al., 2021; Moreno et al., 2021; Wang et al., 2021b, 2021a). The post-loading process of pH-responsive Psomes allows us to control the loading of cargo with Psomes' compartments (Geervliet et al., 2021; Gumz et al., 2019; Moreno et al., 2021). For protein post-loading (Scheme 1), preferred locations involve the membrane and shell/membrane interface. On the other hand, low-molecular weight compounds are preferentially located in the membrane or lumen, which is dependent on the structural characteristic and charge of cargo molecules during loading at acidic conditions (swollen state) and purification at neutral/slightly basic conditions (collapsed state). This principle of pH-responsive Psomes have an undoubted advantage in the case of drug delivery to tumor environment. Thus, the ability of Psomes to switch the membrane structure into diffusible state only at the pH characteristic for the tumor environment may further increase the selectivity of the action of drug molecules by controlled release, as well as protect the drug from degradation during blood circulation. This gives a chance to reduce the dose rate while maintaining the therapeutic effect.

The overall aim of the study was to investigate the potential of RB post-loaded polymersome B (RB-Psome B) for PDT (Scheme 1). We focused on its biophysical properties, as well as the ability to encapsulate RB, to deliver it to the cytoplasm of basal cell carcinoma cells and to modulate phototoxic activity of photosensitizer.



Scheme 1. Preparation of RB-loaded Psome B and comparison of protein and RB post-loaded Psomes B.

2. Materials and methods

2.1. Materials

Rose bengal, fetal bovine serum, penicillin/streptomycin solution, trypsin–EDTA solution, ABDA(9,10-Anthracenediyl-bis(methylene)dimalonic acid) and MTT (3-(4,5-dimethyl-2-thiazolyl)-2,5-diphenyl-2H-tetrazolium bromide) were purchased from Sigma-Aldrich, Taufkirchen, Germany. Dulbecco’s phosphate buffered saline with no calcium and no magnesium (DPBS) was purchased from Biowest, France. 154 CF culture medium was obtained from Gibco, Thermo Fisher Scientific, Waltham, Massachusetts, USA. Chelex 100 Resin was obtained from Bio-Rad. H₂DCFDA were purchased from Molecular Probes, ThermoFisher, Waltham, Massachusetts, USA. Dimethyl sulfoxide (DMSO) was purchased from POCH (Gliwice, Poland). Snake-Skin™ Dialysis Tubing, 3.5K MWCO, 22 mm was obtained from ThermoFisher, Waltham, Massachusetts, USA. Murine basal cell carcinoma lines (AsZ, BsZ, CsZ) were kindly provided by Dr. Ervin Epstein (Children’s Oakland Research Institute, Oakland, USA). Materials for the fabrication of rose bengal-loaded polymersomes are listed in the SI.

2.2. Methods

2.2.1.1. Synthesis of block copolymer (BCP-B)

BCP-B was obtained from a previous study (Wang et al., 2021a). The corresponding synthesis of all intermediates and final BCP-B and molecular parameters of BCP-B determined by ¹H NMR and GPC are described in the SI.

2.2.2. Preparation of rose bengal-loaded polymersomes

A solution of BCP-B (0.5 mg/mL) in 10 mM HCl was prepared and stirred for 30 min until the polymer was totally dissolved. Then, 1 M NaOH was added dropwise until pH value between 5.8 and 5.9. The solution was stirred in the dark (150 rpm) for 3 days. The final solution was passed through a cellulose

ester syringe filter (0.8 μm) and placed in the UV chamber (OmniCure S2000[®], Excelitas Technologies) under irradiation for 180 seconds (1.5 mL at each irradiation). After irradiation, 0.4 M PBS was added to the solution of cross-linked polymersome (Psome B) to reach the final PBS concentration of 10 mM and titrated to pH 5 with 1 M HCl. After this step, rose bengal (50 μM) was added to the solution and stirred overnight. The RB-loaded Psome B (RB-Psome B) was subsequently compacted by NaOH titration to pH 7.4 and moved to dialysis tube (SnakeSkin[™] Dialysis Tubing, 3.5K MWCO, 22 mm, ThermoFisher), submerged in PBS (pH 7.4) and stirred in the dark overnight, with several changes of PBS. After this time, sample fluorescence was measured on PerkinElmer LS-50B spectrofluorometer and compared to the sample obtained before dialysis to define the level of encapsulation of RB as described in point 2.2.5.

2.2.3. Measurements of hydrodynamic diameter and zeta potential

Hydrodynamic diameter measurements were performed using 10 μL of 0.5 mg/mL solution of Psome B and RB-Psome B, which was diluted in 1 mL of distilled water (mQ) and placed in the low volume sizing cuvettes (ZEN0112, Malvern). For zeta potential measurements, 50 μL of Psome B and RB-Psome B solution was added to 1 mL of distilled water (mQ), then the solutions were placed in the folded capillary cells (DTS 1070, Malvern). Measurements were performed with the use of Zetasizer Nano ZS (Malvern Instruments Ltd., Malvern, UK) at 25 °C. The data were analyzed using the Malvern software.

2.2.4. Asymmetrical flow field flow fraction study

Asymmetrical flow field flow fractionation (AF4) in combination with multidetection (MD) was applied to quantify the loading of RB-Psome B, according to the protocol previously established for RB and drug loading of branched glycopolymers (Boye et al., 2010; Gorzkiewicz et al., 2019). Furthermore, AF4-MD was used for the determination of conformation properties. All experimental details can be found in SI.

2.2.5. Spectroscopy studies

Fluorescence spectra were acquired using a PerkinElmer LS-50B spectrofluorometer (Waltham, Massachusetts, USA). Measurements were performed in PBS (pH 7.4 or pH 5), at RT. The excitation wavelength was set to 525 nm and spectra were collected in a wavelength range from 540 nm to 640 nm. Excitation and emission slits were 5 nm and 7 nm, respectively. The measurements were carried out for tested compounds at 1 μM concentration of RB.

2.2.6. Release studies

To determine the rate of photosensitizer release from RB-Psome B under different pH conditions, a 5 ml solution of RB-Psome B in PBS (10 mM, pH 7.4) was enclosed in a dialysis membrane tubing (SnakeSkin[™] Dialysis Tubing, 3.5K MWCO, 22 mm, ThermoFisher, Waltham, Massachusetts, USA) and immersed in 10 mM PBS at a pH of 5 or 7.4 at RT. Samples from the internal phase were collected after 0, 2, 4, 8, and 24 h and the RB fluorescence was analyzed as described in the point 2.2.5. Percentage of release was determined with regards to the first sample, where the drug was not released from RB-Psome B (100% of initial fluorescence).

2.2.7. Singlet oxygen generation

The singlet oxygen generation was studied using the ABDA probe (final concentration: 5 μM). Solutions of RB, RB-Psome B, and free Psome B were prepared in 10 mM HEPES. Evaluated compounds were prepared at RB concentrations of 0.125, 0.25, 0.5, 0.75, and 1 μM . Upon sample preparation, 100 μL of each solution was transferred to a 96-well black plate. All measurements were performed on a

fluorescence microplate reader (Fluoroskan Ascent FL, ThermoFisher Scientific) at an excitation wavelength of 355 nm and an emission wavelength of 430 nm. Samples were mixed before each measurement. The first measurement was recorded without ABDA probe to determine whether RB, Psome B, or RB-Psome B exhibit any fluorescence in this range. Following the first measurement, ABDA was added to each well, and the fluorescence of the probe without irradiation was measured. Next, the plate was immediately placed under a Q.Light Pro Unit lamp (Q.Light, Rorschach, Switzerland) equipped with a filter emitting visible light in the wavelength range 385–780 nm (2.4 J/cm² per minute). Fluorescence was measured in 5 min intervals during irradiation for 5–60 min. The slopes of the fluorescence curves were considered to be a measure of singlet oxygen generation. The results were presented as percentages of the singlet oxygen generation in the control sample (HEPES buffer irradiated with probe).

2.2.8. Cell culture

Murine basal cell carcinoma lines (AsZ and CsZ) were cultured in 154-CF medium with 5% penicillin/streptomycin, 0.05 mM calcium, and 2% chelexed, heat-inactivated fetal bovine serum (FBS). Cells were cultured in T-75 culture flasks at 37 °C, 5% CO₂ and subcultured every 2 or 3 days. The number of viable cells was determined by trypan blue exclusion assay with the use of Countess Automated Cell Counter (Invitrogen, Carlsbad, California, USA). For harvesting the cells, a 0.25% (w/v) trypsin–0.03% (w/v) EDTA solution was used.

2.2.9. ROS generation assay

An H₂DCFDA probe was used to investigate the intracellular production of ROS. For this purpose, AsZ and CsZ cells were seeded in 96-well black plates at a density of 1×10^4 cells per well in 100 μL medium. After incubation for 24 h, the samples (free RB solutions or RB-Psome B) were prepared in Hank's Balanced Salt Solution (HBSS) buffer and added to the cells to obtain final RB concentrations of 0.25, 0.50, 1, or 2 μM. ROS-generating activity of free Psome B was also evaluated at the highest concentration used for preparation of RB-Psome B. Cells were incubated with tested compounds for 5 h (37°C, 5% CO₂). The medium was subsequently removed, 2 μM solution of H₂DCFDA in HBSS was added to each well, and the plates were incubated for the next 20 min in the dark (37°C, 5% CO₂). Next, the cells were washed with HBSS, and background fluorescence (excitation: 485 nm; emission: 530 nm) of nonirradiated cells in 100 μL HBSS was measured on a PowerWave HT Microplate reader (BioTek). The cells were then irradiated using Q.Light Pro Unit lamp for 30 min (2.4 J/cm² per minute), and 2',7'-dichlorofluorescein (DCF) fluorescence was measured immediately. ROS level was calculated as increase in DCF fluorescence intensity and was presented as a percentage of the ROS production in control samples (without treatment). Each measurement was corrected by subtraction of the background fluorescence intensity (before irradiation).

2.2.10. Cytotoxicity

AsZ and CsZ cells were seeded into 96-well transparent plates at a density of 3×10^4 cells per well in 100 μL medium and incubated for 24 h before experiments. Then, free RB and RB-Psome B solutions were prepared in PBS buffer and added to the cells to obtain final RB concentrations of 0.25, 0.5, 0.75, and 1 μM. Cytotoxicity of free Psome B was also evaluated at the highest concentration used for the preparation of RB-Psome B. Cells were incubated with tested compounds for 5 h (37°C, 5% CO₂). The medium was replaced with PBS, and the cells were irradiated with visible light using the Q.Light Pro Unit lamp for 30 min. Immediately after irradiation, PBS was replaced with fresh culture medium, and the cells were incubated for 24 h (post-PDT incubation). So-called “dark” toxicity (without irradiation) was evaluated in parallel. The cell viability was measured by MTT assay. MTT was added to the wells

at a final concentration of 0.5 mg/mL, and the plates were incubated for 2 h (37°C, 5% CO₂). After incubation, formazan crystals were dissolved in DMSO, and the absorbance was read at 570 nm using the PowerWave HT Microplate Spectrophotometer (BioTek, Winooski, VT, USA). Cell viabilities are presented as percentages of the viability in the untreated control.

2.2.11. Cellular Uptake

AsZ and CsZ cells were seeded into 24-well plates at a density of 1×10^5 cells per well and incubated for 24 h (37°C, 5% CO₂). Next, RB and RB-Psome B (5 μM final concentration of RB) were added to each well, and the cells were incubated with the compounds for up to 4 h. Following incubation, the compounds were removed, and the cells were washed with PBS and detached using trypsin-EDTA solution. Fresh culture medium was added to the cells, and the samples were gently mixed and collected for measurements. To estimate cellular uptake, the fluorescence of samples was measured using flow cytometry (LSRII, Becton Dickinson, Franklin Lakes, NJ, USA). The excitation and emission filters were 520 and 570 nm, respectively. The results are presented as the percentage of cells in the population that internalized RB.

2.2.12. Statistics

For statistical significance testing, one-way ANOVA for concentration series and post hoc Tukey's test for pairwise difference testing were used. In all tests, p-values < 0.05 were considered to be statistically significant. Data are presented as arithmetic mean ± SD.

3. Results

3.1. Biophysical characterization of nanocarrier system

The formation of Psome B was carried out by the self-assembly of BCP-B through the use of pH-switch method (Pearson et al., 2013) and photo-crosslinking for 180 s under UV irradiation as presented in Scheme 1. The corresponding details on the synthesis of well-established BCP-B are presented in the SI. BCP-B is attributed by a hydrophilic block, a PEG chain, and a hydrophobic block, composed of pH-responsive monomer, 2-(*N,N'*-di-*iso*-propylamino)ethyl methacrylate, and photo-active crosslinker, 6-(3,4-dimethylmaleimidio)hexyl methacrylate (Scheme 1).

To characterize and evaluate Psome B formation, post-loading of RB in swollen Psome B at pH 5, and the purification of RB-Psome B at pH 7.4, we performed dynamic light scattering measurements of nanoparticles at each preparation step. We were able to obtain preferentially uniform nanoparticles with hydrodynamic diameters of 170 nm at pH 7.4 (Psome B with collapsed membrane) and 200 nm at pH 5 (Psome B with swollen membrane) (**Table 1, Figure S5**). As expected from previous study,²⁹ low values of PDI thoroughly indicate the pH-stability after UV-crosslinking and post-loading of RB by swollen Psome B at pH 5. This does not lead to any disassembly processes of swollen Psome B at acidic pH. The surface charge of empty Psome is slightly positive and rises under acidic conditions, indicating the protonation of tertiary amino groups within Psome membrane (Scheme 1). After preparation and purification of RB-Psome B by dialysis in PBS pH 7.4, the zeta potential of RB-Psome B drops to 0.57 ± 1.40 mV, and its hydrodynamic diameter is 190.10 ± 2.12 .

Table 1. Hydrodynamic diameter and zeta potential of Psome B at different stages of preparation.

| Sample Name | PDI | Z-Average [nm] | Zeta potential [mV] |
|---------------------------------|-----------------|-------------------|---------------------|
| Psome B before crosslinking | 0.14 ± 0.03 | 163.40 ± 2.34 | - |
| Psome B after crosslinking pH 5 | 0.17 ± 0.02 | 200.10 ± 6.64 | 7.60 ± 1.56 |

| | | | |
|-----------------------------------|-----------------|--------------------|-----------------|
| Psome B after crosslinking pH 7.4 | 0.22 ± 0.01 | 171.50 ± 11.70 | 2.19 ± 0.54 |
|-----------------------------------|-----------------|--------------------|-----------------|

Analysis of spectral properties of empty Psome B and RB-Psome B show that empty Psome B has no emission in the spectrum range specific for RB, thus the presence of evaluated Psome B would not disturb further measurements. Moreover, pH conditions have no impact on fluorescence intensity of RB-Psome B. In both states, impermeable (“closed” at pH 7.4) and permeable (“open” at pH 5) RB-Psome B have similar maximum emission wavelength, shifting from 565 (for free RB) to 580 nm (**Figure 1**). Moreover, based on the reduction of fluorescence intensity of RB-Psome B before and after purification by equilibrium dialysis, encapsulation efficiency can be determined. In case of this nanosystem the encapsulation efficiency is approx. 60%.

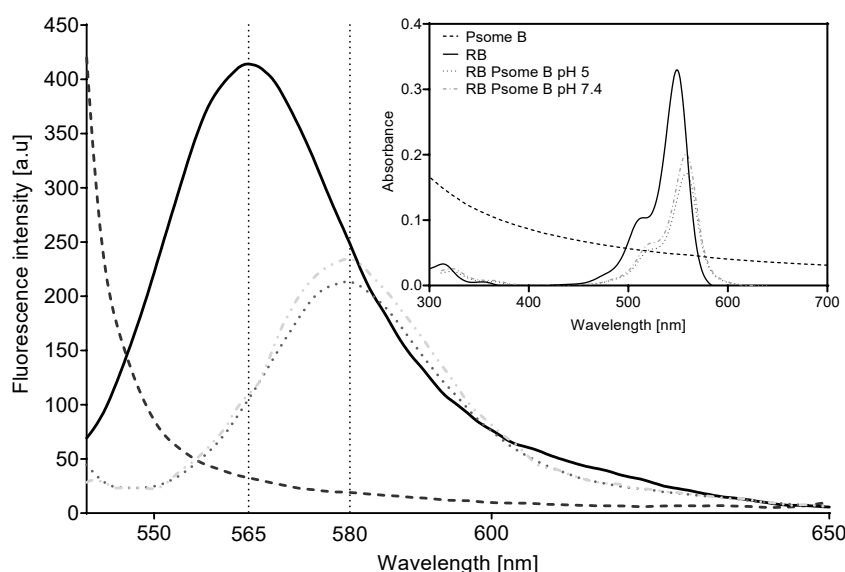


Figure 1. Fluorescence and absorbance spectra of RB, Psome B, “open” RB-Psome B (pH 5) and “closed” RB-Psome B (pH 7.4). The measurements of fluorescence were carried out for the tested compounds at RB concentration of 1 μM and 5 μM , respectively.

3.2. Quantitative and qualitative characterization of RB-Psome B by AF4-MD

In order to quantify the amount of loaded RB as well as to obtain information about the influence of the RB-loading on the Psome B’s structure AF4 in combination with multidetection (AF4-MD) was applied. AF4 enables a versatile separation under gentle conditions without affecting the conformation of Psome B. The quantification of the RB amount was determined using the ultrafiltration effect of the membrane with MWCO of 10k with downstream UV detection. After the calibration of $\text{UV}_{550\text{nm}}$ signal areas according to the injected RB amount, the free RB of the unpurified RB-Psome B mixture was determined and correlated to the loaded RB (Figure S6). It was shown that 31 % of the initial RB amount is loaded into Psome B at pH 6.5 (Table S2). Physico-chemical properties of RB-Psome B were determined by optimized separation by AF4. The multidetection system enables the determination of radius of gyration (R_g) and hydrodynamic radius (R_h) and the consideration of conformation properties. In the fractograms of empty Psome B before and after hollow fiber filtration it is clearly visible that the purification removes smaller species such as non-crosslinked BCPs or smaller micelles in the size region of 10-30 nm (Figure

S7a). The ρ parameter (R_g/R_h) 1.0-1.2 is characteristic for hollow spheres with loaded cargo (Figure S7b) as known from previous studies (Moreno et al, 2021; Wang et al, 2021a).

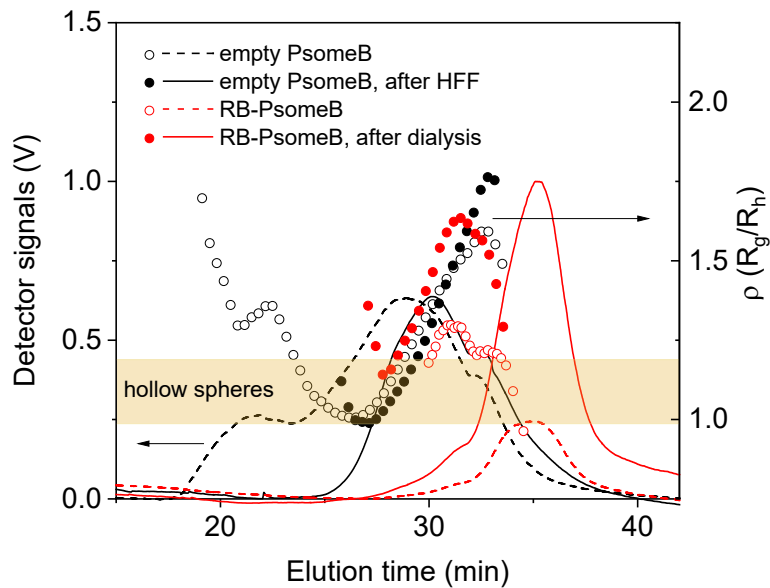


Figure 2. Burchard-Stockmayer plots of Psomes (empty PsomeB -black; RB-PsomeB -red) obtained by AF4-MD, UV signals (before purification -dashed lines; after purification - solid lines) and ρ (R_g/R_h) parameter (before purification - empty circles; after purification -filled circles) vs. elution time, region of characteristic ρ values for hollow spheres is highlighted in yellow.

3.3. Release of RB from RB-Psome B

Release studies proved that at pH 7.4, RB-Psome B are stable, without any significant leak of RB from the system. Due to the swollen membrane of Psome B at pH 5, RB is released from the system in a time-dependent manner. Moreover, the majority of RB is released during the first 4 hours of the experiment (Figure 3).

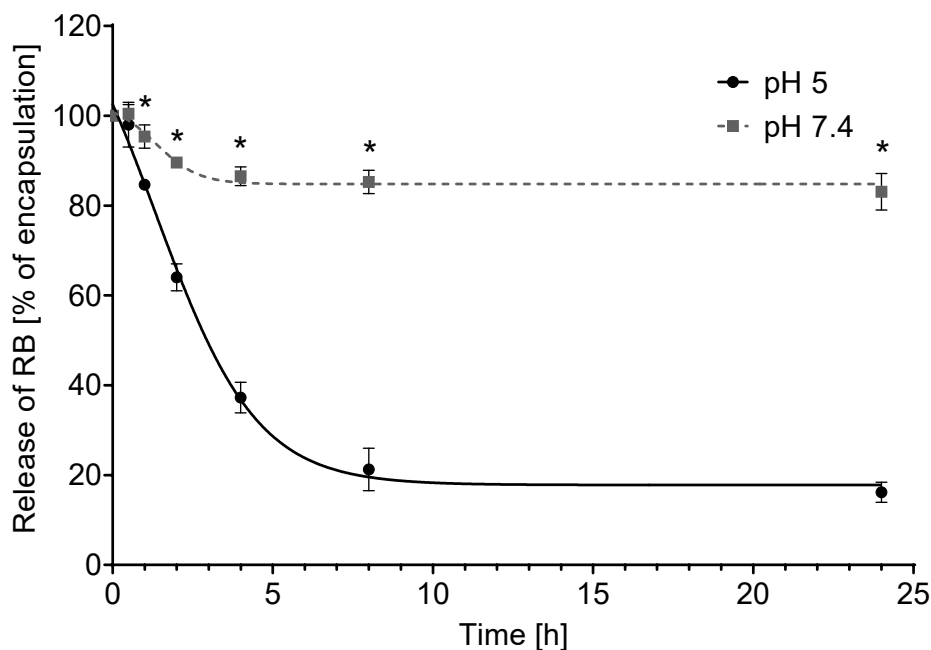


Figure 3. Release of RB from RB-Psome B in pH 5 and pH 7.4 using equilibrium dialysis against PBS. Data presented as mean \pm SD, $n = 3$. * Statistically significant difference at $p < 0.05$ between pH 5 and pH 7.4.

3.4. In vitro photodynamic and phototoxic properties of RB-Psome B

Singlet oxygen generation by the compounds under evaluation was assessed with the use of a highly selective ABDA probe. RB encapsulated in Psome B shows significantly higher ability to generate singlet oxygen than free RB (**Figure 4**). The effect of RB-Psome B is already visible at the lowest concentration tested, whereas the activity of free RB is only detected at higher concentrations. At the highest tested concentration, free RB causes ~2-fold, and RB-Psome B ~6-fold increase in singlet oxygen production relative to the control. At the same time, empty Psome B does not generate singlet oxygen (data not shown).

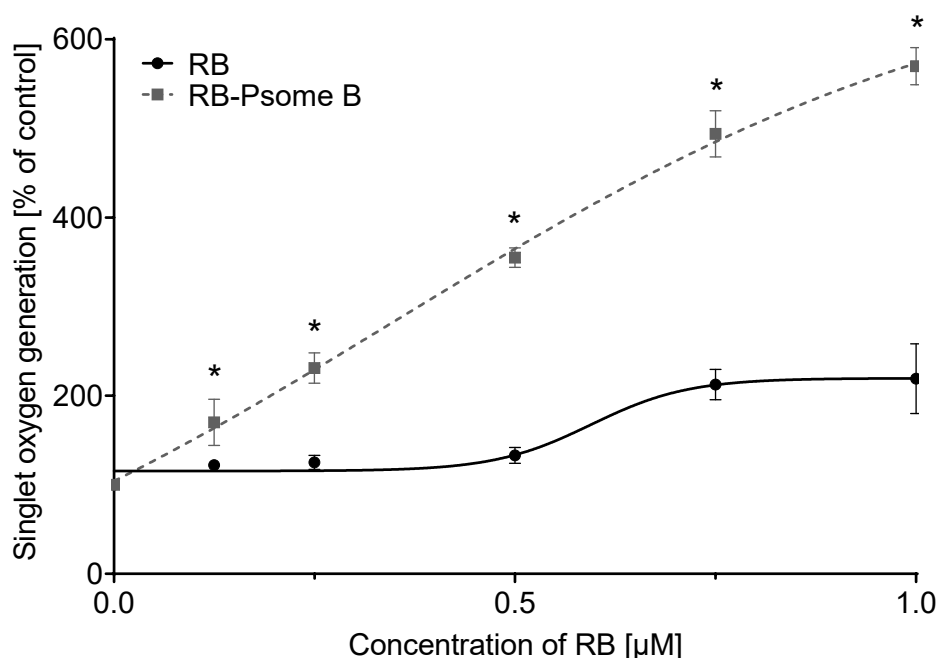


Figure 4. Singlet oxygen generation by free RB and RB-Psome B. The singlet oxygen generation assay was performed using the ABDA probe as an indicator. Data presented as mean \pm SD, $n=3$. * Statistically significant difference at $p < 0.05$ between the RB and RB-Psome B.

Further studies involved the evaluation of uptake, intracellular ROS generation and phototoxicity in two basal cell carcinoma cell line models. The time course of drug uptake in studied cell lines was highly similar for the free and encapsulated form of RB. However, the percentage of cells exhibiting RB-specific fluorescence is significantly higher for AsZ and CsZ lines treated with RB-Psome B, although incubation was performed at equimolar concentration with regard to drug molecules (**Figure 5**).

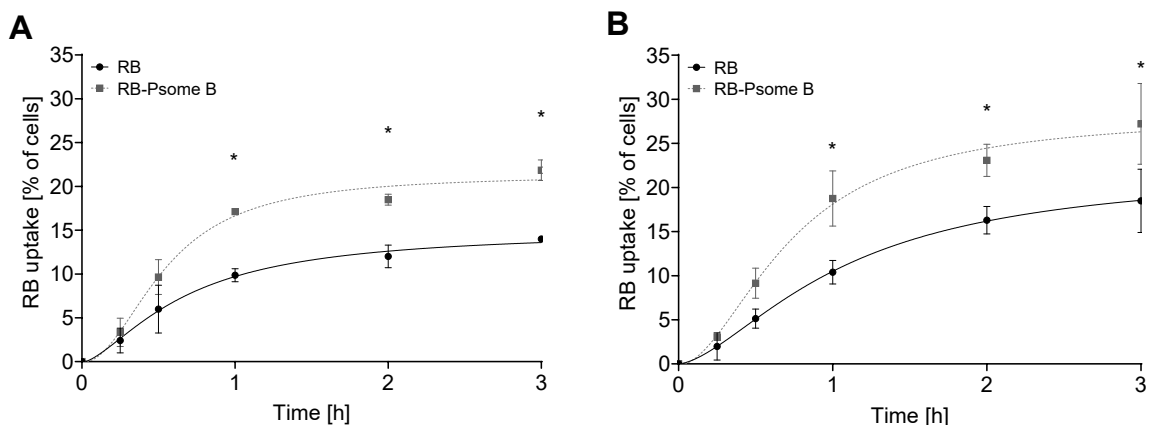


Figure 5. Cellular uptake of free RB and RB-Psome B by: (A) AsZ and (B) CsZ cell lines, evaluated by flow cytometry. Data presented as mean \pm SD, $n = 3$. * Statistically significant difference at $p < 0.05$ between the RB and RB-Psome B.

RB-Psome B generates intracellular ROS more efficiently than free RB (**Figure 6**) in both studied cell lines. This results in a significantly higher phototoxicity of RB co-delivered with Psome B (**Figure 7 A and B**). In AsZ cell line, IC_{50} values for free RB and RB-Psome B are 1.38 and 0.53 μ M, respectively. In case of CsZ cell line, IC_{50} values equal 0.99 and 0.33 μ M for free RB and RB-Psome B. Noteworthy, we do not observe any cytotoxicity of Psome B (data not shown) or dark toxicity of free RB and RB-Psome B under given conditions (**Figure 7 C and D**).

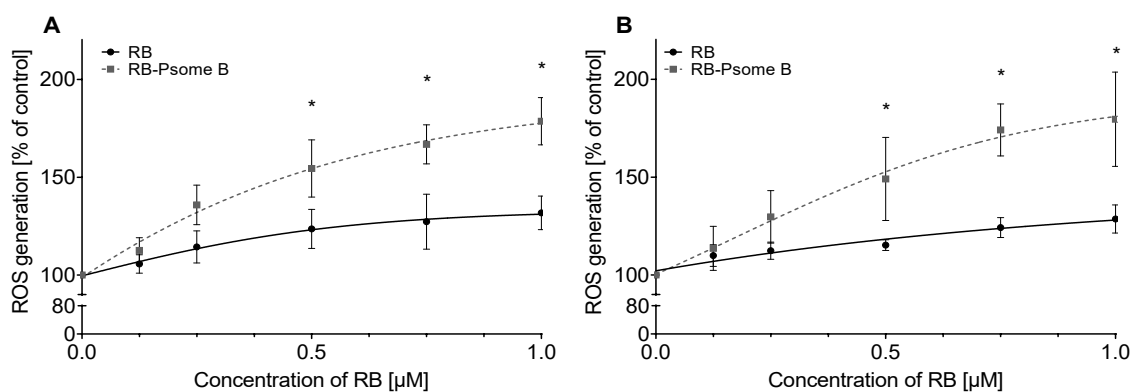


Figure 6. ROS generation by free RB and RB-Psome B. (A) AsZ cell line and (B) CsZ molar ratio upon irradiation determined with the use of the 2',7'-dichlorodihydrofluorescein diacetate (H2DCFDA) probe. Data are presented as percentages of intracellular ROS generation in control (untreated) cells as mean \pm SD, $n = 3$. * Statistically significant difference at $p < 0.05$ between the RB and RB-Psome B.

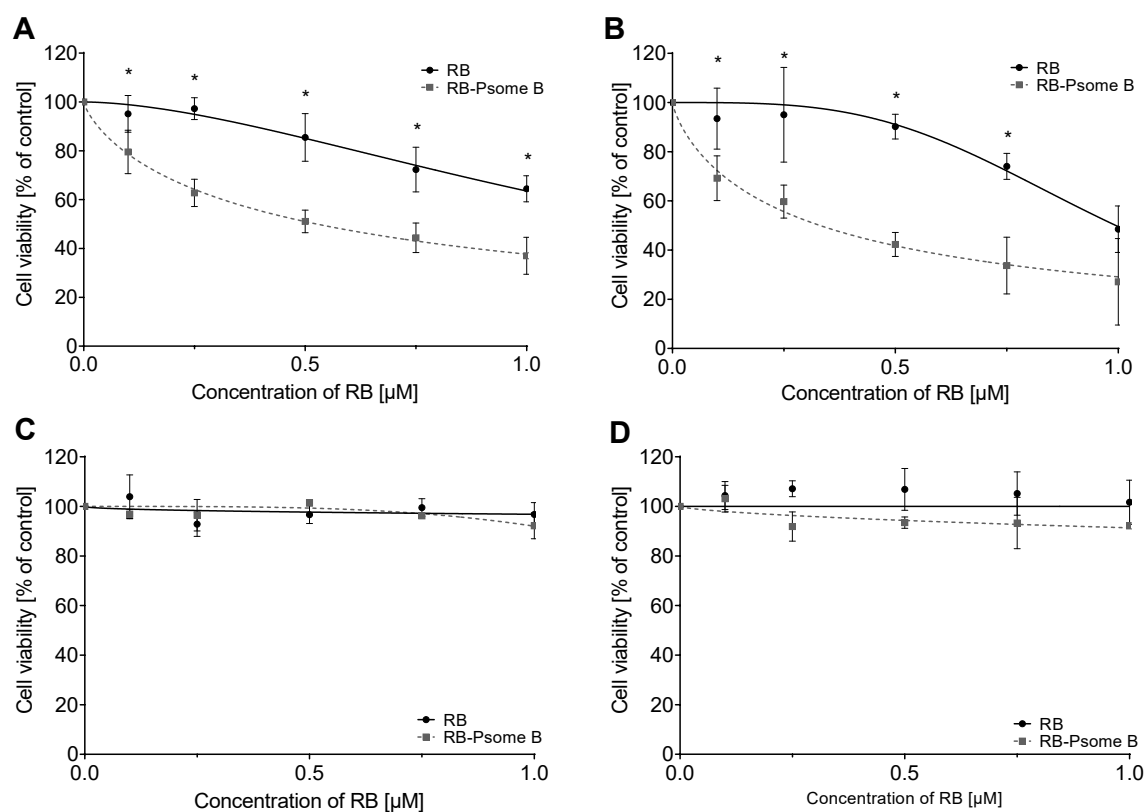


Figure 7. Cytotoxic activity of free RB and RB-Psome B: after irradiation of (A) AsZ, (B) CsZ cell lines, and without irradiation of (C) AsZ and (D) CsZ cell lines. Cell viability was determined using MTT assay. Data are presented as percentages of the viability of control (untreated) cells as mean \pm SD, $n = 3$. * Statistically significant difference at $p < 0.05$ between the RB and RB-Psome B.

4. Discussion

Considering the growing interest in anticancer photodynamic therapy, it is necessary to develop novel compounds allowing to overcome the limitations of currently used photosensitizers. One of the methods involves the use of nanomaterials to act as drug carriers, providing efficient cellular uptake and increasing photodynamic activity. In the living organisms, membranes of cell structures are crucial elements separating different compartments and maintaining controlled transport between them. Thus, current studies focus on the development of nanocarriers mimicking this natural cellular structures, but with controllable shape, size, responsivity and stability in different environments (Iqbal et al., 2020; Kauscher et al., 2019; Messenger et al., 2016). Amphiphilic constructs of low-molecular weight and polymeric compounds used for this purpose allow the spontaneous assembly of vesicles with double-layer membrane similar to the cellular ones, which promotes the placement of lipophilic compounds in the membrane and hydrophilic compounds in the core (Moquin et al., 2018). This in turn may protect the drugs from biodegradation, prolong their half-life and increase cellular uptake. Further application of pH-responsive elements within the vesicle's shell may increase selectivity of the therapy via release of cargo only in the tumor environment (Feng et al., 2018).

Rose bengal is a dianionic fluorescent dye derived from xanthenes, commonly used as an ocular diagnostic tool. Due to the high efficiency of generation of singlet oxygen, RB is considered as PDT agent in anticancer treatment (Demartis et al., 2021; Redmond and Gamlin, 1999). However, its short

half-life, hydrophilic nature, and tendency to aggregation limits the use of RB in PDT of tumors. Due to the short half-life (approx. 30 min), favorable distribution of RB is reduced, necessitating multiple dosing. The tendency of RB to form aggregates in aqueous solutions affects spectral properties of this PS and decreasing the desired singlet oxygen generation, which is the main PDT reaction (Demartis et al., 2021). Finally, RB has a negative charge in physiological environment, which also hampers cellular uptake. Due to this fact, the accumulation of proper RB concentration may be difficult in tumor cells. The above-mentioned limitations can be overcome by the use of appropriate nanocarrier for intracellular delivery of RB.

In our studies, we investigated specific pH-stable polymersome (Psome B) as nanocarrier, composed of amphiphilic block copolymers enriched in UV-crosslinkable and pH-sensitive units (Scheme 1). Amphiphilic architecture enables self-assembling into globular Psome B in aqueous environment (Wang et al., 2021a), whereas cross-linking increases stability of structure and enables modulation of membrane permeability by change of pH (Wang et al., 2021a). Thus, this allowed us to carry out a controlled drug post-loading process with a preferred membrane-integration of RB in RB-Psome B, while the direct loading of RB during the formation of Psome B in aqueous solution may result in undesired aggregation process of RB. Psome B used in this study is designed to swell “open” at $\text{pH} \leq 6.0$ and shrink “close” at $\text{pH} \geq 6.0$ (Wang et al., 2021a). This key characteristic of Psome B is advantageous for our approach in a such way that the swelling (and thus, drug release) would correspond to the pH of tumor environment (Feng et al., 2018). The completely swollen state of Psome B is only given at pH 5 (Moreno et al., 2021). Thus, pH values between 5 and 6 also allow to induce a retarded release profile, when Psome B is only semi-swollen (Wang et al., 2021a). The opening and closing pH values for Psome B can be slightly varied to values up to 6.5 due to varying environmental conditions (Wang et al., 2021a). Swollen state of Psome B during the post-loading process of RB at pH 5 is also indicated by higher cationic surface charge due to protonation state of di-*iso*-propylaminoethyl units in Psome B membrane (Scheme 1). Thus, spherical vesicles can be assumed, supported by first cryo-TEM images (SI) and AF4-MD for both Psome B.

DLS and zeta potential results allowed to postulate the desired encapsulation of RB by Psome B. We observed an increase in hydrodynamic diameter of Psome B at pH 7.4 after RB loading. At the same time surface charge of RB-Psome B is nearly neutral compared to more positively charged empty Psome B (Table 1). This may indicate that RB is integrated in the hydrophobic membrane of Psome B at pH 7.4. Reduction in surface charge of protein post-loaded Psomes (Geervliet et al., 2021; Gumz et al., 2019; Moreno et al., 2021) was also observed and supports the assumption of membrane-integrated RB molecules in Psome B. Furthermore, spherical vesicles can be assumed for empty Psome B, while cauliflower-like shape with rough surface are visible for RB-Psome B, supported by first cryo-TEM images (SI). Both types of Psome B possess diameters in the range of 100 and 130 nm. Cryo-TEM images of RB-Psome B also outline a different state of density for cauliflower-like shape. Results of AF4-MD study support the assumption of vesicular architectures through typical ρ parameters of cargo-loaded hollow spheres (= vesicular structures) in comparison to protein-loaded polymersomes (Geervliet et al., 2021; Gumz et al., 2019; Moreno et al., 2021, 2020a; Wang et al., 2021a). With increasing size, the ρ parameter increases due to higher heterogeneity and potential aggregation. Furthermore, the AF4 results show a shift to higher elution times and a significant increase in size of Psome B with RB loading (Table S3). It can be assumed that the RB molecules accumulate both within the membrane and on the surface due to their small size. The location on the surface facilitates the accessibility to undergo undesired intermolecular interactions resulting in aggregation. However, the ρ parameters reveal still hollow spheres with rough surface on the level of individual RB-Psome B molecules with increasing heterogeneity due to aggregation processes at larger dimensions.

Spectroscopy results allowed to estimate encapsulation rate with significant efficiency (approx. 60%) which is lower in comparison to nanosystem consisting of dendrimersomes but higher than in previously described in the literature (Apartsin et al., 2020; Sztandera et al., 2022; Xu et al., 2019). The experiment showed also red shift of emission wavelength for RB molecules, observed in our previous studies on nanoparticle-based delivery systems. This undoubtedly suggests the emerging interaction of RB with Psome B membrane, (Dabrzalska et al., 2015; Klajnert and Bryszewska, 2002; Sztandera et al., 2021) which is in accordance with the detection of lowered surface charge and increased diameter for RB-Psome. Results from AF4-MD confirm the RB complexation by Psome B with lower loading efficiency. Due to use of different loading parameters (e.g. static vs. flow conditions or use of different MWCO for separating non-complexed RB molecules) for both methods one cannot compare final loading efficiency of RB.

The release study of RB from RB-Psome B smoothly implies the desired stability of the complete nanosystems at physiological pH over the time. On the other hand, the placement of RB-Psome B in acidic conditions makes its membrane permeable for RB, which is released in higher rate than in pH 7.4. Thus, the key characteristic of tunable Psome B membrane brings great promise for the delivery of different anticancer drugs. However, it should be noted that a full release is not necessary in case of photosensitizers, due to the diffusible properties of molecular and singlet oxygen through closed vesicle membranes (Axthelm et al., 2008; Sztandera et al., 2020a). Similar behavior of Psome B is also expected, when RB-Psome should act with closed, semi-permeable or swollen membrane in intra- and extracellular matrix at different pH values.

Considering the application of our nanosystem in the PDT, it must be noted that there are two main mechanisms involved in cell death for this therapy. One of them is previously mentioned generation of singlet oxygen in response to irradiation of photosensitizer. Thus, in the first step we determined the extent of its production by RB and RB-Psome B. The level of singlet oxygen is much higher in the whole concentration range for RB-Psome B compared to free photosensitizer. It should be highlighted that empty Psome B does not generate singlet oxygen by itself. Similar effects were previously observed after RB encapsulation inside dendrimersomes (Sztandera et al., 2022) and complexation of RB with PPI and PAMAM (Sztandera et al., 2021) or cationic phosphorus dendrimers (Dabrzalska et al., 2017). Moreover, the molecular mechanism for all dendritic nanosystems is probably associated with non-covalent interactions of (anionic) RB molecules with (positively charged) structure units of the nanocarrier during the loading and storage process. This preferentially prevents undesired aggregation of RB molecules in the dendritic scaffold of PPI and PAMAM dendrimers (Sztandera et al., 2021). Interestingly, no such effect is observed when RB was conjugated covalently with the same phosphorus dendrimers (Sztandera et al., 2020b). This thoroughly proves the advantage of non-covalent preparations for the delivery of this photosensitizer. Our *in vitro* models additionally confirm the increase of intracellular ROS production by RB-loaded Psome B, leading to enhanced cell death upon irradiation. Interestingly, the cellular uptake is only slightly increased after encapsulation of RB in Psome B. The lack of more profound increase in cellular uptake is most probably due to the almost neutral surface charge of RB-Psome B. The effect of positive surface charge is broadly described in the literature as enabling factor for transmembrane drug delivery (Fröhlich, 2012). Comparing this effect in our study with positively-charged dendrimersome system, we observed a significantly boosted cellular uptake of RB encapsulated in triazine-carbosilane dendrimersomes (Sztandera et al., 2022). Thus, it is reasonable to conclude that the enhanced phototoxic effect of RB-Psome B is solely associated with the increased production of singlet oxygen. Such phenomena undoubtedly show the potential of the developed RB-Psome B nanosystem in anticancer PDT.

5. Conclusions

In summary, we demonstrated the fabrication of RB-loaded polymersome for photodynamic therapy. The developed nanosystem was thoroughly characterized in terms of drug encapsulation, delivery, and release in the tumor environment as well as *in vitro* photodynamic activity. The pH-stable and photo-crosslinked polymersome proved to be suitable systems for loading, storing, and releasing RB molecules. Encapsulation of RB within the polymersome advantageously increases the production of singlet oxygen, which can be immediately transferred into the final photodynamic effect. This gives hope for the development of an efficient drug delivery system in the photodynamic therapy for basal cell carcinoma of the skin. Further *in vivo* studies are necessary to determine the pharmacokinetic and pharmacodynamic parameters of this nanosystem and its performance in living organisms.

Declaration of Competing Interest

The authors declare that they have no known competing financial interests or personal relationships that could have appeared to influence the work reported in this paper.

Acknowledgements

This work was supported by the National Science Centre, Poland (Project UMO-2017/25/B/NZ7/01304 "Phosphorus dendrimers as carriers for photosensitizers - *in vivo* studies") and based upon work from COST Action "Nano2Clinic. Cancer Nanomedicine - from the bench to the bedside" CA17140 supported by COST (European Cooperation in Science and Technology). X. Wang is grateful for a scholarship under the Chinese government award for outstanding students abroad by the China Scholarship Council (CSC).

References

- Allison, R.R., Downie, G.H., Cuenca, R., Hu, X.H., Childs, C.J.H., Sibata, C.H., 2004. Photosensitizers in clinical PDT. *Photodiagnosis Photodyn. Ther.* 1, 27–42.
- Apartsin, E., Knauer, N., Arkhipova, V., Pashkina, E., Aktanova, A., Poletaeva, J., Sánchez-Nieves, J., de la Mata, F.J., Gómez, R., 2020. pH-sensitive dendrimersomes of hybrid triazine-carbosilane dendritic amphiphiles-smart vehicles for drug delivery. *Nanomaterials* 10, 1899.
- Axthelm, F., Casse, O., Koppenol, W.H., Nauser, T., Meier, W., Palivan, C.G., 2008. Antioxidant nanoreactor based on superoxide dismutase encapsulated in superoxide-permeable vesicles. *J. Phys. Chem. B* 112, 8211–8217.
- Bottiroli, G., Cleta Corce, A., Baglioni, P., Monici, M., 1996. Fluorogenic substrates for diagnosis and photodynamic treatment of tumours. WO1997003697A2.
- Boye, S., Polikarpov, N., Appelhans, D., Lederer, A., 2010. An alternative route to dye-polymer complexation study using asymmetrical flow field-flow fractionation. *J. Chromatogr. A* 1217, 4841–4849.
- Dabrzalska, M., Janaszewska, A., Zablocka, M., Mignani, S., Majoral, J.P., Klajnert-Maculewicz, B., 2017. Cationic Phosphorus Dendrimer Enhances Photodynamic Activity of Rose Bengal against Basal Cell Carcinoma Cell Lines. *Mol. Pharm.* 14, 1821–1830.
- Dabrzalska, M., Zablocka, M., Mignani, S., Majoral, J.P., Klajnert-Maculewicz, B., 2015. Phosphorus

- dendrimers and photodynamic therapy. Spectroscopic studies on two dendrimer-photosensitizer complexes: Cationic phosphorus dendrimer with rose bengal and anionic phosphorus dendrimer with methylene blue. *Int. J. Pharm.* 492, 266–274.
- Dees, H.C., Scott, T.C., 2001. Use of halogenated xanthenes as anti-cancer and anti-bacterial agents. CA2415280C.
- Dees, H.C., Scott, T.C., Smolik, J., Wachter, Fisher, G., 2015. Topical medicaments and methods for photodynamic treatment of disease. US8974363B2.
- Demartis, S., Obinu, A., Gavini, E., Giunchedi, P., Rassa, G., 2021. Nanotechnology-based rose Bengal: A broad-spectrum biomedical tool. *Dye. Pigment.* 188, 109236.
- Discher, B.M., Won, Y.Y., Ege, D.S., Lee, J.C.M., Bates, F.S., Discher, D.E., Hammer, D.A., 1999. Polymersomes: Tough vesicles made from diblock copolymers. *Science (80-.)*. 284, 1143–1146.
- Feng, L., Dong, Z., Tao, D., Zhang, Y., Liu, Z., 2018. The acidic tumor microenvironment: A target for smart cancer nano-theranostics. *Natl. Sci. Rev.* 5, 269–286.
- Fröhlich, E., 2012. The role of surface charge in cellular uptake and cytotoxicity of medical nanoparticles. *Int. J. Nanomedicine*.
- Gaitzsch, J., Appelhans, D., Gräfe, D., Schwille, P., Voit, B., 2011. Photo-crosslinked and pH sensitive polymersomes for triggering the loading and release of cargo. *Chem. Commun.* 47, 3466–3468.
- Gaitzsch, J., Appelhans, D., Wang, L., Battaglia, G., Voit, B., 2012. Synthetic bio-nanoreactor: Mechanical and chemical control of polymersome membrane permeability. *Angew. Chemie - Int. Ed.* 51, 4448–4451.
- Gaitzsch, J., Huang, X., Voit, B., 2016. Engineering Functional Polymer Capsules toward Smart Nanoreactors. *Chem. Rev.* 116, 1053–1093.
- Geervliet, E., Moreno, S., Baiamonte, L., Booiijink, R., Boye, S., Wang, P., Voit, B., Lederer, A., Appelhans, D., Bansal, R., 2021. Matrix metalloproteinase-1 decorated polymersomes, a surface-active extracellular matrix therapeutic, potentiates collagen degradation and attenuates early liver fibrosis. *J. Control. Release* 332, 594–607.
- Gorzakiewicz, M., Appelhans, D., Boye, S., Lederer, A., Voit, B., Klajnert-Maculewicz, B., 2019. Effect of the Structure of Therapeutic Adenosine Analogues on Stability and Surface Electrostatic Potential of their Complexes with Poly(propyleneimine) Dendrimers. *Macromol. Rapid Commun.* 40, 1900181.
- Gumz, H., Boye, S., Iyisan, B., Krönert, V., Formanek, P., Voit, B., Lederer, A., Appelhans, D., 2019. Toward Functional Synthetic Cells: In-Depth Study of Nanoparticle and Enzyme Diffusion through a Cross-Linked Polymersome Membrane. *Adv. Sci.* 6, 1801299.
- Hasan, T., 2006. Compositions and methods relating to target-specific photodynamic therapy. PCT Int. Appl. WO2006133271A2.
- Hong, E.J., Choi, D.G., Shim, M.S., 2016. Targeted and effective photodynamic therapy for cancer using functionalized nanomaterials. *Acta Pharm. Sin. B.* <https://doi.org/10.1016/j.apsb.2016.01.007>
- Iqbal, S., Blenner, M., Alexander-Bryant, A., Larsen, J., 2020. Polymersomes for Therapeutic Delivery of Protein and Nucleic Acid Macromolecules: From Design to Therapeutic Applications. *Biomacromolecules* 21, 1327–1350.
- Kakde, D., Jain, D., Shrivastava, V., Kakde, R., Patil, A.T., 2011. Cancer therapeutics- opportunities, challenges and advances in drug delivery. *J. Appl. Pharm. Sci.* 1, 1–10.

- Karges, J., 2022. Clinical Development of Metal Complexes as Photosensitizers for Photodynamic Therapy of Cancer. *Angew. Chemie - Int. Ed.* 61, e202112236.
- Kauscher, U., Holme, M.N., Björnmalm, M., Stevens, M.M., 2019. Physical stimuli-responsive vesicles in drug delivery: Beyond liposomes and polymersomes. *Adv. Drug Deliv. Rev.* 138, 259–275.
- Klajnert, B., Bryszewska, M., 2002. The interaction of tryptophan and ANS with PAMAM dendrimers. *Cell. Mol. Biol. Lett.* 7, 1087–1094.
- Kyropoulou, M., DiLeone, S., Lanzilotto, A., Constable, E.C., Housecroft, C.E., Meier, W.P., Palivan, C.G., 2020. Porphyrin Containing Polymersomes with Enhanced ROS Generation Efficiency: In Vitro Evaluation. *Macromol. Biosci.* 20.
- Messenger, L., Burns, J.R., Kim, J., Cecchin, D., Hindley, J., Pyne, A.L.B., Gaitzsch, J., Battaglia, G., Howorka, S., 2016. Biomimetic Hybrid Nanocontainers with Selective Permeability. *Angew. Chemie - Int. Ed.* 55, 11106–11109.
- Moquin, A., Ji, J., Neibert, K., Winnik, F.M., Maysinger, D., 2018. Encapsulation and Delivery of Neutrophilic Proteins and Hydrophobic Agents Using PMOXA-PDMS-PMOXA Triblock Polymersomes. *ACS Omega* 3, 13882–13893.
- Moreno, S., Boye, S., Ajeilat, H.G. Al, Michen, S., Tietze, S., Voit, B., Lederer, A., Temme, A., Appelhans, D., 2021. Multivalent Protein-Loaded pH-Stable Polymersomes: First Step toward Protein Targeted Therapeutics. *Macromol. Biosci.* 21, 2100102.
- Moreno, S., Sharan, P., Engelke, J., Gumz, H., Boye, S., Oertel, U., Wang, P., Banerjee, S., Klajn, R., Voit, B., Lederer, A., Appelhans, D., 2020a. Light-Driven Proton Transfer for Cyclic and Temporal Switching of Enzymatic Nanoreactors. *Small* 16.
- Moreno, S., Voit, B., Gaitzsch, J., 2020b. The chemistry of cross-linked polymeric vesicles and their functionalization towards biocatalytic nanoreactors. *Colloid Polym. Sci.* 1–16.
- Pearson, R.T., Warren, N.J., Lewis, A.L., Armes, S.P., Battaglia, G., 2013. Effect of pH and temperature on PMPC-PDPA copolymer self-assembly. *Macromolecules* 46, 1400–1407.
- Peters, R.J.R.W., Marguet, M., Marais, S., Fraaije, M.W., Van Hest, J.C.M., Lecommandoux, S., 2014. Cascade reactions in multicompartimentalized polymersomes. *Angew. Chem. Int. Ed. Engl.* 53, 146–150. <https://doi.org/10.1002/ANIE.201308141>
- Pouge, B., O'Hara, J., Swartz, H., Hassan, T., 2005. Methods of adjuvant photodynamic therapy to enhance radiation sensitization. US20050112131A1.
- Prokopovich, P., Perni, S., 2017. PHOTODYNAMIC THERAPY COMPLEX. WO2017077299A1.
- Redmond, R.W., Gamlin, J.N., 1999. A compilation of singlet oxygen yields from biologically relevant molecules. *Photochem. Photobiol.* 70, 391–475.
- Sood, N., 2014. Multi-Functional Polymer Vesicles: Applications in Chemotherapy and Photodynamic Therapy. Publicly Access. Penn Diss.
- Sztandera, K., Gorzkiewicz, M., Bątal, M., Arkhipova, V., Knauer, N., Sánchez-Nieves, J., Mata, F.J. de la, Gómez, R., Apartsin, E., Klajnert-Maculewicz, B., 2022. Triazine–Carbosilane Dendrimersomes Enhance Cellular Uptake and Phototoxic Activity of Rose Bengal in Basal Cell Skin Carcinoma Cells. *Int. J. Nanomedicine* 17, 1139–1154.
- Sztandera, K., Gorzkiewicz, M., Dias Martins, A.S., Pallante, L., Zizzi, E.A., Miceli, M., Bątal, M., Reis, C.P., Deriu, M.A., Klajnert-Maculewicz, B., 2021. Noncovalent Interactions with PAMAM and PPI Dendrimers Promote the Cellular Uptake and Photodynamic Activity of Rose Bengal: The Role of the Dendrimer Structure. *J. Med. Chem.* 64, 15758–15771.

- Sztandera, K., Gorzkiewicz, M., Klajnert-Maculewicz, B., 2020a. Nanocarriers in photodynamic therapy—in vitro and in vivo studies. *Wiley Interdiscip. Rev. Nanomedicine Nanobiotechnology* 12, 1–24.
- Sztandera, K., Marcinkowska, M., Gorzkiewicz, M., Janaszewska, A., Laurent, R., Zabłocka, M., Mignani, S., Majoral, J.P., Klajnert-Maculewicz, B., 2020b. In search of a phosphorus dendrimer-based carrier of rose bengal: Tyramine linker limits fluorescent and phototoxic properties of a photosensitizer. *Int. J. Mol. Sci.* 21, 1–20.
- Thambi, T., Lee, D.S., 2018. Stimuli-responsive polymersomes for cancer therapy, in: *Stimuli Responsive Polymeric Nanocarriers for Drug Delivery Applications: Volume 2: Advanced Nanocarriers for Therapeutics*. pp. 413–438.
- Tu, Y., Peng, F., Adawy, A., Men, Y., Abdelmohsen, L.K.E.A., Wilson, D.A., 2016. Mimicking the Cell: Bio-inspired functions of supramolecular assemblies. *Chem. Rev.* 116, 2023–2078. <https://doi.org/10.1021/acs.chemrev.5b00344>
- Wang, M., Geilich, B.M., Keidar, M., Webster, T.J., 2017. Killing malignant melanoma cells with protoporphyrin IX-loaded polymersome-mediated photodynamic therapy and cold atmospheric plasma. *Int. J. Nanomedicine* 12, 4117–4127.
- Wang, X., Moreno, S., Boye, S., Wang, P., Liu, X., Lederer, A., Voit, B., Appelhans, D., 2021a. Artificial Organelles with Orthogonal-Responsive Membranes for Protocell Systems: Probing the Intrinsic and Sequential Docking and Diffusion of Cargo into Two Coexisting Avidin–Polymersomes. *Adv. Sci.* 8, 2004263.
- Wang, X., Moreno, S., Boye, S., Wen, P., Zhang, K., Formanek, P., Lederer, A., Voit, B., Appelhans, D., 2021b. Feedback-Induced and Oscillating pH Regulation of a Binary Enzyme-Polymersomes System. *Chem. Mater.* 33, 6692–6700.
- Xu, J., Chen, Y., Jiang, X., Gui, Z., Zhang, L., 2019. Development of hydrophilic drug encapsulation and controlled release using a modified nanoprecipitation method. *Processes* 7, 331.

**Oświadczenia współautorów publikacji wchodzących w skład rozprawy
doktorskiej**

Łódź, 7.04.2022
(miejsce, data)

Dr Monika Marcinkowska
Katedra Biofizyki Ogólnej
Wydział Biologii i Ochrony Środowiska
Uniwersytet Łódzki
ul. Pomorska 141/143, 90-236 Łódź

Oświadczenie

Oświadczam, że w pracy:

Sztandera K., Marcinkowska M., Gorzkiewicz M., Janaszewska A., Laurent R., Zabłocka M., Mignani S., Majoral J.P., Klajnert-Maculewicz B. (2020). In Search of a Phosphorus Dendrimer-Based Carrier of Rose Bengal: Tyramine Linker Limits Fluorescent and Phototoxic Properties of a Photosensitizer. *International Journal of Molecular Sciences*, 21(12), 4456 mój udział polegał na syntezie i analizie chemicznej zsintezowanych koniugatów dendrymerów fosforowych z różem bengalskim oraz przygotowaniu części manuskryptu dotyczącego syntezy chemicznej związków (15%).

Monika Marcinkowska

.....
(podpis)

Łódź, 05.04.22
(miejsce, data)

Dr hab. Anna Janaszewska, prof. UŁ
Katedra Biofizyki Ogólnej
Wydział Biologii i Ochrony Środowiska
Uniwersytet Łódzki
ul. Pomorska 141/143, 90-236 Łódź

Oświadczenie

Oświadczam, że w pracy:

Sztandera K., Marcinkowska M., Gorzkiewicz M., Janaszewska A., Laurent R., Zabłocka M., Mignani S., Majoral J.P., Klajnert-Maculewicz B. (2020). In Search of a Phosphorus Dendrimer-Based Carrier of Rose Bengal: Tyramine Linker Limits Fluorescent and Phototoxic Properties of a Photosensitizer. *International Journal of Molecular Sciences*, **21(12)**, 4456 mój udział polegał na opracowaniu koncepcji badań dotyczących analizy biofizycznej zsyntezowanych koniugatów (5%).

Anna Janaszewska
(podpis)

Toulouse, 24th march 2022

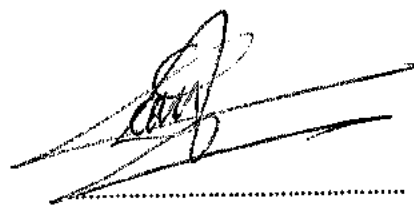
Dr Regis Laurent
Laboratoire de Chimie de Coordination, CNRS
205 Route de Narbonne, BP44099
31077 Toulouse CEDEX 4, France

Statement

I hereby declare that in the article:

Sztandera K., Marcinkowska M., Gorzkiewicz M., Janaszewska A., Laurent R., Zabłocka M., Mignani S., Majoral J.P., Klajnert-Maculewicz B. (2020). In Search of a Phosphorus Dendrimer-Based Carrier of Rose Bengal: Tyramine Linker Limits Fluorescent and Phototoxic Properties of a Photosensitizer. International Journal of Molecular Sciences, 21(12), 4456 my contribution was based on the synthesis of phosphorus dendrimers and revising of the manuscript (5%).

RPB



(signature)

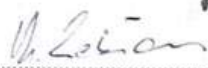
Łódź...16/04/2022.....
(miejsce, data)

Dr hab. Maria Zabłocka
Centrum Badań Molekularnych i Makromolekularnych
Polska Akademia Nauk
ul. Sienkiewicza 112, 90-363 Łódź

Oświadczenie

Oświadczam, że w pracy:

Sztandera K., Marcinkowska M., Gorzkiewicz M., Janaszewska A., Laurent R., Zabłocka M., Mignani S., Majoral J.P., Klajnert-Maculewicz B. (2020). In Search of a Phosphorus Dendrimer-Based Carrier of Rose Bengal: Tyramine Linker Limits Fluorescent and Phototoxic Properties of a Photosensitizer. *International Journal of Molecular Sciences*, 21(12), 4456 mój udział polegał na planowaniu syntezy koniugatów dendrymerów fosforanowych z fózem bengalskim (5%).


.....
(podpis)

Cher Nancy, Madeira, France

(place, date)

26/04/2022

Prof. Serge Mignani
CQM-Centro de Quimica da Madeira,
Universidade da Madeira,
Campus da Penteadá,
9020-105 Funchal, Portugal

Statement

I hereby declare that in the article:

Sztandera K., Marcinkowska M., Gorzkiewicz M., Janaszewska A., Laurent R., Zablocka M., Mignani S., Majoral J.P., Klajnert-Maculewicz B. (2020). In Search of a Phosphorus Dendrimer-Based Carrier of Rose Bengal: Tyramine Linker Limits Fluorescent and Phototoxic Properties of a Photosensitizer. *International Journal of Molecular Sciences*, 21(12), 4456 my contribution was based on the design of phosphorus dendrimers and revising of the manuscript (5%).

Serge Mignani

(signature)

Toulouse
08/04/2022.....
.....
(place, date)

Prof. Jean Pierre Majoral
Laboratoire de Chimie de Coordination, CNRS,
205 Route de Narbonne, BP44099,
31077 Toulouse CEDEX 4, France

Statement

I hereby declare that in the article:

Sztandera K., Marcinkowska M., Gorzkiewicz M., Janaszewska A., Laurent R., Zabłocka M., Mignani S., Majoral J.P., Klajnert-Maculewicz B. (2020). In Search of a Phosphorus Dendrimer-Based Carrier of Rose Bengal: Tyramine Linker Limits Fluorescent and Phototoxic Properties of a Photosensitizer. International Journal of Molecular Sciences, 21(12), 4456 my contribution was based on the design of conjugates of phosphorus dendrimers and revising of the manuscript (5%).



.....
(signature)

Lisboa, 25/03/2022
(place, date)

Ana Sofia Dias Martins
iMed.Ulisboa–Research Institute for Medicines,
Faculdade de Farmácia,
Universidade de Lisboa,
Av. Prof. Gama Pinto, 1649-003 Lisboa, Portugal

Statement

I hereby declare that in the article:

Sztandera K., Gorzkiewicz M., Dias Martins A.S., Pallante L., Zizzi E.A., Miceli M., Bątal M., Pinto Reis C., Deriu M.A., Klajnert-Maculewicz B. (2021). Noncovalent Interactions with PAMAM and PPI Dendrimers Promote the Cellular Uptake and Photodynamic Activity of Rose Bengal: The Role of the Dendrimer Structure. Journal of medicinal chemistry, 64(21), 15758-15771 my contribution was based on the performing of the part of biophysical characterization of complexes of PAMAM and PPI dendrimers with rose bengal (5%)

Ana Sofia Martins
(signature)

Turin, 04/04/2022
(place, date)

Lorenzo Pallante
Polito^{BIO}MedLab
Department of Mechanical and Aerospace Engineering
Politecnico di Torino
Corso Duca degli Abruzzi 24, 10129 Turin, Italy

Statement

I hereby declare that in the article:

Sztandera K., Gorzkiewicz M., Dias Martins A.S., Pallante L., Zizzi E.A., Miceli M., Bątal M., Pinto Reis C., Deriu M.A., Klajnert-Maculewicz B. (2021). Noncovalent Interactions with PAMAM and PPI Dendrimers Promote the Cellular Uptake and Photodynamic Activity of Rose Bengal: The Role of the Dendrimer Structure. *Journal of medicinal chemistry*, 64(21), 15758-15771 my contribution was based on the execution of the part of the computer modeling and partial analysis of the data (7%).

Lorenzo Pallante
(signature)

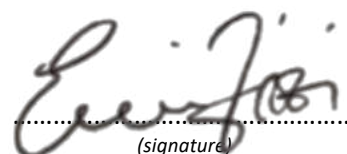
.....Turin, 24/3/22.....
(place, date)

Eric Adriano Zizzi
Polito^{BIO}Med Lab
Department of Mechanical and Aerospace Engineering
Politecnico di Torino
Corso Duca degli Abruzzi 24, 10129 Turin, Italy

Statement

I hereby declare that in the article:

Sztandera K., Gorzkiewicz M., Dias Martins A.S., Pallante L., Zizzi E.A., Miceli M., Bałal M., Pinto Reis C., Deriu M.A., Klajnert-Maculewicz B. (2021). Noncovalent Interactions with PAMAM and PPI Dendrimers Promote the Cellular Uptake and Photodynamic Activity of Rose Bengal: The Role of the Dendrimer Structure. Journal of medicinal chemistry, 64(21), 15758-15771 my contribution was based on the execution of the part of the computer modeling and partial analysis of the data (7%).



.....
(signature)

Turin 04/04/22
(place, date)

Marcello Miceli
Polito^{BIO}MedLab
Department of Mechanical and Aerospace Engineering
Politecnico di Torino
Corso Duca degli Abruzzi 24, 10129 Turin, Italy

Statement

I hereby declare that in the article:

Sztandera K., Gorzkiewicz M., Dias Martins A.S., Pallante L., Zizzi E.A., Miceli M., Bątal M., Pinto Reis C., Deriu M.A., Klajnert-Maculewicz B. (2021). Noncovalent Interactions with PAMAM and PPI Dendrimers Promote the Cellular Uptake and Photodynamic Activity of Rose Bengal: The Role of the Dendrimer Structure. *Journal of medicinal chemistry*, 64(21), 15758-15771 my contribution was based on the execution of the part of the computer modeling and partial analysis of the data (7%).


(signature)

Lisbon, 29th of March 2022
(place, date)

Prof. Catarina Pinto Reis
iMed.Ulisboa–Research Institute for Medicines
Faculdade de Farmácia
Universidade de Lisboa
Av. Prof. Gama Pinto, 1649-003 Lisboa, Portugal

Statement

I hereby declare that in the article:

Sztandera K., Gorzkiewicz M., Dias Martins A.S., Pallante L., Zizzi E.A., Miceli M., Bątal M., Pinto Reis C., Deriu M.A., Klajnert-Maculewicz B. (2021). Noncovalent Interactions with PAMAM and PPI Dendrimers Promote the Cellular Uptake and Photodynamic Activity of Rose Bengal: The Role of the Dendrimer Structure. Journal of medicinal chemistry, 64(21), 15758-15771 my contribution was based on the approving of the final manuscript (2%)

Catarina Pinto Reis
(signature)

Turin, 01/01/2022
(place, date)

Prof. Marco Agostiono Deriu
Polito^{BIO}Med Lab
Department of Mechanical and Aerospace Engineering
Politecnico di Torino
Corso Duca degli Abruzzi 24, 10129 Turin, Italy

Statement

I hereby declare that in the article:

Sztandera K., Gorzkiewicz M., Dias Martins A.S., Pallante L., Zizzi E.A., Miceli M., Bařal M., Pinto Reis C., Deriu M.A., Klajnert-Maculewicz B. (2021). Noncovalent Interactions with PAMAM and PPI Dendrimers Promote the Cellular Uptake and Photodynamic Activity of Rose Bengal: The Role of the Dendrimer Structure. *Journal of medicinal chemistry*, 64(21), 15758-15771 my contribution was based on the revising and approval of final manuscript (5%).


(signature)

Novosibirsk, 25.03.2022

.....
(place, date)

Valeria Arkhipova
Institute of Chemical Biology and
Fundamental Medicine SB RAS,
Novosibirsk, 630090, Russia

Statement

I hereby declare that in the article:

Sztandera K., Gorzkiewicz M., Bątal M., Arkhipova V., Knauer N., Sánchez-Nieves J., de la Mata FJ., Gómez R., Apartsin E., Klajnert-Maculewicz, B. (2022). Triazine–Carbosilane Dendrimersomes Enhance Cellular Uptake and Phototoxic Activity of Rose Bengal in Basal Cell Skin Carcinoma Cells. *International Journal of Nanomedicine*, 17, 1139-1154 my contribution was based on the synthesis of the dendrons (4%).


.....
(signature)

Novosibirsk, 25 March 2022

.....
(place, date)

Nadezhda Knauer
Research Institute of Fundamental and Clinical Immunology,
Novosibirsk, 630099, Russia

Statement

I hereby declare that in the article:

Sztandera K., Gorzkiewicz M., Bałal M., Arkhipova V., Knauer N., Sánchez-Nieves J., de la Mata FJ., Gómez R., Apartsin E., Klajnert-Maculewicz, B. (2022). Triazine–Carbosilane Dendrimersomes Enhance Cellular Uptake and Phototoxic Activity of Rose Bengal in Basal Cell Skin Carcinoma Cells. *International Journal of Nanomedicine*, 17, 1139-1154 my contribution was based on the synthesis of the dendrons (4%).



.....
(signature)

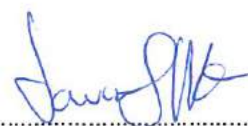
Alcalá de Henares
March 23rd of 2022
(place, date)

Prof. Javier Sánchez-Nieves
Departamento de Química Orgánica y Química Inorgánica
Universidad de Alcalá (UAH)
Alcalá de Henares, 28805, Madrid, Spain

Statement

I hereby declare that in the article:

Sztandera K., Gorzkiewicz M., Bątal M., Arkhipova V., Knauer N., Sánchez-Nieves J., de la Mata FJ., Gómez R., Apartsin E., Klajnert-Maculewicz, B. (2022). Triazine–Carbosilane Dendrimersomes Enhance Cellular Uptake and Phototoxic Activity of Rose Bengal in Basal Cell Skin Carcinoma Cells. *International Journal of Nanomedicine*, 17, 1139-1154 my contribution was based on the revision of the final manuscript (3%)



.....
(signature)

Alcalá de Henares, March
29,2022

.....
(place, date)

Prof. Javier de la Mata
Departamento de Química Orgánica y Química Inorgánica
UAH-IQAR
Alcalá de Henares, 28805, Spain

Statement

I hereby declare that in the article:

Sztandera K., Gorzkiewicz M., Bątal M., Arkhipova V., Knauer N., Sánchez-Nieves J., de la Mata FJ., Gómez R., Apartsin E., Klajnert-Maculewicz, B. (2022). Triazine–Carbosilane Dendrimersomes Enhance Cellular Uptake and Phototoxic Activity of Rose Bengal in Basal Cell Skin Carcinoma Cells. *International Journal of Nanomedicine*, 17, 1139-1154 my contribution was based on the revision of the final manuscript (3%).



F. Javier de la Mata

.....
(signature)

Alcalá de Henares,
March 23th 2022

Prof. Rafael Gómez
Departamento de Química Orgánica y Química Inorgánica
UAH-IQAR
Alcalá de Henares, 28805, Spain

Statement

I hereby declare that in the article:

Sztandera K., Gorzkiewicz M., Bątal M., Arkhipova V., Knauer N., Sánchez-Nieves J., de la Mata FJ., Gómez R., Apartsin E., Klajnert-Maculewicz, B. (2022). Triazine–Carbosilane Dendrimersomes Enhance Cellular Uptake and Phototoxic Activity of Rose Bengal in Basal Cell Skin Carcinoma Cells. *International Journal of Nanomedicine*, 17, 1139-1154 my contribution was based on the revision of the final manuscript (3%).



Rafael Gómez Ramírez
(signature)

Toulouse, 25/03/2022

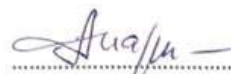
.....
(place, date)

Dr Evgeny Apartsin
Laboratoire de Chimie de Coordination CNRS
Toulouse, 31077, France

Statement

I hereby declare that in the article:

Sztandera K., Gorzkiewicz M., Bałal M., Arkhipova V., Knauer N., Sánchez-Nieves J., de la Mata FJ., Gómez R., Apartsin E., Klajnert-Maculewicz, B. (2022). Triazine–Carbosilane Dendrimersomes Enhance Cellular Uptake and Phototoxic Activity of Rose Bengal in Basal Cell Skin Carcinoma Cells. *International Journal of Nanomedicine*, 17, 1139-1154 my contribution was based on the designing of the part of biophysical experiments, revision and approval of the final manuscript (8%).


.....
(signature)

Łódź 14.06.2022
.....
(miejsce, data)

Mateusz Bątal
Katedra Biofizyki Ogólnej
Wydział Biologii i Ochrony Środowiska
Uniwersytet Łódzki
ul. Pomorska 141/143, 90-236 Łódź

Oświadczenie

Oświadczam, że w pracy:

Sztandera K., Gorzkiewicz M., Dias Martins A.S., Pallante L., Zizzi E.A., Miceli M., Bątal M., Pinto Reis C., Deriu M.A., Klajnert-Maculewicz B. (2021). Noncovalent Interactions with PAMAM and PPI Dendrimers Promote the Cellular Uptake and Photodynamic Activity of Rose Bengal: The Role of the Dendrimer Structure. *Journal of medicinal chemistry*, 64(21), 15758-15771 mój udział polegał na wykonaniu części doświadczenia dotyczącego transportu dkomorkowego (2%)

Sztandera K., Gorzkiewicz M., Bątal M., Arkhipova V., Knauer N., Sánchez-Nieves J., de la Mata FJ., Gómez R., Apartsin E., Klajnert-Maculewicz, B. (2022). Triazine–Carbosilane Dendrimersomes Enhance Cellular Uptake and Phototoxic Activity of Rose Bengal in Basal Cell Skin Carcinoma Cells. *International Journal of Nanomedicine*, 17, 1139-1154 15771 mój udział polegał na wykonaniu części charakterystyki biofizycznej dendrymersomów z enkapsulowanym rozem bengalskim (3%).

M. Mateusz Bątal
.....
(podpis)

Dongguan, China, 16.06.2022
(place, date)

Dr Xueyi Wang
Dongguan Hospital
Southern Medical University
Dongguan 523059, P. R. China

Statement

I hereby declare that in the article:

Sztandera K., Gorzkiewicz M., Wang X., Boye S., Appelhans D., Klajnert-Maculewicz, B. (2022). pH-stable polymersome as nanocarrier for post-loaded rose bengal in photodynamic therapy. *Colloids and Surfaces B: biointerfaces* (in revision process) my contribution was based on the revision and approval of the final manuscript (10%).

Wang Xueyi
(signature)

Dresden, 15.6.2022

(place, date)

Dr Susanne Boye
Leibniz Institute for Polymer Research Dresden
6 Hohe St., 01069 Dresden, Germany

Statement

I hereby declare that in the article:

Sztandera K., Gorzkiewicz M., Wang X., Boye S., Appelhans D., Klajnert-Maculewicz, B. (2022). pH-stable polymersome as nanocarrier for post-loaded rose bengal in photodynamic therapy. Colloids and Surfaces B: biointerfaces (in revision process) my contribution was based on the revision and approval of the final manuscript (5%).



(signature)

Dresden, 17.06.2022
(place, date)

Dr. Dietmar Appelhans
Leibniz Institute for Polymer Research Dresden
6 Hohe St., 01069 Dresden, Germany

Statement

I hereby declare that in the article:

Sztandera K., Gorzkiewicz M., Wang X., Boye S., Appelhans D., Klajnert-Maculewicz, B. (2022). pH-stable polymersome as nanocarrier for post-loaded rose bengal in photodynamic therapy. Colloids and Surfaces B: biointerfaces (in revision process) my contribution was based on the revision and approval of the final manuscript (5%).


.....
(signature)

Leibniz-Institut für Polymerforschung
Dresden e.V.
Hohe Straße 6
01069 Dresden

Düsseldorf, 16.06.2022
(miejsce, data)

Dr Michał Gorzkiewicz
Katedra Biofizyki Ogólnej
Wydział Biologii i Ochrony Środowiska Uniwersytet Łódzki
ul. Pomorska 141/143, 90-236 Łódź

Oświadczenie

Oświadczam, że w pracy:

Sztandera K., Gorzkiewicz M., Klajnert-Maculewicz B. (2020). Nanocarriers in photodynamic therapy—in vitro and in vivo studies. Wiley Interdisciplinary Reviews: Nanomedicine and Nanobiotechnology, 12(3), e1509 mój udział polegał na przygotowaniu rozdziału, korekcie merytorycznej oraz zatwierdzeniu ostatecznej wersji artykułu (30%).

Sztandera K., Marcinkowska M., Gorzkiewicz M., Janaszewska A., Laurent R., Zabłocka M., Mignani S., Majoral J.P., Klajnert-Maculewicz B. (2020). In Search of a Phosphorus Dendrimer-Based Carrier of Rose Bengal: Tyramine Linker Limits Fluorescent and Phototoxic Properties of a Photosensitizer. International Journal of Molecular Sciences, 21(12), 4456 mój udział polegał na planowaniu badań, konsultacji merytorycznej oraz sprawdzeniu i zatwierdzeniu ostatecznej wersji artykułu (5%).

Sztandera K., Gorzkiewicz M., Dias Martins A.S., Pallante L., Zizzi E.A., Miceli M., Bątał M., Pinto Reis C., Deriu M.A., Klajnert-Maculewicz B. (2021). Noncovalent Interactions with PAMAM and PPI Dendrimers Promote the Cellular Uptake and Photodynamic Activity of Rose Bengal: The Role of the Dendrimer Structure. Journal of medicinal chemistry, 64(21), 15758 mój udział polegał na planowaniu badań, konsultacji merytorycznej oraz sprawdzeniu i zatwierdzeniu ostatecznej wersji artykułu (10%).

Sztandera K., Gorzkiewicz M., Bątał M., Arkhipova V., Knauer N., Sánchez-Nieves J., de la Mata FJ., Gómez R., Apartsin E., Klajnert-Maculewicz, B. (2022). Triazine–Carbosilane Dendrimersomes Enhance Cellular Uptake and Phototoxic Activity of Rose Bengal in Basal Cell Skin Carcinoma Cells. International Journal of Nanomedicine, 17, 1139-1154 mój udział polegał na planowaniu badań, konsultacji merytorycznej oraz sprawdzeniu i zatwierdzeniu ostatecznej wersji artykułu (5%).

Sztandera K., Gorzkiewicz M., Wang X., Boye S., Appelhans D., Klajnert-Maculewicz B. (2022). pH-stable polymersome as nanocarrier for post-loaded rose bengal in photodynamic therapy. Colloids and Surfaces B: Biointerfaces (w trakcie recenzji) mój udział polegał na planowaniu badań dotyczących charakterystyki biofizycznej dendrymersomów, konsultacji merytorycznej oraz sprawdzeniu i zatwierdzeniu ostatecznej wersji artykułu (10%).



.....
(podpis)

Łódź, 17 czerwca 2022 r.
(miejsce, data)

Prof. dr hab. Barbara Klajnert-Maculewicz
Katedra Biofizyki Ogólnej
Wydział Biologii i Ochrony Środowiska Uniwersytet Łódzki
ul. Pomorska 141/143, 90-236 Łódź

Oświadczenie

Oświadczam, że w pracy:

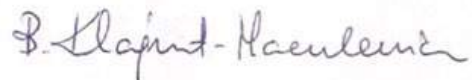
Sztandera K., Gorzkiewicz M., Klajnert-Maculewicz B. (2020). Nanocarriers in photodynamic therapy—in vitro and in vivo studies. *Wiley Interdisciplinary Reviews: Nanomedicine and Nanobiotechnology*, 12(3), e1509 mój udział polegał na korekcie merytorycznej oraz zatwierdzeniu ostatecznej wersji artykułu (10%).

Sztandera K., Marcinkowska M., Gorzkiewicz M., Janaszewska A., Laurent R., Zabłocka M., Mignani S., Majoral J.P., Klajnert-Maculewicz B. (2020). In Search of a Phosphorus Dendrimer-Based Carrier of Rose Bengal: Tyramine Linker Limits Fluorescent and Phototoxic Properties of a Photosensitizer. *International Journal of Molecular Sciences*, 21(12), 4456 mój udział polegał na planowaniu badań, kierowaniu projektem obejmującym badania, konsultacji merytorycznej oraz zatwierdzeniu ostatecznej wersji artykułu (5%).

Sztandera K., Gorzkiewicz M., Dias Martins A.S., Pallante L., Zizzi E.A., Miceli M., Bątał M., Pinto Reis C., Deriu M.A., Klajnert-Maculewicz B. (2021). Noncovalent Interactions with PAMAM and PPI Dendrimers Promote the Cellular Uptake and Photodynamic Activity of Rose Bengal: The Role of the Dendrimer Structure. *Journal of medicinal chemistry*, 64(21), 15758-15771 mój udział polegał na planowaniu badań, kierowaniu projektem obejmującym badania, konsultacji merytorycznej oraz zatwierdzeniu ostatecznej wersji artykułu (5%).

Sztandera K., Gorzkiewicz M., Bątał M., Arkhipova V., Knauer N., Sánchez-Nieves J., de la Mata F.J., Gómez R., Apartsin E., Klajnert-Maculewicz B. (2022). Triazine–Carbosilane Dendrimersomes Enhance Cellular Uptake and Phototoxic Activity of Rose Bengal in Basal Cell Skin Carcinoma Cells. *International Journal of Nanomedicine*, 17, 1139-1154 mój udział polegał na planowaniu badań, kierowaniu projektem obejmującym badania, konsultacji merytorycznej oraz zatwierdzeniu ostatecznej wersji artykułu (5%).

Sztandera K., Gorzkiewicz M., Wang X., Boye S., Appelhans D., Klajnert-Maculewicz B. (2022). pH-stable polymersome as nanocarrier for post-loaded rose bengal in photodynamic therapy. *Colloids and Surfaces B: Biointerfaces* (w trakcie recenzji) mój udział polegał na planowaniu badań, kierowaniu projektem obejmującym badania, konsultacji merytorycznej oraz zatwierdzeniu ostatecznej wersji artykułu (5%).



.....
(podpis)

Łódź, 14.06.2022
(miejsce, data)

Mgr Krzysztof Sztandera
Katedra Biofizyki Ogólnej
Wydział Biologii i Ochrony Środowiska Uniwersytet Łódzki
ul. Pomorska 141/143, 90-236 Łódź

Oświadczenie

Oświadczam, że w pracy:

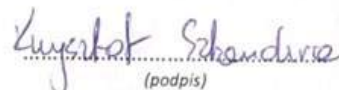
Sztandera K., Gorzkiewicz M., Klajnert-Maculewicz B. (2020). Nanocarriers in photodynamic therapy—in vitro and in vivo studies. *Wiley Interdisciplinary Reviews: Nanomedicine and Nanobiotechnology*, 12(3), e1509 mój udział polegał na zebraniu materiałów oraz przygotowaniu manuskryptu (60%).

Sztandera K., Marcinkowska M., Gorzkiewicz M., Janaszewska A., Laurent R., Zabłocka M., Mignani S., Majoral J.P., Klajnert-Maculewicz B. (2020). In Search of a Phosphorus Dendrimer-Based Carrier of Rose Bengal: Tyramine Linker Limits Fluorescent and Phototoxic Properties of a Photosensitizer. *International Journal of Molecular Sciences*, 21(12), 4456 mój udział polegał na planowaniu i wykonaniu doświadczeń obejmujących analizę biofizyczną koniugatów oraz badania in vitro, analizie i interpretacji wyników, przygotowaniu manuskryptu (50%).

Sztandera K., Gorzkiewicz M., Dias Martins A.S., Pallante L., Zizzi E.A., Miceli M., Bątał M., Pinto Reis C., Deriu M.A., Klajnert-Maculewicz B. (2021). Noncovalent Interactions with PAMAM and PPI Dendrimers Promote the Cellular Uptake and Photodynamic Activity of Rose Bengal: The Role of the Dendrimer Structure. *Journal of medicinal chemistry*, 64(21), 15758- mój udział polegał na planowaniu i wykonaniu doświadczeń obejmujących analizę biofizyczną kompleksów oraz badania in vitro, analizie i interpretacji wyników, przygotowaniu manuskryptu (50 %).

Sztandera K., Gorzkiewicz M., Bątał M., Arkhipova V., Knauer N., Sánchez-Nieves J., de la Mata F.J., Gómez R., Apartsin E., Klajnert-Maculewicz, B. (2022). Triazine–Carbosilane Dendrimersomes Enhance Cellular Uptake and Phototoxic Activity of Rose Bengal in Basal Cell Skin Carcinoma Cells. *International Journal of Nanomedicine*, 17, 1139-1154 - mój udział polegał na planowaniu i wykonaniu doświadczeń obejmujących analizę biofizyczną dendrymersomów oraz badania in vitro, analizie i interpretacji wyników, przygotowaniu manuskryptu (62%).

Sztandera K., Gorzkiewicz M., Wang X., Boye S., Appelhans D., Klajnert-Maculewicz B. (2022). pH-stable polymersome as nanocarrier for post-loaded rose bengal in photodynamic therapy. *Colloids and surfaces B: biointerfaces* mój udział polegał na planowaniu i wykonaniu doświadczeń obejmujących analizę biofizyczną polimersomów oraz badania in vitro, analizie i interpretacji wyników, przygotowaniu manuskryptu (65%).


(podpis)